“As to the heart: it moves itself, and doth never stop, except it be for eternity.”

Translated words of observations made by Leonardo da Vinci during his anatomical studies.

Understanding altered intrinsic heart rate in type 2 diabetes

Sajida Parveen

A thesis submitted for the degree of

Doctor of Philosophy

at the University of Otago, Dunedin, New Zealand,

October 2019

Abstract

Heart rate (HR) is generated by sinoatrial node (SAN) intrinsic pacemaking and modulated by autonomic innervation. Within the SAN, intrinsic (*ex vivo*) HR is determined by the mutual entrainment of the sarcolemmal voltage membrane (Vm) and intracellular Ca^{2+} clocks. The Vm clock involves membrane ion channels, such as the hyperpolarisation-activated cyclic nucleotide-gated channel 4 (HCN4), transient type (T-type) and long-lasting type (L-type) Ca^{2+} channels and the ion transporter Na^{+}-Ca^{2+} exchanger 1 (NCX1). The Ca^{2+} clock primarily involves the intracellular Ca^{2+} store, the sarcoplasmic reticulum (SR), and the Ca^{2+} release protein the ryanodine receptor 2 (RyR2), the Ca^{2+} uptake protein the sarco(endo)plasmic reticulum Ca^{2+}-ATPase (SERCA2a) and its regulator phospholamban. Conduction of the AP within the SAN occurs via the coupling protein connexin 45 (cx45). Additionally, the presence of the non-neuronal cardiac intrinsic cholinergic system within cardiomyocytes suggests it might also be present in the SAN cardiomyocytes and have the capacity to modulate intrinsic HR.

Disruption of HR control occurs in patients and animal models with type 2 diabetes (DM). Interestingly, in the DM Zucker Diabetic Fatty (ZDF) rats, intrinsic HR was significantly decreased compared to non-diabetic (nDM) controls. This suggests DM impairs the intrinsic ability of the SAN to generate a normal HR. Therefore, the overall aim of this research was to investigate whether the decreased intrinsic HR in DM was due to changes in the Vm and / or Ca^{2+} clocks, cx45 and / or increased non-neuronal intrinsic cholinergic system activity. The SAN / hearts of 19 – 22 week-old nDM and DM ZDF rats were used to investigate protein expression of the key SAN clock, cx45 and cholinergic proteins via western blotting, intrinsic HR

contributions from HCN4, SERCA2a and muscarinic type 2 (M_2) receptor via Langendorff, and SAN cellular / tissue morphology via immunohistochemistry.

For the Vm clock, a significant increase in HCN4 (nDM 0.83 ± 0.07 versus DM 1.67 ± 0.19, *p<0.05*) and NCX1 (nDM 1.74 ± 0.32 versus DM 3.83 ± 0.81, *p<0.05*) protein expression was found in DM. For the Ca^{2+} clock, a significant increase in phospholamban (nDM 0.96 ± 0.06 versus DM 1.51 ± 0.18, *p<0.05*), with no change to SERCA2a protein expression (nDM 2.77 ± 0.55 versus DM 3.33 ± 0.38, *p>0.05*) or SERCA2a to phospholamban ratio (nDM 2.97 ± 0.68 versus DM 2.37 ± 0.34, *p>0.05*) was found in DM. A significant increase in the M_2 receptor expression (nDM 1.14 ± 0.18 versus DM 3.14 ± 0.80, *p<0.01*) was also found in DM. The functional effects on intrinsic HR were investigated by increasing ivabradine (HCN4 inhibitor), external Ca^{2+} ($[Ca^{2+}]_o$) and carbachol (M_2 stimulus) to challenge HCN4 and SERCA2a, and determine cholinergic responsiveness respectively in DM. Ivabradine reduced intrinsic HR in nDM but not DM (interaction *p<0.05*), $[Ca^{2+}]_o$ decreased intrinsic HR in DM but not nDM (interaction *p<0.05*), and carbachol decreased intrinsic HR in nDM and DM to equal measure (interaction *p>0.05*). For immunohistochemistry, no difference in cellular / tissue distribution of key SAN clock, cx45 or cholinergic proteins was observed, or in the levels of fibrosis (*p>0.05*) and fat (*p>0.05*) within the DM SAN.

Collectively, this study presents novel mechanisms that are altered in pacemaking in the type 2 DM SAN. From this research, I conclude, the lower intrinsic HR in DM is, in part, a result of changes to both the Vm and Ca^{2+} clock due to non-functional HCN4 channels and compromised SERCA2a activity that would prolong diastolic depolarisation and repolarisation respectively.

Alhamdulillah

Acknowledgements

I find myself with countless heartfelt thanks to give and not enough words to express the sentiment. Firstly, I would like to express my deepest gratitude to both my supervisors Associate Professor Pete Jones and Associate Professor Regis Lamberts for entrusting me to embark on this PhD journey. I will always be thankful for the continuous support, open door, guidance and the individual valuable insights on the many different aspects of this PhD experience. I highly appreciate the time that has been given to me to improve my scientific research skills. To my PhD chair, Associate Professor Kirk Hamilton, thank you for being approachable, a listening ear and owning a positive manner.

I would also like to thank the previous and current members of the Jones and Lamberts labs. In particular, many special thanks to Dr Akash Chakraborty and Dr Michelle Munro for their friendships, unwavering support, teaching and advice in the lab, department and with my thesis writing. Besides the support received at the University of Otago, I would also like to extend my warm thanks to Dr Halina Dobrzynski and Dr Sunil Logantha at the University of Manchester, UK. Halina has always kindly provided her expertise and the valuable opportunity to re-enter her lab in Manchester with Sunil, who trained me to have capable hands in isolating the sinoatrial node.

Last but not least, I express infinite thanks and love for all my own. Countless thanks to my family back in the UK that has listened, supported and encouraged me throughout this journey at the other side of the globe, patiently bearing my time away, and for always being my

strength – my words cannot express how grateful I truly am. To my amazing friends. Thank you very much Swati, for literally being there since day one, for experiencing my good and bad with me, for our stimulating research conversations and so much more. Thanks again to Akash for all your kindness, for bearing my frustrations and ways, and for being there. Special thanks also to my bestie Mariam, Mimi, Eloise and Caroline (adventurers), Sharon, Karolina and Madita for the unforgettable moments, laughter, warmth, time and close friendships in my life.

Contents

List of figures

List of tables

List of abbreviations

AP	Action potential
Ca^{2+}	Calcium
$[Ca^{2+}]_i$	Intracellular Ca^{2+}
$[Ca^{2+}]_o$	External Ca^{2+}
CaMKII	Ca^{2+} / calmodulin-dependent protein kinase II
cAMP	Cyclic adenosine monophosphate
CCS	Cardiac conduction system
CICR	Calcium-induced calcium release
Cs^+	Caesium
Cx	Connexin
DM	Type 2 diabetes
E_m	Membrane potential
$GABA_A$	Gamma-aminobutyric acid type A channel
GAPDH	Glyceraldehyde-3-phosphate dehydrogenase
$G_{\alpha s}$	G alpha stimulatory
$G_{\alpha\beta\gamma i}$	G alpha, beta and gamma inhibitory
HCN4 / I_f	Hyperpolarisation-activated cyclic nucleotide-gated channel 4 / current
HR	Heart rate
HRV	Heart rate variability
I_K	Potassium current
$I_{K,r}$	K^+ current rapid
$I_{K,s}$	K^+ current slow
$I_{K,ur}$	K^+ current ultra-rapid
I_{Na}	Na^+ current
I_{st}	Sustained current
I_{to}	Transient outward K^+ current
K^+	Potassium
K_{ACh} / I_{KACh}	Acetylcholine K^+ channels / current
K_{ATP}	ATP-sensitive K^+ channel
LCRs	Local Ca^{2+} releases
L-type Ca^{2+} / $I_{Ca,L}$	Long-lasting type calcium channel / current

LV	Left ventricle
M_2	Muscarinic type 2 receptor
Na^+	Sodium
$[Na^+]_i$	Intracellular Na^+
NCX1 / I_{NCX1}	Na^+-Ca^{2+} exchanger 1 / current
nDM	Non-diabetic
NMDA	N-methyl-D-aspartate channel
PBS	Phosphate-buffered saline
PBST	Phosphate-buffered saline tween
PKA	Protein kinase A
RyR2 / 3	Ryanodine receptor 2 / 3
SAN	Sinoatrial node
SERCA2a	Sarco(endo)plasmic reticulum Ca^{2+}-ATPase 2a
SR	Sarcoplasmic reticulum
SVC	Superior vena cava
TBS	Tris-buffered saline
T-tubules	Transverse tubules
T-type Ca^{2+}/ $I_{Ca,T}$	Transient type calcium channel / current
Vm	Voltage membrane
ZDF	Zucker Diabetic Fatty

Type 2 diabetes and the type 2 Zucker Diabetic Fatty ($ZDF^{fa/fa}$) rats are referred to as 'DM' throughout the thesis. When referring to type 1, comparing type 1 and type 2 diabetes or emphasising type 2 diabetes it will be clearly stated.

CHAPTER 1

Introduction

1.1. Type 2 diabetes and cardiovascular disease

Type 2 diabetes (DM) is a metabolic disease arising due to continued hyperglycaemia, insulin resistance and dysfunctional insulin secretion, which increases the risk of developing cardiovascular disease including initiating and advancing heart failure (1-3). The global increasing prevalence of DM coincides with the rising prevalence of DM-induced cardiovascular disease, which will add to the healthcare burden (4-7). DM patients with cardiovascular disease present a greater mortality risk than patients with cardiovascular disease or DM alone (1, 8). Types of cardiovascular disease associated with DM can include, but are not limited to, coronary heart disease, atherosclerosis, myocardial infarction, ischemic heart disease, DM cardiomyopathy, heart failure and cardiac conduction system (CCS) abnormalities (9-12). The CCS includes the sinoatrial node (SAN), the atrioventricular node and the His-Purkinje system (13-15).

The heart beats about 3 billion times during an average life-span (16). The origin of this normal heart rhythm is the SAN (**Figure 1.1**) (17). The DM state is known to affect the whole heart including the primary pacemaker, the SAN (5, 18-22). For this reason, SAN dysfunction is not necessarily exclusive and can coincide with other (DM-induced) cardiovascular diseases making it difficult to define specific disease aetiologies. The SAN is an organised and coupled anatomic structure appropriate for its function to generate, propagate and modulate heart rate (HR) facilitated by both intrinsic SAN pacemaking, connexins (cx) and autonomic input (see pacemaking section 1.3, cx section 1.4 and autonomic innervation section 1.5 below) (23). Sick sinus syndrome has been associated with DM inpatient case reports, but further studies are required to fully establish this relationship (9, 24, 25). SAN dysfunction might encompass faults in the initiation and / or propagation of the action potential (AP). Though it is recognised

that DM promotes SAN abnormalities, increases the prevalence of arrhythmias and risk of sudden cardiac death, and notably, pacemaker or cardioverter-defibrillator implantation commonly occur in DM patients although the survival benefits of such treatments is questionable, yet, despite these acknowledgements, the changes in the underlying mechanisms in DM remain under-researched (5, 18-21, 24, 26-29).

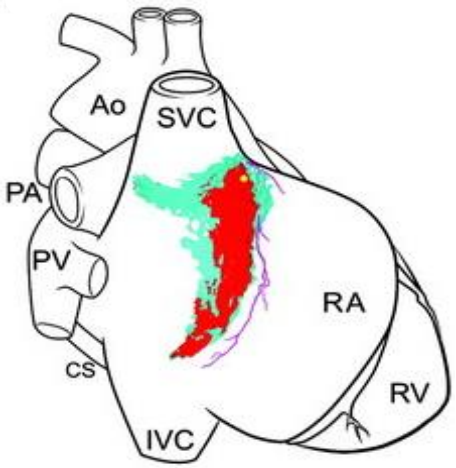

Figure 1.1. The sinoatrial node in the heart. A schematic representation of the heart highlighting the location of the **sinoatrial node** (SAN) **centre** in **red**, **SAN periphery** in **blue** and the **SAN artery** in **purple**. The action potential originates within the sinoatrial node centre propagates through the atria and slows in the atrioventricular node. This allows the atria to contract and fill the ventricles with blood. The action potential then travels down the His-Purkinje fibres and enables a synchronised ventricular contraction (13, 15). Abbreviations: aorta (Ao), superior vena cava (SVC), inferior vena cava (IVC), right atria (RA), right ventricle (RV), coronary sinus (CS), pulmonary vein (PV) and pulmonary artery (PA). Image modified from: (30).

DM *per se* has pathological consequences for many other bodily systems and these might influence direct or indirect secondary effects to the cardiovascular system. For example, the risk of (cardiac) autonomic dysfunction increases with DM disease duration and poor

glycaemic control (31). Hence, despite acknowledgement of both intrinsic and autonomic influences on HR and the above associations on type 2 DM-induced SAN dysfunction, the primary focus of research has been on the autonomic neuropathic influence to the SAN rather than type 2 DM intrinsic SAN remodelling. Since SAN pacemaking is primarily mediated by intrinsic mechanisms (the voltage membrane (Vm) and Ca^{2+} clocks, see pacemaking section 1.3), and modulated by neuronal innervation, it is important to evaluate both in DM.

1.2. The sinoatrial node

1.2.1 Location

The heterogeneous SAN is located at or below the base of the superior vena cava (SVC) adjacent to the crista terminalis, a thick band of atrial muscle, on the posterior wall of the right atria (14, 30). In humans, the SAN is an extensive crescent-like tissue structure (32). SAN cardiomyocytes are embedded in connective tissue which also encompasses the SAN artery serving as its landmark (14, 30, 32, 33). The human SAN has also been described to have a 'tail' interdigitating into the atrial musculature (also seen with the rat SAN) (34). A transitional paranodal / periphery region that is an intermediate between SAN cardiomyocytes and atrial cardiomyocytes connects the 'true' SAN and right atrial tissues (33, 35, 36). The precise location, shape, vascularisation and innervation of the SAN can vary inter- and intra-species; perhaps accounting for functional differences and HR ranges seen within and across species.

1.2.2 Location of the rat sinoatrial node

In some species such as the rat, the SAN and a nodal-like tract form an n-shape around the SVC (**Figure 1.2**) (14, 37, 38). The posterior wall of the right atria with the SVC side closest to the right atrial appendage represents the SAN (circled in red in Figure 1.2) as it displays

continuous spontaneous beating (37). The left SVC side represents a tract of nodal-like cardiomyocytes as it displays non-continuous spontaneous beating (37). The nodal-like cardiomyocytes extend down the inter-atrial groove and have been suggested to form inter-nodal pathways between the SAN and the atrioventricular node (37). The lead (dominant) pacemaking site, defined as SAN cardiomyocytes with the fastest intrinsic rhythm which primarily mediate HR generation, were typically found to be located near the crista terminalis within the SAN, however, it has also been located in the inter-atrial groove within the nodal-like tract (37).

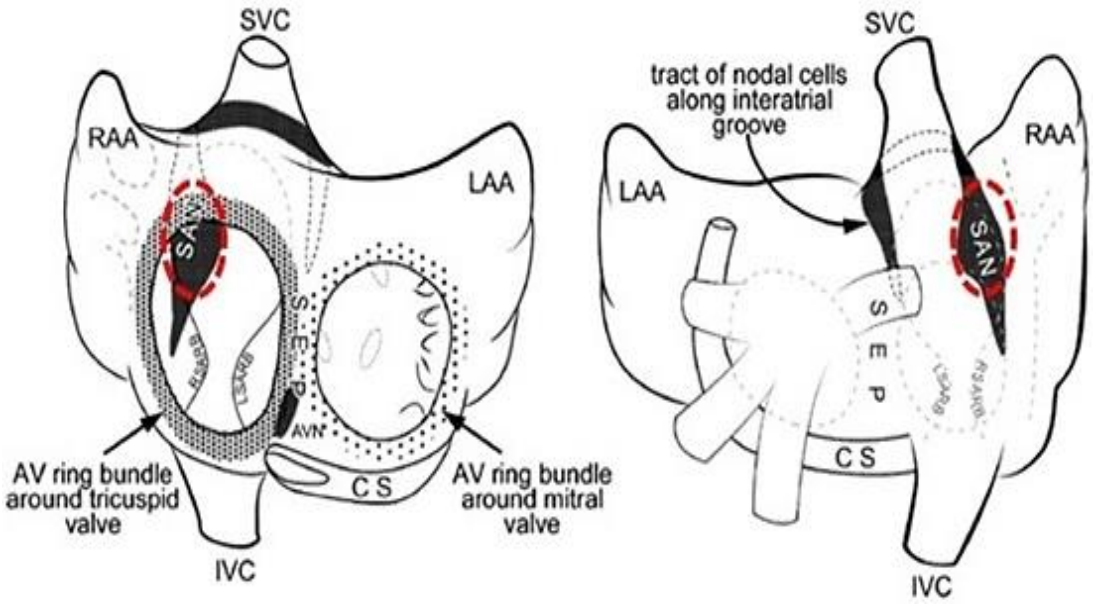

Figure 1.2. Schematic representation of the rat atria. An anterior view on the left and posterior view on the right of the rat atrial tissue. The dark black shading marks the rat sinoatrial node (circled red) and tract of nodal-like inter-atrial cardiomyocytes forming the n-shape, and the dotted shading marks the atrioventricular ring bundle comprising the tricuspid and mitral valves. Abbreviations: sinoatrial node (SAN), superior vena cava (SVC), inferior vena cava (IVC), right atrial appendage (RAA), left atrial appendage (LAA), septum (SEP), atrioventricular node ((AV)N), left sinoatrial node ring bundle (LSARB), right sinoatrial node ring bundle (RSARB) and coronary sinus (CS). Image modified from: (37).

1.2.3 Cellular architecture

The cardiomyocytes forming the CCS differ structurally and functionally between each other and from the working (atrial and ventricular) cardiomyocytes (13-15). Three types of SAN cardiomyocyte shapes have been described to exist: elongated spindle shaped (most prominent), spindle shaped and spider shaped (fastest intrinsic rate) (39-42). The spindle shaped SAN cardiomyocytes have also been identified in the rat SAN (43, 44). The lead pacemaking SAN cardiomyocytes are small, loosely organised and are known to be interweaving in comparison to working cardiomyocytes (14, 39, 42). The SAN exhibits poor electrical coupling, scarce mitochondria, a higher density of nuclei, poorly established transverse tubules (T-tubules, sarcolemmal invaginations that infiltrate into the cardiomyocyte for effective excitation-contraction coupling) and sarcoplasmic reticulum (SR, intracellular Ca^{2+} store), plentiful but disorganised myofilaments and presents a highly elastic extracellular matrix component (14, 39, 40, 42, 45).

1.2.4 General electrical characteristics

The SAN retains automaticity with the fastest intrinsic rhythm compared to all other cardiomyocytes, enabling it to independently generate spontaneous cyclic APs (intrinsic HR) that propagate ultimately effecting a globally synchronised contraction of the heart, and whilst doing so it also re-sets other CCS pacemaking via a phenomenon termed overdrive suppression (15, 35, 46). Central SAN tissue is protected from the hyperpolarisation effects of the right atrial myocardium by poor electrical coupling (14). Electrical coupling is arbitrated in part by cx (see cx section 1.4 below) and cell-to-cell contact (14, 33, 35). Furthermore, the central SAN compared to the SAN periphery (intermediate between the SAN and right atria) retains a high density of specific ion channels, such as the hyperpolarisation-activated cyclic

nucleotide-gated channel 4 (HCN4 / funny current (I_f), see pacemaking section 1.3 below) which enable pacemaking (14, 21). Structurally, the surrounding connective tissue and the transitional SAN periphery also prevent hyperpolarisation of the SAN (14, 33, 35).

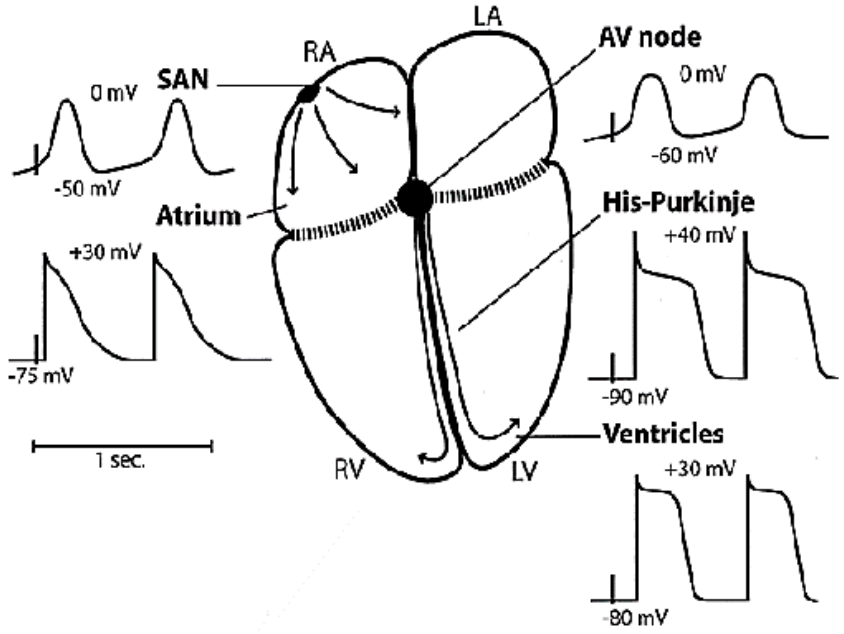

Figure 1.3. Cardiac action potentials. The different types of action potentials generated from different cardiac tissue regions. Abbreviations: sinoatrial node (SAN), atrioventricular node (AV), right atria (RA), left atria (LA), right ventricle (RV) and left ventricle (LV). Image reproduced from: (41).

The SAN AP characteristics also differ from other CCS and working cardiomyocytes (**Figure 1.3**) (14, 35, 47). Healthy *in vivo* and isolated *ex vivo* SAN myocardium displays cyclic spontaneous depolarisations whereas the healthy *in vivo* and isolated *ex vivo* working myocardium does not (35). The SAN electrical voltage begins at a less negative membrane potential (48). The AP is small in amplitude compared to an AP originating from the working myocardium, AP duration decreases as it propagates in all directions through different tissues in the heart which is associated with an increase in coupling and conduction velocity amongst the different

cardiomyocyte types, as well as being influenced by changing molecular expression of proteins (32, 35, 48). Characteristics of the SAN AP include diastolic depolarisation, slow upstroke, small amplitude overshoot plateau, slow and low repolarisation, and no stable resting membrane potential (14, 35, 49).

The functional role, primarily AP initiation, AP propagation and contraction, of each cardiomyocyte type is made possible by specific molecular expression. The differences in AP characteristics in different cardiomyocytes / tissue regions and species is due to differences in molecular expression of Ca^{2+} handling proteins, ion channels and transporters, cx and receptors, which might further be separated by different isoforms types (14, 21, 47, 50). For example, human SAN versus periphery / paranodal region versus atria mRNA expression (**Table 1.1**) (32, 35). The roles of some components in Table 1.1 in mediating HR generation, propagation and / or modulation will be introduced in the following pacemaking section 1.3. The SAN has been established to be distinct from the paranodal region and right atria appropriate for its independent spontaneous pacemaking function (32).

The SAN has been shown to have dual pacemaking sites and mechanisms, comprising of lead (dominant) and latent (supplementary) pacemaking cardiomyocytes and a shift in the pacemaking site from lead to latent can result (51-54). The different pacemaking mechanisms are likely to be due to subtle differences in expression. For example, this notion arises due to the findings that Cs^{+} inhibits diastolic depolarisation in the SAN periphery but not SAN centre (i.e. Cs^{+}-sensitive is the latent diastolic depolarisation mechanism and Cs^{+}-insensitive is the lead diastolic depolarisation mechanism) (51, 52). Perhaps, these sites and mechanisms provide a safety net for the continuation of automaticity. Four different types of APs have

been recorded in the central SAN of the rat; one representative of a 'true' lead pacemaking AP and three types of latent pacemaking APs (55). Since SAN cardiomyocytes are not depolarised by a previous initiator, as are all other cardiomyocytes in a healthy heart, the question of how the SAN initiates the heartbeat is raised.

Table 1.1. mRNA expression differences in different cardiac tissue regions in human. A comparative summary of mRNA expression in the healthy human sinoatrial node (SAN), paranodal region and right atria of membrane ion channel / transporter isoform(s) and their corresponding currents, intracellular Ca^{2+} handling proteins, connexins and receptors. The phase(s) of the action potential the proteins contribute to or their effect on heart rate is also presented. The components investigated in this thesis are highlighted in red. Key: high expression (+++), modest expression (++), low expression (+) and negligible (-). Table generated based upon findings of: (21, 32, 41, 56).

Additional Information	mRNA Transcript	Sinoatrial Node	Paranodal Region	Right Atria
Membrane Ion Currents and Transporters				
I_{Na} Upstroke in SAN periphery	$Na_v1.2$	+++	+	++
	$Na_v1.4$	+	++	++
	$Na_v1.5$	+	++	+++
$I_{Ca,T}$ Mid diastolic depolarisation / early upstroke	**$Ca_v3.1$**	+++	++	++
$I_{Ca,L}$ Late diastolic depolarisation / upstroke / plateau	**$Ca_v1.2$**	++	+++	+++
	$Ca_v1.3$	+++	++	++
I_f Diastolic depolarisation only in SAN / cardiac conduction system	HCN1	+++	++	++
	HCN2	+	++	+++
	HCN3	-	-	-
	HCN4	+++	++	++
I_{to} Early phase 1 repolarisation	$K_v1.4$	++	+	++
	$K_v4.2$	++	+++	+
	$K_v4.3$	++	++	+++
$I_{K,ur}$ Phase 1 / 2 repolarisation	$K_v1.5$	+	++	++
$I_{K,r}$	ERG	++	+++	+++

Phase 2 repolarisation				
$I_{K,s}$ Phase 2 repolarisation	K_vLQT1	++	++	++
I_{K1} Resting potential / terminal repolarisation, absent in SAN	K_{ir}2.1	+	+	++
	K_{ir}2.3	+	++	++
Na^+-Ca^{2+} Exchanger Couples the calcium and membrane clock during mid-late diastolic depolarisation / upstroke	**NCX1**	+++	+++	+++
Sarcolemmal Ca^{2+} ATPase Calcium extrusion	PMCA1	+	++	+
	PMCA4	+++	++	++
Intracellular Ca^{2+} Handling Proteins				
Ryanodine Receptor Local calcium release during mid-late diastolic depolarisation / upstroke	RyR2	+	+++	+++
	RyR3	++	++	+
Sarco(endo)plasmic Reticulum Ca^{2+} ATPase Calcium uptake during repolarisation	**SERCA2a**	++	+++	+++
SERCA2a Regulators	Sarcolipin	+	+++	+++
	Phospholamban	++	+++	+++
Connexins Intercellular conduction mediating action potential propagation				
Large	Cx40	++	+++	+++
Medium	**Cx43**	++	+++	+++
Small	**Cx45**	++	++	+
Receptors				
Adrenergic Autonomic modulation for heart rate increase	α1a	++	++	+
	α2a	+	++	+
	β1	++	++	+++
	β2	+	++	++
Muscarinic Autonomic modulation for heart rate decrease	**M_2**	+	+	+

1.3. Pacemaking

1.3.1 Ca^{2+}-induced Ca^{2+} release

The Ca^{2+}-induced Ca^{2+} release (CICR) hypothesis refers to a phenomenon where Ca^{2+} entry into the cardiomyocyte via transient type (T-type / $I_{Ca,T}$) and long-lasting type (L-type / $I_{Ca,L}$) Ca^{2+} channels present on the sarcolemma / T-tubules binds to the SR Ca^{2+} release channel the ryanodine receptor 2 (RyR2) triggering mass Ca^{2+} release from the intracellular Ca^{2+} store the SR (57-59). This CICR hypothesis has been supported by experiments using skinned cardiomyocytes where Ca^{2+} did not instantaneously result in myofilament shortening and contraction (58, 60). After each beat, the SR Ca^{2+} store is replenished by the cardiac sarco(endo)plasmic reticulum Ca^{2+}-ATPase 2a (SERCA2a) (60). The SAN cardiomyocyte causes its own CICR by spontaneously releasing Ca^{2+} via the SR Ca^{2+}release channel (RyR2 → Na^{+}-Ca^{2+} exchanger 1 (NCX1 / I_{NCX1}) → T-type and L-type Ca^{2+} channels → RyR2), and is one of the major contributions to SAN automaticity (see following section 1.3.2), whereas CICR in the working cardiomyocytes occurs upon sarcolemmal depolarisation due to SAN originating AP (depolarisation → T-type and L-type Ca^{2+} channels → RyR2) (21, 47). The specific differences in spontaneous rhythmicity between species and in the SAN cardiomyocytes compared to working cardiomyocytes are also suggested to be due to differences in the spatial arrangement (see section 1.3.5) and phosphorylation levels (16).

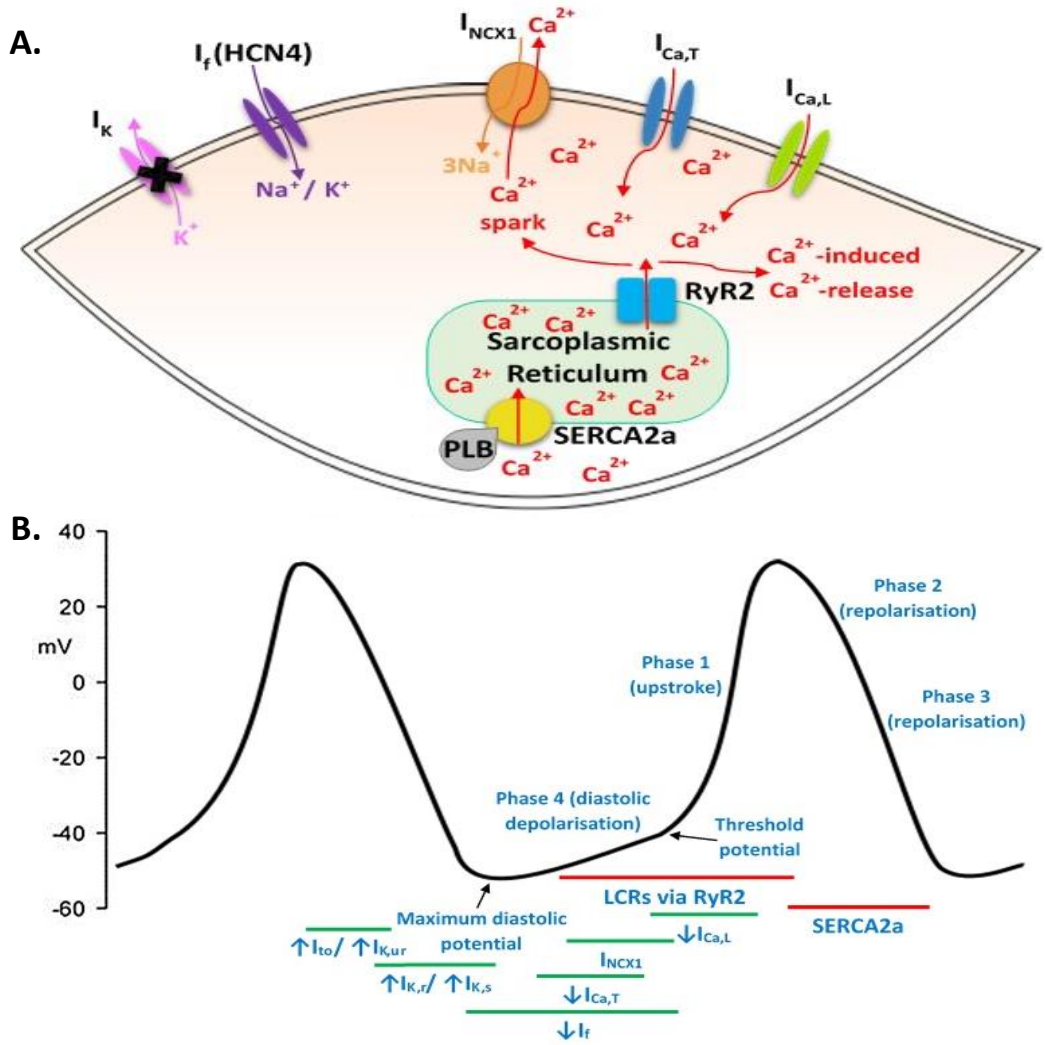

Figure 1.4. Sinoatrial node pacemaking and action potential. (A.) The voltage membrane and intracellular Ca^{2+} clocks that mediate sinoatrial node (SAN) pacemaking. Ca^{2+} movement is highlighted in red. (B.) The various phases of the SAN action potential and summary of the main **voltage membrane clock** ion currents (**green**) and **Ca^{2+} clock** events (**red**) involved in pacemaking. Diastolic depolarisation is enabled by the activation of hyperpolarisation-activated cyclic nucleotide-gated channel 4 (HCN4 / I_f), transient-type Ca^{2+} channels ($I_{Ca,T}$) and local Ca^{2+} releases (LCRs) via ryanodine receptor 2 (RyR2) that trigger the activity of the Na^+-Ca^{2+} exchanger 1 (I_{NCX1}), which collectively depolarise the membrane potential with the influx of net inward currents (phase 4). This accumulating strong positive feedback activates long-lasting type Ca^{2+} channels ($I_{Ca,L}$) that enable Ca^{2+} entry and eventually trigger mass Ca^{2+} release from the intracellular Ca^{2+} store the sarcoplasmic reticulum via RyR2 (phase 1). Repolarisation is predominantly enabled by Ca^{2+} uptake into the sarcoplasmic reticulum via the sarco(endo)plasmic reticulum Ca^{2+}-ATPase 2a (SERCA2a) and the activation of various K^+ channels (I_{to}, $I_{K,ur}$, $I_{K,r}$, $I_{K,s}$) (phase 2 and 3). Upward arrows relate to outward currents and downward arrows relate to inward currents. Original figure.

1.3.2 The Vm and Ca^{2+} clocks

During pacemaking (intrinsic HR), diastolic depolarisation increases the membrane potential towards threshold effecting an AP (14, 21, 47). This function is enabled by the synergistic interaction of the Vm and Ca^{2+} clocks mediated by the specific expression of various ion channels / transporters located at the sarcolemma and Ca^{2+} handling proteins located at the SR respectively (32, 49, 50, 61-63). The current understanding of the *de novo* generation of the heartbeat within the SAN cardiomyocyte is illustrated in **Figure 1.4** (21, 47, 50).

Phase 4 early diastolic depolarisation initiates with the inactivation and decay of the voltage-dependent outward K^+ currents (I_K) (63-65), and activation of HCN4 (I_f) responsible for pacemaker potential enabled via an inward mixed Na^+ and K^+ current (21, 49, 62). During mid-diastolic depolarisation, inward Ca^{2+} entry occurs via activation of the T-type Ca^{2+} channels along with the initiation of spontaneous local Ca^{2+} releases (LCRs) via RyR2 (also possibly by RyR3 or inositol triphosphate receptor type 2 (32, 35, 66, 67)) from the Ca^{2+} store the SR located near the cardiomyocyte sarcolemma (50, 61, 68). This initiates forward-mode NCX1 that couples both clocks by extruding Ca^{2+} for accumulative Na^+ influx which continues sarcolemmal depolarisation (69), mediating further Ca^{2+} entry via the L-type Ca^{2+} channels and also possibly via the inward sustained current (I_{st}) (70-75)). This strong positive feedback mechanism (continuation of LCRs and NCX1, and increasing $I_{Ca,L}$ contribution) builds-up and promotes a strong contribution from $I_{Ca,L}$ that triggers AP threshold and a mass CICR from the SR contributing to **phase 1** AP upstroke (76). L-type Ca^{2+} channel contribution also ensures necessary Ca^{2+} entry to later refill the SR for the subsequent cycle (72, 77). This occurs within the lead SAN cardiomyocyte(s) which propagates membrane depolarisation outwards to adjacent cardiomyocytes and globally across the heart facilitating a synchronised contraction

(68, 70). For relaxation cytosolic Ca^{2+} needs to be depleted. During **phase 2** early repolarisation the Ca^{2+} within the SR is restored via the strong activity of the SERCA2a pump (~70% in human and rabbit, ~92% in rat), or extruded via NCX1 (~28% in human and rabbit, ~7% in rat), plasma membrane Ca^{2+}-ATPase and mitochondrial Ca^{2+} uniporters mediating the repolarisation phase of the AP (47, 60, 78, 79). SERCA2a and phospholamban, a negative regulator of SERCA2a activity in its dephosphorylated state, partly influence a critical determinant for the persistence of pacemaking; SR Ca^{2+} load, LCR number, LCR size and LCR period (the time taken between the next spontaneous release due to the refilling rate of SERCA2a) (80, 81). There is also the activation of the ultra-rapid and transient outward K^+ channels (21, 32). **Phase 3** late repolarisation results in the activation of the rapid and slow activating delayed rectifier K^+ channels that are responsible for the downward AP slope returning membrane potential to hyperpolarising levels so the cycle can begin again with HCN4 activation (21, 32).

1.3.3 The T-type and L-type Ca^{2+} channels

Ca^{2+} channels are heterotetrameric proteins consisting of the channel pore, voltage sensing and gating α_1 subunit, and accessory subunits α_2 / δ and β (82, 83). There are currently 10 α_1 subunit genes known (82). The T-type Ca^{2+} channels are divided into 3 classes: $Ca_v3.1$ (α_{1G}), $Ca_v3.2$ (α_{1H}) and $Ca_v3.3$ (α_{1I}) (82). The L-type Ca^{2+} channels are divided into 4 classes: $Ca_v1.1$ (α_{1S}), $Ca_v1.2$ (α_{1C}), $Ca_v1.3$ (α_{1D}) and $Ca_v1.4$ (α_{1F}) (82). The isoforms highly expressed in the SAN / heart and investigated in this thesis are $Ca_v3.1$ (T-type) and $Ca_v1.2$ (L-type) (32, 82, 84). T-type and L-type Ca^{2+} channels activate and deactivate at more negative and positive potentials respectively (83). T-type Ca^{2+} channel activity is entirely voltage-dependent, whilst L-type Ca^{2+} channel deactivation is voltage and SR Ca^{2+} release dependent (83).

1.3.4 Electrical characteristics of the rat sinoatrial node

Research on SAN electrophysiology has predominantly occurred in larger animals (14, 43, 55) and mice (17, 42, 47). Hence, little is known about rat SAN electrophysiology or the specifics of molecular mediators involved. In the research that has occurred, spontaneous APs have been observed in rat SAN cardiomyocytes presenting I_f that is responsible for continuous diastolic depolarisations (43). Four different types of APs have been recorded in the central SAN of the rat; one representative of a 'true' lead pacemaking AP and three types of latent pacemaking APs (55). The research also demonstrated activation of I_{st}, its name acquired from little inactivation during depolarising pulses (Na^+ carrier ion), over the slow diastolic depolarisation range and during AP upstroke (43, 71). The L-type Ca^{2+} channel is primarily involved in the rising phase and delayed-rectifier K^+ channel / current rapid ($I_{K,r}$) in repolarisation (43). It has been suggested deactivation of $I_{K,r}$ at maximum diastolic depolarisation might initiate or even be responsible for slow diastolic depolarisation (43, 51, 52). Further research is needed on the AP characteristics and mechanisms involved in the rat SAN.

1.3.5 Spatial organisation

Robust pacemaking relies on intra-cellular spatial arrangement and location of the various molecular machinery (45, 85). Since SAN cardiomyocytes have a poorly developed T-tubule system (sarcolemmal invaginations), the distance and position of the sarcolemmal components (NCX1, T-type and L-type Ca^{2+} channels) from the sarcoplasmic reticulum (RyR2 / 3 and possibly inositol triphosphate receptor type 2) are considered of utmost importance for clock coupling (45, 85). A high degree of co-localisation and strong immuno-labelling of mediators implicated in pacemaking is seen just beneath the SAN cardiomyocyte sarcolemma

where automaticity takes place (RyR2-NCX1, SERCA2a) compared to the relatively uniform protein distribution in ventricular cardiomyocytes (16, 86). This suggests spontaneous LCRs at the periphery are sufficient for initial AP initiation and excitation-contraction coupling (CICR), without global cellular activation of the non-peripheral mediators within the SAN cardiomyocytes (45, 86-88).

1.3.6 Pacemaking regulation

The intrinsic biochemical molecular mediators and the respective regulators (Ca^{2+}, adenylyl cyclases, protein kinase A (PKA), Ca^{2+} / calmodulin-dependent protein kinase II (CaMKII), phosphodiesterases) of both clocks collectively integrate and modulate the mutually entrained intrinsic clocks and allow for a physiological flexible *in vivo* HR (16, 73). Many of the proteins involved in pacemaking (HCN4, L-type Ca^{2+} and K^{+} channels, RyR2 and phospholamban) are subject to intrinsic (basal / *ex vivo*) and autonomic phosphorylation by primarily PKA and / or CaMKII (81, 89-91). The coupling points and tight regulation ensures synchronisation and robustness where co-ordinated timing of events is also of absolute importance (21, 73). Pacemaking rate is also influenced by extrinsic signals such as neuronal (see autonomic innervation section 1.5 below), hormonal and mechanical stimulus (stretch) (14, 92). The SAN adapts to these intrinsic and extrinsic signals, possibly by alteration of the lead pacemaking site shifting to a point anywhere between the SVC and inferior vena cava (lead versus latent pacemaking sites), again allowing a flexible range of pacing rates to meet bodily demands (14, 92). Adaptation is made possible due to the subtle differences in cell type and protein expression in different areas of the SAN. The heterogeneous nature of the SAN is indicative of its complexity and numerous mechanisms involved in mediating pacemaking. The heterogeneous intrinsic and extrinsic influences on pacemaking might be of significance for

reasons such as to serve as a back-up if one mechanism fails and might clarify why lead pacemaking site shifts happen (14).

1.3.6.1 PKA and CaMKII

Within the SAN cardiomyocytes, PKA and CaMKII activity can be triggered by intrinsic (independent of sympathetic activity-induced β-adrenergic signalling) and extrinsic signals (dependent on sympathetic activity-induced β-adrenergic signalling) (16, 50, 93). Both kinases are activated by the following pathways: (1) extrinsically via β-adrenergic input → Gα stimulatory ($G_{\alpha s}$) protein → Ca^{2+}-inhibited adenylyl cyclases and / or (2) intrinsically via Ca^{2+}-activated adenylyl cyclases. Adenylyl cyclases from either pathway use ATP to generate the second messenger cyclic adenosine monophosphate (cAMP) → PKA → increase in intracellular Ca^{2+} ($[Ca^{2+}]_i$) that results in Ca^{2+} / calmodulin binding to CaMKII and thereby its activation (94-96). As mentioned above, the kinases directly phosphorylate proteins involved in cardiac contractility (L-type Ca^{2+} channels, RyR2, phospholamban) (94). PKA and CaMKII are expressed in working and SAN cardiomyocytes (81, 96-98). The CaMKII isoform predominantly expressed in cardiomyocytes is CaMKII-δ followed by CaMKII-γ (99). Inhibition of PKA and CaMKII using a PKA inhibitor peptide and KN-93 respectively, reduced rabbit SAN cardiomyocyte LCRs and spontaneous firing rate in a concentration-dependent manner (81, 97). This indicates the importance of PKA and CaMKII during intrinsic (basal / *ex vivo*) and β-adrenergic pacemaking (81, 97).

1.4. Connexins

AP propagation occurs through intercellular gap junction channels called cx that couple the cytosol of neighbouring cardiomyocytes and other cell types, thus enabling bilateral permeability to ions and other small metabolites (100, 101). Five main cx types are present in the heart; cx40, cx43, cx45, cx30.2 and cx37 (32, 100, 102). The cx vary in size of unitary conductance and permeability, as well as expression profile, which differs across regions of the heart and species (100). Conductance is dependent on pH, free Ca^{2+}, extracellular fatty acids, and on the (de/)phosphorylation state of the cx with the number of phosphorylation sites varying across species (100, 103). Cx within the SAN have small conductance and are sparse compared to the atria (104). Generalised cx expression within the heart is illustrated in **Figure 1.5** and the major cardiac cx are discussed below.

The large (based on conductance) cx40 (conductance of 120 – 200pS), responsible for fast synchronised conduction, has been found in the distal region of the atrioventricular node and the ventricular conduction system (100, 102, 103, 105). Cx40 has been shown to co-localise with cardiomyocytes expressing cx43 or cx45 in some species (47, 100, 105, 106). In human, cx40 is not expressed in the SAN but is present in the atria and ventricular conduction system (47). In the rat, cx40 protein is expressed in the ventricular conduction system and not in the working myocardium (47, 103, 107). The medium cx43 (conductance of 45 – 75pS) is robustly present throughout the working myocardium presenting an immunofluorescence pattern that appears as prominent end-to-end cardiomyocyte labelling (100, 102). The small cx45 (conductance of 20 – 40pS) is present in the CCS and low expression is also seen in the rat working myocardium whereas in human atria there is widespread expression; presenting an immunofluorescence pattern that appears as dispersed defined spots (102, 103, 105, 107).

Cx30.2 protein expression has been shown in the murine SAN, atrioventricular node and His-bundle (108-110) and mRNA expression has also been found in the rat SAN (35). Cx37 is present in the endocardial endothelium (100, 102, 103).

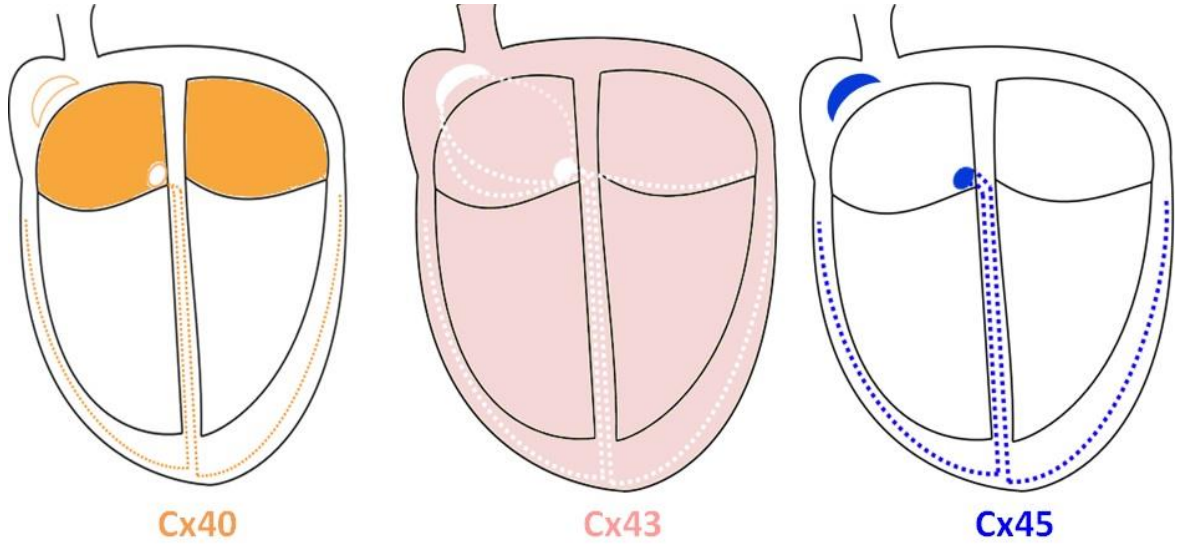

Figure 1.5. Generalised connexin expression within the heart. Schematic representation of differential connexin (cx) expression within different heart regions. **Cx40** (**orange**) typically expressed in the atria and cardiac conduction system, **cx43** (**pink**) abundantly expressed within the working myocardium and **cx45** (**blue**) predominantly expressed in the cardiac conduction system. Original figure.

The central SAN is poorly coupled and lacks cx43, which protects from the inhibitory hyperpolarising effects of the right atria (35). However, cx43 expressing atrial cardiomyocytes infiltrate aspects of the SAN appearing as cx43-positive islands upon immuno-labelling (106). Intercellular coupling (as well as Na^+ channels (I_{Na}, $Na_v1.5$)) progressively increases outwards from the SAN mediating fast succinct propagation of the AP (32, 35). The small cx45 mediates propagation in the SAN, however, it has also been suggested that over-lapping cell-to-cell contact of the SAN cardiomyocytes with each other might influence outwards continuation of

the electrical current (35, 39). As well as specific cx profile expression in heart regions where no overlap exists; cardiomyocytes might also express more than one cx type particularly in zones of tissue mergers, for example, SAN periphery / atrial cardiomyocyte expression of cx45 and cx43 (100, 106).

1.5. Autonomic innervation to the sinoatrial node

1.5.1 Autonomic control

The autonomic control centres for the heart are located in the medulla oblongata within the brain stem that relay inputs and outputs from higher brain centres (hypothalamus) (111-113). Innervation can be divided into cardiac extrinsic or intrinsic, involving neuronal networks between the heart and central nervous system, and neuronal networks within the cardiac layers respectively (111, 112, 114). All cardiac chambers and layers (epicardium, myocardium, and endocardium) have been found to be well innervated, which challenges the old perceptions of the CCS receiving greater innervation compared to other regions (111, 112, 115-118). Originally, it was reported that no direct contact exists between the SAN cardiomyocyte sarcolemma and nerve endings, however, this dogma is also being challenged since input for fine-tuning via neuronal discharge would be diluted as they are released into interstitial spaces (39, 119, 120). Tailoring of the beat-to-beat control is likely to reside with the intrinsic neuronal network, presumed to have independent neuronal activity, while the extrinsic central nervous system will take superiority in situations of stress (113, 121, 122).

1.5.2 Cardiac sympathetic and parasympathetic sinoatrial node modulation

In vivo, the SAN is extrinsically modulated by sympathetic and parasympathetic innervation by the release of norepinephrine and acetylcholine neurotransmitters, which act on the adrenergic and cholinergic receptors present on the SAN cardiomyocyte sarcolemma to increase and decrease *in vivo* HR respectively (115, 123). *In vivo* HR is collectively determined by the intrinsic HR (SAN pacemaking) and sympathetic and parasympathetic influences (124).

In human and in rat, the predominant β-adrenergic receptor isoform expressed is β_1 (117, 125). Greater expression of β-adrenergic receptors is typically present within the SAN compared to the working myocardium (32, 117, 125-127). The β-adrenergic pathway and its phosphorylation targets are presented in **Figure 1.6**. In SAN cardiomyocytes, a greater level of basal phosphorylation exists compared to ventricular cardiomyocytes for phospholamban, RyR2 and L-type Ca^{2+} channels enabling a net effect of promoting spontaneous cyclic LCRs i.e. continuation of pacemaking (81).

As described in section 1.3.6.1, β-adrenergic receptors are coupled with $G_{\alpha s}$ proteins (91, 128, 129). β-$G_{\alpha s}$ stimulation activates Ca^{2+}-inhibited adenylyl cyclases that produce cAMP that in turn results in PKA activation and phosphorylation of pacemaking proteins, which collectively result in effects of increased *in vivo* HR (91, 130, 131). The diastolic depolarisation slope is steepened by phosphorylation and direct cAMP binding to HCN4 which increases the open probability and the number of channel contributions (132-134). The mid-diastolic depolarisation / upstroke phase is enhanced by increased RyR2 open probability and its Ca^{2+} release kinetics (81, 135, 136). Additionally, greater L-type Ca^{2+} channel open probability (long

openings and short closings) increase the height and speed of the upstroke phase (137, 138). Repolarisation is also faster due to increased phospholamban phosphorylation resulting in decreased SERCA2a inhibition which increases pump rate and there is increased conductance through various I_K (87, 139-143).

The neuronal cholinergic receptor isoform responsible for lowering HR is the muscarinic type 2 (M_2) receptor which is expressed in the human and rat in approximately the following manner SAN = atria > ventricle (32, 117, 118, 144-146). The M_2 pathway and its targets are also presented in **Figure 1.6**. M_2 receptors are coupled to Gαβγ inhibitory ($G_{\alpha\beta\gamma i}$) proteins (91, 128, 147). M_2-$G_{\alpha i}$ activation results in the inhibition of adenylyl cyclases that consequently decrease cAMP levels and PKA activity (131). This limits cAMP-induced I_f activation, therefore, reducing the slope of and slowing diastolic depolarisation (128, 148). Moreover, the collective phosphorylation contributions to HR (discussed above) are restricted resulting in lengthened AP duration (128, 148). While, M_2-$G_{\beta\gamma i}$ stimulation results in activation of the inwardly rectifying acetylcholine K^+ channels (K_{ACh} / I_{KACh}) which hyperpolarises the SAN cardiomyocytes (128, 145, 149-152). Furthermore, acetylcholine effects on HR might be concentration-dependent; it has been suggested at low concentrations (0.01 µM) I_f is inhibited with no effect on I_{KACh} (slowing rate without hyperpolarisation) however, at higher concentrations (>0.1 µM) I_f is inhibited and I_{KACh} is also activated (slowing rate with hyperpolarisation) (148, 153).

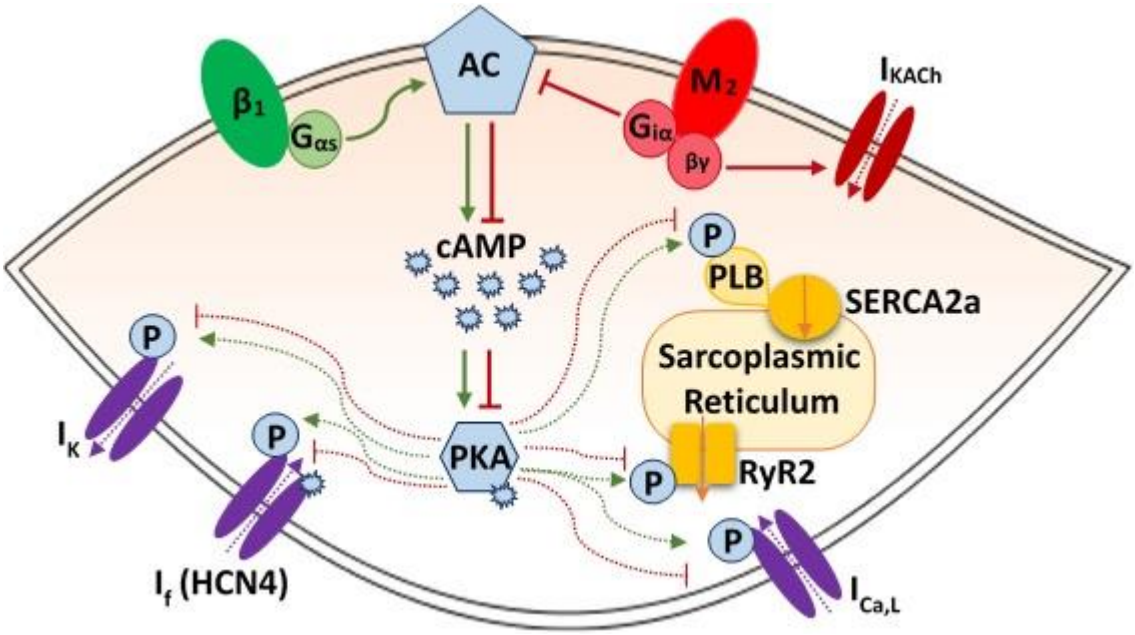

Figure 1.6. Autonomic influence to the sinoatrial node. The basic **β-adrenergic** (**green**) and neuronal **cholinergic** (**red**) pathways. The β-adrenergic receptors (β_1) are bound to Gα stimulatory ($G_{\alpha s}$) proteins. Stimulation of the β-$G_{\alpha s}$ complex results in activation of adenylyl cyclases (AC) that generate cyclic adenosine monophosphate (cAMP) which activates protein kinase A (PKA). PKA mediated phosphorylation of proteins, denoted by 'P', collectively results in increased heart rate (HR). Whilst, M_2 receptors are coupled to Gαβγ inhibitory ($G_{\alpha\beta\gamma i}$) proteins. M_2-$G_{\alpha i}$ activation inhibits adenylyl cyclases which subsequently results in lower cAMP levels and PKA activity. This limits basal and β-adrenergic phosphorylation contributions to HR. M_2-$G_{\beta\gamma i}$ stimulation results in activation of the acetylcholine K^+ channel (I_{KACh}) that hyperpolarises SAN cardiomyocytes. Other abbreviations: hyperpolarisation-activated cyclic nucleotide-gated channel 4 (HCN4 / I_f), ryanodine receptor 2 (RyR2), sarco(endo)plasmic reticulum Ca^{2+}-ATPase 2a (SERCA2a), phospholamban (PLB), long-lasting type Ca^{2+} channel ($I_{Ca,L}$) and K^+ channels (I_K). Original figure.

In physiology, a balance of both sympathetic and parasympathetic mechanisms are accepted to be acting simultaneously however to differing degrees maintaining cardiovascular output (113). Generally, in humans, sympathetic input increases during the day, while parasympathetic input has been suggested to apply a vagal brake, prevailing during times of rest and at night (113, 118, 154, 155). The net autonomic influence to the SAN in humans is

parasympathetic however there are constant beat-to-beat fluctuations that echo the dual influence of sympathetic and parasympathetic input, allowing heart rate variability (HRV) (113). In conscious rats, the net autonomic influence to the heart during the dark (active) period is sympathetic (normal sympathetic contribution in different rat strains can vary) which is presented with increased HR compared to the light (inactive period) (156, 157). This greater sympathetic input might not, however, be as effective at the cardiac level as the effects of acetylcholine have been shown to outweigh the effects of norepinephrine in the isolated rat atria (158). Whether the dominance of parasympathetic effects in the heart is in part attributed to the additional presence of the non-neuronal cardiac intrinsic cholinergic system (see following section 1.6) remains to be clarified. Imbalance of this sympathovagal innervation can result in cardiac arrhythmias as acknowledged in the DM state (9).

1.6. The non-neuronal cardiac intrinsic cholinergic system

Traditionally, cholinergic input has only been associated with *in vivo* parasympathetic physiology, however, research provides evidence for the existence of a non-neuronal cardiac intrinsic cholinergic system (159). The intrinsic cholinergic system encompasses synthesis, storage and release of acetylcholine by cardiomyocytes and is thought to act in an autocrine and paracrine manner (**Figure 1.7**) (159, 160). The intrinsic cholinergic system is present in the rat adult atrial and ventricular cardiomyocytes (160, 161).

A strong association of the intrinsic cholinergic system being positively influenced by the neuronal cholinergic system has been shown (i.e. neuronal / exogenous application of acetylcholine increases activation, transcription and expression of the intrinsic cholinergic

system) (159, 160). This might suggest a limited function of the intrinsic cholinergic system *ex vivo*, however, continuous synthesis of basal acetylcholine levels have been detected in rat cultured cardiomyocytes using acetylcholinesterase inhibitors (the enzyme responsible for acetylcholine breakdown) (160).

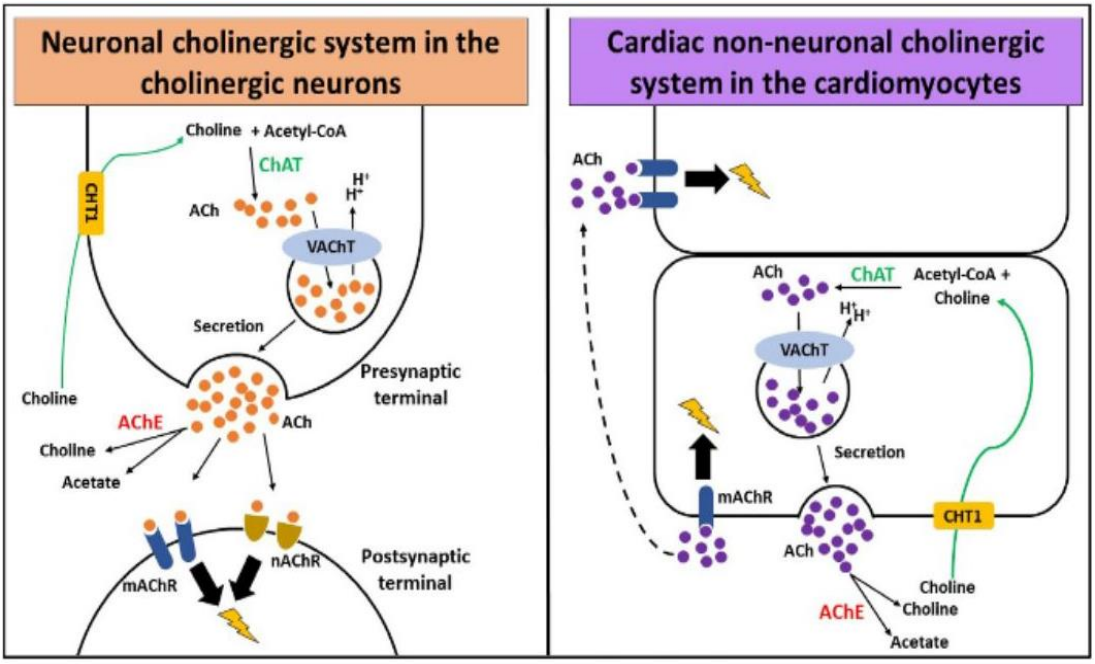

Figure 1.7. The neuronal and non-neuronal cardiac intrinsic cholinergic systems. Cholinergic neurones and cardiomyocytes are equipped for acetylcholine (ACh) synthesis via choline acetyltransferase (ChAT) using choline and acetyl-coenzyme A, storage and transport via vesicular acetylcholine transporter (VAChT), breakdown via acetylcholinesterase (AChE) and re-uptake via high-affinity choline transporter (CHT1). The ACh released via cholinergic neurones at the presynaptic terminal binds to muscarinic (mAChR) and nicotinic (nAChR) receptors at the postsynaptic terminal. The ACh released via cardiomyocytes binds to mAChR expressed on the sarcolemma in an autocrine-paracrine manner enabling signalling (159, 160). Image reproduced from: (159).

1.7. The (diabetic) sinoatrial node

As mentioned in section 1.1, DM promotes SAN dysfunction, increases the risk of arrhythmias and sudden cardiac death, and therefore warrants investigation of any changes to underlying mechanisms (5, 18-21, 26). This section presents current knowledge on the DM SAN.

Histological investigation of the DM SAN in humans (non-diabetic (nDM) age range 44 – 56 years-old versus DM age range 56 – 73 years-old) presented ischemia, necrosis and apoptosis that left remnants of a-nuclear '*ghost*' SAN cardiomyocytes amongst isles of normal SAN cardiomyocytes (162). However, these intrinsic structural changes might not only be caused by DM but might also be age-induced (162). The underlying trigger(s) as to why SAN cardiomyocytes decrease via necrosis and apoptosis during DM in humans is not clear. Hyperglycaemia is known to initiate metabolic abnormalities and substrate imbalance causing augmented oxidative stress and free radical production resulting in cellular injury and apoptosis possibly within cardiomyocytes and nerve cells (163).

A reduced intrinsic (*ex vivo*) HR has been found in rats with an induced metabolic syndrome (via 20% sucrose in drinking water) and in rats on a high fat diet (45% versus 10% fat in control) protocols compared to their respective controls; both protocols give rise to a pre-DM state (55, 164). Both models also present increased susceptibility to arrhythmias. In addition, four types of AP patterns with variable firing frequencies were found between lead and latent pacemaking cardiomyocytes (55). A significant increase in I_f in rats with metabolic syndrome suggests remodelling of the Vm clock, however, the Ca^{2+} clock was not investigated (55). Increased tyrosine hydroxylase labelling, as well as increased adipose tissue surrounding SAN

cardiomyocytes compared to control was also shown (55). This highlights increased dependence on sympathetic input (also seen in our DM rat model, see below (165)) and perhaps functional uncoupling between lead versus latent SAN cardiomyocytes heightening the risk of SAN originating arrhythmias perhaps even explaining the four types of AP patterns seen (55, 165). Whether these Vm clock findings are mirrored in DM remains to be determined.

A study from our lab, directly measured *in vivo* left efferent cardiac sympathetic input and β-adrenergic receptor responsiveness in 20 week-old DM Zucker Diabetic Fatty (ZDF) rats (165). A 45% increase in cardiac sympathetic activity and a double mean firing rate in DM compared to nDM controls were found (165). Immuno-histochemical staining revealed no change in the total number of axons or number of sympathetic axons per nerve; confirming the increased sympathetic activity rather than density in the DM rats. β_1 expression was increased by 17% in the right atrium of the DM rats, whilst in the left ventricle (LV) β_1 expression was decreased by 23% (165). Furthermore, in another study from our lab, β-adrenergic chronotropic responsiveness was found to be significantly increased in the conscious DM ZDF rats *in vivo* (166). Collectively, this primarily suggests an augmented *in vivo* cardiac sympathetic β-adrenergic pathway in the DM ZDF rats. Parasympathetic nerve activity to the DM ZDF heart has also been found to be significantly increased (Bussey *et al*., unpublished data).

1.7.1 Rhythm and diabetes

HR is not metronomic; beat-to-beat variability in the R-R interval is used as a measure of HRV (167). Traditionally, HRV is attributed to autonomic innervation, and thus HRV measure is thought to be an indirect non-invasive clinical assessor of autonomic tone, however, this

dogma is again being questioned (167, 168). To what degree the sympathetic and parasympathetic inputs play a role is also debated (167). It has been suggested that HRV cannot be assumed as a true evaluator of cardiac autonomic status, rather HRV measure is reliant on HR; when HR is slow HRV and R-R interval increase, and vice versa (168). This would suggest that (increases in) sympathetic activity (corresponding to high HRs) decreases HRV and (increases in) parasympathetic activity (corresponding to low HRs) increases HRV. HRV has also shown to be present in isolated hearts under baseline conditions (168). Additionally, HRV might also be influenced by a mutual entrainment of a central circadian clock (the autonomic tone at a particular time of day or night prescribing a degree of HRV via ionic conductance) and a local cardiac circadian clock (responsible for ion channel expression in the SAN over 24 hours) (169, 170). Thus, interpretation of HRV data in DM (described below) does not necessarily equate to underlying autonomic influence. At rest, typically a high HRV is favourable and a low HRV unfavourable, whilst the opposite is preferred in an active state. Low HRV i.e. a more static HR, is associated with increased morbidity and mortality; not necessarily cardiac related (167, 171).

1.7.2 *In vivo* diabetic heart rate

A characteristic change described in the literature regarding DM animal models and patients is an altered HR and reduced HRV displaying a greater risk of arrhythmias (8, 19, 165, 172, 173). DM-induced changes in HR have been inconsistent. *In vivo* HR recordings in DM rodent models have been variable, with studies reporting it to be similar (19, 165, 174) or faster (175, 176), but mostly to be slower (166, 177-182). Typically in humans, a higher resting and sleeping HR has been detected *in vivo* that presents an increased risk of major cardiovascular events, all-cause death and cardiovascular death (183-191). Studies have also shown a lower

resting HR, notably not only in chronic heart failure patients (8, 25, 192). Maximum HR has been shown to be significantly lower (165, 185). These discrepancies might arise due to differences in the severity or duration of DM, animal models or possible changes in central and local circadian influences, in addition to the time these measurements were taken. Despite these discrepancies, most studies do find a chronotropic imbalance in DM. These alterations have been suggested as a primary indicator for DM-induced autonomic neuropathy and CCS defects (9, 25).

In part, due to the build-up of *in vivo* DM HR data, many investigations on DM HR changes have been on autonomic neuropathy, and research on the possible changes in the intrinsic pacemaking mechanisms in type 2 DM has been undermined (31). Indeed, follow up studies in humans show decreased autonomic function early on in DM that continues to decline, which was also correlated with reduced HRV when compared to nDM (171, 193). A reduced HRV was also detected in nDM which was attributed to an ageing effect (171). Some have suggested that alterations in HRV are the result of an increase and decrease in sympathetic and parasympathetic innervation respectively resulting in electrical imbalance (9, 25, 190). DM patients typically show a loss of parasympathetic tone during the night, and continuous or increased sympathetic tone during the day and night compared to nDM (113, 194, 195). The day-night circadian sympathovagal rhythm modulation is lost in DM especially those with symptoms of cardiac autonomic neuropathy; of note with most cardiovascular incidents occurring early morning or also known as the ‘dead in bed syndrome’ (194, 195). However, these studies cannot indefinitely associate reduced HRV to altered cardiac autonomic dysfunction as there could be intrinsic changes altering variability, or determine whether these reductions result due to sympathetic or parasympathetic dysfunction (171).

1.7.3 Intrinsic diabetic heart rate

Nevertheless, intrinsic type 2 DM HR data is also accumulating and becoming noticed. Significant intrinsic HR reductions have been found in a study from our lab (~32% decrease) as well as others in the DM ZDF model and many other models compared to respective nDM control (19, 165, 174, 196-198). This reduced intrinsic HR is seen at 6 (pre-DM, insulin resistant), 12 (DM) and 24 (prolonged DM) weeks in the DM ZDF compared to age-matched nDM controls. Moreover, an age-induced decline was also present in both groups, however, this was more pronounced in the DM animals (196). A significant reduction in HR has also been shown in the DM (*db / db*) mouse (174). Collectively, these intrinsic HR reductions are suggestive of intrinsic pacemaking changes. Why the intrinsic HR is lower in type 2 DM compared to nDM controls in regards to protein expression and function is unknown and will be the subject of investigation in my thesis.

1.8. Summary

A significantly decreased **intrinsic** HR is present in type 2 DM in rodents. Current knowledge of possible intrinsic pacemaking protein remodelling occurring in type 2 DM remains unknown. The overall **aim** of this thesis was to investigate HR control of the SAN in type 2 DM rats. I determined DM protein expression differences of key Vm and Ca^{2+} clocks, cx45 and cholinergic proteins at the SAN level (**Chapter 3**). I investigated intrinsic HR effects by challenging the Vm and Ca^{2+} clocks, and the cholinergic system in DM (**Chapter 4**). I further went on to explore the DM SAN structure and cellular protein expression patterns (**Chapter 5**). Finally, in **Chapter 6** I looked into the effects of anaesthetics on the recording of standard animal parameters.

CHAPTER 2

Methodologies

2.1. Ethics

Ethical approval for use of experimental animals and protocols was granted by the University of Otago Animal Ethics Committee and all experiments conducted were in compliance with the New Zealand (NZ) Animal Welfare Act 1999 and University guidelines (ET29-15 and AUP18-115).

2.2. Animal model: the Zucker Diabetic Fatty rat

Zucker type 2 Diabetic Fatty (DM ZDF$^{fa/fa}$) rats have a dysfunctional leptin receptor due to a homozygous missense mutation in the leptin receptor gene and reduced insulin gene transcription due to inherited defective β-cells (199-202). Hence, around 12-weeks of age ZDF$^{fa/fa}$ rats become obese, hyperglycaemic, hyperlipidemic and insulin resistant in part due to hyperphagia, developing an obese DM phenotype (202-204). The DM rats were compared to their in-strain normoglycaemic lean non-diabetic (nDM) control rats (heterozygous (ZDF$^{fa/+}$) or homozygous (ZDF$^{+/+}$)). The rats were housed in groups of 2 – 4 per cage at room temperature 21°C ± 1°C with a 12-hour light-dark cycle and provided unlimited access to a slightly high fat rat chow that promoted and accelerated the onset of the type 2 DM phenotype (205) (Purina 5008, LabDiet®) and water until required. The rats used in my thesis were all adult male aged between 19 – 22 week-old (no significant age difference was present between the groups), which is known to have a prevalent onset of DM (165, 166, 182, 206, 207). Female ZDF rats were not used as they do not spontaneously develop the DM phenotype observed in males (204, 205, 208, 209). The rats were acquired from the Hercus Taieri Resource Unit, Dunedin, NZ.

2.3. Rat heart isolations

2.3.1 Anaesthesia

Rats (n=31 per group) were weighed, and anaesthetised in two different ways (**Figure 2.1**) to investigate any effects of anaesthesia on *in vivo* heart rate (HR), intrinsic (*ex vivo*) HR or blood glucose (**Chapter 6**). The anaesthetics used were either 5% isoflurane (nDM n=8 and DM n=9) (Merial, provided by the Animal Welfare Office, Dunedin, NZ) with 1 L/min oxygen in a gas chamber (Technident Industries Ltd, NZ and Medical Supplies and Services Int Ltd, England) or 50 mg/kg intraperitoneal sodium pentobarbital injection (nDM n=23 and DM n=22) (provided by the Animal Welfare Office, Dunedin, NZ). Once anaesthetised the rats were placed on a heated pad for echocardiography, and isoflurane anaesthesia was maintained at 3% with 1 L/min oxygen using a nose cone. For some rats (isoflurane n=3 per group and sodium pentobarbital n=9-10 per group), a tail tip blood glucose reading was taken 5-minutes post-anaesthesia just before echocardiographic assessment using strips for a glucometer (ACCU-CHECK® Performa). Following echocardiography and to prepare the animals for the excision of the heart, the rats were then deeply anaesthetised, judged by the loss of pedal withdrawal due to a toe pinch, using either 5% isoflurane with 1 L/min oxygen or additional intraperitoneal sodium pentobarbital administration (100 mg/kg). The rats remained anaesthetised for a total maximum of 25 minutes.

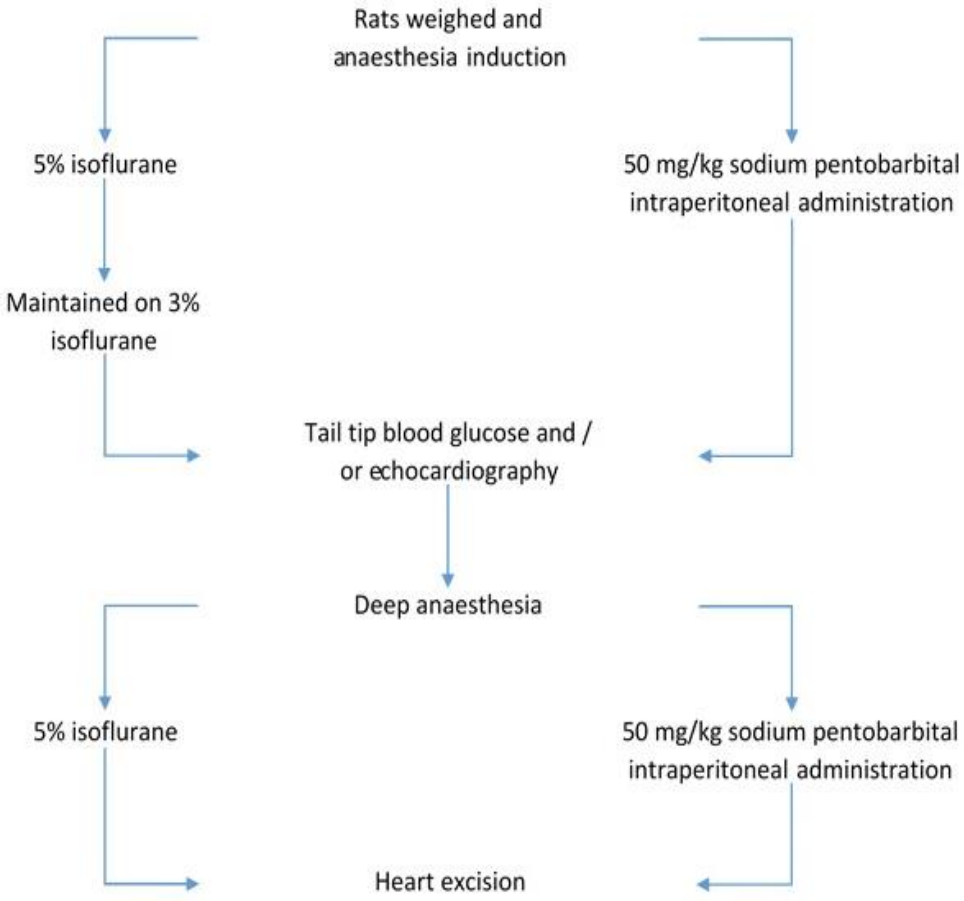

Figure 2.1. Flow diagram explaining how rats were anaesthetised. Original figure.

2.3.2 Echocardiography

To obtain *in vivo* HR under anaesthesia, echocardiography was performed using the ML6-15 probe on an echocardiogram ultrasound machine (Vivid Q, General Electric Healthcare). The rat thorax was first trimmed to remove the fur and expose the thoracic skin. Echocardiography measurements were captured in the long axis at a 45° angled lateral position of the rat. A 2D image of the heart and a minimum of 5 M-mode recordings with clear systolic and diastolic waves were captured. *In vivo* HR under anaesthesia was obtained by measuring 5 diastole-to-diastole cardiac cycles (R-R interval) per image with 3 images analysed in total per rat resulting in 15 HR readings that were averaged (**Figure 2.2**).

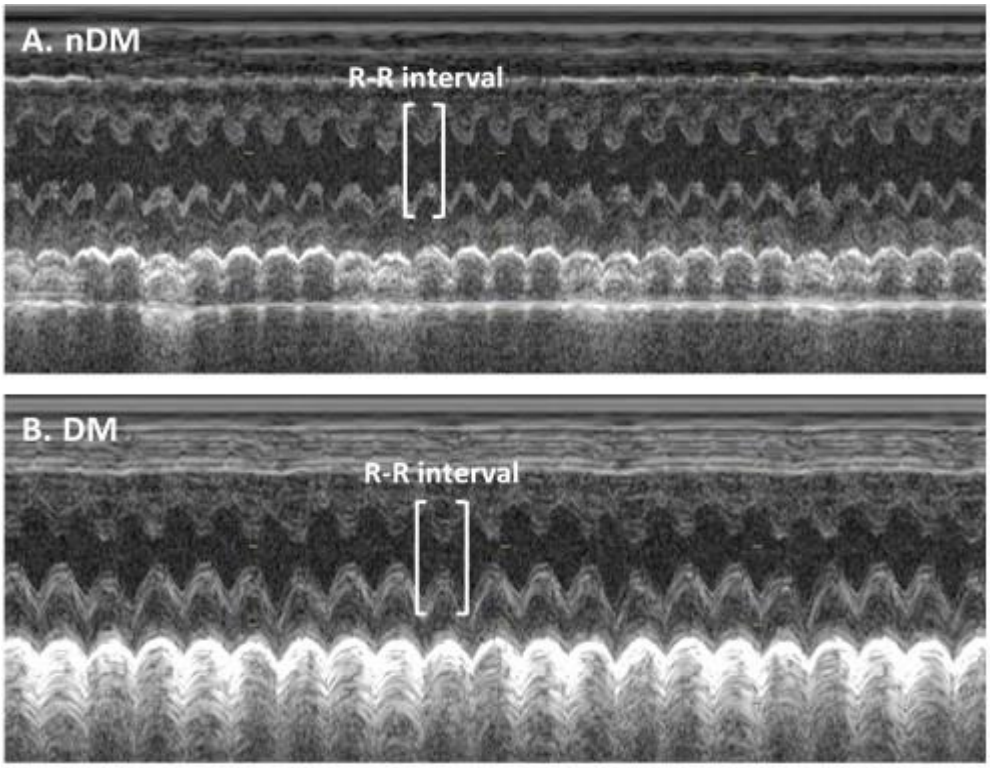

Figure 2.2. *In vivo* heart rate under anaesthesia. Typical M-mode images that were taken during echocardiography for *in vivo* heart rate (HR) analysis in non-diabetic (A. nDM) and diabetic (B. DM) rats. R-R interval was used to calculate HR. In these images, a higher *in vivo* HR can be observed when comparing the number and width of R-R intervals in the nDM compared to DM. Original figure.

2.3.3 Buffers

For experiments using the Langendorff, an arresting and working buffer was used, both were based on the Krebs-Henseleit buffer and differed only in terms of $CaCl_2$ concentration and temperature (**Table 2.1**) (210). The buffer components provided ionic and metabolic nutrients mimicking blood composition, whilst the bicarbonate worked to maintain pH (at 7.4), collectively allowing maintained cardiac tissue viability and excitability (211). Both buffers were gassed with carbogen (95% O_2 and 5% CO_2), which also helped in balancing pH. $CaCl_2$ was the last to be added to the buffer solution in order to prevent precipitation and possible vessel occlusion.

Table 2.1. Krebs-Henseleit cardiac buffer. The components of the arresting and working Krebs-Henseleit buffers used for rat heart isolations and the Langendorff experiments.

Ingredients	Concentration (mM)	Manufacturer
Sodium chloride	118.5	Lab supply
Potassium chloride	4.7	Lab supply
Magnesium sulphate	1.2	Fisher scientific
Potassium dihydrogen orthophosphate	1.2	Fisher scientific
Sodium hydrogen carbonate	25	Lab supply
D-Glucose	11	AppliChem
Calcium chloride	0.5 (arresting) or 1 (working)	LabServ

2.3.4 Heart tissue retrieval

Once surgical anaesthesia had been achieved, the rats were placed in the supine position to allow access to the thoracic cavity. The thoracic skin was excised, and an incision just below the xiphoid process of the sternum through the pectoral muscles was made to expose and cut along the diaphragm using large dissecting forceps and scissors. Direct bilateral cuts were made along the length of the rib cage allowing the anterior rib cage and xiphoid process to be clamped backwards, exposing the beating heart. Any obstructing thymus, pericardium, fat or connective tissue was removed using fine dissecting forceps and scissors. The aorta and superior vena cava (SVC) were located and briefly clamped using forceps as far up the vessels as possible in order to include the sinoatrial node (SAN) region present at the base of the SVC before the aorta and SVC were cut. The heart was then quickly excised out of the thoracic cavity and instantly placed in ice-cold arresting buffer containing 0.5 mM $CaCl_2$ (to reduce contraction without Ca^{2+} withdrawal to the heart and lessen possible ischaemic injury between the period of excision and restoration by perfusion (211)). A thorax blood glucose

reading was also taken. DM rats that displayed a 'high' blood glucose reading, above the maximal reading of 33.3 mmol/L detected by the glucometer, were excluded from the blood glucose analysis only.

2.4. Langendorff setup

2.4.1 Overview

The Langendorff technique allows the isolated rat heart to be perfused; flushing out blood, providing adequate oxygen, nutrients and maintaining pH through the buffer solution that ensures cardiac sustainability, and therefore enables a functional experiment to be conducted *ex vivo* (211). Of great importance to the heart's viability, and thus the functional experiment, is swift precise cannulation of the heart to install retrograde perfusion of the aorta and ensuing coronary perfusion can be enabled following the closure of the aortic valves.

2.4.2 The Langendorff apparatus

A simplified schematic depiction of the Langendorff apparatus is presented in **Figure 2.3**. The isolated rat hearts were tied by the aorta onto the Langendorff cannula and working buffer containing 1 mM $CaCl_2$ warmed to 37°C was retrograde perfused into the aorta with flow increasing from ~0.5 ml/min to an average rate of ~12 ml/min, which is within range of a physiological coronary flow (211).

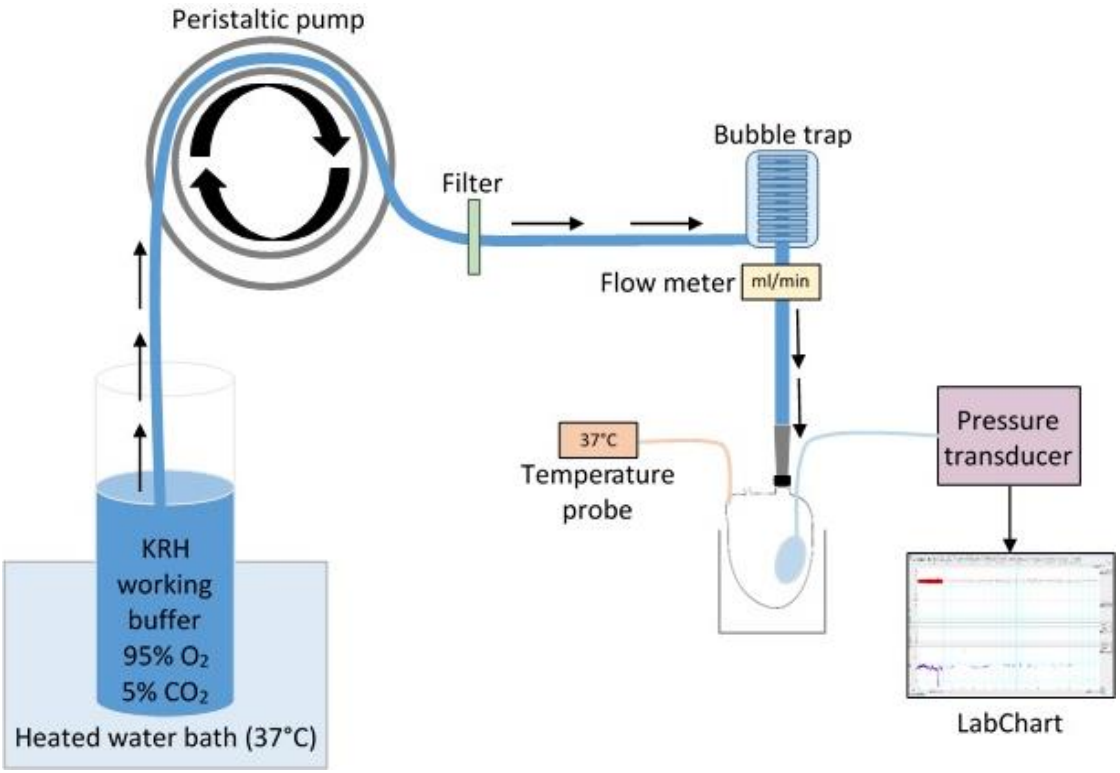

Figure 2.3. The Langendorff experimental setup. The water bath heats the carbogenated Krebs-Henseleit (KRH) working buffer and the water circulation around the Langendorff setup to maintain 37°C. The peristaltic pump moves the buffer through the inflow line (blue) through the filter, bubble trap and cannula to eventually reach and nourish the isolated heart. The water-filled balloon at the end of the pressure transducer is inserted into the left ventricle and real-time pressure changes upon contraction are measured, which relays input to the LabChart software on a computer. Real-time coronary flow and temperature are monitored by the flow meter and temperature probe respectively. Original figure.

The cannula was a blunted 14-gauge needle with circular indented grooves that enabled secure tightening of the aorta to the cannula using braided thread (5 metric, 2 USP, Resorba, Germany). The cannula was inserted and tied to the aorta cautiously to prevent rupture of the aortic valve and then flow was increased. The apex of the left ventricle (LV) was gently pierced which introduced a tiny hole in order to allow leakage of thebesian flow and relieve LV wall pressure (211). Together, this ensured thorough coronary perfusion and pressure to the heart for continued cardiac function *ex vivo*. The working buffer, bubble trap and heart chamber

were heated to 37°C by a heating circulator pump (LAUDA Alpha A24, Germany). Tubing was wrapped in foil to reduce heat loss. The working buffer was suctioned in through the inflow tube by a peristaltic pump (MINIPUL S3, Gilson, France) and, the flow was controlled and measured by the pump controller and flow meter, respectively (ML175 STH Pump Controller, ADInstruments and ME3 PXN Inline Flow Probe, Transonic Systems Inc., USA). The working buffer travelled through the 0.45 µm sterilised filter that removed occluding particles, bubble trap which functioned to reduce any air bubbles present and cannula to sustain the isolated heart by aortic retrograde perfusion. The real-time flow was presented (T402 Transit-Time Tubing Flow Meter, Transonic Systems Inc., USA). The pump controller, flow meter and pressure transducer were connected to a bridge amp and PowerLab system (ML224 Quad Bridge Amp, ADInstruments, Australia and PowerLab ML870 8/30 ADInstruments, Australia) which presented and recorded the signal trace to LabChart software (LabChart® 7 and 8 Pro, ADInstruments, NZ).

To record intrinsic HR, either the LV (avoiding the septa) was gently pierced with a 27-gauge needle which served as a detector, or a custom-made deflated balloon was inserted into the LV following removal of the left atria and then the balloon was slowly filled with 250 µl of water using a micro-syringe again ensuring no air bubbles were present. The needle or balloon was linked to a pressure transducer via a water-filled catheter making sure no air bubbles were present (Physiological Pressure Transducer, ADInstruments, NZ). Using the LabChart software intrinsic HR was derived from the LV pressure trace during sinus rhythm. The needle was used for short measurements of intrinsic HR (~20 minutes), while, the balloon was more suitable for longer measurements of intrinsic HR (~4 hours). No significant differences were found in intrinsic HRs recorded from either method in both groups. **Figure 2.4** shows representative nDM and DM intrinsic HR traces.

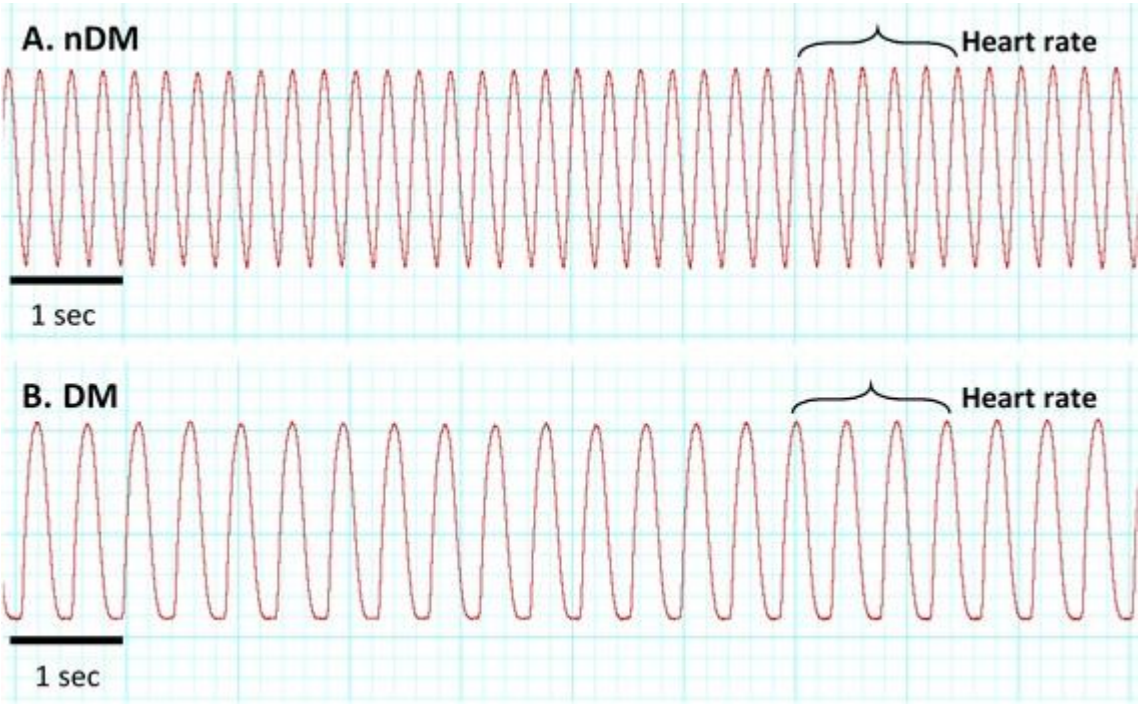

Figure 2.4. ***Ex vivo*** **intrinsic heart rate traces.** Representative LabChart left ventricular pressure traces in non-diabetic (A. nDM) and diabetic (B. DM) isolated rat hearts. The left ventricular pressure waves are used as an indirect measure of intrinsic heart rate (HR). The wave forms are uniform in morphology indicative of normal regular sinoatrial node (SAN) heart rhythm. In these images, a higher intrinsic HR can be observed when comparing the number and width of the pressure waves in the nDM compared to DM. Original figure.

2.4.3 Challenging the Vm and Ca^{2+} clocks, and evaluating the cholinergic and caffeine responses

To determine whether the decrease in intrinsic HR in DM was due to remodelling of the voltage membrane (Vm) and / or Ca^{2+} clocks, Langendorff hearts (n=7-10 per group) were sequentially perfused with increasing external Ca^{2+} ($[Ca^{2+}]_o$) and ivabradine (HCN4 inhibitor) targeting the Ca^{2+} and Vm clocks respectively. Additionally, the response to cholinergic stimulus by the muscarinic type 2 (M_2) receptor agonist carbachol was investigated. Lastly, caffeine, a sarcoplasmic reticulum (SR) Ca^{2+} store depletor, was also added to indirectly determine maximal SR Ca^{2+} load. $[Ca^{2+}]_o$, ivabradine, carbachol or caffeine in 37°C working buffer were sequentially changed with working buffer washout periods occurring in-between

conditions. These conditions were perfused through the isolated hearts to measure effects on intrinsic HR using the balloon method (protocol outlined in **Table 2.2**, results in **Chapter 4**). Drug concentrations were predetermined based on initial common findings in the literature and then altered accordingly due to preliminary Langendorff experiments in Sprague-Dawley rats and experimental aims (212-217). Typically, 3 µM ivabradine (clinically relevant) is used for isolated heart Langendorff experiments in mouse (213), guinea-pig (218) and rabbit (219) over a longer period of perfusion time (30 – 60 minutes). In my study, the higher concentrations of ivabradine over a shorter period were selected to obtain a faster response due to the length of the entire Langendorff protocol and testing of multiple conditions. Carbachol concentrations used in isolated heart Langendorff experiments are quite variable in the literature (1 µM used in mouse (217), 0.01 – 1 µM used in the rat (215, 216) and 10 µM used in rabbit (220)). In my study, lower concentrations of carbachol were used compared to the literature due to the higher concentrations resulting in detrimental decreases in intrinsic HR. Wash times were also determined by the preliminary Langendorff experiments.

$[Ca^{2+}]_o$ was modulated to primarily assess intrinsic HR effects on increased SAN cardiomyocyte Ca^{2+} load and Ca^{2+} cycling (Ca^{2+} clock) in nDM versus DM hearts. $[Ca^{2+}]_o$ tested were 1 (baseline), 0.5, 1, 1.5, 2, 2.5 and 3 mM for 5 minutes each. The hearts were then allowed to recover by switching back to 1 mM Ca^{2+} normal working buffer washout for 30 minutes. The following different conditions all included the baseline 1 mM Ca^{2+} in the working buffer. Next, ivabradine (Sigma-Aldrich) was perfused to determine intrinsic HR on HCN4 inhibition, a primary Vm clock channel contributor within the SAN. Ivabradine concentrations used were 1, 3, 5 and 10 µM for 10 minutes each (212-214). Again, hearts were allowed to recover by switching back to 1 mM Ca^{2+} normal working buffer washout for 45 minutes. Next, carbachol (Sigma-Aldrich) was perfused to investigate intrinsic HR effects on increased muscarinic

stimulation. Carbachol concentrations explored were 1, 2, 3, 4, 5 and 10 nM for 5 minutes each (215-217). Carbachol was washed out of the hearts for 15 minutes using 1 mM Ca^{2+} normal working buffer. After which, 20 mM caffeine (Sigma-Aldrich) in working buffer was perfused. Finally, the hearts were washed out one last time with 1 mM Ca^{2+} normal working buffer for 10 minutes before tissue dissection.

Table 2.2. Langendorff protocol challenging intrinsic sinoatrial node clocks, and evaluating the cholinergic and caffeine responses. Langendorff protocol for testing effects of increasing external Ca^{2+} ($[Ca^{2+}]_o$, 0.5-3 mM), ivabradine (Ivab, 1, 3, 5 and 10 µM), carbachol (Carb, 1-5 and 10 nM) and caffeine (Caff) on intrinsic heart rate in non-diabetic versus diabetic. From the 1st wash, all experiments were carried out in 1mM Ca^{2+}.

Condition	Baseline 1mM $[Ca^{2+}]_o$	↑ $[Ca^{2+}]_o$	Wash 1	↑ Ivab	Wash 2	↑ Carb	Wash 3	20mM Caff	Wash 4
Time (minutes)	5	30	30	40	45	30	15	10	10

2.4.4 Langendorff data analysis

Langendorff data traces were analysed using LabChart 8.0 Pro (ADInstruments, NZ) using the 'blood pressure' analysis plugin. The pressure waves that are obtained from LV contraction were used as an indirect measure of intrinsic HR. A minimum 10-second time frame was chosen for analysis with the condition that a minimum of 10 LV pressure waves exist. If 10 LV pressure waves did not occur in the 10-second window then the time frame was increased to at least include 10 LV pressure waves. A part of the pressure wave trace in sinus rhythm was selected. An averaged HR measurement was derived from the blood pressure analysis. For experiments where working buffer included alterations of Ca^{2+} or drugs, the 10-second time frame was selected from the last 2 minutes of the 5 or 10-minute LabChart trace recording.

For this experiment, isolated hearts with a continuous unstable arrhythmogenic or extremely low HR trace were excluded (n=2).

2.5. Heart tissue processing

Cardiac tissue from nDM and DM ZDF rats was isolated and processed accordingly for either immunohistochemistry or western blotting.

2.5.1 Tissue for immunofluorescence and histology

The SAN / right atria including the SVC and ventricular tissue were dissected from the whole heart and placed in 4% formalin (Sigma-Aldrich) diluted in 1x phosphate-buffered saline (PBS) (**Table 2.3**) for 24 hours at 4°C. The formalin worked to cross-link proteins which increased stability and preserved tissue for longer periods. Next, tissue was placed in 1x PBS for 24 hours at 4°C. Then in 30% D+-sucrose (Lab Supply) solution diluted in 1x PBS until the sample sunk. The tissue remained in the solution for at least 24 hours or if left longer; a maximum of 3 days, before tissue was embedded. The sucrose displaced the water from the tissue, which minimised ice crystals from forming within the cells and consequent cell rupture upon freezing. The freezing process was as follows: an aluminium foil well was coated in protective cryomatrix (Thermo Scientific), the tissue sample was placed in the well and further coated with cryomatrix until the sample was covered. Tissue orientation was marked on the foil well. The aluminium foil well was then placed on an aluminium foil boat and sat on liquid nitrogen to allow slow freezing. Once frozen, the foil well was further wrapped in aluminium foil, and the sample was stored in the liquid nitrogen until later storage at -80 °C. nDM and DM samples used for immunofluorescence and histology were blinded at this time point and revealed post-analysis of images captured.

2.5.2 Tissue cryosectioning for immunofluorescence and histology

The SAN is a heterogeneous tissue structure that needed to be located in a plane which provided a consistent way of locating the SAN and enabled maximal surface area. SAN / right atria and ventricular tissue were cut in the transverse plane. I.e. the SAN / right atria were cryosectioned from the SVC down towards the inferior vena cava. Rat tissue was sectioned using a cryostat (Leica CM1850 / CM1950) at -23 °C. The tissue samples were allowed to sit in the cryostat and adjust to the temperature set in order to prevent cracks in the frozen tissue and cryomatrix. Cryomatrix was used to attach the tissue to the cryostat chuck (approximate tissue orientation was known) and allowed to solidify for 5 minutes. The cryostat knife was angled at roughly 7°. Tissue was cryosectioned at 20 µm. The serial tissue sections were adhered to labelled Superfrost Plus slides (LabServ) and stored at -20 °C until further use. These tissue sections were either used for immunofluorescence or histology labelling.

Table 2.3. Phosphate-buffered saline buffer. pH to 7.4.

Ingredients	Concentration (mM)	Manufacturer
Sodium chloride	137	Lab Supply
Potassium chloride	2.7	Sigma
Disodium phosphate	100	VWR Global Science
Potassium dihydrogen phosphate	2	Thermo Scientific

2.5.3 Sinoatrial node tissue isolation for western blotting

To isolate SAN tissue, the right atria was cut open separating the anterior and posterior walls like a flap, which exposed the SAN seen as the 'translucent window' along either side of the base of the SVC and posterior wall of the right atria (**Figure 2.5**). This translucent region was adjacent to the *crista terminalis* and was excised as the SAN sample which should include the

lead pacemaking region within the rat and be reasonably connexin 43 (cx43) absent (37). Tissue for western blotting was excised and snap-frozen in liquid nitrogen and stored at -80°C.

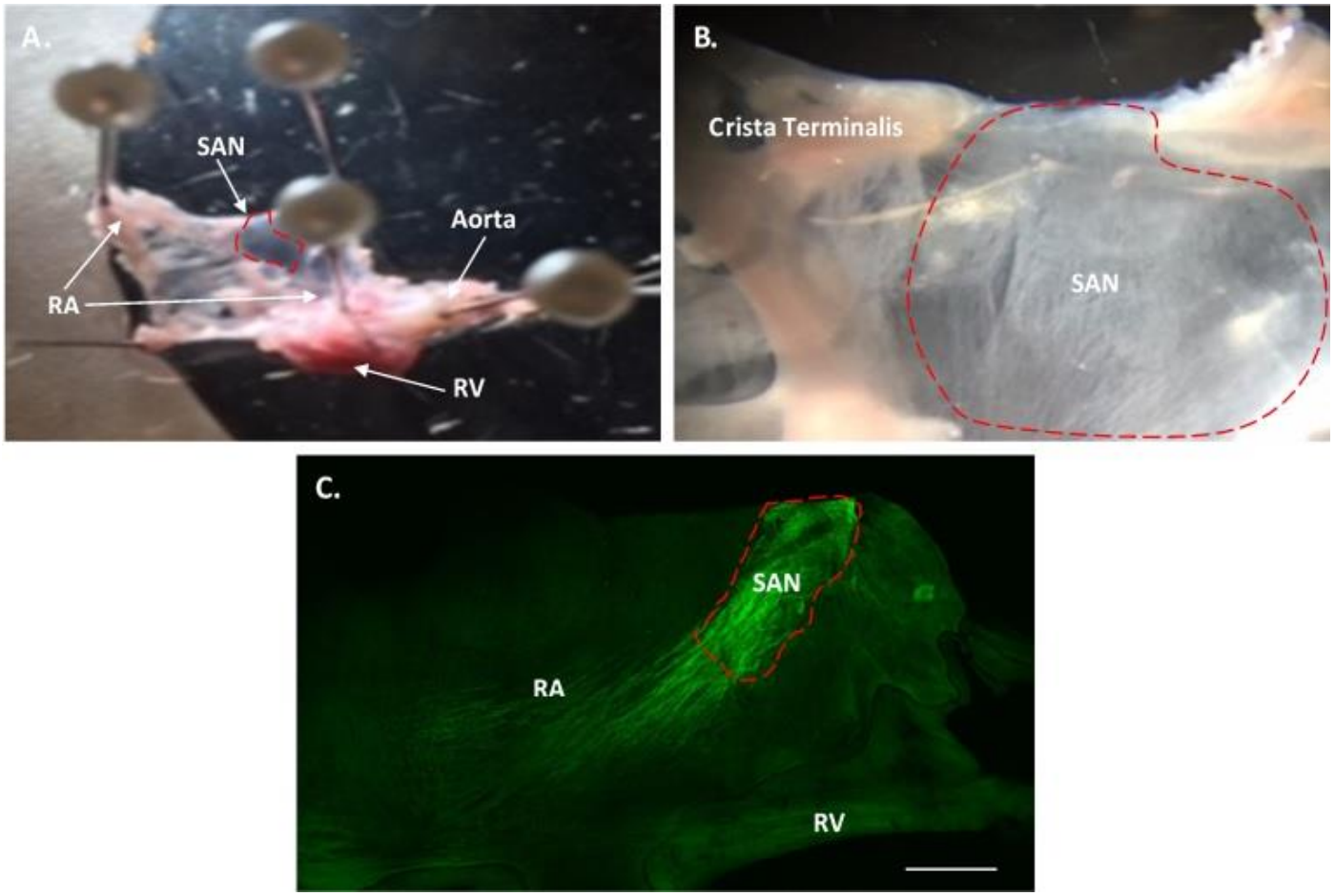

Figure 2.5. Rat sinoatrial node tissue isolation for western blotting. (A. and B.) Photos of the opened up pinned down right atria (RA) and right ventricle (RV), revealing the translucent sinoatrial node (SAN) region at the base of the superior vena cava. (C.) Whole-mount immuno-fluorescent labelled tissue showing the translucent region (dashed red area) that would be isolated labels positive for hyperpolarisation-activated cyclic nucleotide-gated channel 4 (HCN4), a positive marker of the SAN. HCN4 labelling also extends into the RA. 10x tile NA 0.45, 1000 µm scale bar. Original figure.

2.6. Immunohistochemistry

2.6.1 Immunofluorescence

For immunofluorescence labelling, the primary antibodies selected were not raised in the same species as the sample of interest (rat) and were from different species to avoid non-specific binding. Both monoclonal and polyclonal primary antibodies were used in this thesis (**Table 2.4**). The fluorophore-conjugated secondary antibodies selected were raised against the species of the primary antibodies and the secondary antibodies were raised in the same species to minimise non-specific binding and lower background fluorescence.

2.6.2 Finding the sinoatrial node

Every 10th SAN / right atrial tissue cryosection per sample was labelled for HCN4 in order to locate the SAN. The SAN was determined to be immuno-labelled as HCN4-positive with the presence of the SAN nodal artery, and the surrounding atria as HCN4-negative (**Figure 2.6**). Transverse cryosections selected for multiple immunofluorescence and histology were based on maximal SAN area determined by the area of HCN4-positive labelling.

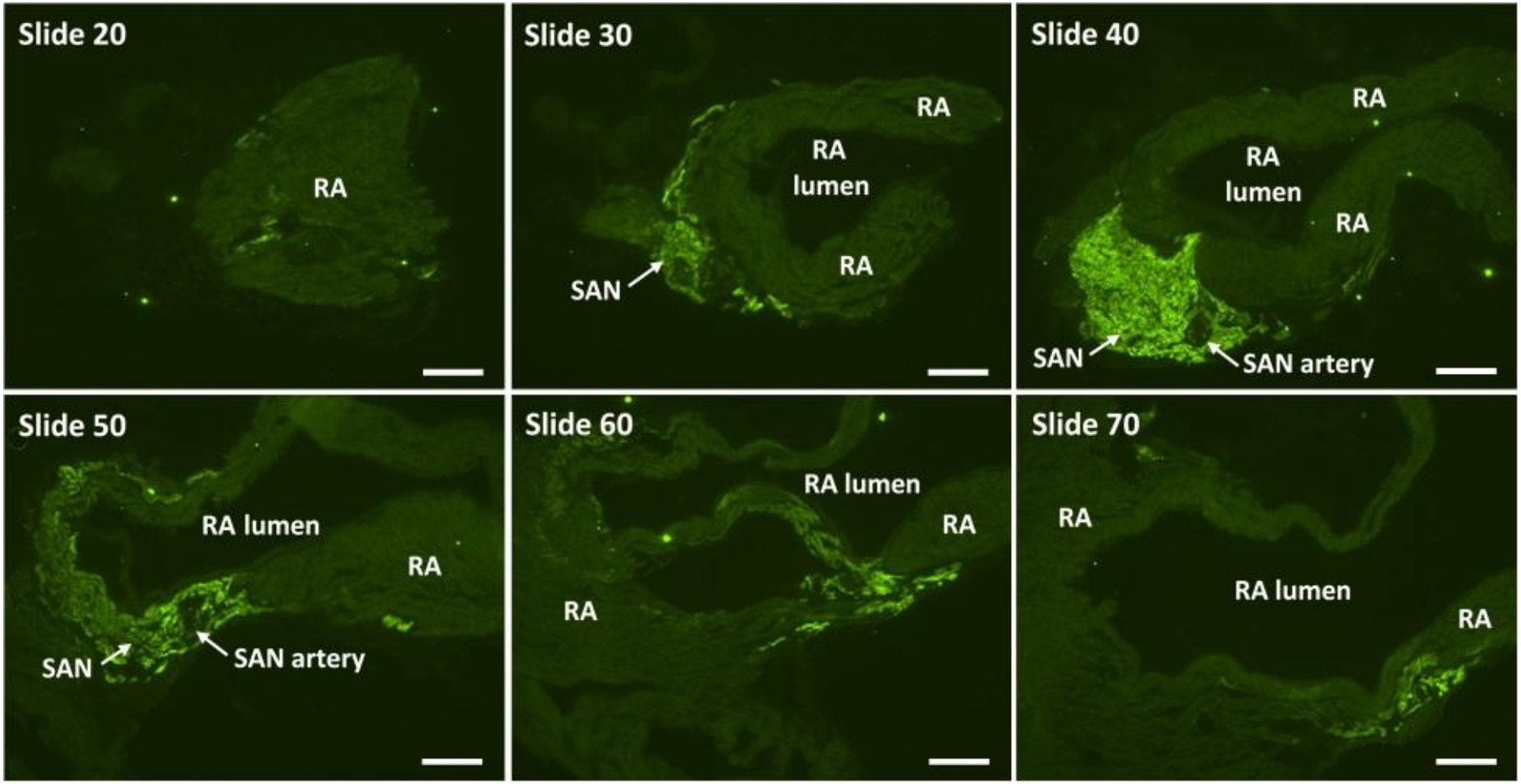

Figure 2.6. Locating the sinoatrial node for immunohistochemistry labelling. The start and end of the sinoatrial node (SAN) through the right atria (RA) of one sample in the transverse plane; detected by hyperpolarisation-activated cyclic nucleotide-gated channel 4 (**HCN4**) positive (**bright green**) immuno-labelling in the SAN and its absence in the RA (dull green). The presence of the SAN artery can also be seen. In this example, slides selected for immunohistochemistry would range from slide 35 – slide 45. 10x NA 0.2, 200 µm scale bar. Original figure.

2.6.3 Sinoatrial node multiple immunofluorescence labelling

Multiple immunofluorescence labelling was carried out on nDM and DM SAN tissue cryosections (n=7 per group, 1 SAN cryosection per protein per n) (**Chapter 5**). A boundary was drawn around each tissue cryosection using an ImmEdge pen (Vector Laboratories), tissue was fixed in 4% formalin in 1x PBS for 5 minutes, and washed 3x using 1x PBS for 10 minutes each. Next, tissue was permeabilised using either 0.1% (HCN4 and connexin 45 (cx45)) or 1% (all other proteins) Triton X-100 (Millipore) in 1x PBS for 30 minutes, washed 3x using 1x PBS for 10 minutes each, and blocked using 1% bovine serum albumin (Thermo Fisher) in 1x PBS for 30 minutes. Then washed 3x using 1x PBS for 10 minutes each, and incubated in a humidified environment with primary antibodies (goat cx43 and protein of interest) appropriately diluted in 1% bovine serum albumin in 1x PBS, overnight at 4°C (**Table 2.4**). The following day, tissue sections were washed 3x using 1x PBS for 10 minutes each and incubated with Alexa secondary antibodies diluted in 1% bovine serum albumin in 1x PBS, for 1 hour at room temperature in the dark (**Table 2.5**). Following this, slides were washed 2x using 1x PBS for 10 minutes each, then incubated with 1 mg/ml Hoechst 33342 (Invitrogen) diluted in 1x PBS for 10 minutes to stain the nuclei. Then washed 2x with 1x PBS for 10 minutes each, prior to application of TrueBlack quencher (Biotium) for 30 seconds to minimise any lipofuscin (oxidised proteins and lipids present within lysosomes) and general background autofluorescence in order to preserve fluorescent signal-to-noise ratio. Finally, tissue cryosections were washed a further 3x with 1x PBS for 10 minutes each, before coverslips were attached to glass slides using Vectashield H-1000 anti-fade mounting medium (Vector Laboratories) and the edges of the coverslips (22x60 mm, thickness 0.13 – 0.16 mm, Lab Supply) were sealed with nail varnish and allowed to dry and set in a dark environment for at least 2 hours. Immuno-labelling for all nDM and DM samples per protein were carried out in

parallel on the same day to minimise labelling variation and imaged as soon as possible (within a maximum of 4 days).

Negative controls included tissue autofluorescence, secondary antibodies only (**Figure 2.7**), a primary antibody with a non-matching secondary antibody, and for multiple immuno-labelling cross-reactivity's of the secondary antibodies was also checked. Positive labelling was assessed as fluorescence greater than the corresponding negative and tissue autofluorescence, in addition to, where possible, visualisation of the expected labelling pattern seen in longitudinal atrial cardiomyocytes. Immunofluorescence was used as it enables semi-quantification of the fluorescent signal, as well as visualisations of the cellular location and pattern of the protein of interest within the SAN. Application of TrueBlack post immunofluorescence protocol was found to produce images with greater intensity compared to TrueBlack use before the start of the immunofluorescence protocol. Additionally, no significant difference was found in average fluorescent intensity when comparing post immunofluorescence protocol TrueBlack use to no use.

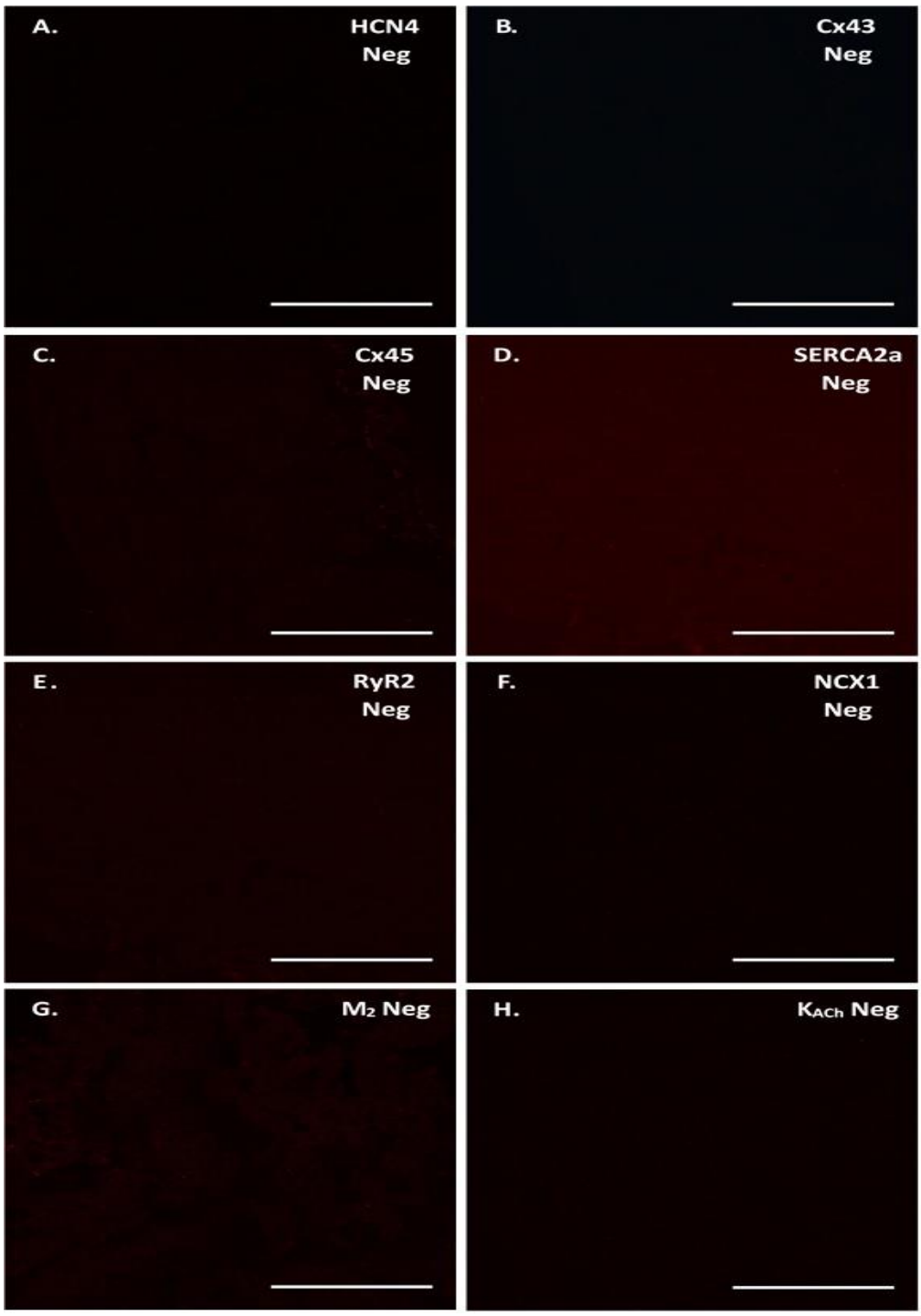

Figure 2.7. Immunofluorescent negatives. No primary antibody with Alexa-488 and Alexa-568 secondary antibody negatives imaged at the respective confocal settings used for each immuno-labelled protein. (A.) Hyperpolarisation-activated cyclic nucleotide-gated channel 4 (HCN4) negative, (B.) connexin 43 ((cx)43) negative, (C.) Cx45 negative, (D.) sarco(endo)plasmic reticulum Ca^{2+}-ATPase 2a (SERCA2a) negative, (E.) ryanodine receptor 2 (RyR2) negative, (F.) Na^{+}-Ca^{2+} exchanger 1 (NCX1) (G.) muscarinic type 2 (M_2) receptor negative and (H.) acetylcholine K^{+} channel (K_{ACh}) negative. No immunofluorescence signal for any protein was observed. 60x NA 1.4, 50µm scale bar.

Table 2.4. Primary antibodies used for immunofluorescence. List of primary antibodies, dilutions and source of antibodies used for immunofluorescence.

Primary Antibody	Clonality	Dilution	Species	Manufacturer
HCN4	Polyclonal	1:100	Rabbit	Alomone
Cx43	Polyclonal	1:1000	Goat	Abcam
Cx45	Polyclonal	1:200	Rabbit	Alomone
NCX1	Polyclonal	1:200	Rabbit	Louch lab, University of Oslo
RyR2	Polyclonal	1:200	Rabbit	Alomone
SERCA2a	Polyclonal	1:500	Rabbit	Badrilla
M_2	Polyclonal	1:200	Rabbit	Sigma-Aldrich

Table 2.5. Secondary antibodies used for immunofluorescence. Fluorescent Alexa secondary antibodies, dilutions and source of antibodies used for immunofluorescence.

Secondary Antibody	Dilution	Species	Manufacturer
488 anti-goat	1:400	Donkey	Abcam
568 anti-rabbit	1:400	Donkey	Abcam

2.6.4 Confocal laser scanning microscopy

The SAN was identified as a cx43 negative region with the presence of the SAN artery. Immunofluorescent labelling was viewed and captured with the widefield fluorescence microscope used for locating the SAN in each sample only (Olympus U-RFL-T, Japan) or the confocal laser scanning microscope (Nikon Eclipse A1 Plus Inverted TiE, Japan). Confocal laser microscopes enhance image resolution by minimising out of focus light by use of a pinhole (**Figure 2.8**). The pinhole enables emission light to be received from one focal point rather than above, below or around the focal point as seen in widefield fluorescence microscopy (221, 222).

For locating the SAN, 4x (numerical aperture (NA) 0.2), 10x (NA 0.2) and 20x (NA 0.2) images were captured. For multiple immunofluorescence labelling of the SAN, a 10x (NA 0.45) overview and four 60x (NA 1.4) oil-immersion Z stacks (0.35 µm Z step for a total of 2 µm) were captured. The 60x confocal settings were selected using the 10x maximum and minimum SAN fluorescence samples per protein imaged; ensuring minimal under or over saturation of pixels. Following, the blinded nDM and DM samples were imaged in a random manner to prevent bias. The refractive index of the immersion oil (Type F Nikon, 1.51), glass coverslip (0.13 – 0.16 mm thickness, ~0.17mm has a refractive index of 1.51 (https://www.microscopyu.com/microscopy-basics/coverslip-correction)) and the Vectashield mounting medium (1.45) relatively matched making them suitable for oil immersion imaging.

Alexa-488 was excited by a 488 nm laser (500 – 550 filter range) and Alexa-568 was excited by a 561 nm (570 – 620 filter range). Hoechst 33342 nuclei stain was excited by a 405 nm laser (425 – 475 filter range). The filters allowed passage of the appropriate emission wavelengths. For multiple immunofluorescence imaging, bleaching and spectral cross-talk of fluorescence emission (i.e. one fluorophore emission detected by filter for the second fluorophore emission) was minimised by using sequential laser scanning of the tissue sections, and the order in which the lasers were used; 561 nm first then 488 nm and last 405 nm laser, as the longest wavelength (561 > 488 > 405) has less energy and cannot bleed-through into the filter for a shorter wavelength.

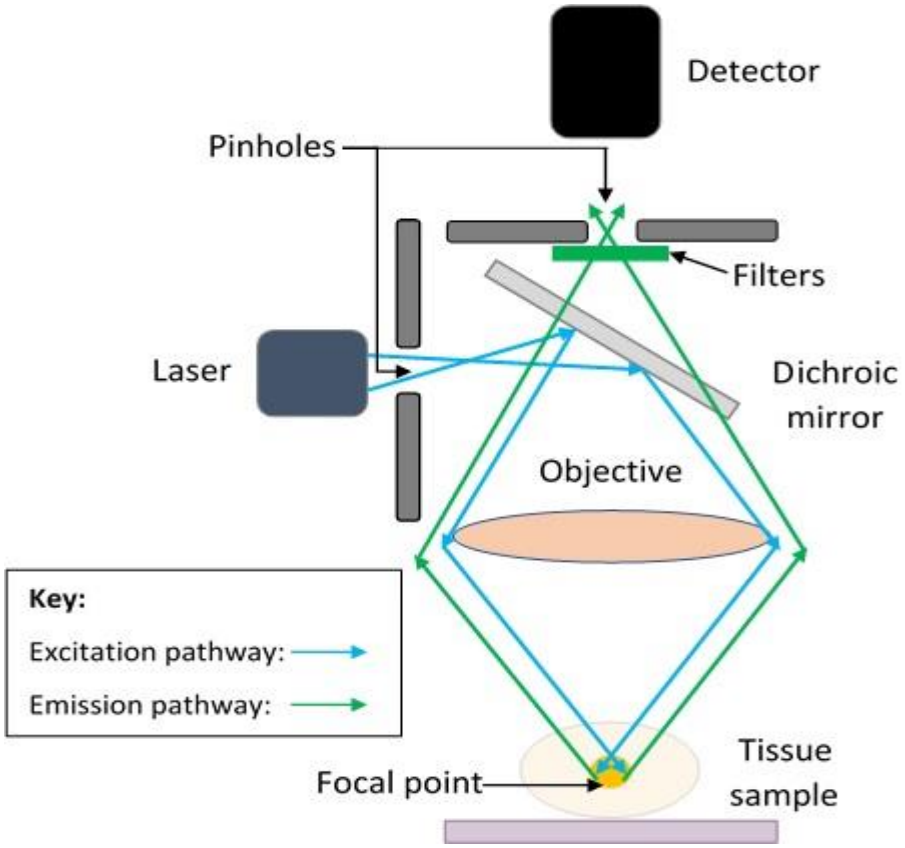

Figure 2.8. The basic principle of confocal laser scanning microscopy. **Excitation** (**blue arrows**) and **emission** (**green arrows**) pathways on a simplified confocal microscope. The pinholes work to remove out of focus light and allow in focus light to pass through. The dichroic mirror reflects light of a defined shorter wavelength and allows light of a longer wavelength to pass through. The filter enables passage of only wanted wavelengths of light. Collectively this reduces background fluorescent noise and increases resolution from the tissue sample. The detector picks up the fluorescent signal from the scanned focal point and scanning continues across the sample to form an image pixel by pixel on a computer screen (221). Original figure.

2.6.5 Immunofluorescent image analysis

The 60x images were quantified using ImageJ software (version 1.51u, Java 1.8.0_66). An IJ-IsoData thresholding approach was applied to semi-quantify the mean fluorescent signal and background (**Figure 2.9**). The algorithm separates signal from background per image by setting an initial threshold, then the averages of the pixels at or below the initial threshold and pixels above are calculated. Averages of these 2 values are calculated, then the threshold is

increased and the process is replicated until the threshold is greater than the composite average, threshold = (average background + average signal) / 2 (223). This approach allows for quantification of fluorescent signal and prevents false values that are influenced by the degree of unlabelled and or background present in each image. This was repeated for each of the four 60x SAN images per sample. Following, the average mean background was subtracted from average mean IJ-IsoData thresholding signal for each nDM and DM sample and these values were statistically analysed (see section 2.8 below).

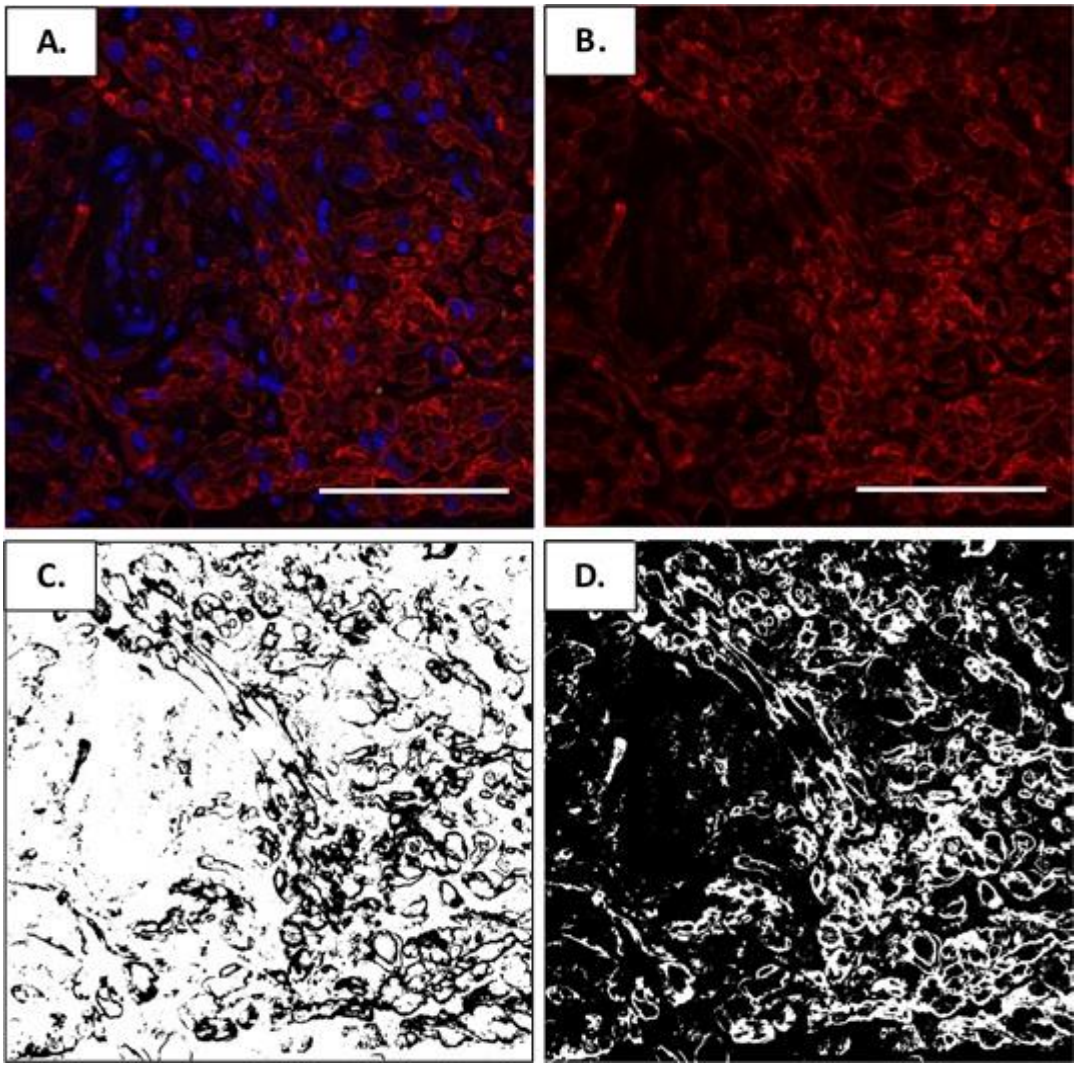

Figure 2.9. Fluorescent image intensity quantification using Image J. (A.) A multiple immuno-labelled Z-stack image is averaged and flattened to a 2D-image, in this example hyperpolarisation-activated cyclic nucleotide-gated channel 4 (**HCN4**) is in **red** and **nuclei** in **blue**. (B.) The multiple immuno-labelled image is split, **HCN4** membrane labelling only in **red**, and a mean intensity measurement is taken. (C.) The IJ-Isodata thresholding approach is applied which separates fluorescent signal from the background; black outline represents the signal intensity picked up by the algorithm which is reasonably true for HCN4 membrane labelling, another mean intensity measurement is taken. (D.) Background mean signal intensity is also calculated, black now represents the background and is the inverse image of C. Mean fluorescent signal intensity for an image is calculated by subtracting background mean intensity from IJ-Isodata thresholding mean intensity. 60x NA 1.4, 50µm scale bar. Original figure.

2.6.6 Histological stains

Histology stains (**Chapter 5**) were carried out by me within the Histology Service Unit, University of Otago. Fresh filtered solutions were used to carry out the following protocols. Histology staining for all nDM and DM samples per stain was carried out on the same day and imaged the following day (n=7 per group, 1 SAN cryosection per protein per n).

2.6.6.1 Masson's trichrome

Masson's trichrome stain was used to determine extracellular matrix / connective tissue between the nDM and DM SAN as a measure of fibrosis. Frozen 20 µm SAN tissue cryosections on slides were taken from the -20 °C freezer and thawed at room temperature for 5 minutes. Slides were placed in distilled water for 30 seconds, fixed using 10% formalin (Thermo Fisher) for 1 minute and rinsed in running tap water then distilled water for 30 seconds each. The nuclei were stained using 0.5% celestine blue for 2 minutes, placed in running water for 30 seconds, nuclei further stained using Gill's haematoxylin for 1 minute and placed in running water for 1 minute. Following, slides were placed in Scott's water for 1 minute, which acts as a gentle blueing reagent of nuclear chromatin and nuclear membranes altering the soluble red haematoxylin into an insoluble blue dye, and also minimises the loss of tissue sections. Slides were placed in running water for 1 minute, stained using 0.5% acid fuchsin for 1 minute, which differentiates cytoplasm / muscle from connective tissue, rinsed in 4x change of distilled water and left in the water until the dye no longer leaked from the tissue into the water (about 2 minutes). Next, slides were placed in 1% phosphomolybdic acid for 2 minutes, which contests with the acid fuchsin, drained, and placed in 0.5% methyl blue for 1 minute to stain collagen / connective tissue. Slides were then rinsed in 4x change of distilled water and left for any excess dye to leak out (about 2 minutes). To differentiate the stains slides were then placed in 1% acetic acid for 1 minute 30 seconds, subsequently placed in 3x 100% alcohol for

30 seconds each for dehydration, and cleared in 3x xylene (Thermo Fisher) for 1 minute each, and finally mounted using non-aqueous DPX mounting medium (Merck) and coverslips attached (22x60 mm), then left to dry. Constituents of the various solutions used are listed in **Table 2.6**.

Table 2.6. Compositions of solutions used for Masson's trichrome stain.

Solution	Ingredients	Manufacturer
0.5% Celestine blue	Celestine blue B 2.5g	Sigma-Aldrich
	Amonium iron (III) sulphate dodecahydrate 25g	Sigma-Aldrich
	Glycerol 70ml	Sigma-Aldrich
	Distilled water 500ml	-
Gill's haematoxylin	Ready to use	Leica Biosystems
Scott's water	Magnesium sulphate 10g	Scharlab
	Sodium hydrogen carbonate 1g	BDH Laboratory
	Distilled water 1L	-
0.5% Acid fuchsin	Acid fuchsin 0.5g	Raymond A Lamb
	Glacial acetic acid 0.5ml	Sigma-Aldrich
	Distilled water 100ml	-
1% Phosphomolybdic acid	Phosphomolybdic acid 1g	AnalaR
	Distilled water 100ml	-
0.5% Methyl Blue	Methyl blue 0.5g	Amber Scientific
	Glacial acetic acid 0.625ml	Sigma-Aldrich
	Distilled water 25ml	-
1% Acetic acid	Glacial acetic acid 1ml	Sigma-Aldrich
	Distilled water 100ml	-

2.6.6.2 Oil Red O

Oil Red O stain was used to investigate fat droplets present within or amongst the nDM and DM SAN cardiomyocytes. The dye solution used has a high affinity to fat and is insoluble to the hydrophobic fat droplets. Constituents of the solutions used are given in **Table 2.7**. Frozen 20 µm SAN tissue cryosections were taken from the -20 °C freezer and thawed at room temperature for 5 minutes. Tissue sections were fixed in 10% neutral buffered formalin (Thermo Fisher) for 1 minute, washed in running tap water and then in distilled water for 30 seconds each. Fat droplets were stained using Oil Red O working solution, a fat-soluble dye, for 10 minutes. Next, slides were washed in running tap water for 2 minutes. Nuclei were stained by Gill's haematoxylin for 10 seconds. Then slides were washed in running tap water for 2 minutes, Scott's water for 1 minute and again in running tap water for 1 minute. Aqueous Immu-Mount (Thermo Scientific) mounting medium was used for preservation of the tissue section, coverslips (22x60 mm) were gently attached to prevent any movement of possible fat droplets and their edges were sealed with nail varnish. Liver tissue sections (20 µm) provided by the Histology Service Unit (University of Otago) were used as positive controls.

Table 2.7. Compositions of solutions used for Oil Red O stain.

Solution	Ingredients and Quantity	Manufacturer
Oil Red O stock solution	Oil Red O 0.5g	Raymond A Lamb
	Absolute isopropyl alcohol, 70% alcohol 100ml	Lab Supply
Oil Red O working solution	Oil Red O stock 24ml	-
	Distilled water 16ml	-
Gill's haematoxylin	Ready to use	Leica Biosystem
Scott's water	Magnesium sulphate 10g	Scharlab
	Sodium hydrogen carbonate 1g	BDH Laboratory
	Distilled water 1L	-

2.6.7 Image capture and stain quantification

Histology stained slides were captured using a slide scanner (Leica Aperio, scanner console version 102.0.7.5). The image zoom magnification ranged from 2x – 40x. Aperio ImageScope software (Leica, version 12.3.0.5056) was used to select the SAN region for analysis. The SAN region was identified by the appearance of unorganised and less densely packed cardiomyocytes in comparison to the right atrial cardiomyocytes with the presence of the SAN artery, in addition, the nearest HCN4-positive labelled tissue section was also used as a guide. Fibrosis and fat deposits within the SAN were semi-quantified using 4x images on Adobe Photoshop CS5.1 software (version 12.1). The SAN region was cropped out from the surrounding right atrial tissue. Masks were created on the blinded samples in order to define the colour intensity range for pixels to be identified as blue and red for fibrosis and fat droplets respectively, the masks were also independently verified by another researcher (**Figure 2.10**). The software calculated the total number of pixels in the SAN region, then based on the mask application to the SAN region, calculated pixel count for fibrosis and fat droplets per SAN

image. This was then calculated to a percentage value for fibrosis and fat per SAN image. Fibrosis was analysed within the SAN which excludes the connective border surrounding or neighbouring the SAN (that provides physiological protection from hyperpolarisation effects of the right atria).

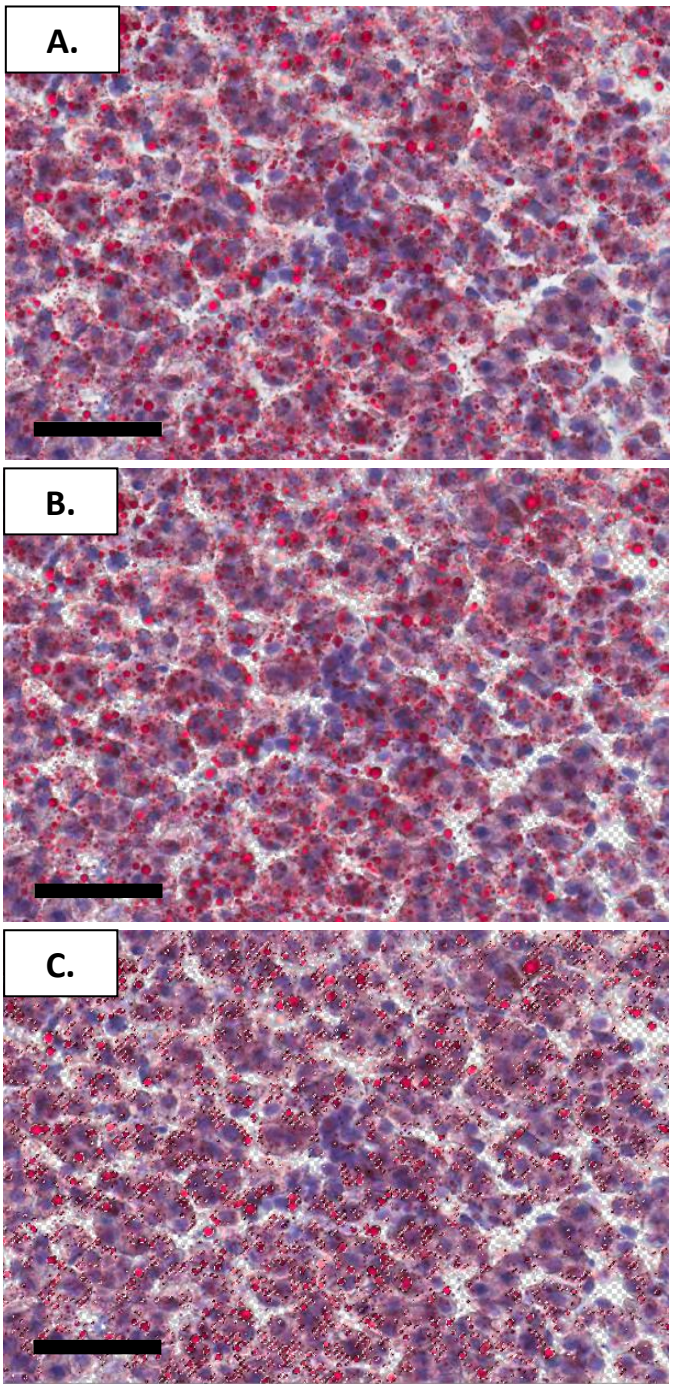

Figure 2.10. Histology image quantification using Photoshop. (A.) Oil Red O stained image of liver tissue section where **fat droplets** are stained in **red**, other **tissue** in **pink** and **nuclei** in **purple**. This image gives a total pixel count of 784168 arbitrary units (a.u.) (B.) The background (white pixels) are removed which now gives a pixel count of 743981 a.u. (C.) The pre-determined mask, that defines the colour range to be picked up, is applied and as can be seen by the speckled outlines present the majority of red i.e. fat droplets stained are selected, which provides a pixel count of 146748 a.u. The percentage of fat droplets in this image is 19.7% ((100 / 743981) x 146748). 40x, 50µm scale bar. Original figure.

2.7. SDS-PAGE and western blotting

2.7.1 Tissue homogenate preparation

Tissue (SAN and LV) homogenisation was carried out using the Bullet Blender Storm 24® (Next Advance Inc., USA). The LV sample was used to represent a part of the working myocardium that abundantly expresses cx43 (37). Cx43 expression in the SAN samples and LV sample was compared to determine the relative purity of the SAN samples. For adequate protein extraction, two SANs with the closest intrinsic HR's were pooled together and counted as one 'n' (12 - 14 animals were used in total resulting in an n=6-7 per group). The frozen tissue was cut, placed with stainless steel beads (0.9 - 2.0 mm bead blend, Lab Supply) and radioimmunoprecipitation assay (RIPA) lysis buffer with protease inhibitors and dithiothreitol cocktail added on the day of homogenisation (**Table 2.8** and **Table 2.9**). The tissue was blended until sufficient homogenisation had been achieved. The homogenate samples were placed on ice for 15 minutes and clarified via centrifuging for 30 minutes at 15000 rcf at 4°C (Centrifuge 5430R, Germany). Homogenate protein concentrations were determined at 280 nm using Gen data analysis software (Biotek) with the RIPA buffer cocktail used as a blank, successively, homogenate samples were flash-frozen in liquid nitrogen and stored at -80°C.

Table 2.8. Radioimmunoprecipitation lysis buffer.

Ingredients	Concentration	Manufacturer
Triton X-100	1% (vol/vol)	Lab Supply
SDS (Sodium dodecyl sulphate)	0.1% (w/vol)	Thermo Scientific
Tris-HCl (pH 7.4)	50 mM	VWR Global Science
NaCl	150 mM	Lab Supply
EDTA (Ethylene diamine tetraacetic acid)	1 mM	Sigma

Table 2.9. List of protease inhibitors and dithiothreitol. The protease inhibitors and dithiothreitol (DTT) added to the radioimmunoprecipitation lysis buffer. Note: DTT is a reducing agent used to prevent oxidation.

Ingredients	Concentration	Protease target	Manufacturer
Benzamide	1 mM	Trypsin	Thermo Fisher
Leupeptin	2 µg/ml	Cysteine	Sigma
Aprotinin	2 µg/ml	Serine	Sigma
Pepstatin A	2 µg/ml	Aspartyl proteases	Sigma
PMSF (Phenylmethylsulfonyl fluoride)	0.525 mM	Serine	Sigma
DTT (Dithiothreitol)	2.5 mM	-	Thermo Fisher

2.7.2 SDS-PAGE

SDS PAGE was carried out using the traditional Laemmli method (224). Acrylamide resolving gels of various percentages were cast using 1.5 mm gel casting plates (Bio-Rad) (**Table 2.10**). Methanol was used to form a flat resolving gel surface and polymerisation was allowed for 45 minutes. Following resolving gel polymerisation, the methanol was removed and the stacking gel (**Table 2.11**) was placed on top of the resolving gel. A 10 or 15-well comb of 1.5 mm thickness was immersed in the stacking gel solution to form protein loading wells. The stacking gel was also set to polymerise for 45 minutes. The comb was then removed, wells were rinsed with distilled water, and gels were set up in a vertical electroporator tank (Bio-Rad) filled with 1x running buffer (**Table 2.12**).

Table 2.10. Resolving gels. The components used to cast the resolving gels at different percentages. Note: different gel percentages were used for different proteins to ensure appropriate resolution of the different molecular weights. 6%: ryanodine receptor 2 (RyR2). 8%: hyperpolarisation-activated cyclic nucleotide-gated channel 4 (HCN4), Na^+-Ca^{2+} exchanger 1 (NCX1), sarco(endo)plasmic reticulum Ca^{2+}-ATPase 2a (SERCA2a), Ca^{2+} / calmodulin-dependent protein kinase II (CaMKII), connexin 45 ((cx)45), cx43 and glyceraldehyde-3-phosphate dehydrogenase (GAPDH). 10%: muscarinic type 2 (M_2) receptor, phospholamban, L-type ($Ca_v1.2$) and T-type ($Ca_v3.1$) Ca^{2+} channels and GAPDH.

Ingredients	6% gel (µl)	8% gel (µl)	10% gel (µl)	Manufacturer
MilliQ-H_2O	4632	4232	3832	Lab Supply
Tris-HCl (1.5 M, pH 8.8)	2000	2000	2000	VWR Global Science
Acrylamide / Bis acylamide (40%, 37.5:1)	1200	1600	2000	Bio-Rad
SDS (Sodium dodecyl sulphate) (10%)	80	80	80	Thermo Scientific
APS (Ammonium persulfate) (10%)	80	80	80	Sigma
TEMED (Tetramethylethylenediamine)	8	8	8	Acros Organics

Table 2.11. Stacking gel.

Ingredients	4% gel (µl)	Manufacturer
MilliQ-H_2O	5032	Lab Supply
Tris-HCl (1.5 M, pH 6.8)	2000	VWR Global Science
Acrylamide / Bis acylamide (40%, 37.5:1)	800	Bio-Rad
SDS (Sodium dodecyl sulphate) (10%)	80	Thermo Scientific
APS (Ammonium persulfate) (10%)	80	Sigma
TEMED (Tetramethylethylenediamine)	8	Acros Organics

Table 2.12. Running buffer.

Ingredients	Concentration	Manufacturer
Glycine	192 mM	Thermo Scientific
Tris	25 mM	VWR Global Science
SDS (Sodium dodecyl sulphate)	1% (w/vol)	Thermo Scientific

2.7.3 Western blotting

A protein marker (10 µl for ryanodine receptor 2 (RyR2) and 6 µl for all other proteins, precision plus protein dual colour, Bio-Rad) was loaded into the first well to view protein movement and estimate molecular weight. 70 µg (RyR2) or 40 µg (all other proteins) of nDM and DM SAN homogenate samples were mixed (1:1) with 2x Laemmli blue buffer (**Table 2.13**). The samples were denatured by heat block incubation at 37°C for 30 minutes followed by vortex and centrifugation of the samples at 15000 rcf (Centrifuge 5418, Germany) for 2 minutes at room temperature. Samples were run at 60 V through the stacking gel and into the resolving gel for approximately 40 minutes visualised via the bromophenol blue dye. Then at

100 V through the resolving gel until the desired protein separation had been achieved. The total running time varied from 1.5 – 6 hours depending on the molecular weight of the protein of interest.

Table 2.13. 2x Laemmli buffer.

Ingredients	Concentration	Manufacturer
Tris-HCl (pH 6.8)	125 mM	VWR Global Science
Glycerol	20% (w/vol)	VWR Global Science
SDS (Sodium dodecyl sulphate)	4% (w/vol)	Thermo Scientific
Bromophenol blue	0.004% (w/vol)	Sigma
2-Mercaptoethanol	10% (w/vol)	Sigma

The classic wet transfer approach was utilised for binding of proteins from the gel to the nitrocellulose membrane (0.45 µm pore size, Bio-Rad) using a transfer tank (Bio-Rad). A transfer sandwich of sponge, filter paper, gel, nitrocellulose membrane, filter paper and sponge was made and sealed in a cassette. The nitrocellulose membrane was placed in the direction towards the cathode and the gel in the direction towards the anode ensuring protein transfer onto the membrane. The gel was immersed in cold 1x transfer buffer (**Table 2.14**) with an ice pack and transfer took place at 45 V overnight (RyR2) or at 60 V for 3 hours (all other proteins) at 4°C. Post transfer the nitrocellulose membrane was washed using 1x PBS for removal of transfer buffer and gel remnants before being stained using ponceau S (0.1 g (weight/ vol) in 5% acetic acid (vol/ vol)) to determine transfer quality and imaged using the Syngene PXi 4 (GeneSys v1.6.9.0 software, Synoptics, Cambridge, UK). The ponceau S was then washed off using 0.5% tween (LabChem) PBS (PBST) until cleared and blocked using 5% non-fat milk in PBST either overnight at 4°C or for 2 hours at room temperature (RyR2 only) on a shaker. The following day the membrane was washed 3x in 1x PBS for 5 minutes each.

Table 2.14. Transfer buffer. Note: SDS was only added to the ryanodine receptor 2 protein transfer buffer.

Ingredients	Concentration	Manufacturer
Glycine	192 mM	Thermo Scientific
Tris	25 mM	VWR Global Science
Methanol	20% (vol/vol)	Lab Supply
SDS	0.01% (w/vol)	Thermo Scientific

Primary antibodies (**Table 2.15**) were diluted in 20% foetal bovine serum albumin and 1x PBS or 1x tris-buffered saline (TBS) (**Table 2.16**). Primary antibody incubation was carried out for 4 hours (RyR2 only) or 2 hours (all other proteins) at room temperature. This was followed by 3x 5-minute washes in PBST and then 3x 1x PBS washes. Secondary antibodies diluted in 1x PBS or TBS were incubated for 1 hour 30 minutes at room temperature (**Table 2.15** (dilution) and **Table 2.17**). 3x 5-minute PBST and 3x 1x PBS washes followed. The membrane was then incubated in SuperSignal West Pico Plus Chemiluminescent Substrate working solution (Thermo Scientific) for 5 minutes at room temperature ensuring the nitrocellulose membrane was covered with solution. The membrane was then placed between clear plastic sheets before chemiluminescence signal detection and capture using Syngene PXi 4. Syngene PXi 4 exposure times were adjusted to obtain suitable image capture per protein without over exposure (over exposed bands could be detected by the Studio Lite software used for western blot analysis).

Table 2.15. Primary antibodies for western blotting. Primary and secondary antibody dilutions used for western blot. Antibodies were diluted in 20% foetal bovine serum (vol/vol) in 1x PBS and 0.01% NaN_3 (w/vol) or 1x TBS (Ca^{2+} / calmodulin-dependent protein kinase II (CaMKII)).

Primary Antibody	Clonality	Primary Antibody Dilution	Species	Manufacturer	Secondary Antibody Dilution
HCN4	Polyclonal	1:1000	Rabbit	Alomone	1:10000
Cx43	Polyclonal	1:5000	Rabbit	Sigma-Aldrich	1:20000
GAPDH	Monoclonal	1:1000	Mouse	GeneTex	1:10000
Cx45	Polyclonal	1:1000	Rabbit	Alomone	1:10000
SERCA2a	Polyclonal	1:5000	Rabbit	Badrilla	1:10000
NCX1	Monoclonal	1:1000	Rabbit	Abcam	1:10000
CaMKII δ	Polyclonal	1:7000	Rabbit	Thermo Fisher	1:5000
RyR2	Monoclonal	1:1000	Mouse	Abcam	1:10000
Phospholamban	Monoclonal	1:5000	Mouse	Badrilla	1:10000
M_2	Monoclonal	1:1000	Rabbit	Abcam	1:10000
$Ca_v1.2$ α_{1C}	Polyclonal	1:1000	Rabbit	Alomone	1:10000
$Ca_v3.1$ α_{1G}	Polyclonal	1:1000	Rabbit	Alomone	1:10000

Table 2.16. Tris-buffered saline buffer. pH to 7.6.

Ingredients	Concentration (M)	Manufacturer
Tris	0.5	VWR Global Science
Sodium chloride	1.5	Lab Supply

Table 2.17. Secondary antibodies for western blotting. Antibodies were diluted in 1x PBS or 1x TBS.

Secondary Antibody	Species	Manufacturer
Anti-Rabbit	Goat	Abcam
Anti-Mouse	Goat	Abcam

2.7.4 Membrane stripping

Due to the small quantities of the SAN homogenates, the nitrocellulose membranes were stripped using stripping buffer (**Table 2.18**) to remove the primary and secondary antibody, and then re-used. The nitrocellulose membrane was stripped with pre-heated 50°C stripping buffer solution and placed in a 50°C pre-heated water bath for 40 minutes. Next, the membrane was washed 3x using PBST for 5 minutes each, before 3 further washes in 1x PBS. To confirm the membrane strip, the membrane was incubated in SuperSignal West Pico Plus Chemiluminescent Substrate working solution for 5 minutes, then imaged as before using the Syngene PXi v4 for a minimum of 10 minutes. If membrane strip was successful (no labelling remained) then the membrane was washed 3x in PBST and incubated in 5% non-fat milk PBST block overnight at 4°C. Otherwise, another 10-minute strip would occur in the same manner and the membrane would be re-checked for confirmation of the membrane strip as before. The following day the protocol was repeated for the next protein. A maximum of 3 – 4 strips and probes were possible from one membrane as each strip would also result in a loss of protein from the membrane. The proteins were probed in different orders during technical repeats and the strip / re-probe protocol.

Table 2.18. Stripping buffer.

Ingredients	Concentration	Manufacturer
Tris-HCl (pH 6.8)	0.5M	VWR Global Science
SDS (Sodium dodecyl sulphate)	10% (w/vol)	Thermo Scientific
2-Mercaptoethanol	1% (vol/vol)	Sigma

2.7.5 Western blot analysis

The western blot images were analysed using the Studio Lite software (version 5.2) where the average value of the background around each band was subtracted. Protein expression was semi-quantified and normalised to the housekeeping protein, glyceraldehyde-3-phosphate dehydrogenase (GAPDH).

2.8. Statistical analysis

Prism (version 7.02, GraphPad software) and SigmaPlot (version 14.0, Systat software) were used for statistical analysis. A *p-value <0.05* was regarded as statistically significant. All data are presented as mean values ± the standard error of the mean (mean ± SEM). nDM and DM grouped data were analysed using an unpaired or paired t test (Prism). Where the F statistic was significant for an unpaired t test and thus data did not meet equality of variance, the non-parametric Mann Whitney test was used. For Langendorff experiments where Ca^{2+} and drug concentrations were altered, intrinsic HRs and the difference from baseline for each concentration per group were tested for outliers using the robust regression and outlier removal (ROUT) method with a false discovery rate set to 5% (225). A two-way ANOVA with repeated measures and Holm-Sidak post hoc test for multiple comparisons (SigmaPlot) was used to compare Ca^{2+} and drug intrinsic HR changes between the nDM and DM groups. Non-linear regression (Prism) was used to compare normalised intrinsic HR responses between nDM and DM.

CHAPTER 3

Expression of Sinoatrial Node Clocks, Connexins and Cholinergic Proteins in the Type 2 Diabetic Sinoatrial Node

3.1. Introduction

Type 2 diabetes (DM) has adverse effects on *in vivo* and intrinsic (*ex vivo*) heart rate (HR) in animal models and humans (*in vivo* HR only) (19, 165, 173, 183). However, the DM-induced pathological remodelling of the sinoatrial node (SAN) remains unknown. To evaluate potential DM remodelling in the intrinsic SAN clocks, the expression levels of the key voltage membrane (Vm) and Ca^{2+} clock proteins were investigated. The proteins explored included the Vm clock proteins hyperpolarisation-activated cyclic nucleotide-gated channel 4 / funny current (HCN4 / I_f), Na^+-Ca^{2+} exchanger 1 (NCX1 / I_{NCX1}), long-lasting (L-type / $I_{Ca,L}$) and transient-lasting (T-type / $I_{Ca,T}$) Ca^{2+} channels and the Ca^{2+} clock proteins sarco(endo)plasmic reticulum Ca^{2+}-ATPase 2a (SERCA2a), phospholamban and ryanodine receptor 2 (RyR2). To determine whether the protein facilitating action potential (AP) propagation within the SAN is affected by DM, connexin 45 (cx45) expression was also examined. Additionally, the expression of the muscarinic type 2 (M_2) receptor was studied to assess whether increased parasympathetic input to the heart (Bussey *et al*., unpublished data) resulted in upregulation of cholinergic proteins at the SAN level. Lastly, Ca^{2+} / calmodulin-dependent protein kinase II (CaMKII) protein expression was also investigated in the DM SAN due to its emerging pathological roles in the DM heart (207, 226, 227).

Why are these clock, cx45, cholinergic and CaMKII proteins important to investigate? The role of these proteins being essential in mediating and / or modulating physiological pacemaking and propagating the AP has been extensively characterised (Chapter 1) (21, 50, 228, 229). Additionally, CaMKII is subject to a variety of post-translational modifications such as auto-phosphorylation, oxidation, O-GlcNAcylation and S-nitrosylation (230, 231). These modifications are amplified in the DM setting resulting in chronically active CaMKII (94, 207,

226, 230, 232, 233). Chronically active CaMKII results in pathological alterations to Ca^{2+} handling and cycling, disrupting pacemaking and cardiac function (94, 95). Moreover, there is evidence that these proteins are subject to expression level alterations in type 1 DM and other cardiovascular diseases, which is summarised in **Table 3.1**. The literature in Table 3.1 presents mRNA (type 1 and type 2 DM) and / or protein (type 1 DM) expression changes in the clock, cx and CaMKII profiles. As far as I know, no mRNA or protein data is available for the M_2 receptor expression in the type 1 DM SAN. Also, to the best of my knowledge, no current data exists on the protein expression of the SAN clock, cx, cholinergic and CaMKII proteins in the type 2 DM SAN.

Table 3.1. A summary of the literature describing mRNA and protein expression levels in diabetes and other cardiovascular pathologies in humans and / or animal models. Key: A significant (*p<0.05*) increase (upward arrow) or decrease (downward arrow) is marked. Abbreviations: sinoatrial node (SAN), hyperpolarisation-activated cyclic nucleotide-gated channel 4 (HCN4), Na^{+}-Ca^{2+} exchanger 1 (NCX1), long-lasting type Ca^{2+} channel (L-type Ca^{2+} channel), transient type Ca^{2+} channel (T-type Ca^{2+} channel), sarco(endo)plasmic reticulum Ca^{2+}-ATPase 2a (SERCA2a), ryanodine receptor 2 (RyR2), connexin 45 (cx45), connexin 43 (cx43), muscarinic type 2 receptor (M_2 receptor) and Ca^{2+} / calmodulin-dependent protein kinase II (CaMKII).

Mediator	mRNA in type 2 diabetic SAN	Protein in type 1 diabetic SAN	mRNA in type 1 diabetic SAN	mRNA and / or protein in other cardiac chambers and / or aetiologies	References
HCN4	↓	↓	No change.	↓ exercise training, atrial tachyarrhythmias & heart failure. ↑ atrial fibrillation.	(197, 234-241).
NCX1	No change.	↓	↑	↑ dilated & ischemic cardiomyopathy, coronary artery disease & heart failure. No change also reported in heart failure, dilated cardiomyopathy & valvular heart disease. ↓ in type 1 diabetes.	(197, 234, 236, 241-247).
L-type Ca^{2+} Channel	↓ ($Ca_v1.2$), ↓ ($Ca_v1.3$).	↓ ($Ca_v1.3$).	-	↓ $Ca_v1.2$ in pulmonary hypertension induced right atrial hypertrophy.	(197, 234, 241, 248-250).
T-type Ca^{2+} Channel	↓ ($Ca_v3.1$), ↓ ($Ca_v3.2$).	↓ ($Ca_v3.1$).	↑ ($Ca_v3.1$), ↑ ($Ca_v3.2$).	↑ $Ca_v3.1$ & $Ca_v3.2$ right ventricular hypertrophy. No difference in $Ca_v3.1$ in pulmonary hypertension induced right atrial hypertrophy.	(197, 234, 236, 241, 250, 251).

SERCA2a	No change.	↓	No change.	↓ dilated & ischemic cardiomyopathy, coronary artery disease, heart failure & type 1 diabetes. No change also reported in dilated cardiomyopathy.	(197, 234, 236, 243, 246, 252-257).
Phospholamban	No change.	-	No change.	↓ & no change also found in dilated cardiomyopathy. ↓ in type 1 diabetes.	(197, 236, 246, 253, 255-257).
RyR2	↑	↓ / no change.	No change.	No change in dilated cardiomyopathy. ↓ in type 1 diabetes.	(197, 234, 236, 241, 246, 255, 256).
Cx45	↓	↓ / no change.	↑	↑ in human ventricular tissue in ischemic & dilated cardiomyopathy. But, ↓ also in human ventricular tissue in ischemic & idiopathic cardiomyopathy.	(197, 236, 241, 258-260).
Cx43	↓	-	No change.	↓ in human ventricular tissue in ischemic, dilated & idiopathic cardiomyopathy.	(197, 236, 258, 259).
M_2 receptor	-	-	-	↑ in human diabetic atria & in sudden infant deaths. ↑ in whole heart of type 1 but not type 2 diabetes. No change in dilated & ischemic cardiomyopathy.	(261-265).
CaMKII	-	↑ oxidised CaMKII.	-	↑ oxidised, phosphorylated or O-GlcNAcylated CaMKII in right atria / ventricular tissue of type 2 diabetes.	(207, 226, 232, 233).

The animal models from type 1 (mRNA and protein) and type 2 (mRNA only) DM SAN studies all presented significantly reduced intrinsic HR (197, 234, 236). This itself suggests the importance of these expression changes in either being responsible for, or a manifestation of, the low intrinsic HR in DM (197, 234, 236).

3.2. Aims and hypothesis

The **aim** of this study was to determine the expression levels of the key molecular proteins involved in the SAN clocks (Vm clock: HCN4, NCX1, L-type and T-type Ca^{2+} channels and Ca^{2+} clock: SERCA2a, phospholamban and RyR2), conduction pathway (cx45), the cholinergic pathways (M_2 receptor) and CAMKII in the DM SAN.

I **hypothesised** a decrease of the Vm clock proteins, HCN4, NCX1, L-type and / or T-type Ca^{2+} channel, and Ca^{2+} clock proteins, RyR2 and SERCA2a, an increase in phospholamban, a decrease in cx45, and an increase in M_2 receptors and CaMKII in the SAN of DM ZDF rats compared to their nDM littermates.

3.3. Methodology

Detailed methodology used in this study can be found in Chapter 2. Experimental techniques applied here include echocardiography, heart tissue retrieval, Langendorff, LabChart analysis, SDS-PAGE, western blotting and statistical analysis.

3.4. Results

3.4.1 Animal characterisation

Table 3.2 lists the standard measurements for the Zucker Diabetic Fatty (ZDF) rat characterisation. The ZDF$^{fa/fa}$ rats had significantly increased blood glucose compared to their ZDF$^{fa/+,\ +/+}$ littermates, indicating their diabetic (DM) state. The ZDF$^{fa/fa}$ rats that presented a 'high' blood glucose reading above the maximum reading of 33.3 mmol/L on the glucometer (3 out of 14 rats) were excluded from the blood glucose analysis only in Table 3.2. No difference in the body weight existed between the ZDF$^{fa/fa}$ and ZDF$^{fa/+,\ +/+}$ rats. Also, consistent with previous studies, a markedly reduced intrinsic HR was confirmed within the isolated hearts of ZDF$^{fa/fa}$ rats in addition to a significantly lower *in vivo* HR also being present. This data was collected using sodium pentobarbital anaesthesia. Collectively, this confirmed the DM status of the ZDF$^{fa/fa}$ rats.

Table 3.2. Animal characteristics from non-diabetic (nDM) and diabetic (DM) rats used for western blotting. nDM n=12 and DM n=14, mean ± SEM, unpaired t test or Mann-Whitney test (weight and *ex vivo* intrinsic heart rate).

Parameter	nDM (ZDF$^{fa/+,\ +/+}$)	DM (ZDF$^{fa/fa}$)	*P value*
Weight (g)	379 ± 6	392 ± 10	*>0.05*
Blood glucose (mmol/L)	10.7 ± 0.5	31.4 ± 0.7	** <0.0001*
***In vivo* heart rate (bpm)**	343 ± 8	289 ± 10	** <0.001*
***Ex vivo* intrinsic heart rate (bpm)**	188 ± 12	148 ± 6	** <0.01*

3.4.2 Connexins within the sinoatrial node

3.4.2.1 No difference in cx43 expression within the non-diabetic and type 2 diabetic sinoatrial node

In order to determine the expression levels of both the Vm and Ca^{2+} SAN clocks, cx45 and cholinergic proteins, it was important to confirm the tissue samples isolated were SAN in origin. Absence of connexin 43 (cx43) within the SAN is an indicator of a relatively pure (central) SAN sample (266, 267). However, small levels of cx43 in the SAN homogenates are likely to arise from the inclusion of the SAN periphery during isolation and / or cx43 islands existing within the SAN as seen during immunofluorescence (267). Six out of fourteen SAN samples displayed cx43 islands present within or neighbouring the SAN region which were not directly connected to the right atrial tissue (**Figure 3.1**). During SAN dissection, the cx43 islands cannot be visually known hence their exclusion was not possible. There was no significant difference in cx43 expression in the nDM and DM SAN samples (nDM 2.70 ± 0.50 versus DM 3.48 ± 1.13, *p=0.53*). Whether cx43 presence arises due to larger cx43 expression within some SAN samples, more cx43 islands, or better isolation of the central SAN cannot be determined. The cx43 presence within the SAN was also compared to a left ventricle (LV) sample where cx43 is expressed abundantly. In **Figure 3.1**, it can be observed that the nDM and DM SAN samples contained considerably less cx43 compared to the LV sample, indicating that they were relatively pure SAN samples.

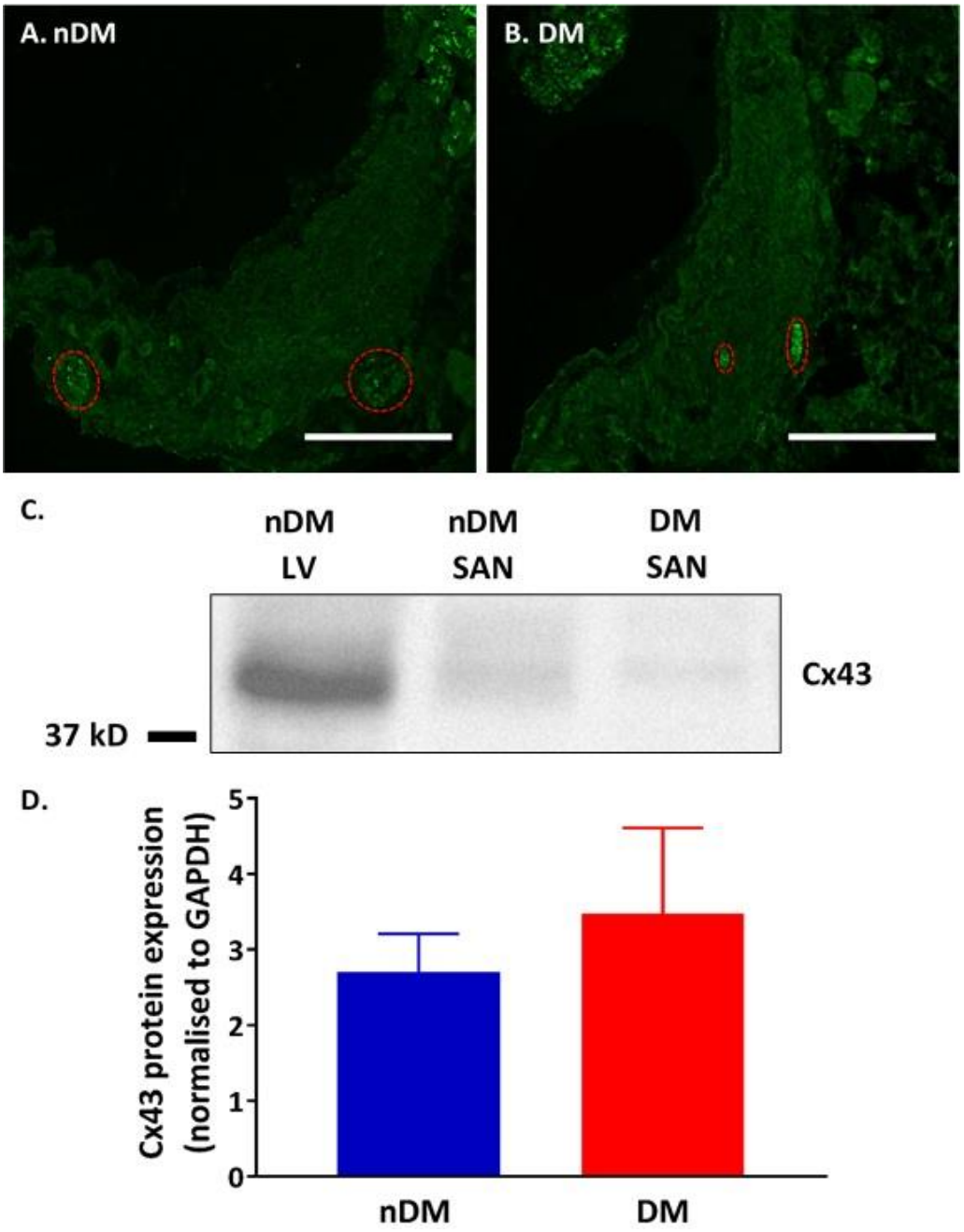

Figure 3.1. Connexin 43 expression within the sinoatrial node. A typical example of non-diabetic (A. nDM) and diabetic (B. DM) sinoatrial node (SAN, dull green) with connexin 43 (**cx43**, **bright green**) islands highlighted in red circles. The cx43 islands in the immunofluorescent images vary in size, location and intensity. (C.) Representative western blot comparison of cx43 presence within the nDM and DM SAN samples, in addition to a nDM left ventricle (LV) sample, where cx43 is expressed abundantly. (D.) No significant difference was found in the cx43 expression between the nDM and DM SAN. (A. and B.) 10x NA 0.45, 200µm scale bar, cx43 islands visualised in 6 / 14 SANs, nDM n=7 and DM n=7 (C. and D.) nDM n=9 and DM n=8, 2 – 5 technical replicates, (D.) mean ± SEM, *p>0.05*, Mann-Whitney test.

3.4.2.2 Cx45 expression is unchanged in the type 2 diabetic sinoatrial node

Upon confirmation that the SAN samples were relatively free of contaminating right atrial tissue, cx45 expression was examined in the nDM and DM SAN. Cx45 expression was not different between the nDM and DM SAN (nDM 0.97 ± 0.15 versus DM 1.00 ± 0.08, *p=0.87*, **Figure 3.2**). This suggests a change in cx45 protein levels within the SAN is not responsible for the low intrinsic HR present in the DM SAN.

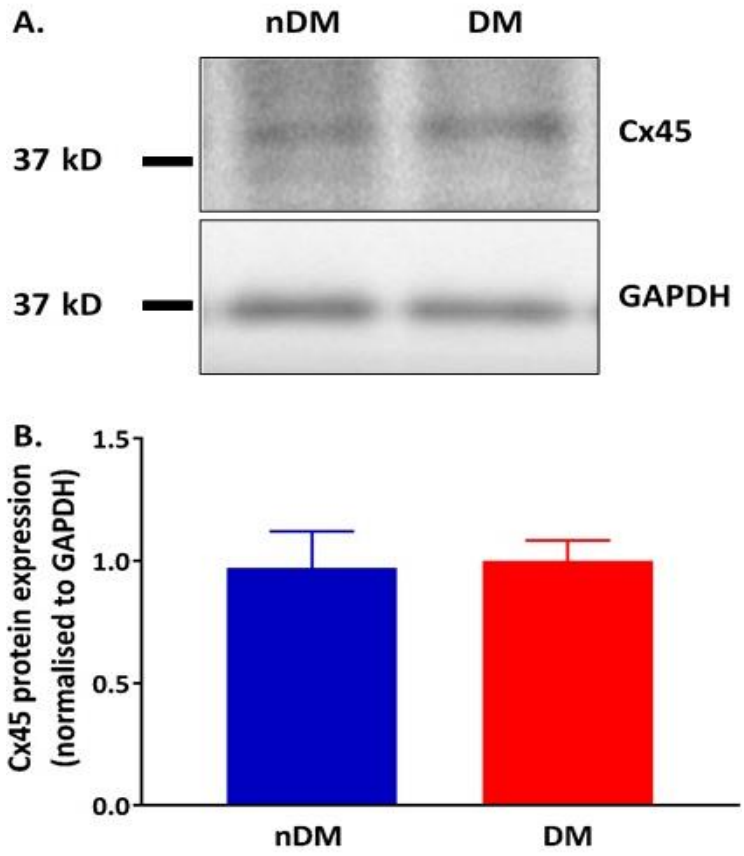

Figure 3.2. Connexin 45 expression within the sinoatrial node. (A.) Representative western blot of connexin 45 (cx45) and glyceraldehyde-3-phosphate dehydrogenase (GAPDH) as a loading control in the non-diabetic (nDM) and diabetic (DM) sinoatrial node (SAN) tissue. (B.) No significant difference was found in the cx45 expression between the nDM and DM SAN. nDM n=6 and DM n=7, 1 technical replicate, mean ± SEM, *p>0.05*, unpaired t test.

3.4.3 Vm clock expression: upregulated HCN4 and NCX1 but unchanged L-type and T-type Ca^{2+} channels in the type 2 diabetic sinoatrial node

Next, the expression levels of the Vm clock proteins HCN4, NCX1, L-type ($Ca_v1.2$) and T-type ($Ca_v3.1$) Ca^{2+} channels were examined. HCN4 expression was significantly increased in the DM SAN compared to the nDM SAN (nDM 0.83 ± 0.07 versus DM 1.67 ± 0.19, *p=0.0005*, **Figure 3.3**). The NCX1 expression was markedly upregulated in the DM SAN (nDM 1.00 ± 0.16 versus DM 1.52 ± 0.15, *p=0.04*, **Figure 3.4**). However, L-type (nDM 0.86 ± 0.07 versus DM 0.97 ± 0.10, *p=0.43*, **Figure 3.5**) and T-type (nDM 0.89 ± 0.13 versus DM 0.85 ± 0.13, *p=0.81*, **Figure 3.6**) Ca^{2+} channel expression were not different in the DM SAN.

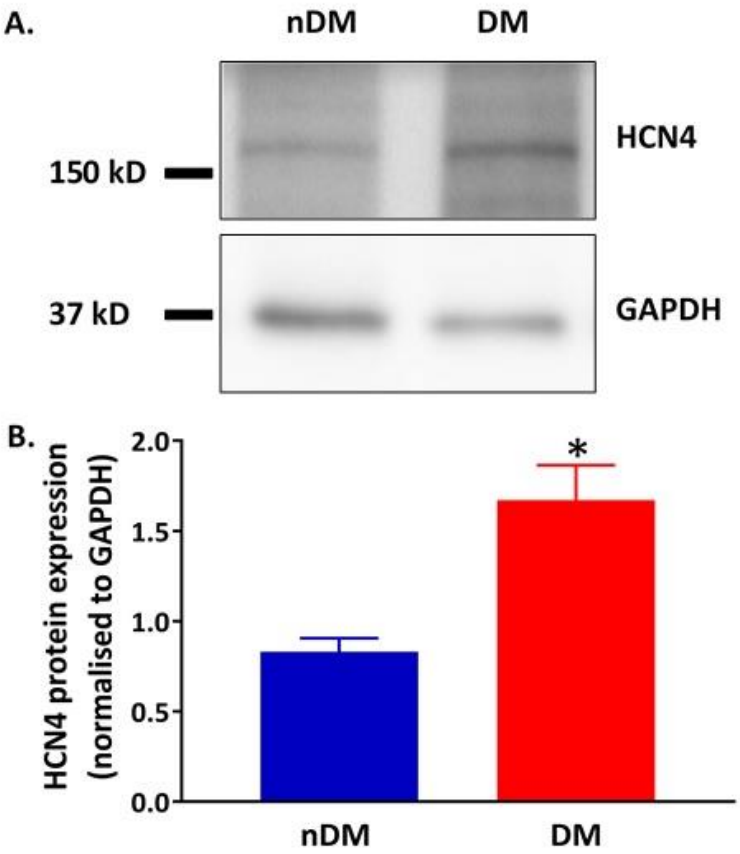

Figure 3.3. Hyperpolarisation-activated cyclic nucleotide-gated channel 4 expression within the sinoatrial node. (A.) Representative western blot of hyperpolarisation-activated cyclic nucleotide-gated channel 4 (HCN4) and glyceraldehyde-3-phosphate dehydrogenase (GAPDH) as a loading control in the non-diabetic (nDM) and diabetic (DM) sinoatrial node (SAN) tissue. (B.) A significantly increased HCN4 expression was found in the DM compared to the nDM SAN. nDM n=9 and DM n=8, 3 – 6 technical replicates, mean ± SEM, * $p<0.05$, Mann-Whitney test.

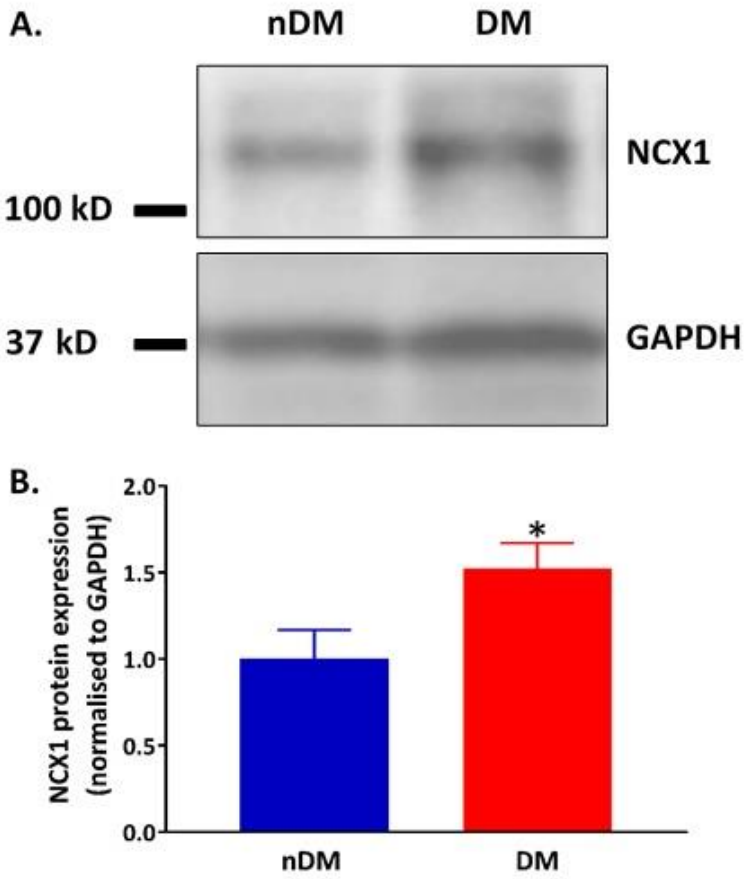

Figure 3.4. Na^{+}-Ca^{2+} exchanger 1 expression within the sinoatrial node. (A.) Representative western blot of Na^{+}-Ca^{2+} exchanger 1 (NCX1) and glyceraldehyde-3-phosphate dehydrogenase (GAPDH) as a loading control in the non-diabetic (nDM) and diabetic (DM) sinoatrial (SAN) tissue. (B.) A significantly increased NCX1 expression was found in the DM compared to nDM SAN. nDM n=6 and DM n=7, 3 – 4 technical replicates, mean ± SEM, * *p<0.05*, unpaired t test.

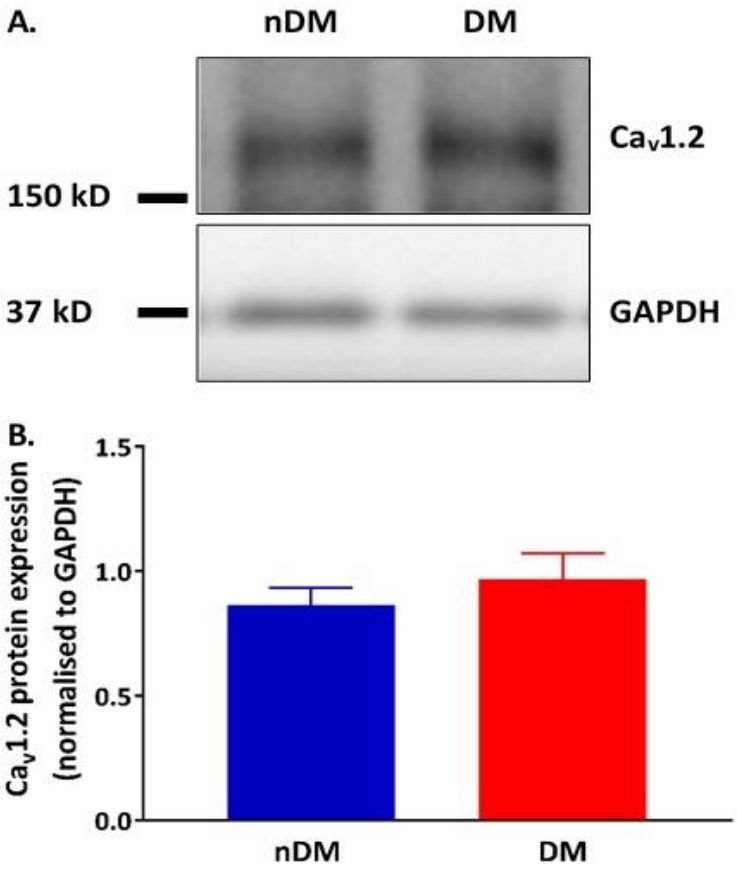

Figure 3.5. L-type Ca^{2+} channel expression within the sinoatrial node. (A.) Representative western blot of L-type Ca^{2+} channel ($Ca_v1.2$) and glyceraldehyde-3-phosphate dehydrogenase (GAPDH) as a loading control in the non-diabetic (nDM) and diabetic (DM) sinoatrial node (SAN) tissue. (B.) No significant difference was found in the $Ca_v1.2$ expression between the nDM and DM SAN. nDM n=6 and DM n=7, 1 technical replicate, mean ± SEM, *p>0.05*, unpaired t test.

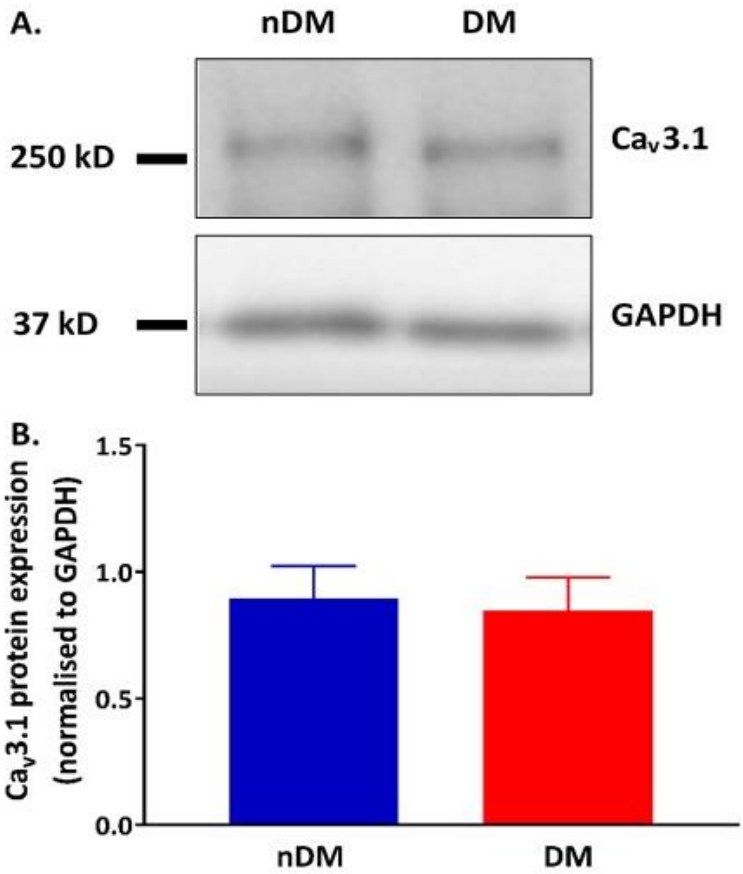

Figure 3.6. T-type Ca^{2+} channel expression within the sinoatrial node. (A.) Representative western blot of T-type Ca^{2+} channel ($Ca_v3.1$) and glyceraldehyde-3-phosphate dehydrogenase (GAPDH) as a loading control in the non-diabetic (nDM) and diabetic (DM) sinoatrial node (SAN) tissue. (B.) No significant difference was found in the $Ca_v3.1$ expression between the nDM and DM SAN. nDM n=5 and DM n=5, 1 technical replicate, mean ± SEM, *p>0.05*, unpaired t test.

3.4.4 Ca^{2+} clock expression: upregulated phospholamban with no change to SERCA2a in the type 2 diabetic sinoatrial node

Following, the expression of the Ca^{2+} clock proteins SERCA2a, phospholamban and RyR2 were examined. No change was found in SERCA2a expression (nDM 2.77 ± 0.55 versus DM 3.33 ± 0.38, *p=0.41*, **Figure 3.7**), but a significant increase in phospholamban was observed in the DM compared to the nDM SAN (nDM 0.96 ± 0.06 versus DM 1.51 ± 0.18, *p=0.03*, **Figure 3.8**). However, when comparing the SERCA2a to phospholamban ratio (a proxy for SERCA2a activity

(257, 268, 269)) no significant difference was found between the groups (nDM 2.97 ± 0.68 versus DM 2.37 ± 0.34, *p=0.43*, **Figure 3.9**). Unfortunately, RyR2 expression within the SAN could not be determined by western blot, because low amounts of total protein obtained from the rat SAN were not sufficient to accurately determine the very large RyR2 protein (see Figure 3.i in the Appendix).

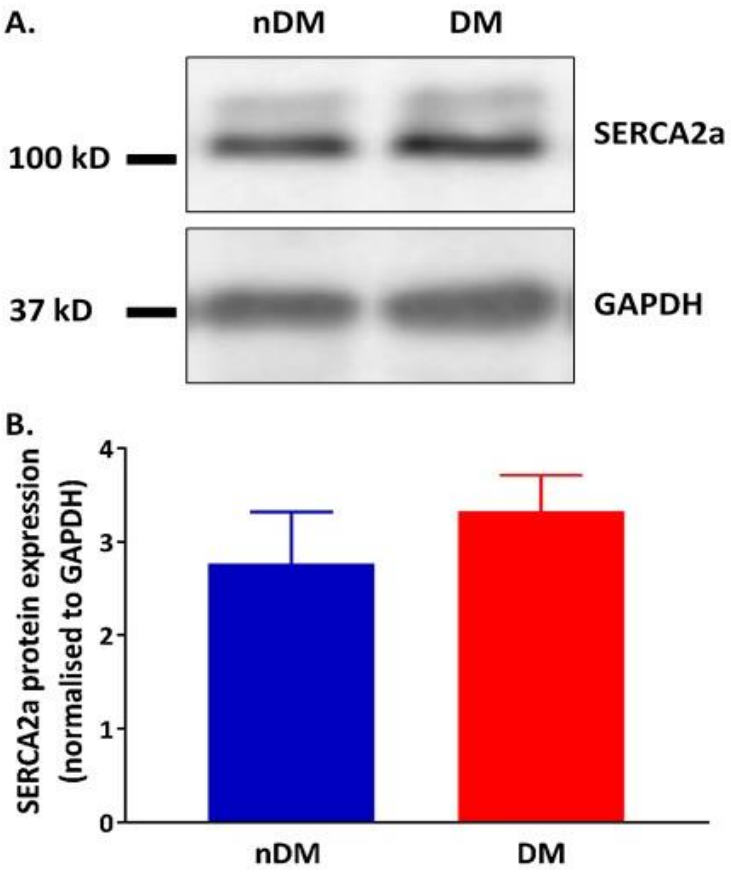

Figure 3.7. Sarco(endo)plasmic reticulum Ca^{2+}-ATPase 2a expression within the sinoatrial node. (A.) Representative western blot of sarco(endo)plasmic reticulum Ca^{2+}-ATPase 2a (SERCA2a) and glyceraldehyde-3-phosphate dehydrogenase (GAPDH) as a loading control in the non-diabetic (nDM) and diabetic (DM) sinoatrial node (SAN) tissue. (B.) No significant difference was found in the SERCA2a expression between the nDM and DM SAN. nDM n=6 and DM n=7, 3 – 4 technical replicates, mean ± SEM, *p>0.05*, unpaired t test.

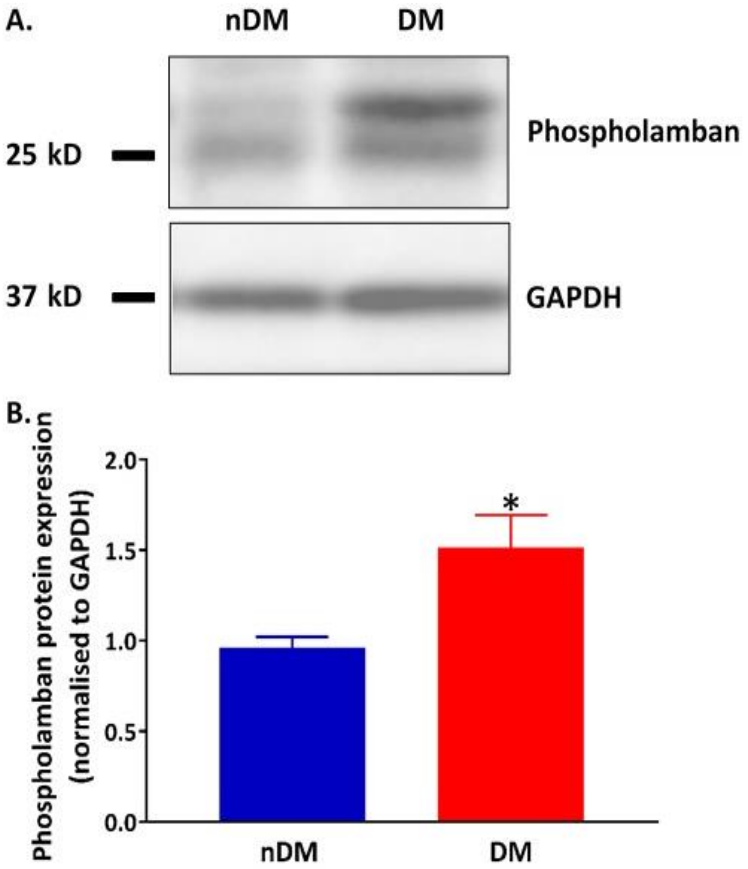

Figure 3.8. Phospholamban expression within the sinoatrial node. (A.) Representative western blot of phospholamban and glyceraldehyde-3-phosphate dehydrogenase (GAPDH) as a loading control in the non-diabetic (nDM) and diabetic (DM) sinoatrial node (SAN) tissue. (B.) A significantly increased phospholamban expression was found in the DM compared to nDM SAN. nDM n=6 and DM n=7, 2 technical replicates, mean ± SEM, * *p<0.05*, Mann-Whitney test.

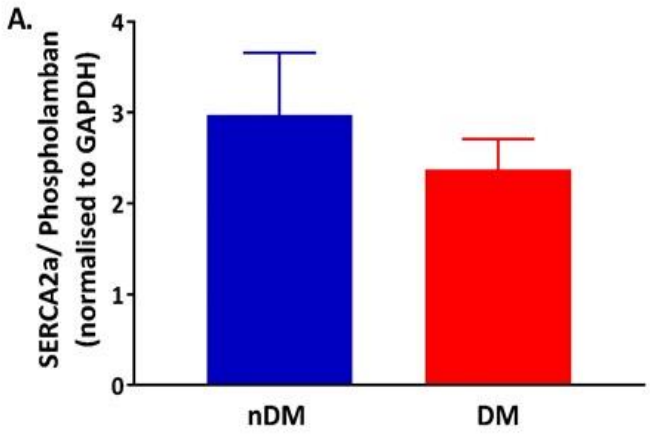

Figure 3.9. Sarco(endo)plasmic reticulum Ca^{2+}-ATPase 2a to phospholamban ratio within the sinoatrial node. (A.) No difference was found between the sarco(endo)plasmic reticulum Ca^{2+}-ATPase 2a (SERCA2a) to phospholamban ratio in the non-diabetic (nDM) and diabetic (DM) sinoatrial node (SAN). nDM n=6 and DM n=7, mean ± SEM, *p>0.05*, unpaired t test.

3.4.5 Increased M_2 receptor in the type 2 diabetic sinoatrial node

Next, the expression of the cholinergic protein the M_2 receptor was investigated in the DM SAN. A significantly upregulated M_2 expression was found in the DM SAN (nDM 1.14 ± 0.18 versus DM 3.14 ± 0.80, *p=0.002*, **Figure 3.10**).

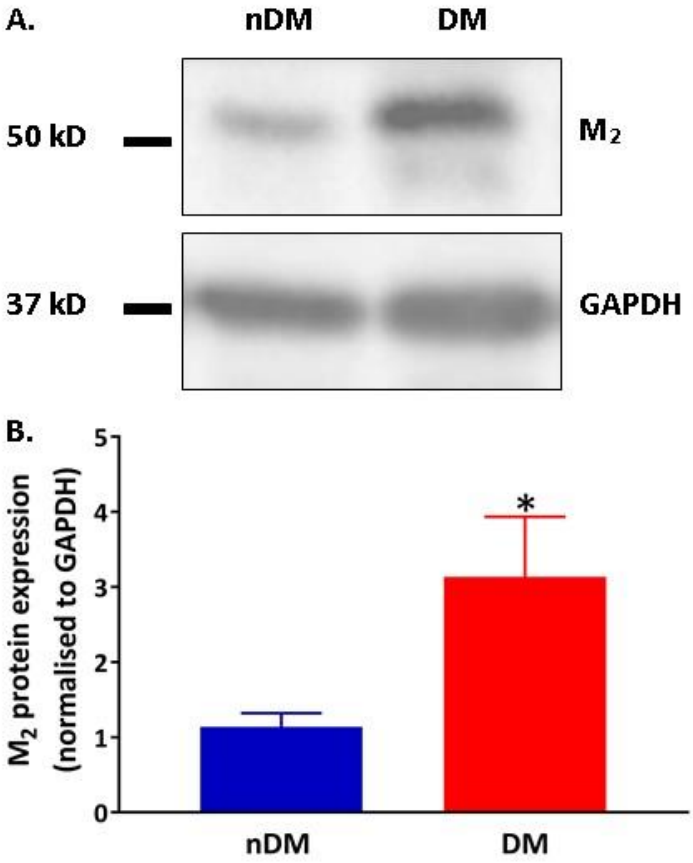

Figure 3.10. Muscarinic type 2 receptor expression within the sinoatrial node. (A.) Representative western blot of muscarinic type 2 (M_2) receptor and glyceraldehyde-3-phosphate dehydrogenase (GAPDH) as a loading control in the non-diabetic (nDM) and diabetic (DM) sinoatrial node (SAN) tissue. (B.) A significantly increased M_2 expression was found in the DM compared to nDM SAN. nDM n=6 and DM n=7, 3 technical replicates, mean ± SEM, * *p<0.01*, Mann-Whitney test.

3.4.6 Increased total CaMKII in the type 2 diabetic sinoatrial node

The expression of total CaMKII (δ isoform) was also determined in the nDM and DM SAN due to its emerging associations with DM cardiovascular disease (207, 226, 227) and role in the SAN pacemaking control (97, 270). CaMKII expression was significantly upregulated in the DM SAN (nDM 1.19 ± 0.25 versus DM 2.42 ± 0.33, *p=0.01*, **Figure 3.11**).

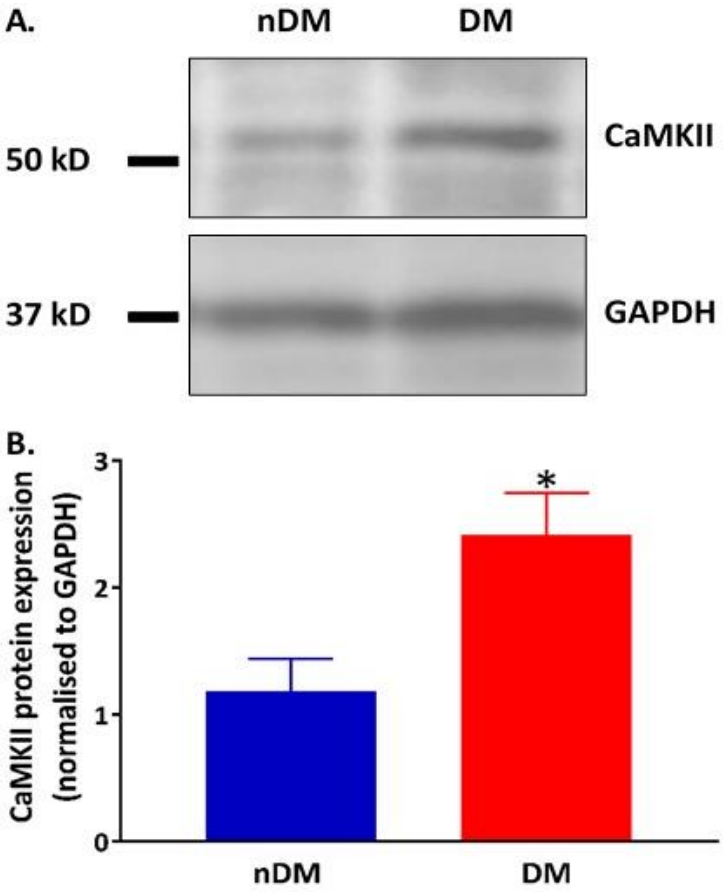

Figure 3.11. Ca^{2+} / calmodulin-dependent protein kinase II expression within the sinoatrial node. (A.) Representative western blot of Ca^{2+} / calmodulin-dependent protein kinase II (CaMKII) and glyceraldehyde-3-phosphate dehydrogenase (GAPDH) as a loading control in the non-diabetic (nDM) and diabetic (DM) sinoatrial node (SAN) tissue. (B.) A significantly increased CaMKII expression was found in the DM compared to nDM SAN. nDM n=6 and DM n=7, 3 - 4 technical replicates, mean ± SEM, * *p<0.05*, unpaired t test.

The relative changes in expression as determined by western blot are summarised in **Table 3.3**.

Table 3.3. A summary of the relative expression changes in the voltage membrane and Ca^{2+} clocks, connexins and cholinergic proteins between the non-diabetic (nDM) and diabetic (DM) sinoatrial node (SAN). Note: western blots for all nDM and DM SAN samples can be found in Figure 3.ii in the Appendix. Abbreviations: hyperpolarisation-activated cyclic nucleotide-gated channel 4 (HCN4), Na^{+}-Ca^{2+} exchanger 1 (NCX1), long-lasting type (L-type) and transient type (T-type) Ca^{2+} channels, sarco(endo)plasmic reticulum Ca^{2+}-ATPase 2a (SERCA2a), ryanodine receptor 2 (RyR2), muscarinic type 2 (M_2) receptor, connexin 45 (cx45), connexin 43 (cx43) and Ca^{2+} / calmodulin-dependent protein kinase II (CaMKII).

Protein	nDM : DM ratio	*P Value*
HCN4	1 : 2.01	** <0.01*
NCX1	1 : 1.52	** <0.05*
L-type Ca^{2+} Channel	1 : 1.12	*0.43*
T-type Ca^{2+} Channel	1 : 0.95	*0.80*
SERCA2a	1 : 1.20	*0.41*
Phospholamban	1 : 1.58	** <0.05*
RyR2	1 : 9.89	*N/A*
M_2 receptor	1 : 2.75	** <0.01*
Cx45	1 : 1.03	*0.87*
Cx43	1 : 1.29	*0.53*
CaMKII	1 : 2.04	** <0.05*

3.5. Discussion

In this chapter, the expression levels of the key Vm and Ca^{2+} clock, cx45 and cholinergic proteins were compared in the nDM and DM SAN. The main findings of this study are: (a) significantly increased expression of HCN4, NCX1, phospholamban, M_2 receptor and total

CaMKII in the DM SAN and (b) no difference in cx43, cx45, L-type and T-type Ca^{2+} channels, SERCA2a and SERCA2a to phospholamban ratio in the DM SAN.

3.5.1 Can these findings explain the lower intrinsic heart rate in type 2 diabetes?

3.5.1.1 Vm clock

3.5.1.1.1. HCN4

The presence of HCN4 in the SAN avoids quiescence by preventing the occurrence of a steady resting membrane potential and initiating early-mid diastolic depolarisation promoting HR generation (21, 271). HCN4 knockout is embryonically lethal and HCN4 presence has been shown to be essential for cardiac development and continued embryogenesis (13, 272, 273). Transgenic studies show *in vivo* HR with HCN4 overexpression remains unchanged (274), however, HCN4 knockdown presents differing results with reports of no change in mean *in vivo* HR but with increased SAN pauses (275, 276) and significant decreases resulting in bradycardia (274, 277, 278) compared to respective controls. Why there are differing results with *in vivo* HR and HCN4 knockdown remains unknown. Spontaneous firing rates (a proxy for intrinsic HR) of isolated SAN cardiomyocytes exhibited no difference with HCN4 overexpression (274) and were significantly decreased with HCN4 knockdown (274-278) compared to respective controls. Additionally, SAN cardiomyocytes with HCN4 knockdown displayed more hyperpolarised membrane potentials, therefore, taking longer to reach AP threshold (275, 276). Collectively, the research demonstrates the need for HCN4 for diastolic depolarisation promoting (intrinsic) HR generation and maintaining a relatively 'stable' rhythm.

In my study, HCN4 protein expression was significantly increased in DM compared to nDM SAN. The DM SAN HCN4 results are opposed to the protein and mRNA expression findings in the type 1 DM and type 2 DM SAN respectively where significant decreases in HCN4 were found (**Table 3.1**) (197, 234, 235, 241). The upregulated HCN4 in the DM ZDF SAN was surprising, and did not support the hypothesis, as it would oppose the lower intrinsic HR observed in DM. This would suggest a compensation to maintain the physiological intrinsic HR (seen with HCN4 overexpression) rather than the DM decrease (seen with HCN4 knockdown). The apparent mismatch between HCN4 expression and reduced intrinsic HR in DM requires additional studies. Therefore, in **Chapter 4** the functional contribution of HCN4 channels to intrinsic HR generation in the nDM and DM SAN will be investigated using the HCN4 inhibitor ivabradine.

3.5.1.1.2. NCX1

The markedly increased NCX1 in the DM SAN did not support my hypothesis of reduced NCX1 expression being responsible for lower intrinsic HR in DM. It suggests that, the upregulated NCX1 might not be a direct contributor to the lower DM intrinsic HR; however, this is likely to be dependent on NCX1 mode of function. NCX1 and possible DM SAN NCX1 functional contributions to different parts of the action potential are considered below. These NCX1 findings are in contrast to the protein and mRNA expression findings in the type 1 DM and type 2 DM SAN where significant reductions and no change in NCX1 were shown respectively (**Table 3.1**) (197, 234, 241).

NCX1 has several functions throughout the cardiac AP. NCX1 forward mode (Ca^{2+} efflux Na^{+} influx) functions to couple both SAN clocks during mid-late diastolic depolarisation, promoting

the triggering of the AP upstroke and HR generation (21, 69, 279). NCX1 reverse mode (Na^+ efflux Ca^{2+} influx) functions to contribute to the intracellular Ca^{2+} ($[Ca^{2+}]_i$) transient during the late-plateau phase of the AP upstroke (79, 280). NCX1 forward mode is again active during repolarisation aiding in Ca^{2+} efflux and cardiomyocyte relaxation (79). The exact timing of NCX1 transition to forward-reverse-forward mode during the AP is difficult to determine and remains debatable (280). This switch is dependent on Na^+ and Ca^{2+} gradients as well as membrane potential (E_m) (79, 281). More simply, forward mode Ca^{2+} efflux is preferred during a negative E_m and high $[Ca^{2+}]_i$ (during diastolic depolarisation ($E_m < I_{NCX1}$) and repolarisation ($E_m = I_{NCX1}$)), while during a positive E_m and high intracellular Na^+ ($[Na^+]_i$) reverse mode Ca^{2+} influx is preferred (during AP upstroke / plateau ($E_m > I_{NCX1}$)) (79, 282). The physiological contribution of NCX1 in the forward mode is suggested to be greater than its contribution in the reverse mode; the affinity for $[Ca^{2+}]_i$ being greater than extracellular Ca^{2+} (unless $[Na^+]_i$ is greatly increased, AP duration is prolonged, if SR Ca^{2+} or I_{Ca} entry is inhibited) (79, 280-282). The local rise in $[Ca^{2+}]_i$ enabled by the presence of functioning Ca^{2+} channels is likely to avert NCX1 reverse mode Ca^{2+} influx (83). Also, the unitary Ca^{2+} influx via L-type Ca^{2+} channels is much more effective, being ~1000 times greater compared to NCX1 (i.e. 1 L-type Ca^{2+} channel for ~1000 NCX1) (83, 283). So, with forward mode activity dominating, I suggest the functional importance of NCX1 in pacemaking to be SAN clock coupling during diastolic depolarisation and initiation of AP upstroke > repolarisation (species dependent) = / > reverse mode Ca^{2+} influx during AP upstroke / plateau.

3.5.1.1.3. Diabetic NCX1 during diastolic depolarisation

Complete NCX1 knockout is embryonically lethal (284-286), while overexpression has been shown to maintain basal *in vivo* and intrinsic HR (287, 288). It has been suggested that forward mode NCX1 might either directly contribute to and / or accelerate diastolic depolarisation,

however, whether this is likely could be disputed as the NCX1 overexpression studies demonstrated no quickening of either basal *in vivo* or intrinsic HR (287). Support for NCX1 implication in diastolic depolarisation arises from experiments where forward mode NCX1 is inhibited by the use of low Na^+ solutions which results in cessation of spontaneous AP generation in guinea-pig SAN (279). Furthermore, in these experiments, HCN4 inhibition alone results in slowing but not the cessation of the AP, but with the addition of low Na^+ solution the cessation of spontaneous AP again results (279). Additional supporting evidence comes from a SAN and atrial specific NCX1 knockout model that exhibits significantly decreased *in vivo* HR (attributed to a junctional escape rhythm) and absence of spontaneous firing rates (a proxy for intrinsic HR) of isolated SAN cardiomyocytes (289, 290). So, knockout of HCN4 results in significantly reduced intrinsic HR, but pacemaking is not completely abolished, whereas SAN / atrial specific NCX1 knockout results in SAN / atrial standstill or SAN exit block (289, 291). Collectively, this highlights the importance of NCX1 for pacemaking, which possibly even outweighs the significance of HCN4's contribution to diastolic depolarisation and HR generation. This implies that the upregulated NCX1 in the DM SAN in its forward mode function during diastolic depolarisation would at least maintain clock coupling and intrinsic HR generation, rather than cause the lower intrinsic HR in DM. In addition, why the forward mode NCX1 should (primarily) contribute to diastolic depolarisation with the significantly increased HCN4 expression warranted follow up.

3.5.1.1.4. Diabetic NCX1 during upstroke-plateau

The physiological role of NCX1 mediated Ca^{2+} influx is suggested to be negligible in the nDM SAN (83). However, in the DM SAN the increased reverse mode function might simply arise due to enhanced NCX1 expression and / or because the DM SAN requires Ca^{2+} influx via NCX1. The increased reverse mode NCX1 would provide a greater contribution of Ca^{2+} influx to the

$[Ca^{2+}]_i$ transient and SR refilling for subsequent AP cycle (79, 280). Several potential reasons for the need for augmented Ca^{2+} influx in the DM SAN can exist. First, an increased requirement for NCX1 mediated Ca^{2+} influx would not appear to be due to decreased Ca^{2+} influx through the more effective T-type and L-type Ca^{2+} channels (no change in expression of the Ca^{2+} subunits investigated). Still, whether the function of the Ca^{2+} channels in DM is affected remains unknown. In opposition to this view, overexpression of NCX1 resulted in an increased peak $I_{Ca,L}$ with delayed inactivation of the channel (292). Collectively, delayed $I_{Ca,L}$ inactivation along with reverse mode NCX1 would provide greater Ca^{2+} contribution to the $[Ca^{2+}]_i$ transient which might result in Ca^{2+} overload and significant lengthening of the AP at 50% and 90% repolarisation (292, 293). Whether this occurs in the DM SAN cardiomyocytes remains to be evaluated.

Secondly, increased reverse mode Ca^{2+} influx might be required due to reduced SR Ca^{2+} content in the DM SAN. The quantity of Ca^{2+} released from the SR depends on the trigger (I_{Ca}) and SR Ca^{2+} content (294). Reductions in SR Ca^{2+} content can arise due to reduced SERCA2a activity and / or increased Ca^{2+} release by RyR2, possibly due to increased β-adrenergic stimulation (165) and increased CaMKII in the DM ZDF model (see section 3.5.2.2 below) (80, 294, 295). The lack of a difference in SERCA2a to phospholamban ratio between the nDM and DM SAN expression suggests that SERCA2a activity is unaffected. Unfortunately, RyR2 expression in the SAN could not be completely assessed due to the low quantity of total protein extracted from the SAN and requires future study. In **Chapter 4**, the SR Ca^{2+} content will be indirectly investigated by determining the intrinsic HR response achieved in the nDM and DM hearts upon administration of caffeine (an SR Ca^{2+} store depletor).

3.5.1.1.5. Diabetic NCX1 during repolarisation

Another reason for NCX1 upregulation in the DM SAN might be to aid in repolarisation through its forward mode function (79, 296). However, how successful NCX1 might be with this increased dependency of this role within the rat DM SAN could also be questioned since the role of NCX1 in Ca^{2+} decay and extrusion physiologically in rodents is quite minimal (16, 78). To evaluate this NCX1 (and SERCA2a) function further, the effect of increasing external Ca^{2+} ($[Ca^{2+}]_o$) on intrinsic HR in the nDM and DM hearts will be investigated in **Chapter 4**. Additionally, the increased influence of NCX1 on Ca^{2+} extrusion in the DM SAN might come at the expense of decreasing SR Ca^{2+} content as more NCX1 could be competing with SERCA2a for cytosolic Ca^{2+} removal (60, 79). As mentioned before, the SR Ca^{2+} content will be assessed (**Chapter 4**).

3.5.1.2 Ca^{2+} clock: SERCA2a and phospholamban

In the Ca^{2+} clock, despite the significantly upregulated phospholamban and with no change to SERCA2a expression, no difference was found in the SERCA2a to phospholamban ratio. These results suggest unaffected Ca^{2+} uptake into the SR, but whether SERCA2a activity is compromised requires quantification as a mismatch between expression levels and function can exist (253, 297, 298). Inhibition of SERCA2a decreases local Ca^{2+} releases (LCRs), spontaneous firing rate in isolated SAN cardiomyocytes and reduces diastolic depolarisation rate indicative of the necessity of SERCA2a activity and SR refilling for basal pacemaker function and accordingly HR generation (80). Therefore, SERCA2a activity (via increasing $[Ca^{2+}]_o$) and SR Ca^{2+} content (using caffeine) will be studied in the nDM and DM SAN (**Chapter 4**). The lack of difference in SERCA2a expression mirrors the type 2 and type 1 DM mRNA findings but not the significantly decreased protein in type 1 DM SAN previously reported, however, phospholamban has not been previously reported to increase in the DM SAN but

has been shown to be increased in other type 1 DM cardiac tissue (**Table 3.1**) (197, 234, 236, 246, 256, 297).

Also, the phosphorylation status of phospholamban (a negative regulator of SERCA2a) should be explored in the future. This will indicate the extent of phospholamban inhibition on SERCA2a activity and therefore the rate of decline of $[Ca^{2+}]_i$ during repolarisation between the nDM and DM SAN. Greater inhibition of phospholamban on SERCA2a lengthens repolarisation and AP duration (80, 81, 299). An increase in phospholamban protein expression has been previously reported in non-SAN tissue in type 1 DM with significantly reduced phosphorylation at sites serine-16 and threonine-17 (246, 256, 257). Insulin treatment of the type 1 hearts restored phospholamban protein levels and phospholamban phosphorylation levels (256). However, whether reduced phospholamban phosphorylation exists in the DM SAN remains to be examined in the future. This is particularly relevant because the markedly increased expression of CaMKII could potentially shift the phosphorylation from the protein kinase A (PKA) serine-16 regulated site to the CaMKII threonine-17 regulated site (300).

3.5.2 Modulators of intrinsic and *in vivo* heart rate

3.5.2.1 Cholinergic protein: M_2 receptor

The DM SAN presented significantly increased M_2 receptor expression, as hypothesised. M_2 receptors are the target of acetylcholine released by parasympathetic nerves to the heart at the SAN cardiomyocyte level and by cardiomyocytes via the non-neuronal intrinsic cardiac cholinergic system, which physiologically results in lowering *in vivo* HR (117, 145, 159). Additionally, in the isolated DM heart, an enhanced non-neuronal intrinsic cholinergic system within SAN cardiomyocytes might result in lowering intrinsic HR. The upregulated M_2 receptor

might be due to augmented parasympathetic nerve activity to the DM SAN (Bussey *et al*., unpublished data) and could account for the reduced *in vivo* HR found in some DM ZDF rats, as seen in this study and previously in our lab (182). Additionally, it is possible that the significantly increased M_2 receptor results due to increased expression and / or activity of the non-neuronal cardiac intrinsic cholinergic system. In isolated rat cardiomyocytes, external application of acetylcholine or pilocarpine (a cholinergic agonist) was found to increase protein expression of choline acetyltransferase (intrinsic acetylcholine synthesis) through M_2 receptor activation, however, whether this also resulted in changes to M_2 receptor protein expression was not investigated (160). Although, in isolated rat ventricular cardiomyocytes, pyridostigmine (acetylcholine inhibitor) resulted in decreased mRNA expression of choline acetyltransferase, vesicular acetylcholine transporter and M_2 receptor (301). Collectively, this suggests M_2 receptor activity is implicated in controlling changes to M_2 receptor expression and this activity is regulated by neuronal and non-neuronal cholinergic systems. Transgenic overexpression of the M_2 receptor results in significantly enhanced R-R interval duration *in vivo* (a measure for bradycardiac response) upon phenylephrine administration compared to control (302). This suggests increased M_2 receptor expression can enhance cholinergic responses *in vivo* in DM.

Does greater cholinergic activity follow greater M_2 receptor expression? Typically, research investigating alterations in DM cardiac neuronal input have used indirect measures of neuronal activity (via heart rate variability, receptor expression, radioactivity, enzyme activities, circulating neurotransmitters) rather than providing more conclusive direct evidence of cardiac nerve recordings as they are invasive and often difficult to acquire (303-309). Hence, predominantly the available literature cannot directly address this question.

Nonetheless, previous research from our lab in the DM ZDF model has found markedly increased cardiac sympathetic activity to the heart from direct nerve recordings, which has also shown markedly increased β_1-adrenergic receptor protein expression in the right atria (165). Therefore, in line with this, I suggest that the increase in M_2 receptor expression found in the DM SAN relates to the increased parasympathetic nerve activity determined in the DM rats (Bussey *et al*., unpublished data) and possibly further amplified in a positive-feedback manner via the non-neuronal intrinsic cholinergic activity (i.e. neuronal acetylcholine-induced increases in the intrinsic cholinergic system activity and expression, and also M_2 receptor activity and expression) (159). Furthermore, my finding is supported by previous studies that reported increased M_2 receptor expression in type 1 and type 2 DM hearts but did not investigate direct nerve recordings (**Table 3.1**) (261, 263, 310). Additionally, separate studies reported indirect measures of increased parasympathetic input to the type 1 DM heart, including the SAN, but did not report receptor expression (217, 309). The responsiveness to cholinergic stimulation on intrinsic HR between the nDM and DM SAN will be assessed in **Chapter 4**.

3.5.2.2 CaMKII

CaMKII (δ, the predominant cardiac isoform) expression was also significantly upregulated in the DM SAN (311, 312). This finding was not surprising as an emerging pathological role for chronically active CaMKII has been shown in the DM heart (207, 226, 227). The physiological role of CaMKII in increasing *in vivo* HR (HR modulation) in response to increased sympathetic input is well known (via phosphorylation actions on L-type Ca^{2+} channels, phospholamban, RyR2) (96, 312). Less considered is the involvement of CaMKII for basal (*ex vivo*) intrinsic SAN cardiomyocyte pacemaker firing (HR generation) (97, 270). Evaluation of CaMKII involvement

in rabbit SAN cardiomyocyte pacemaking using a CaMKII inhibitor (KN-93) has revealed a marked ~50% reduction in $I_{Ca,L}$ (97). The $I_{Ca,L}$ steady-state inactivation was found to be markedly enhanced i.e. a significant number of channels were inactive upon CaMKII inhibition and unavailable for pacemaking (97). In support of CaMKII effects on the L-type Ca^{2+} channels was the presence of phosphorylated (active) CaMKII beneath the SAN cardiomyocyte membrane whilst total CaMKII (inactive) was uniformly distributed throughout the SAN cardiomyocyte as shown by immunofluorescence (97). This implies CaMKII in SAN cardiomyocytes is primarily required for basal $I_{Ca,L}$ for pacemaking and remains functionally active during isolated SAN cardiomyocytes pacemaking (intrinsic HR) responses.

Chronically / pathologically active CaMKII (via auto-phosphorylation, oxidation, O-GlcNAcylation or S-nitrosylation mechanisms) disrupts physiological excitation-contraction coupling and can cause a multitude of cardiac complications including arrhythmias (altered electrical remodelling and Ca^{2+} homeostasis) and SAN dysfunction (94, 226, 230, 232). Oxidised CaMKII can also result in SAN fibrosis (230, 232). Fibrosis will be histologically examined in the nDM and DM SAN in **Chapter 5**. Transgenic overexpression of myocardial CaMKII and cardiomyocytes incubated in a high glucose environment exhibited a prolonged AP duration (227, 312, 313). The prolongation was predominantly attributed to lengthy and re-occurring openings of $I_{Ca,L}$ ($Ca_v1.2$) and increased RyR2 Ca^{2+} release (227, 312, 313). Transgenic overexpression also found lengthened AP and significant effects to the SR: SR Ca^{2+} content was decreased, SR Ca^{2+} leak and diastolic Ca^{2+} spark frequency was increased (313). The SR effects were mostly attributed to chronic CaMKII effects on RyR2 and reduced SERCA2a / phospholamban expression (313). Again, slow inactivation of $I_{Ca,L}$ was reported to potentially

contribute to Ca^{2+} overload (313). Collectively, this suggests the effects of upregulated CaMKII are mainly acting on $I_{Ca,L}$, RyR2 and SR Ca^{2+} content that might also be the case in the DM SAN.

Therefore, the phosphorylation status of CaMKII should be examined in future, as well as the location of phosphorylated CaMKII, in the nDM and DM SAN cardiomyocytes. This will provide an indication of the activity of the kinase and distribution within the DM SAN (cardiomyocytes). An increase in chronically active CaMKII might also suggest increased $[Ca^{2+}]_i$ as it is known to be one of the causes for chronically active CaMKII (314). As mentioned previously, SR Ca^{2+} content using caffeine will be determined in the nDM and DM hearts in **Chapter 4**. Prolonged and recurrent Ca^{2+} transients predispose CaMKII to a chronically active state (230). A mechanism for increased DM SAN CaMKII (potentially phosphorylated) might result from continued β-adrenergic stimulation to the DM ZDF hearts (165, 230). Chronic activation effects (*in vivo* and / or *ex vivo*) of CaMKII on slow inactivation of $I_{Ca,L}$ and increased RyR2 Ca^{2+} leak might disrupt Ca^{2+} handling within the DM SAN, lengthening the AP and lowering intrinsic HR (227, 312, 313). Additional studies on $I_{Ca,L}$ and RyR2 Ca^{2+} release characteristics in the DM SAN are needed.

3.6. Summary

In summary, my study has successfully compared the expression levels of the key Vm clock (HCN4, NCX1, L-type and T-type Ca^{2+} channels) and Ca^{2+} clock (SERCA2a and phospholamban), cx45, and cholinergic (M_2 receptor) proteins in the nDM and DM SAN. The protein expression changes of both clocks and of cx45 is interesting, as not one sole perpetrator seems to be responsible for the low intrinsic HR in DM, but rather a complex combination. However,

protein expression does not necessarily parallel a matched functional activity of proteins. Therefore, in the next chapter, the altered Vm and Ca^{2+} clock and cholinergic proteins were functionally challenged in the isolated nDM and DM hearts, and assessed based upon intrinsic HR responses.

CHAPTER 4

Challenging the Sinoatrial Node Clocks and Cholinergic Systems in the Type 2 Diabetic Sinoatrial Node

4.1. Introduction

In Chapter 3, the expression levels of some voltage membrane (Vm) clock and cholinergic proteins were found to be altered, and the Ca^{2+} clock remained unchanged with respect to the sarco(endo)plasmic reticulum Ca^{2+}-ATPase 2a (SERCA2a) to phospholamban ratio in the type 2 diabetic (DM) sinoatrial node (SAN) compared to non-diabetic (nDM). How these findings in Vm and Ca^{2+} clock expression relate to the decreased intrinsic (*ex vivo*) heart rate (HR) in DM remains to be explored. It is well acknowledged that protein expression levels do not necessarily correlate with function (16, 315). Given the unexpected direction of change in the expression levels of some of the proteins studied in the DM SAN (discussed in Chapter 3), it was important to consider whether altered protein function was also present. The contributions of the selected proteins to pacemaking and their respective effect on HR alteration is discussed below.

4.1.1 HCN4

A key component of the SAN's intrinsic pacemaking ability is the presence and contribution of the hyperpolarisation-activated cyclic nucleotide-gated channel 4 (HCN4, funny current (I_f)). As highlighted previously, HCN4 is responsible for the diastolic depolarisation that allows the action potential (AP) threshold to be reached, triggered and HR is generated (21, 271). Decreased HCN4 function (knockdown) results in significant intrinsic bradycardia, whereas increased HCN4 function (overexpression) results in unaltered spontaneous firing rates (a proxy for intrinsic HR) compared to control (234, 235, 274-278). Given the decreased intrinsic HR in DM, it would, therefore, be expected that HCN4 would be decreased; however, Chapter 3 shows this is not the case. Indeed, the data presents significantly increased HCN4 protein expression in the DM SAN which would suggest maintained intrinsic HR. However, as eluded

to above expression does not necessarily equal function, and HCN4 channels within the DM SAN might not be fully functional. Therefore, the contribution of HCN4 to intrinsic HR generation in the DM hearts was investigated using the selective HCN inhibitor ivabradine.

4.1.2 SERCA2a and the SR

The coupled clock hypothesis demonstrates an essential role of the Ca^{2+} clock to pacemaking generation (21, 50). The Ca^{2+} clock components of interest in this study are SERCA2a activity and sarcoplasmic reticulum (SR) Ca^{2+} content. SERCA2a activity is a key determinant of cytosolic Ca^{2+} decay and SR refilling during repolarisation (16, 316). In turn, SR refilling governs the diastolic depolarisation rate (80). Limiting SERCA2a function in SAN cardiomyocytes prolongs cytosolic Ca^{2+} decay, decreases SR Ca^{2+} content, decreases the number and size of spontaneous local Ca^{2+} release (LCR) events, and decreases firing rate, which lengthens repolarisation and diastolic depolarisation, collectively lowering intrinsic HR (16, 80, 234, 316, 317). This also results in diminished HR responses upon stress (16, 80, 234, 316, 317). Therefore, to indirectly assess SERCA2a activity, the intracellular Ca^{2+} ($[Ca^{2+}]_i$) load was enhanced by increasing external Ca^{2+} concentration ($[Ca^{2+}]_o$) and the effect of SR Ca^{2+} depletion was evaluated using caffeine (a RyR2 agonist) (16, 78, 253, 318-320).

4.1.3 Cholinergic systems

Cholinergic input modulates various parts of the SAN AP (diastolic depolarisation, AP amplitude and repolarisation) through effects of adenylyl cyclase inhibition (decreases cAMP levels) and hyperpolarisation (via acetylcholine K^+ channel (K_{ACh} / I_{KACh})) of the membrane potential (128, 148). Combined these effects reduce HCN4 function and prolong diastolic depolarisation (128, 148). Chapter 3 shows a significantly increased muscarinic type 2 (M_2)

receptor. Thus, the functional cholinergic responsiveness of the DM heart to cholinergic stimulation was examined using carbachol (an M_2 agonist).

The isolated heart lacks autonomic input so why study the cholinergic responses? The influence of the non-neuronal intrinsic cholinergic system on *in vivo* HR was shown by mouse cardiac-specific knockout studies of choline acetyltransferase (acetylcholine synthesis) and vesicular acetylcholine transporter (acetylcholine storage) (321, 322). There were no differences in baseline *in vivo* HR, however, after being stressed (saline injection or exercise) prolonged HR recovery was exhibited, suggesting the influence of both the neuronal and non-neuronal intrinsic cholinergic systems on *in vivo* HR regulation (321, 322). This indicates the presence of an intrinsic cholinergic system in the SAN cardiomyocytes, though as far as I know, this has not been directly investigated and the extent of its control on intrinsic HR remains unknown. Investigating the functional cholinergic responsiveness of the DM heart will also, in part, be attributed to this non-neuronal intrinsic cholinergic system.

4.2. Aims and hypothesis

The **aim** of this study was to investigate the effects of ivabradine, $[Ca^{2+}]_o$, caffeine and carbachol on intrinsic HR of the DM heart.

The **hypothesis** was a greater decrease in intrinsic HR with increasing HCN4 inhibition, a blunted increase in intrinsic HR with increasing $[Ca^{2+}]_o$, a reduced intrinsic HR response to caffeine application and a greater decrease in intrinsic HR with increasing carbachol in the isolated heart of the DM ZDF rats compared to their nDM littermates.

4.3. Methodology

Detailed methodology used in this study can be found in Chapter 2. Experimental techniques applied here included heart tissue retrieval, Langendorff, LabChart and statistical analysis.

4.4. Results

4.4.1 Animal Characterisation

Table 4.1 presents the standard measurements for the Zucker Diabetic Fatty (ZDF) rat characterisation. The ZDF$^{fa/fa}$ rats had markedly increased body weight and blood glucose compared to their ZDF$^{fa/+,\ +/+}$ littermate controls. The ZDF$^{fa/fa}$ rats that exhibited a 'high' blood glucose reading above the maximum of 33.3 mmol/L on the glucometer (3 out of 7 rats) were excluded from the blood glucose analysis only in Table 4.1. As shown previously in Chapter 3 and by earlier studies, the ZDF$^{fa/fa}$ hearts had a significantly lower intrinsic HR compared to ZDF$^{fa/+,\ +/+}$ hearts. No *in vivo* HR data is available for these rats as echocardiography was not performed to minimise possible anaesthetic induced stress and influence to the heart before the Langendorff experiment. These data were obtained using sodium pentobarbital anaesthesia. Together, the data confirmed the diabetic (DM) phenotype of the ZDF$^{fa/fa}$ rats.

Table 4.1. Animal characteristics from non-diabetic (nDM) and diabetic (DM) rats used for Langendorff experiments. nDM n=10 and DM n=7, mean ± SEM, unpaired t test.

Parameter	nDM (ZDF$^{fa/+, +/+}$)	DM (ZDF$^{fa/fa}$)	*P value*
Weight (g)	373 ± 7	400 ± 6	* *<0.05*
Blood glucose (mmol/L)	11.1 ± 0.4	31.1 ± 1.4	* *<0.0001*
***Ex vivo* intrinsic heart rate (bpm)**	162 ± 7	127 ± 12	* *<0.05*

4.4.2 Vm clock: the effect of HCN4 inhibition on intrinsic heart rate

The significantly increased HCN4 protein expression and decreased intrinsic HR (Chapter 3) was assessed by determining the effect of HCN4 inhibition on intrinsic HR using the selective HCN inhibitor ivabradine (323-327). The effect of increasing ivabradine concentrations on intrinsic HR in the nDM and DM hearts is shown in **Figure 4.1**. The nDM hearts presented a marked decline in intrinsic HR with increasing ivabradine concentrations compared to respective baseline (*p<0.05*, Figure 4.1A). In contrast, the DM hearts exhibited no change in intrinsic HR with increasing ivabradine concentrations compared to respective baseline (*p>0.05*, Figure 4.1A). There was a significant interaction of ivabradine and DM on intrinsic HR (interaction *p<0.01*). A significant DM difference in absolute intrinsic HR was found between the nDM and DM hearts at all ivabradine concentrations (*p<0.001*, Figure 4.1A). This difference also remained at the higher ivabradine concentrations following normalisation (*p<0.05*, Figure 4.1B). In nDM, a normalised decreasing intrinsic HR response to ivabradine was plotted (Figure 4.1C). The ivabradine IC50 value for the nDM hearts was 5.0 ± 0.3 µM. This was not plotted for DM as no intrinsic HR response to ivabradine was observed. Given the significant increase in HCN4 expression in the DM SAN, yet, the lack of an intrinsic HR decrease

to ivabradine might indicate the presence of non-functional HCN4 channels within the DM SAN.

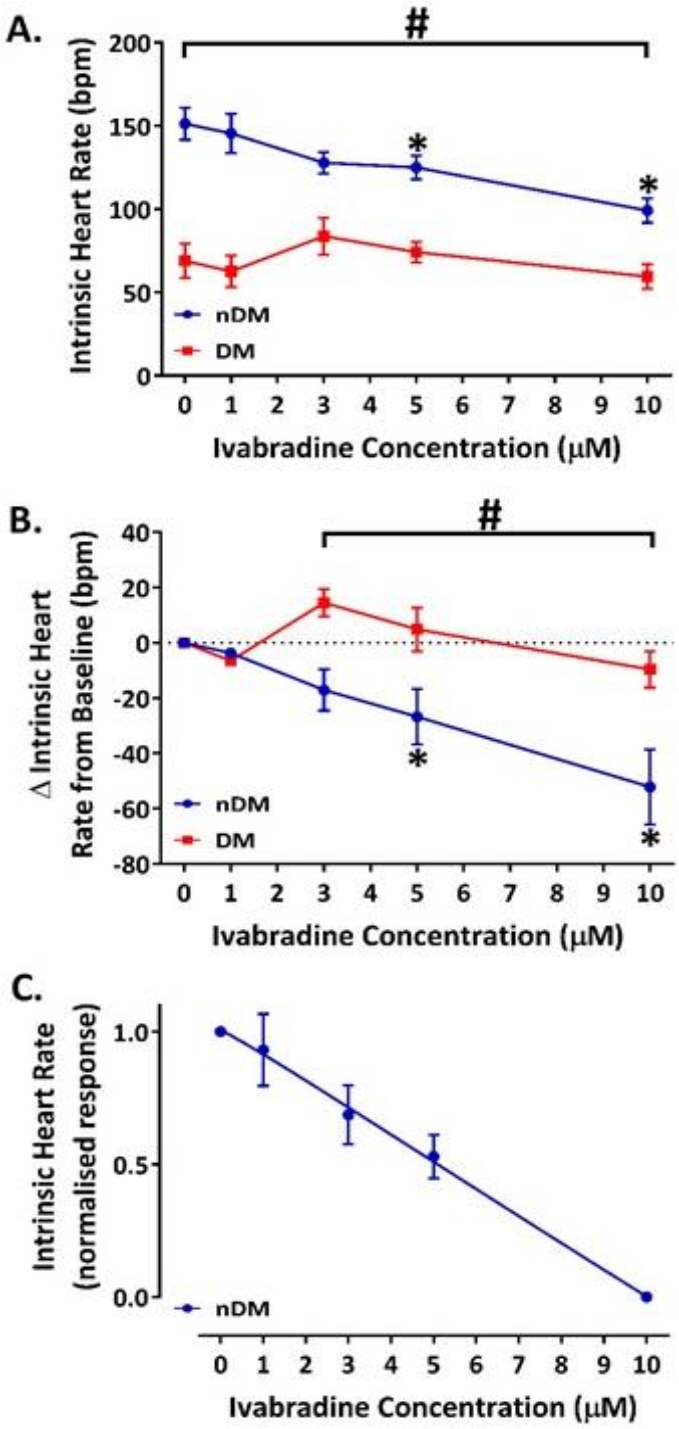

Figure 4.1. Ivabradine effects on intrinsic heart rate. (A.) Intrinsic heart rate (HR) in non-diabetic (nDM) and diabetic (DM) hearts with increasing ivabradine concentrations. (B.) Absolute change in intrinsic HR from respective baselines in nDM and DM with increasing ivabradine concentrations. (C.) Normalised response to ivabradine in nDM hearts. n=6-9 per group, mean ± SEM, # nDM vs. DM $p<0.05$, * intrinsic HR at concentration vs. respective baseline $p<0.05$, interaction significant $p<0.01$. (A. and B.) Two-way ANOVA with repeated measures, Holm-Sidak post hoc test. (C.) Non-linear regression variable slope.

4.4.3 Ca^{2+} clock (and Vm clock): the effect of increasing external Ca^{2+} on intrinsic heart rate

In the Ca^{2+} clock, the unaltered SERCA2a to phospholamban expression ratio suggests unaffected SERCA2a activity in the DM SAN. In an attempt to indirectly evaluate SERCA2a activity (and Na^{+}-Ca^{2+} exchanger 1 (NCX1)) during repolarisation, the effect of increasing SAN cardiomyocyte Ca^{2+} load (entry via Ca^{2+} channels and NCX1) by increasing $[Ca^{2+}]_o$ on intrinsic HR was compared in the nDM and DM hearts (79, 83, 328, 329). The effect of increasing $[Ca^{2+}]_o$ on intrinsic HR in the nDM and DM hearts is presented in **Figure 4.2**. There was a significant interaction of $[Ca^{2+}]_o$ and DM on intrinsic HR (interaction *p<0.05*). A marked DM difference in intrinsic HR was found at all $[Ca^{2+}]_o$ tested (*p<0.001*, Figure 4.2A) which persisted at the higher $[Ca^{2+}]_o$ after normalisation of the nDM and DM baselines (*p<0.05*, Figure 4.2B). The intrinsic HR was unchanged in nDM hearts with rising $[Ca^{2+}]_o$ compared to respective baseline (*p>0.05*, Figure 4.2A), whilst the DM hearts displayed significantly reduced intrinsic HR with increasing $[Ca^{2+}]_o$ compared to respective baseline (*p<0.05*, Figure 4.2A). These results were further investigated by determining the absolute change in intrinsic HR from nDM and DM baselines, with the marked decrease in intrinsic HR in DM still present at the higher $[Ca^{2+}]_o$ (Figure 4.2B). In DM, a normalised decreasing intrinsic HR response to rising $[Ca^{2+}]_o$ can be found (Figure 4.2C). From the graph in Figure 4.2C, the $[Ca^{2+}]_o$ IC50 value for the DM hearts was 2.5 mM. This was not plotted for nDM as no intrinsic HR response to $[Ca^{2+}]_o$ was found. Given the unaltered SERCA2a to phospholamban ratio in the DM SAN, but the declining intrinsic HR with increasing $[Ca^{2+}]_o$ suggests compromised SERCA2a activity within the DM heart.

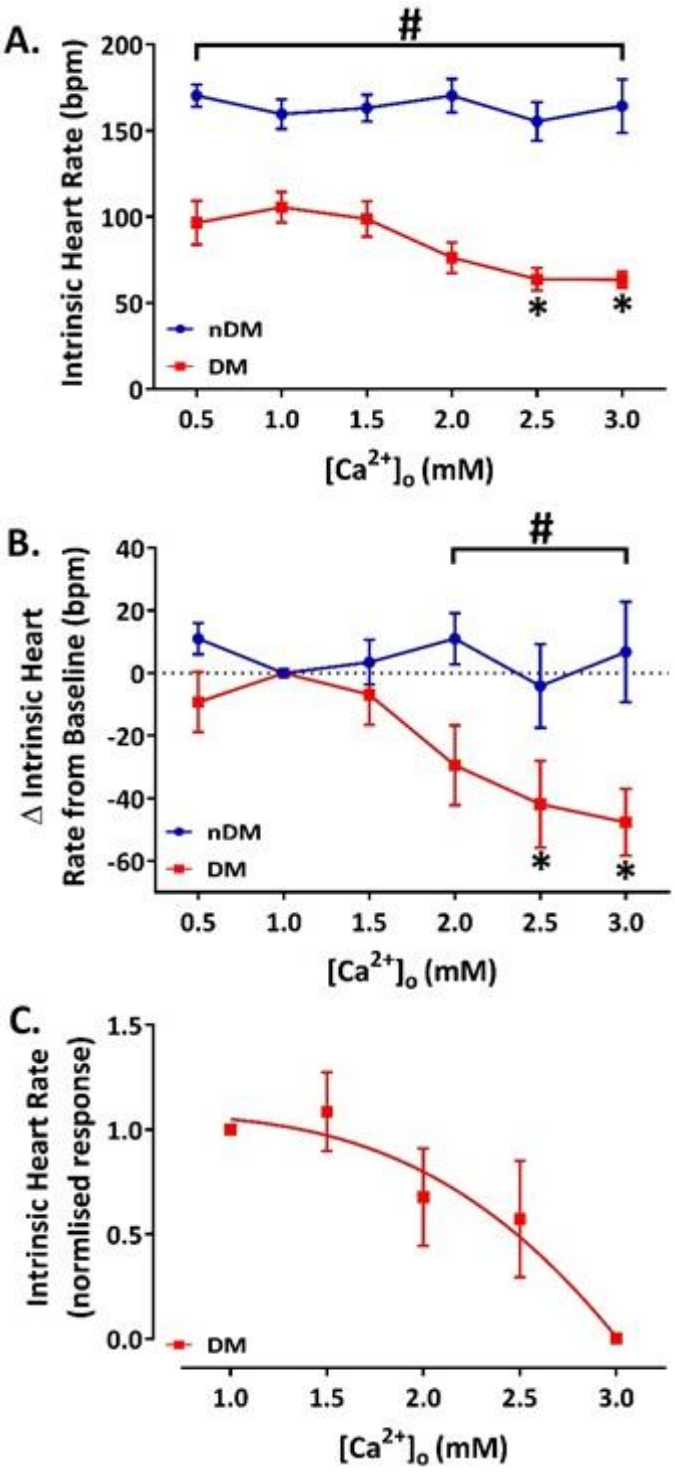

Figure 4.2. External Ca^{2+} concentration effects on intrinsic heart rate. (A.) Intrinsic heart rate (HR) in non-diabetic (nDM) and diabetic (DM) hearts with increasing external Ca^{2+} concentration ($[Ca^{2+}]_o$). (B.) Absolute change in intrinsic HR from respective baselines in nDM and DM with increasing $[Ca^{2+}]_o$. (C.) Normalised response to $[Ca^{2+}]_o$ in DM hearts. n=7-9 per group, mean ± SEM, # nDM vs. DM *p<0.05*, * intrinsic HR at concentration vs. respective baseline (1mM $[Ca^{2+}]_o$) *p<0.05*, interaction significant *p<0.05*. (A. and B.) Two-way ANOVA with repeated measures, Holm-Sidak post hoc test. (C.) Non-linear regression variable slope.

4.4.4 Ca^{2+} clock: the effect of SR Ca^{2+} depletion on intrinsic heart rate response

To indirectly assess SR Ca^{2+} content, the intrinsic HR response achieved upon emptying of the SR within the nDM and DM hearts was evaluated. This intrinsic HR response was measured during the initial caffeine-induced SR Ca^{2+} release determined by initial rapid and increased contraction, as observed on the left ventricle (LV) pressure traces. The effect of (20 mM) caffeine on the intrinsic HR response in the nDM and DM hearts is presented in **Figure 4.3**. No significant interaction of caffeine and DM on intrinsic HR was found (interaction $p>0.05$). A DM difference in absolute intrinsic HR was present ($p<0.01$, Figure 4.3A), however, following normalisation of the nDM and DM baselines, the caffeine-induced intrinsic HR response was absent (interaction $p>0.05$, Figure 4.3B). Both nDM and DM hearts presented significantly increased intrinsic HR on emptying of the SR Ca^{2+} content using caffeine from their respective baselines ($p<0.05$, Figure 4.3A). The lack of a difference in a caffeine-induced HR response seems to be in contrast to the $[Ca^{2+}]_o$ results presented in the previous section 4.4.3 and suggests unchanged SR Ca^{2+} content.

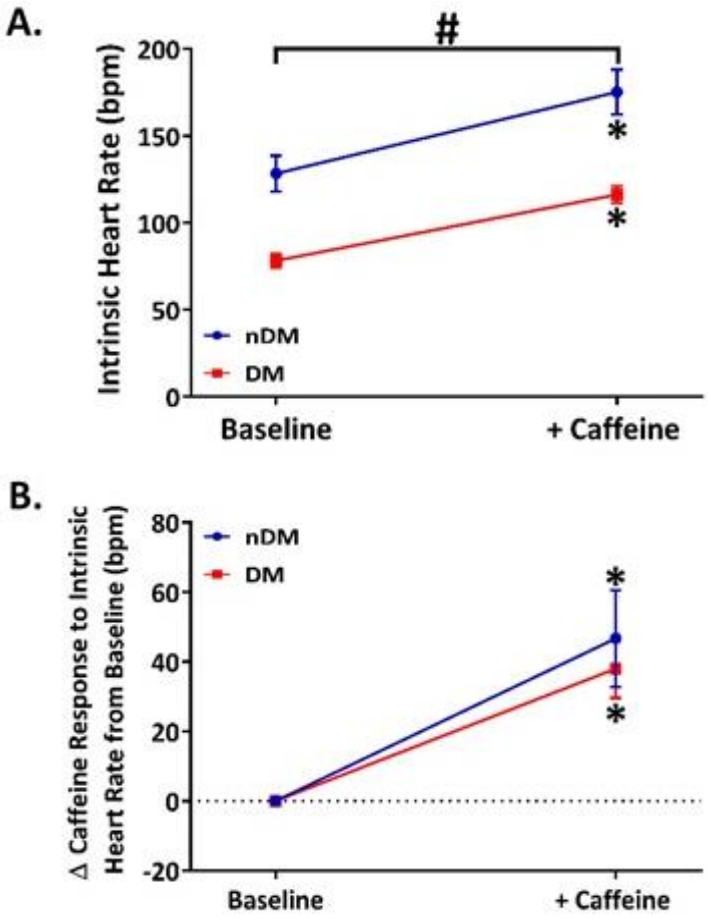

Figure 4.3. Effects of caffeine on intrinsic heart rate. (A.) Intrinsic heart rate (HR) in non-diabetic (nDM) and diabetic (DM) hearts at baseline and caffeine response. (B.) Absolute change in intrinsic HR from baseline in nDM and DM with caffeine. n=5-6 per group, mean ± SEM, # nDM vs. DM *p<0.01*, * intrinsic HR at concentration vs. respective baseline *p<0.05*. Two-way ANOVA with repeated measures, Holm-Sidak post hoc test.

4.4.5 Cardiac cholinergic response: the effect of M_2 receptor stimulus on intrinsic heart rate

As shown in Chapter 3, the expression of the M_2 receptor was markedly elevated in the DM SAN. To evaluate whether these expression findings affected responsiveness to cholinergic input in the nDM and DM hearts, the effect on intrinsic HR was studied using the cholinergic agonist carbachol. The effect of increasing carbachol concentration on intrinsic HR in the nDM and DM hearts is shown in **Figure 4.4**. There was no significant interaction of carbachol and

DM on intrinsic HR (interaction *p>0.05*). A significant DM difference in intrinsic HR was present at low carbachol concentrations (*p<0.05*, Figure 4.4A), which was absent after normalisation of nDM and DM baselines (*p>0.05*, Figure 4.4B). Both the nDM and DM hearts presented significantly decreased intrinsic HR with rising carbachol concentrations compared to respective baselines (*p<0.05*, Figure 4.4A), however, no DM difference was observed (*p>0.05*, Figure 4.4B). In nDM and DM, a normalised decreasing intrinsic HR response to carbachol can be found (Figure 4.4C), which along with IC50 values (nDM 4.5 ± 1.2 nM versus DM 4.2 ± 0.7 nM, *p>0.05*, Figure 4.4D) confirmed no difference in HR responsiveness to carbachol. Given the significantly increased M_2 receptor protein expression in the DM SAN, but the lack of an increased HR response to carbachol, suggests functional uncoupling in the cholinergic pathways within the DM heart.

4.4.6 Baseline intrinsic heart rates throughout the Langendorff protocol

The baseline intrinsic HR throughout the time course of the Langendorff protocol is shown in **Figure 4.5**. A progressive decline in baseline intrinsic HR throughout the time course of the Langendorff experiments existed, which did not fully recover to the initial baseline HR for both the nDM and DM hearts (Figure 4.5B). However, throughout the protocol, a difference in baseline intrinsic HR remained between the nDM and DM hearts (*p<0.01*, Figure 4.5A).

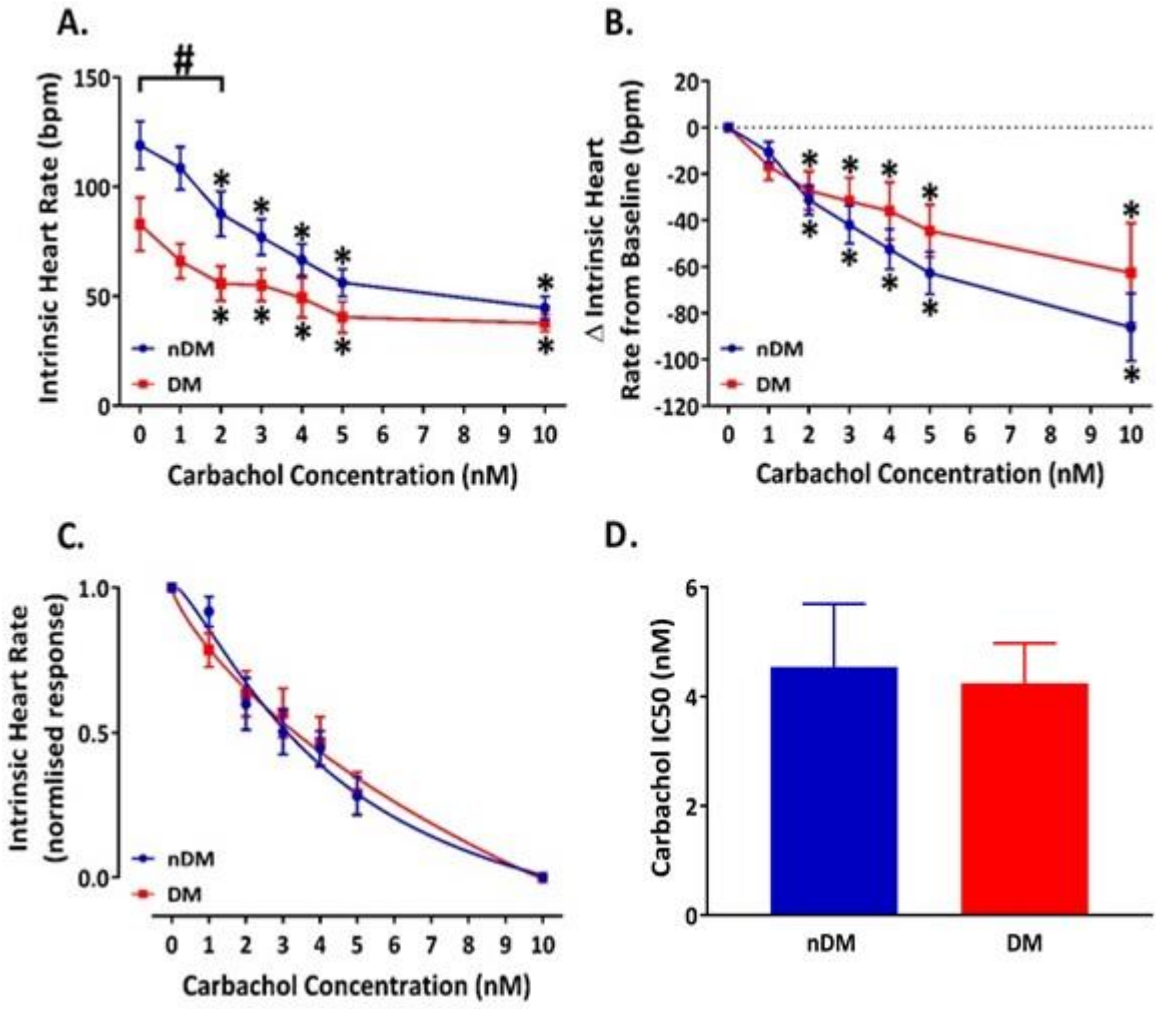

Figure 4.4. Carbachol effects on intrinsic heart rate. (A.) Intrinsic heart rate (HR) in non-diabetic (nDM) and diabetic (DM) hearts with increasing carbachol concentrations. (B.) Absolute change in intrinsic HR from baseline in nDM and DM with increasing carbachol concentrations. (C.) Normalised response to carbachol in nDM and DM hearts. (D.) Comparison of carbachol IC50 values in nDM and DM. n=4-9 per group, mean ± SEM, # nDM vs. DM $p<0.05$, * intrinsic HR at concentration vs. respective baseline $p<0.05$. (A. and B.) Two-way ANOVA with repeated measures, Holm-Sidak post hoc test. (C.) Non-linear regression variable slope. (D.) Unpaired t test.

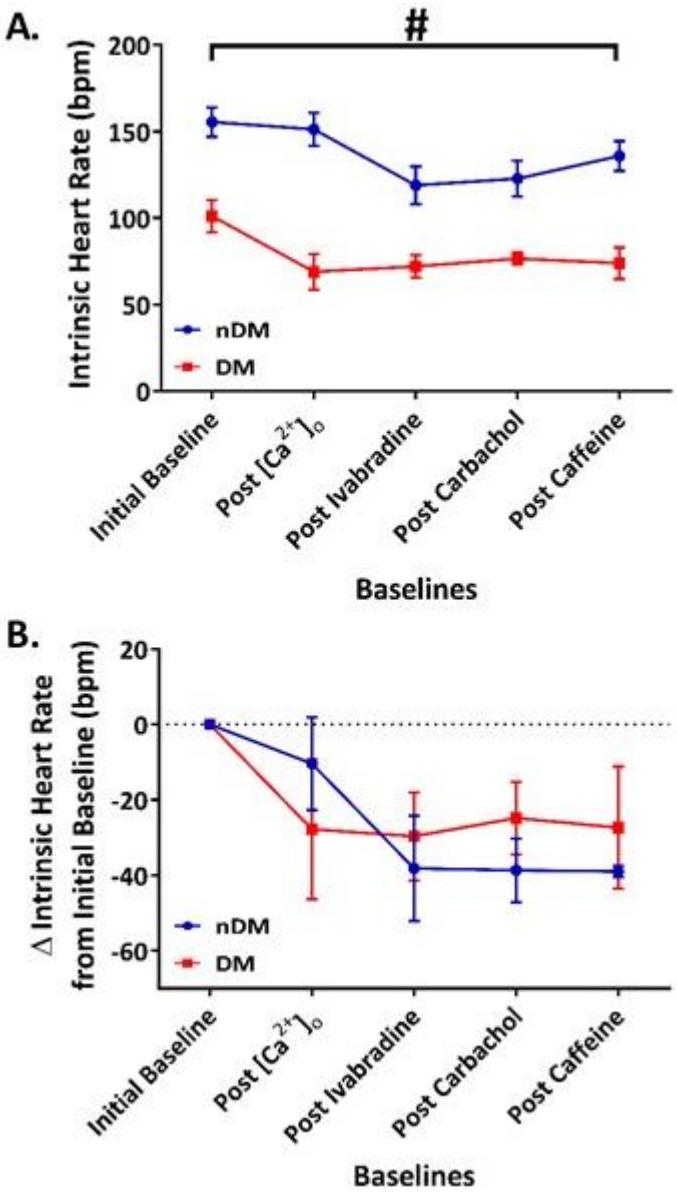

Figure 4.5. Baseline intrinsic heart rates throughout the Langendorff experiments. (A.) Baseline intrinsic heart rate (HR) in non-diabetic (nDM) and diabetic (DM) hearts throughout the course of the Langendorff protocol. (B.) Absolute change in intrinsic HR from the initial baseline in nDM and DM throughout the Langendorff protocol. n=6-9 per group, mean ± SEM, # nDM vs. DM *p<0.01*. (A. and B.) Two-way ANOVA with repeated measures, Holm-Sidak post hoc test.

4.5. Discussion

In this study, I investigated the effects of challenging HCN4 channels (Vm clock) using the inhibitor ivabradine, as well as SERCA2a and SR (Ca^{2+} clock) using $[Ca^{2+}]_o$ and caffeine

respectively, and M_2 receptor (cholinergic system) using the agonist carbachol on intrinsic HR in the nDM and DM isolated hearts. The key findings of this chapter are: (a) ivabradine significantly decreased intrinsic HR in nDM hearts, but had no effect on intrinsic HR in DM hearts; (b) $[Ca^{2+}]_o$ significantly decreased intrinsic HR in DM hearts, but had no effect on intrinsic HR in nDM hearts; (c) no difference in intrinsic HR response to caffeine application was found between nDM and DM; and (d) carbachol significantly decreased intrinsic HR to equal measure in nDM and DM hearts.

4.5.1 Can HCN4 protein expression and function explain the low intrinsic heart rate in type 2 diabetes?

Due to the mismatch between the lower intrinsic HR and the significant increase in HCN4 protein expression in the DM SAN, the contribution of HCN4 channels to intrinsic HR generation was investigated. As a result of the significant increase in HCN4 protein expression, I hypothesised, a larger decrease in intrinsic HR on increasing ivabradine concentrations in the DM hearts. In the nDM hearts, the inhibition of HCN4 using ivabradine resulted in a decrease in intrinsic HR, however, surprisingly, and not in support of my hypothesis, the intrinsic HR in DM hearts remained unchanged even at 10 µM ivabradine. Why this is the case is unclear, but could indicate that although there is increased HCN4 expression in the SAN of DM hearts, HCN4 channels are inactive. As far as I know, such a mismatch between HCN4 protein expression and function has not been previously reported. The effect of ivabradine cannot be solely attributed to HCN4 as ivabradine inhibits all HCN isoforms 1-4 (330). However, although ivabradine can inhibit all HCN isoforms, within the SAN of the rat HCN4 expression (~80%) dominates over HCN2 expression (~20%) (235, 331). No detectable HCN1 or HCN3 protein expression has been found in the rat SAN (235, 331). Therefore, the ivabradine-induced

decline in intrinsic HR in the nDM hearts is likely to be primarily due to the inhibition of HCN4, with a potential smaller contribution from HCN2 inhibition. Together, my data suggest that impaired HCN channel contribution to diastolic depolarisation during intrinsic HR generation due to non-functional HCN4 (and HCN2) channels in the DM SAN, despite the increased HCN4 protein expression. This impaired HCN channel contribution would suggest a depressed and prolonged slope of diastolic depolarisation that would result in a decreased intrinsic HR in DM (**Figure 4.6**). However, HCN4 (and HCN2) channel recordings and action potential measurements in DM SAN cardiomyocytes would be needed to confirm this.

The complete lack of HR reduction by ivabradine in DM has also not been previously reported and is in contrast to the type 1 DM SAN findings. In the type 1 DM SAN, a significant prolongation of the cycle length by 18% compared to 26% in control on ivabradine use was attributed to significantly decreased protein expression of HCN4 and HCN2 channels (i.e. there was a lesser effect of HCN4 and HCN2 inhibition in the type 1 DM SAN) (235). In another study, a significant decrease in HCN4 expression also exhibited significantly decreased I_f in isolated type 1 DM SAN cardiomyocytes (no ivabradine use) (234). Collectively, this literature supports my proposed hypothesis rather than my experimental findings. As mentioned in section 4.1.1, a model of HCN4 overexpression with increased density of I_f found no alterations to spontaneous firing rate (a proxy for intrinsic HR), however, HCN4 knockdown resulted in significantly decreased spontaneous firing rate (274). This suggests overexpression of HCN4 function is likely to be limited by other pacemaking components, but knockdown of HCN4 function can impair *in vivo* and intrinsic HR control. To the best of my knowledge, there are no reports of increased HCN4 protein expression with decreased HCN4 function.

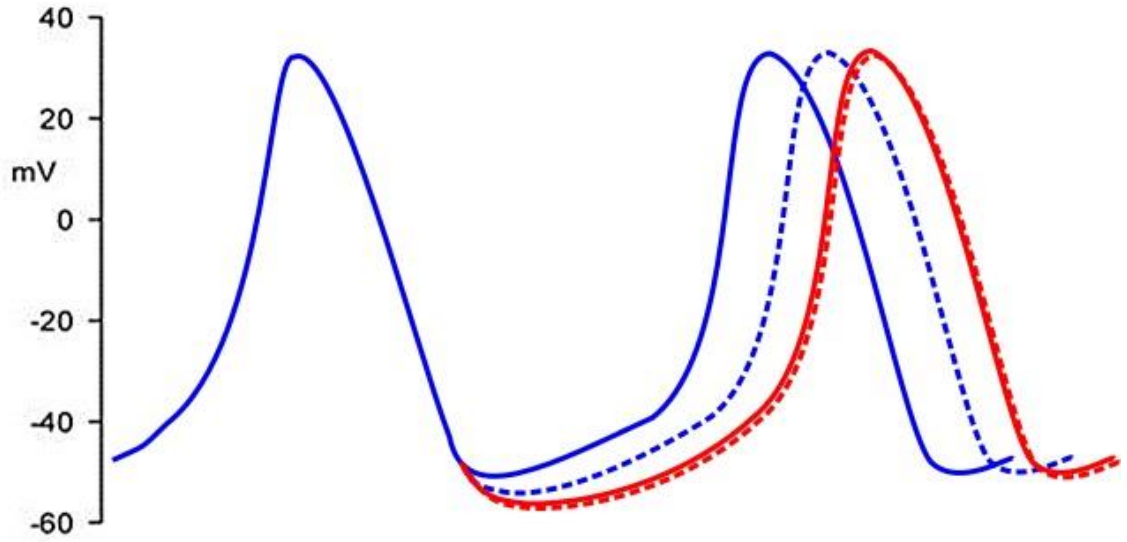

Figure 4.6. Proposed remodelling of the sinoatrial node action potential on hyperpolarisation-activated cyclic nucleotide-gated channel 4 inhibition in diabetes. A schematic sinoatrial node (SAN) action potential (AP) without ivabradine (blue solid) and with ivabradine (blue dashed) in non-diabetic (**nDM**) SAN and diabetic (**DM**) SAN without (red solid) and with ivabradine (red dashed). Ivabradine depresses and lengthens diastolic depolarisation in nDM, but has no effect on the DM AP due to non-functional hyperpolarisation-activated cyclic nucleotide-gated channel 4 (HCN4) channels. In DM, the lack of functional HCN4 might be responsible for the depression and prolongation of the diastolic depolarisation slope accounting for the lower intrinsic heart rate compared to nDM. Original figure.

The idea of non-functional HCN4 (and HCN2) channels in the DM SAN is in line with the mechanism of how ivabradine inhibits HCN channels. Ivabradine requires an open channel state in order to occupy a cavity below the pore from the intracellular side of the HCN channel, affecting its ion conduction pathway (325, 326, 332, 333). Ivabradine mediated HCN inhibition has been suggested to be HR dependent (324, 327). At a slower HR, it might take longer to reach maximal HCN inhibition as not all HCN channels are contributing to diastolic depolarisation at any given time. This suggests that even in the same species a change in baseline HR induced by a disease (like DM) might affect the efficacy of ivabradine.

Consequently, it would be interesting to determine the effects of prolonged ivabradine exposure or use ivabradine in combination with β-adrenergic stimulation to increase DM HR. Possible reasons as to why non-functional HCN4 (and HCN2) might exist in the DM SAN will be discussed in **Chapter 7**.

4.5.2 Can changes in Ca^{2+} clock protein expression and function explain the low intrinsic heart rate in type 2 diabetes?

4.5.2.1 SERCA2a and NCX1 (Ca^{2+} and Vm clock)

SERCA2a and NCX1 activity were indirectly examined by investigating the effects of increasing $[Ca^{2+}]_o$ on intrinsic HR in DM. The results showed no increase in intrinsic HR in either group. Instead, the nDM and DM hearts presented no change and a significantly decreasing intrinsic HR on increasing $[Ca^{2+}]_o$, respectively. The effects of Ca^{2+} on the SAN, intrinsic HR and pacemaking proteins are considered below.

4.5.2.2 The effects of increasing external Ca^{2+} on the sinoatrial node and intrinsic heart rate

The literature on the effects of increasing $[Ca^{2+}]_o$ on intrinsic HR is not straightforward and presents inconsistencies. The changes induced by increasing $[Ca^{2+}]_o$ on intrinsic HR show a biphasic response in the absolute change in HR (roughly a bell-shaped curve) (334, 335). Typically, the maximal increases in HR (~+30 bpm) are achieved at much higher, non-physiological, $[Ca^{2+}]_o$ (~8 mM), which were not used in this study (334, 336, 337). However, others have reported no significant change in intrinsic HR with increasing $[Ca^{2+}]_o$ (335).

At extremely high $[Ca^{2+}]_o$ (10 mM), significant decreases in AP amplitude, maximum diastolic potential and threshold potential (i.e. threshold level has become less negative) have been found, which collectively demonstrate a more depolarised than hyperpolarised state (**Figure 4.7**) (334, 338-340). However, similar effects on AP shape have also been reported at low $[Ca^{2+}]_o$ (0.22 mM), as well as a report of no significant effects on maximum diastolic potential or threshold potential (334, 338-340). Although the slope / rate of diastolic depolarisation was significantly increased, the associated decrease in threshold potential meant no significant difference in intrinsic HR from 2.5 mM to 10 mM $[Ca^{2+}]_o$ (**Figure 4.7**) (334, 341).

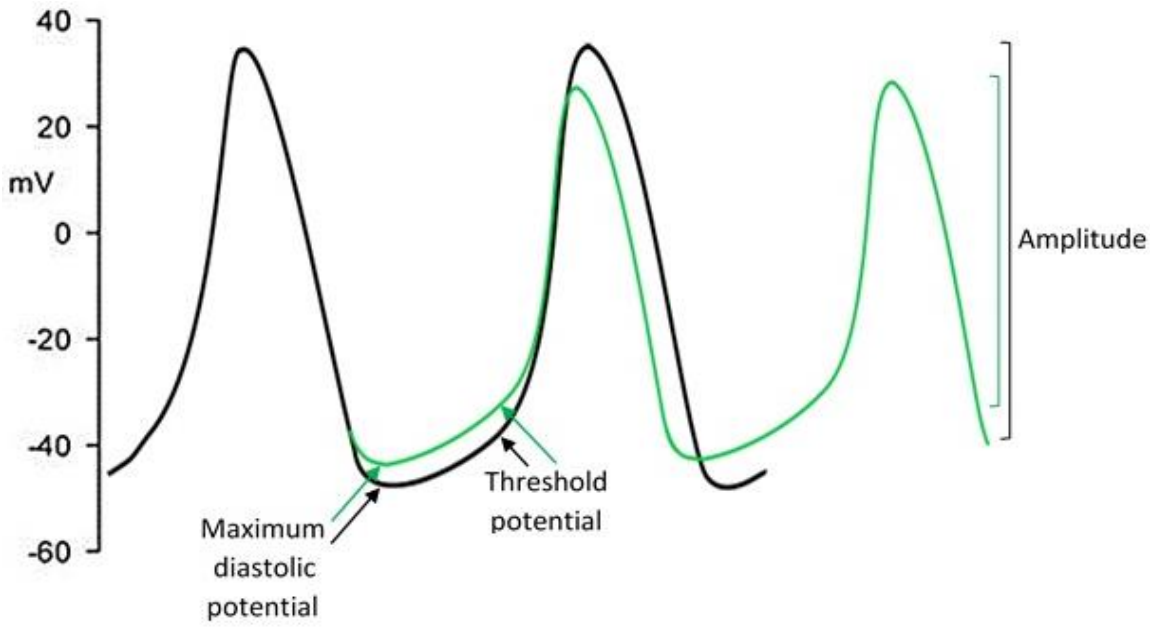

Figure 4.7. The effects of increased external Ca^{2+} on the sinoatrial node action potential. A schematic sinoatrial node action potential (AP) at physiological external Ca^{2+} concentration ($[Ca^{2+}]_o$) (black) and at **extremely high $[Ca^{2+}]_o$** (10 mM) (**green**). The extremely high $[Ca^{2+}]_o$ decreases maximum diastolic potential and threshold potential (a more depolarised state), and AP amplitude (black arrows compared to green arrows). To reach the threshold potential / AP take-off (~-40 mV), there is an accumulation of strong positive feedback mechanism of local Ca^{2+} releases and Na^+-Ca^{2+} exchanger 1 and the long-lasting type Ca^{2+} channels. The strong mass contribution from the long-lasting type Ca^{2+} channels triggers AP take-off (76, 342). Even though the slope / rate of diastolic depolarisation has quickened, the accompanying decrease in threshold potential presents no difference in heart rate. This original figure was made to illustrate the findings of Seifen et al., 1964 (334).

High $[Ca^{2+}]_o$ has also been found to shorten AP duration overall (early repolarisation is quickened and late repolarisation is prolonged) (335, 338, 339, 343). In Purkinje fibres, Ca^{2+} rich solutions have been found to quicken the time- and voltage-dependent current changes that promote repolarisation (344). It has been suggested low $[Ca^{2+}]_o$ decreases Ca^{2+} influx and increases intracellular ($[Na^+]_i$) activity, while high $[Ca^{2+}]_o$ increases Ca^{2+} influx and decreases $[Na^+]_i$ activity (335). (335, 345, 346).

Collectively, these studies suggest Ca^{2+} can act on membrane potential parameters affecting AP shape, duration and consequently, intrinsic HR (84, 334). These studies presented in the literature also highlight the resilience of the SAN to cope with extremely high $[Ca^{2+}]_o$ and continue pacemaking. This suggests pacemaking proteins, including SERCA2a and NCX1, can be expected to compensate for increased $[Ca^{2+}]_o$. Therefore, in my study, it is not surprising that the nDM heart is able to cope with the maximal increase of 3mM $[Ca^{2+}]_o$ (maintained intrinsic HR), however, I suggest that the observed incapability of the DM heart (declining intrinsic HR) is due to compromised Ca^{2+} handling and cycling.

4.5.2.3 Do we expect increased intracellular Ca^{2+} with increased external Ca^{2+}?

In rabbit SAN cardiomyocytes, transient (T-type) and long-lasting (L-type / $I_{Ca,L}$) type Ca^{2+} channels present an increasing current amplitude with increasing $[Ca^{2+}]_o$ (0.5 – 10 mM) (77). In the DM SAN, further amplification of $[Ca^{2+}]_i$ is anticipated due to the 1.5-fold expression increase in NCX1 (via reverse mode activity) and CaMKII. Constitutively active (unknown in the DM SAN) and transgenic overexpression of CaMKII results in $I_{Ca,L}$ facilitation (high and prolonged open probability) (313, 347, 348). Therefore, in the setting of increasing $[Ca^{2+}]_o$, the literature supports that, $[Ca^{2+}]_i$ increases as well. For maintained homeostasis in this condition, increased Ca^{2+} influx must equal increased Ca^{2+} efflux, or be compensated for by enhanced SR refilling (329, 349). The DM SERCA2a and NCX1 repolarisation mechanisms are considered in the condition of increasing $[Ca^{2+}]_o$ and $[Ca^{2+}]_i$ below.

4.5.3 The effects of increasing external Ca^{2+} on SERCA2a and NCX1 in type 2 diabetic hearts

4.5.3.1 Ca^{2+} repolarisation mechanisms: SERCA2a activity and SR Ca^{2+} content

SERCA2a activity and SR refilling regulate repolarisation and diastolic depolarisation of the following AP (16, 80). As mentioned in section 4.1.2, limiting SERCA2a activity in SAN cardiomyocytes significantly prolonged $[Ca^{2+}]_i$ decay, reduced SR Ca^{2+} content, decreased size and number of the succeeding spontaneous LCRs, and firing rate (80). These findings suggest that the succeeding LCRs are dependent on SERCA2a activity, that a certain SR Ca^{2+} threshold is needed for the occurrence of spontaneous LCRs and, SR Ca^{2+} content determines LCR size and number (16, 80). A decrease in the size and number of LCRs postpones and decreases the amplitude of LCR-induced NCX1 activity, depressing the rate of diastolic depolarisation (80). Collectively, this prolongs cycle length during repolarisation and diastolic depolarisation mechanisms thereby decreases firing rate (a proxy for intrinsic HR) (80).

Taking the above study into consideration, I suggest that the decreasing intrinsic HR with increasing $[Ca^{2+}]_o$ in DM is partly attributed to compromised SERCA2a activity and SR refilling, irrespective of the unaltered SERCA2a to phospholamban ratio. In the setting of increasing $[Ca^{2+}]_o$, Ca^{2+} influx does not equal Ca^{2+} efflux and / or is not compensated for by SR refilling. In the DM SAN cardiomyocytes, as with the above study, a decreased SERCA2a activity would lengthen repolarisation and, prolong and depress the rate of diastolic depolarisation, which could account for the lower intrinsic HR observed in DM. This requires further confirmation by direct targeting of the SERCA2a pump (possibly by the inhibitor thapsigargin) and, as mentioned previously, investigation of the phosphorylation status of phospholamban. I also propose that there is greater dependency on the significantly upregulated NCX1 for Ca^{2+}

extrusion as a result of compromised SERCA2a activity in the DM SAN (see below). Why there might be compromised SERCA2a activity with unchanged protein expression will be explored in **Chapter 7**.

In support, is data showing the dependency of repolarisation on SERCA2a compared to NCX1 in rodent hearts (78). About 92% of the $[Ca^{2+}]_i$ is pumped back into the SR by SERCA2a compared to the ~7% extruded by NCX1 (78). On the other hand, if SERCA2a activity is unaffected it should be able to compensate for increased $[Ca^{2+}]_i$ particularly at the higher $[Ca^{2+}]_o$ as more Ca^{2+} is available, despite the upregulated NCX1, as the efficiency of SERCA2a pump is greater than NCX1 (60, 316, 350, 351). An effect of increased NCX1 activity might be reduced SR content, however, the reduction might not be so significant when compared to the effects on SR content with decreased SERCA2a activity.

SERCA2a and the SR, in the SAN and ventricular cardiomyocytes, are also known to compensate to some degree to rises in $[Ca^{2+}]_i$ although there appears to be a limited ability to increase SR content significantly (16, 61, 78, 253, 318, 319, 329, 352, 353). A diminished SERCA2a activity would also suggest lower SR Ca^{2+} content as more $[Ca^{2+}]_i$ is extruded by the upregulated NCX1 (329, 354-356). Yet, the lack of difference in the intrinsic HR achieved between nDM and DM hearts upon caffeine application suggests unaltered SR Ca^{2+} content in DM. This finding was surprising and implies opposition to the effects of increasing $[Ca^{2+}]_o$ where I propose compromised SERCA2a activity in DM. However, this might be explained by a weak dependency of the SR Ca^{2+} content on SERCA2a activity (354, 357).

In a tamoxifen-induced cardiac-specific SERCA2a knockout study, SR Ca^{2+} content was only reduced to 38% compared to control, despite a large decrease in SERCA2a protein expression to less than 5% (354). Another study investigating SERCA2a inhibition (via thapsigargin) in rat ventricular cardiomyocytes also found a given decrease in SERCA2a activity resulted in a relatively smaller decrease in SR Ca^{2+} content (a non-linear relationship) (357). Thapsigargin application presented a decreased amplitude of systolic Ca^{2+} transient but there was a limited effect on caffeine-induced increase in $[Ca^{2+}]_i$ (357). The study suggested changes in SERCA2a results in changes to RyR2 Ca^{2+} release without large changes to SR Ca^{2+} content (357). RyR2 release characteristics require future investigation in the DM SAN. Collectively, these studies show changes to SERCA2a activity and RyR2 release can occur without significant alterations to SR Ca^{2+} content. As with the limited ability to significantly increase SR Ca^{2+}, there also appears to be a limited ability to significantly decrease SR Ca^{2+}, which might be the case in DM hearts.

The method of assessing SR Ca^{2+} content used in this study is not a direct quantification and would require a more direct assessment in the future. Also, caffeine was the last condition to be tested in the nDM and DM hearts and the isolated hearts had been on the Langendorff for ~4 hours. Therefore, possible remaining effects of prior conditions and the time duration of the experiment might have affected SR load. More research studies on the effects of altered SERCA2a expression and activity, and SR Ca^{2+} content in the SAN will be discussed in **Chapter 7**.

4.5.3.2 Ca^{2+} repolarisation mechanisms: NCX1 activity

In ventricular cardiomyocytes, NCX1 overexpression with unaltered SERCA2a presented a faster rise and decay of $[Ca^{2+}]_i$ transients and increased SR Ca^{2+} content compared to control (351). However, partial inhibition of SERCA2a, to mimic pathological states, resulted in decreased SR Ca^{2+} content with $[Ca^{2+}]_i$ transients prolonged until they became comparable to the control (351). These findings suggested under pathophysiological conditions of compromised SERCA2a activity, NCX1 upregulation compensates to maintain $[Ca^{2+}]_i$ homeostasis via forward mode Ca^{2+} efflux (Ca^{2+} influx is also likely as SR Ca^{2+} content was increased in NXC1 overexpression without thapsigargin) (351).

As mentioned previously in rodent hearts, NCX1 is responsible for ~7% of the $[Ca^{2+}]_i$ decay during repolarisation, which is minimal compared to SERCA2a (78). I suggest that in the DM SAN, the upregulated NCX1 will have a greater contribution to Ca^{2+} extrusion compared to the nDM SAN. The declining intrinsic HR on increasing $[Ca^{2+}]_o$ suggests a few mechanisms that might result due to greater Ca^{2+} extrusion via the upregulated NCX1 in the DM SAN. This includes: (a) NCX1 Ca^{2+} extrusion lengthens repolarisation as a result of compromised SERCA2a activity (as discussed above), (b) this causes situations of increased diastolic $[Ca^{2+}]_i$, (c) competition with compromised SERCA2a comes at the expense of decreasing SR Ca^{2+} content, and (d) decreased size and number of LCRs for the subsequent cycle, lengthening diastolic depolarisation and AP trigger. These suggested alterations of prolonged repolarisation and / or diastolic depolarisation might account for the lower intrinsic HR in DM. These effects will become more pronounced with further increases of $[Ca^{2+}]_o$ during the experiment and might exist in the DM SAN under physiological levels of $[Ca^{2+}]_o$ resulting in the decreased intrinsic HR. The proposed effect on the nDM and DM SAN AP on increased $[Ca^{2+}]_o$ is presented in

Figure 4.8. The effects of altered SERCA2a to NCX1 expression and activity will be further discussed in **Chapter 7**.

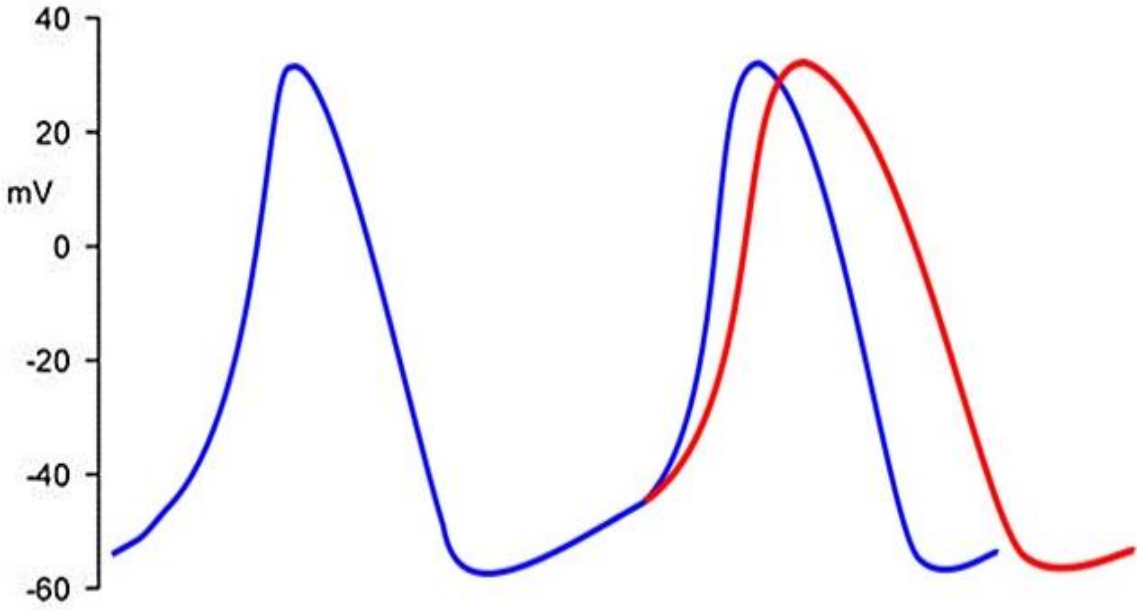

Figure 4.8. Proposed remodelling of the sinoatrial node action potential on increased external Ca^{2+} in diabetes. A schematic **non-diabetic** sinoatrial node (SAN) action potential (AP) (**blue**) and proposed lengthening of the repolarisation phase of the **diabetic** SAN AP due to decreased sarco(endo)plasmic reticulum Ca^{2+}-ATPase 2a function (**red**). Original figure.

In consideration of my findings and literature, I suggest in the DM SAN there is decreased SERCA2a function that is compensated for by the upregulated NCX1. This increased SERCA2a and NCX1 competition during repolarisation might result in reduced SR Ca^{2+} content and SR Ca^{2+} contribution to the succeeding SAN AP cycle (diastolic depolarisation / upstroke). Future direct assessments targeting individual proteins are required to validate these proposed effects (SERCA2a via inhibitor thapsigargin, NCX1 via inhibitor XIP) (358). Collectively, I suggest these mechanisms lengthen repolarisation and diastolic depolarisation resulting in lower intrinsic HR in DM.

4.5.4 Can cholinergic protein expression and function explain the low intrinsic heart rate in type 2 diabetes?

The intrinsic HR responsiveness to the cholinergic agonist carbachol was tested due to the expression findings of an upregulated M_2 receptor in the DM SAN. The nDM and DM hearts exhibited significantly declining intrinsic HR from baseline with rising carbachol concentrations, however, interestingly no difference in cholinergic responsiveness was found. This did not support the hypothesis of enhanced cholinergic responsiveness due to the increased M_2 receptor in the DM SAN. Instead, increased M_2 receptor expression with no increase in cholinergic responsiveness suggests a disassociation / uncoupling at the cardiomyocyte level. The cholinergic responses observed can be attributed to the neuronal cholinergic system (M_2 → G-proteins → I_{KACh} and I_f) and / or the non-neuronal intrinsic cholinergic system (M_2 → acetylcholine-induced acetylcholine release and production) (160). The results suggest a degree of functional uncoupling in either the sensitivity of the M_2 receptor and / or in the intracellular G-protein pathways and / or in the K_{ACh} responses (and / or other downstream molecules such as regulators of G-protein signalling proteins (RGS) (discussed further in **Chapter 7**)). The M_2 receptor downstream target also includes I_f (predominantly by decreasing cAMP (359)). The unchanged responsiveness in the DM SAN could be suggested to, in part, be attributed to no carbachol-induced effect on HCN channels due to the channels being non-functional (i.e. the effect present in DM is entirely due to I_{KACh}), which might prolong recovery from carbachol-induced hyperpolarisation effects, in addition to other possible altered mechanisms (sensitivity and uncoupling).

A reduced *in vivo* and intrinsic HR responsiveness to carbachol was found in a genetic type 1 DM model compared to control (i.e. absolute change in HR was lower) (217). While the

expression of the M_2 receptor or K_{ACh} was not investigated, enhanced I_{KACh} desensitisation and deactivation, with unchanged I_f sensitivity to carbachol was found in the SAN cardiomyocytes (217). This suggested that I_{KACh}, rather than I_f, seems to be responsible for the reduced response in a severe type 1 DM genetic model (217). In the future, a direct assessment of the I_{KACh}, along with its desensitisation and decay characteristics, in the nDM and DM SAN cardiomyocytes will enable more insight into the functional contribution from the channel during SAN cholinergic responses. This might provide an indication of the cause for DM unchanged cholinergic responsiveness and its implications for *in vivo* HR (reduced HR variability, no brake to sympathetic input?), which includes innervation from sympathetic and parasympathetic systems.

The expression of the G-protein inhibitory and subunits ($G_{\alpha\beta\gamma i}$) that are coupled to the M_2 receptor requires investigation, as a mismatch in the expression of $G_{\alpha\beta\gamma i}$ and / or other downstream molecules (i.e. significantly increased M_2 receptors but possibly unchanged or significantly decreased $G_{\alpha\beta\gamma i}$) might deem the additional M_2 receptors as non-functional. In regards to this, the lack of difference in cholinergic responsiveness is surprising as a previous study using similarly aged DM ZDF rats found significantly increased expression of G_i in right atrial and LV tissue (165). An increase in the G_i protein in the SAN would also suggest increased cholinergic responsiveness in DM, rather than the similar responses found between the nDM and DM hearts (unless other downstream molecules are altered, **Chapter 7**). Still, the expression levels of G_i specifically in SAN tissue requires direct investigation in future.

The collective findings from my study and others in this DM ZDF model (increased parasympathetic nerve activity (Bussey *et al*., unpublished data), significantly increased M_2

receptor and G_i protein (165)), would propose amplification of the non-neuronal intrinsic cholinergic system (159, 160). However, the unchanged cholinergic responsiveness in DM suggests a depressed response for the given level of the M_2 receptor. This finding is opposed by the strong positive influence of neuronal cholinergic system on the non-neuronal intrinsic cholinergic system (acetylcholine-induced acetylcholine production), which promotes transcriptional activity and protein expression of the intrinsic cholinergic system (159, 160, 301). The lack of an amplified non-neuronal cholinergic response might be explained by no change or a decrease in the expression and / or function of the rate-limiting high-affinity choline transporter responsible for choline uptake from the extracellular environment into the cardiomyocyte (159).

The level of contribution from the neuronal and non-neuronal systems in the cholinergic response shown here remains to be clarified in DM. This is likely to depend on where the functional uncoupling occurs in the neuronal and non-neuronal cholinergic pathways within the DM SAN cardiomyocyte. Also, how long the intrinsic cholinergic system can remain active *ex vivo* remains to be investigated and is likely to depend on factors such as substrate availability, as the rate-limiting step of intrinsic acetylcholine synthesis is dependent on choline uptake / re-uptake by the high-affinity choline transporter (159, 360).

4.6. Summary

To conclude, this study has investigated components of the Vm clock (HCN4) and Ca^{2+} clock (SERCA2a and SR Ca^{2+} store), and cholinergic mediator (M_2 receptor) in the nDM and DM hearts. I suggest, the effects on intrinsic HR indicate no contribution of HCN4 (and HCN2)

channels which prolong diastolic depolarisation, compromised SERCA2a activity which prolongs repolarisation and diastolic depolarisation, and unaltered neuronal and non-neuronal cholinergic responses in the DM SAN. The suggested prolongation of diastolic depolarisation and repolarisation could individually and collectively account for the decreased intrinsic HR found in DM (**Figure 4.9**). Collectively, the data suggest that defects in both the Vm and Ca^{2+} clock are responsible for the lower intrinsic HR in DM.

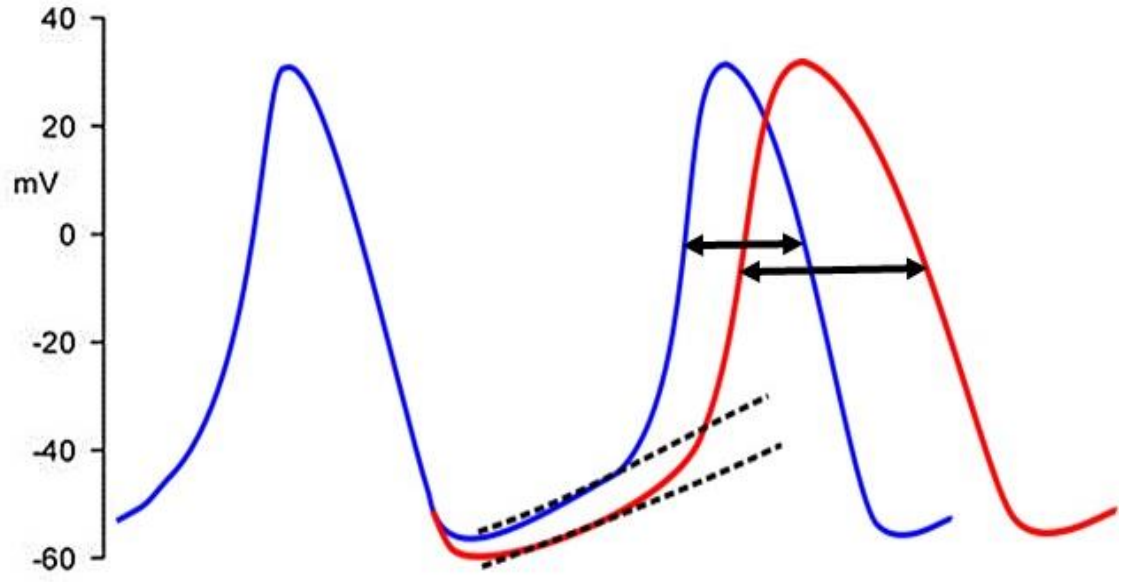

Figure 4.9. Proposed remodelling of the diabetic sinoatrial node action potential. A schematic **non-diabetic** sinoatrial node (SAN) action potential (AP) (**blue**) and proposed lengthening of the diastolic depolarisation and repolarisation phase of the **diabetic** SAN AP due to non-functional hyperpolarisation-activated cyclic nucleotide-gated channels and decreased sarco(endo)plasmic reticulum Ca^{2+}-ATPase 2a function respectively (**red**). Original figure.

CHAPTER 5

Morphology of the Type 2 Diabetic Sinoatrial Node

5.1. Introduction

The sinoatrial node (SAN) has an organised anatomical structure to enable its pacemaking and propagating function (14, 361). Physiologically, the SAN is predominantly compartmentalised by surrounding connective tissue / fibrosis (primarily consisting of fibroblasts, collagen and elastin), which is suggested to insulate the SAN from mechanical and hyperpolarising effects of the neighbouring right atria (14, 30, 32, 33, 361-363). Distinct SAN extensions that merge with the right atria form the specialised conduction pathways that electrically couple the SAN and right atria, and form zones of connexin 45 (cx(45)) and cx43 expressing transitional cardiomyocytes in the SAN periphery, which collectively mediates propagation (14, 30, 32, 33, 100, 104, 106, 361-364). Together, this allows the relatively small SAN to electrically drive the right atria (14). SAN integrity is maintained by viable SAN cardiomyocytes and their electrical coupling (361).

As shown in Chapter 3, the expression of the coupling protein cx45 remained unaltered between the non-diabetic (nDM) and type 2 diabetic (DM) SAN. SAN cardiomyocyte coupling has also been suggested to be mediated by cell-to-cell contact (not just via cx45) (14, 35, 39, 105, 234, 361). Pacemaking and coupling, enabled by cx45 and cell-to-cell contact, can be disrupted by increased fibrosis (accumulation of extracellular matrix), (fibrotic) lesions devoid of SAN cardiomyocytes and therefore also devoid of pacemaking proteins (e.g. hyperpolarisation-activated cyclic nucleotide-gated channel 4 (HCN4)) and, accumulation of triglyceride and lipid droplets (fat) within the SAN (55, 365-369).

SAN fibrosis has been found to be inversely correlated to heart rate (HR) (361). An increase in fibrosis slows pacemaking and conduction, increases beat-to-beat variability and promotes competition between lead (dominant) and latent (supplementary) pacemaking cardiomyocytes within the SAN by forming pathologically insulated pacemaking clusters, which can result in uncoordinated pacemaking and SAN originating arrhythmias (361, 370). The lead (dominant) pacemaking cardiomyocytes refer to cardiomyocytes with the fastest intrinsic rhythm mediating HR generation, typically located in the SAN centre (51-54).

Lesions within the SAN typically arise from SAN cardiomyocyte apoptosis and might or might not involve replacement with fibrosis (162, 361, 371). SAN cardiomyocyte apoptosis decreases the volume of spontaneous pacemaking cardiomyocytes and might increase the volume of non-excitable tissue (fibrosis / fibrotic lesions), which increases the electrotonic load, and as with an increase in fibrosis, slows pacemaking and conduction, and / or causes SAN originating arrhythmias (95, 372). Fibrotic lesions and SAN cardiomyocyte apoptosis are commonly associated with atrial fibrillation and alternating tachycardia-bradycardia arrhythmias (361, 373, 374).

Additionally, the ability of the Ca^{2+} and voltage membrane (Vm) clock proteins, cx45 and cholinergic receptor proteins to generate, propagate or modulate a normal HR depends on their cellular location and a relatively uniform distribution throughout the SAN cardiomyocyte and SAN tissue (i.e. there should be no obvious (fibrotic) lesions due to a loss of SAN cardiomyocytes) (86, 368, 375-378).

As far as I know, the SAN has not been investigated for the presence of fibrosis or fat droplet accumulation in an animal model of type 2 DM. Also, the cellular location and pattern of the key SAN clock, cx45 and cholinergic proteins have not been investigated in the DM SAN. Together, this indicates the importance of investigating SAN morphology at the cellular and tissue level in being implicated in the low intrinsic HR in DM.

5.2. Aims and hypothesis

The **aim** of this study was to determine the cellular location, pattern and intensity of the key proteins involved in the SAN clocks (Vm clock: HCN4 and Na^{+}-Ca^{2+} exchanger 1 (NCX1), and Ca^{2+} clock: sarco(endo)plasmic reticulum Ca^{2+}-ATPase 2a (SERCA2a) and ryanodine receptor 2 (RyR2)), conduction pathway (cx45) and cholinergic (muscarinic type 2 (M_2) receptor) systems, the presence of (fibrotic) lesions devoid of HCN4, fibrosis and fat levels in the SAN in DM.

I **hypothesised** a disruption in the location and pattern of the key pacemaking and cx45 proteins; increased HCN4 and NCX1 (Vm clock), unchanged SERCA2a and decreased RyR2 (Ca^{2+} clock), unchanged cx45 and increased M_2 receptor immunofluorescent signal intensity; the presence of (fibrotic) lesions devoid of HCN4; an increase in fibrosis around, and fat accumulation around or within the SAN cardiomyocytes, in the SAN of DM ZDF rats compared to their nDM littermates.

5.3. Methodology

Detailed methodology used in this study can be found in Chapter 2. Experimental techniques applied here include heart tissue isolation, heart tissue processing and cryosectioning, immunohistochemistry, confocal microscopy, image and statistical analysis.

5.3.1 Use of immunofluorescence and western blotting

The immunofluorescence study presented in this chapter was carried out in parallel to western blotting (Chapter 3). The immunofluorescence technique allowed visualisation of the cellular location and pattern of the pacemaking, cx45 and cholinergic proteins and to determine whether these are altered between the nDM and DM SAN tissue. Additionally, it enabled quantification of the immunofluorescent signal intensity as a measure of protein expression, whilst the more sensitive method of western blotting was carried out to better represent protein expression changes within a more complete SAN tissue sample (versus the one tissue cryosection used per animal during immunofluorescence). Western blotting also enabled a more accurate measure of protein expression changes by analysis of the correct molecular band and prevented quantification of non-specific labelling detected by the polyclonal antibodies, which cannot be excluded during quantification of the immunofluorescent signal.

5.4. Results

5.4.1 Animal characterisation

Table 5.1 presents the standard animal characteristics for the Zucker Diabetic Fatty (ZDF) rats. Unfortunately, the statistical significance of blood glucose between the ZDF$^{fa/+,\ +/+}$ and ZDF$^{fa/fa}$

rats could not be compared due to the high number of ZDF$^{fa/fa}$ rats that were excluded as a result of a 'high' blood glucose reading (>33.3 mmol/L, 5 out of 7 rats). If included the Mann-Whitney (non-parametric) test has a *p*-value of *0.0006* (ZDF$^{fa/+,\ +/+}$ 20.0 ± 1.2 mmol/L versus ZDF$^{fa/fa}$ 32.9 ± 0.2 mmol/L, *p<0.001*), indicating the diabetic (DM) state of the ZDF$^{fa/fa}$ rats. Also, consistent with previous data in this thesis, a markedly decreased intrinsic HR was found in the ZDF$^{fa/fa}$ hearts. No significant differences were determined in body weight or *in vivo* HR, which was measured under isoflurane anaesthesia.

Table 5.1. Animal characteristics for non-diabetic (nDM) and diabetic (DM) rats used for immunofluorescence and histology. nDM n=7 and DM n=7 (blood glucose DM n=2), mean ± SEM, unpaired t test.

Parameter	nDM (ZDF$^{fa/+,\ +/+}$)	DM (ZDF$^{fa/fa}$)	*P value*
Weight (g)	391 ± 8	391 ± 8	*>0.05*
Blood glucose (mmol/L)	20.0 ± 1.2	32.0 ± 0.2	-
***In vivo* heart rate (bpm)**	312 ± 8	293 ± 12	*>0.05*
***Ex vivo* intrinsic heart rate (bpm)**	208 ± 14	146 ± 11	* *<0.01*

5.4.2 Immuno-labelling of the type 2 diabetic sinoatrial node

5.4.2.1 Outlining the sinoatrial node and gross morphology

In order to compare the cellular and gross tissue distribution of the SAN proteins in the nDM and DM SAN, it was important to delineate the SAN tissue from the surrounding right atrial tissue. **Figure 5.1** shows a typical 10x overview of an nDM and DM SAN sample in the transverse plane, triple immuno-labelled for SAN marker HCN4, and cx43 and nuclei. HCN4-

positive and cx43-negative labelling were found in a distinctive area that also included the SAN artery, whereas this labelling pattern was not found in the surrounding area enclosing the right atrial lumen. This was the case for all samples used. Hence, cx43 was used as a negative marker to delineate the SAN for further imaging. During imaging, care was taken to avoid imaging of the SAN periphery, which was visually identified as SAN extension regions merging with the right atria and / or overlap of HCN4-positive and cx43-positive immuno-labelling within SAN peripheral cardiomyocytes. Importantly, no obvious gross structural abnormalities (i.e. lesions with absent HCN4 protein expression) were observed between the nDM and DM SAN (**Figure 5.1**).

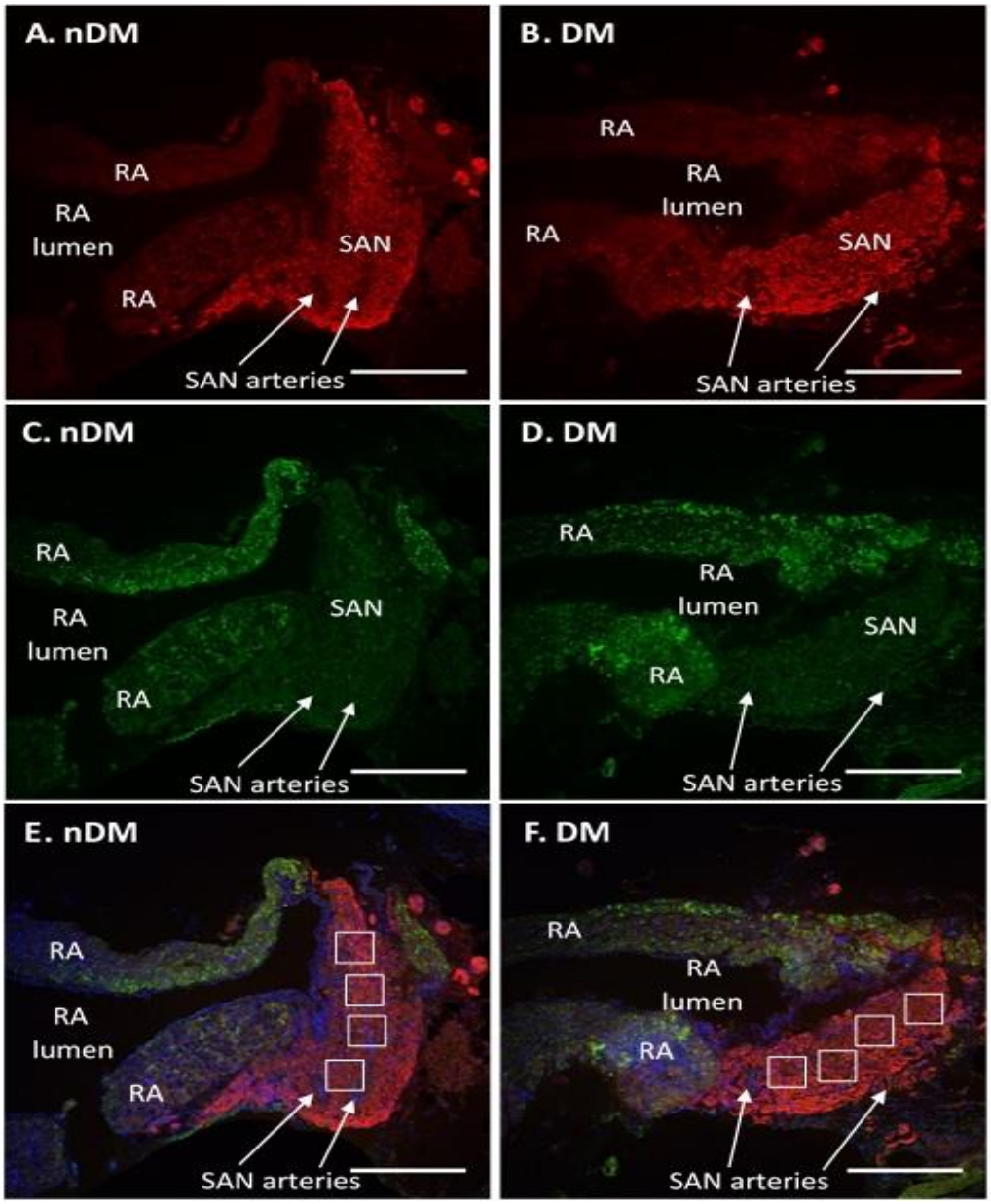

Figure 5.1. Delineating and gross morphology of the sinoatrial node. (A. and B.) Triple immunofluorescent labelling in non-diabetic (nDM) and diabetic (DM) tissue in the transverse plane showing hyperpolarisation-activated cyclic nucleotide-gated channel 4 (**HCN4**, **red**) present only in the sinoatrial node (SAN) and absent in the right atria (RA). No obvious structural abnormalities (lesions) with absent HCN4 immuno-labelling were observed between the nDM and DM SAN. (C. and D.) Connexin 43 (**cx43**, **green**) present only in the RA and absent in the SAN. (E. and F.) Merged images clearly illustrate defined regions of the SAN and RA, and includes **nuclei** labelling (**blue**). For all subsequent immuno-labelling, cx43 was used as a negative marker for the SAN along with the protein of interest. The small squares demonstrate how four 60x images in the SAN were captured. nDM n=7 and DM n=7, 10x NA 0.45, 200µm scale bar.

5.4.2.2 No difference in cx45 immuno-labelling location, pattern and intensity in the type 2 diabetic sinoatrial node

After establishing a way to delineate the SAN, the cellular location, pattern and intensity of the SAN proteins were investigated between the nDM and DM SAN. **Figure 5.2** presents cx45 immuno-labelling in the nDM and DM SAN. A typical punctate labelling pattern was observed in the nDM and DM SAN cardiomyocytes. In both groups, this labelling pattern was not exclusively present on the sarcolemma (where neighbouring cardiomyocytes are expected to couple) but was also localised to the nuclei and intracellularly (102, 103, 105). No significant difference in cx45 signal intensity was found between the nDM and DM SAN (nDM 215 ± 41 versus DM 224 ± 46, *p=0.89*). This suggests cx45 cellular localisation and expression is not altered in DM.

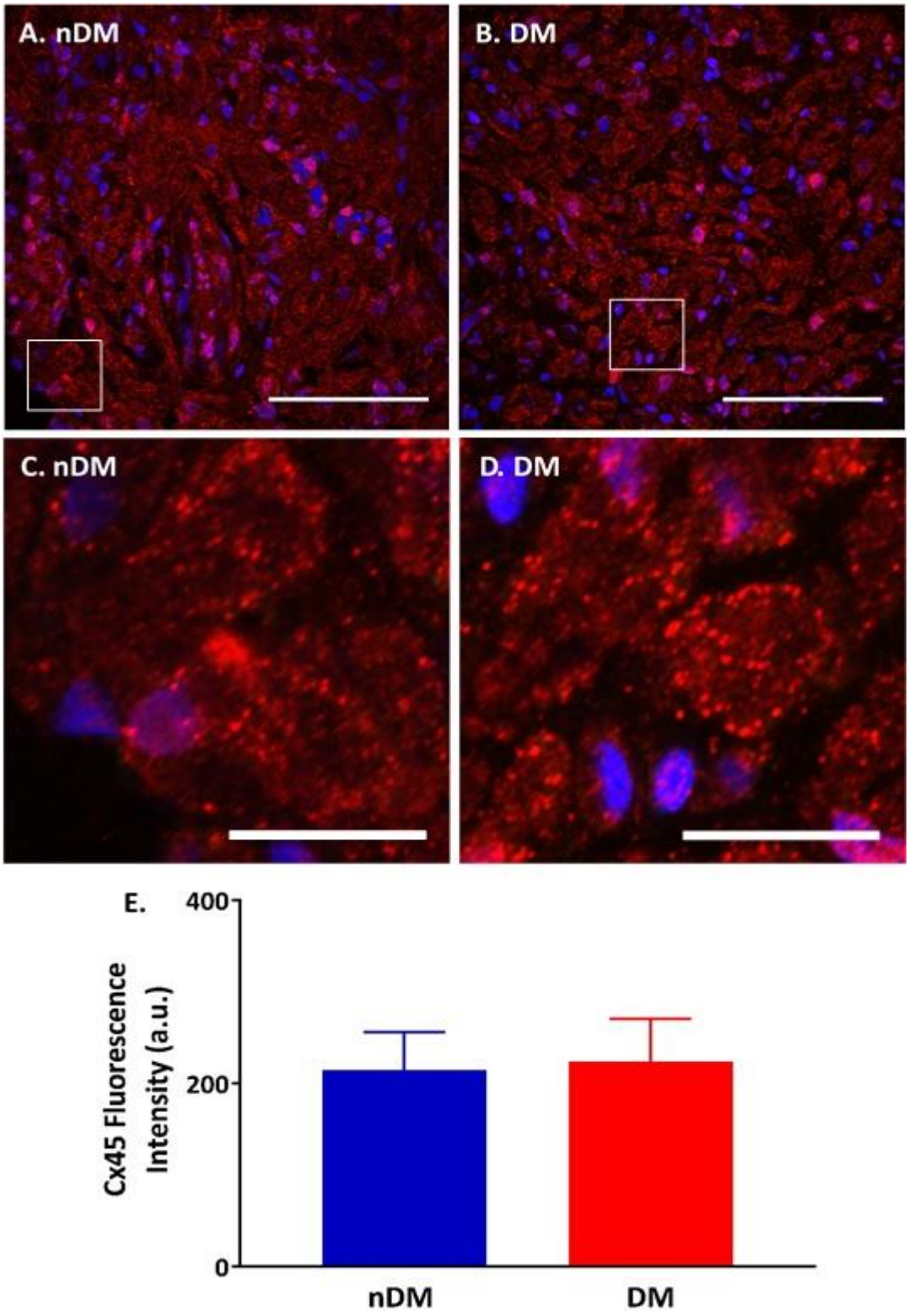

Figure 5.2. Connexin 45 immuno-labelling in the sinoatrial node. Representative (A. and C.) non-diabetic (nDM) and (B. and D.) diabetic (DM) sinoatrial node (SAN) connexin 45 (**cx45**, **red**) and **nuclei** (**blue**) immunofluorescence labelling. (C. and D.) The magnified image displays the punctate labelling pattern. (E.) No significant difference was seen in cx45 intensity between nDM and DM SAN. nDM n=5 and DM n=6, 60x NA 1.4, (A. and B.) 50µm scale bar, (C. and D.) 10µm scale bar, (E.) mean ± SEM, *p>0.05*, unpaired t test.

5.4.2.3 Vm clock: no difference in HCN4 and NCX1 immuno-labelling location, pattern and intensity in the type 2 diabetic sinoatrial node

The Vm clock protein (HCN4 and NCX1) immuno-labelling was compared between the nDM and DM SAN. HCN4 immuno-labelling and intensity quantification in the nDM and DM SAN is presented in **Figure 5.3**. In nDM and DM SAN cardiomyocytes, HCN4 labelling was observed on the sarcolemma and no evident labelling was present intracellularly. The presence of round and elongated spindle-shaped SAN cardiomyocytes can be observed in the nDM and DM tissue. There was no difference in the HCN4 intensity between the nDM and DM SAN (nDM 660 ± 81 versus DM 689 ± 72, *p=0.80*). NCX1 immuno-labelling was observed on the SAN cardiomyocyte sarcolemma and intracellularly in nDM and DM SAN. No significant difference in NCX1 labelling intensity between nDM and DM SAN was found (nDM 715 ± 62 versus DM 893 ± 160, *p=0.33*, **Figure 5.4**). This suggests HCN4 and NCX1 cellular location and (based on this immuno-labelling data alone) expression is not altered in DM.

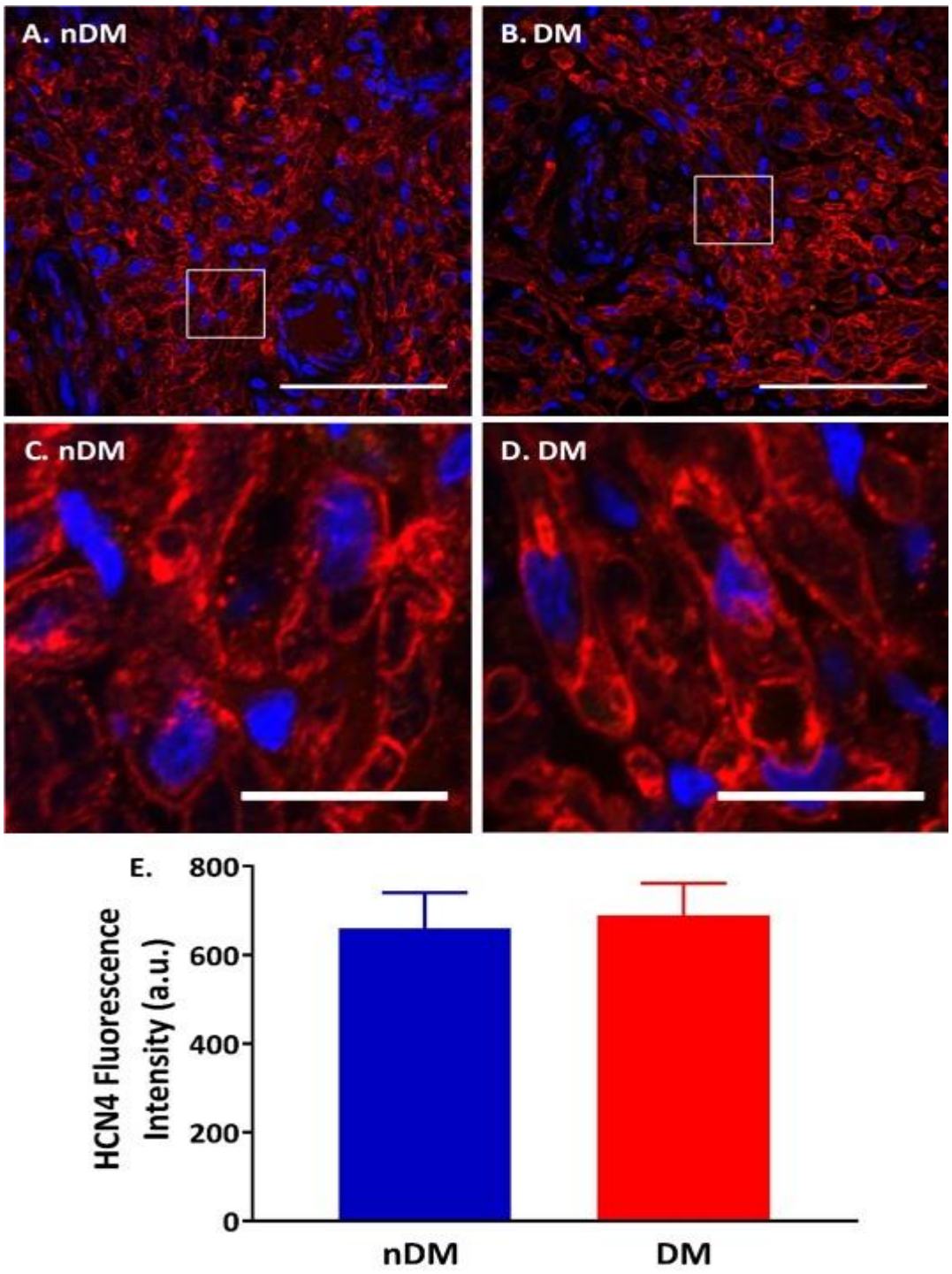

Figure 5.3. Hyperpolarisation-activated cyclic nucleotide-gated channel 4 immuno-labelling in the sinoatrial node. Representative (A. and C.) non-diabetic (nDM) and (B. and D.) diabetic (DM) sinoatrial node (SAN) hyperpolarisation-activated cyclic nucleotide-gated channel 4 (**HCN4**, **red**) and **nuclei** (**blue**) immunofluorescence labelling, with the presence of the SAN artery. (C. and D.) Magnified images highlight membrane specific labelling. (E.) No significant difference was seen in HCN4 intensity between nDM and DM SAN. nDM n=4 and DM n=5, 60x NA 1.4, (A. and B.) 50µm scale bar, (C. and D.) 10µm scale bar, (E.) mean ± SEM, *p>0.05*, unpaired t test.

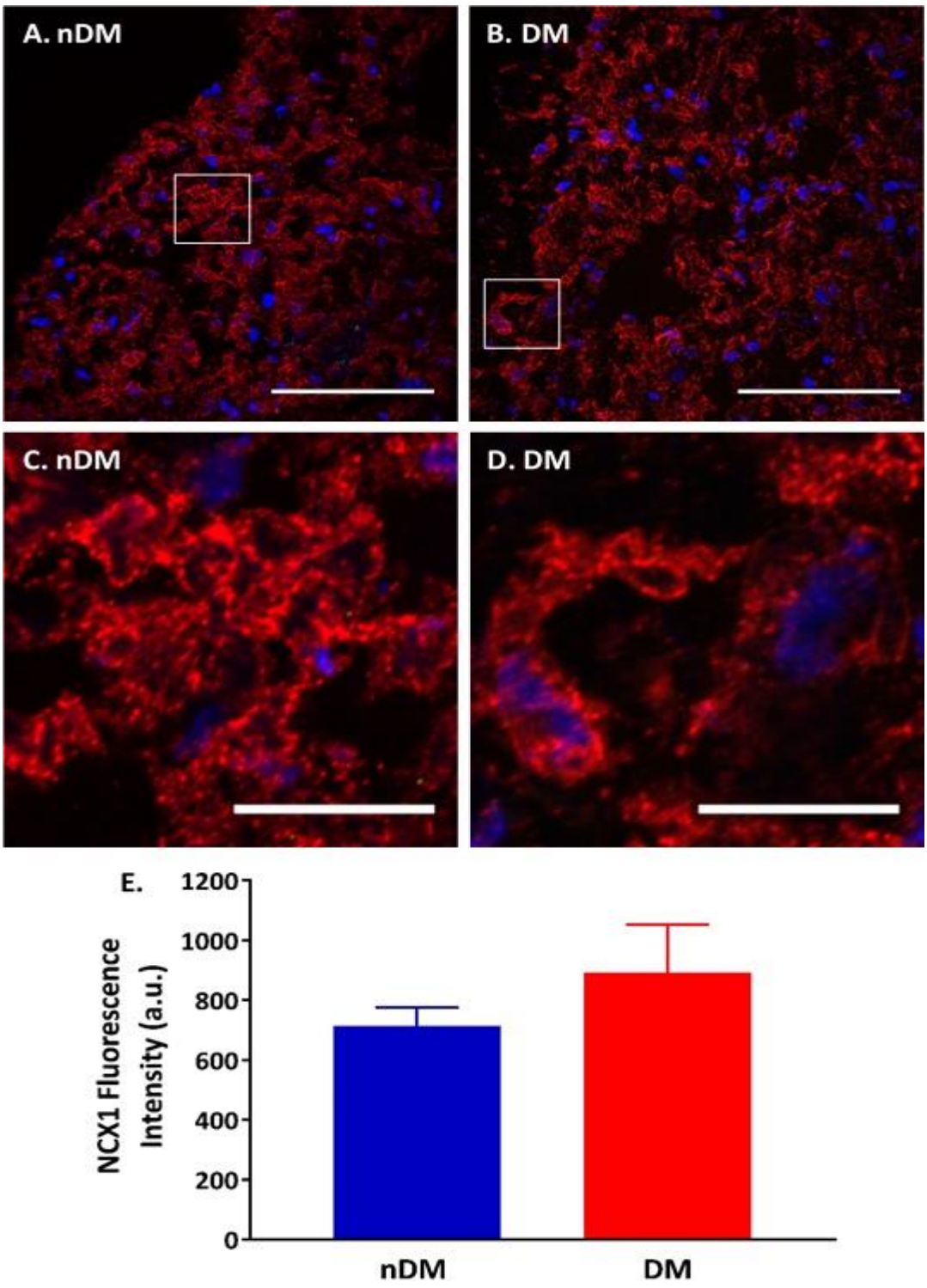

Figure 5.4. Na^+-Ca^{2+} exchanger 1 immuno-labelling in the sinoatrial node. Representative (A. and C.) non-diabetic (nDM) and (B. and D.) diabetic (DM) sinoatrial node (SAN) Na^+-Ca^{2+} exchanger 1 (**NCX1**, **red**) and **nuclei** (**blue**) immunofluorescence labelling. (C. and D.) The magnified images present a membrane and intracellular labelling pattern. (E.) No significant difference was seen in NCX intensity between nDM and DM SAN. nDM n=5 and DM n=5, 60x NA 1.4, (A. and B.) 50µm scale bar, (C. and D.) 10µm scale bar, (E.) mean ± SEM, *p>0.05*, unpaired t test.

5.4.2.4 Ca^{2+} clock: no difference in SERCA2a and RyR2 immuno-labelling location, pattern and intensity in the type 2 diabetic sinoatrial node

Having found no change in the immuno-labelling of the Vm clock proteins, the Ca^{2+} clock proteins (SERCA2a and RyR2) were immuno-labelled in the nDM and DM SAN. SERCA2a labelling and intensity quantification are presented in **Figure 5.5**. An intracellular labelling pattern can be visualised in nDM and DM SAN cardiomyocytes. There was no difference in the SERCA2a signal intensity between the nDM and DM SAN (nDM 565 ± 29 versus DM 595 ± 33, *p=0.52*). RyR2 labelling and intensity quantification are presented in **Figure 5.6**. The intracellular labelling pattern can be observed within nDM and DM SAN cardiomyocytes. No difference in the RyR2 intensity existed between the nDM and DM SAN (nDM 462 ± 138 versus DM 474 ± 26, *p=0.86*). This suggests SERCA2a and RyR2 cellular location and expression is not altered in DM.

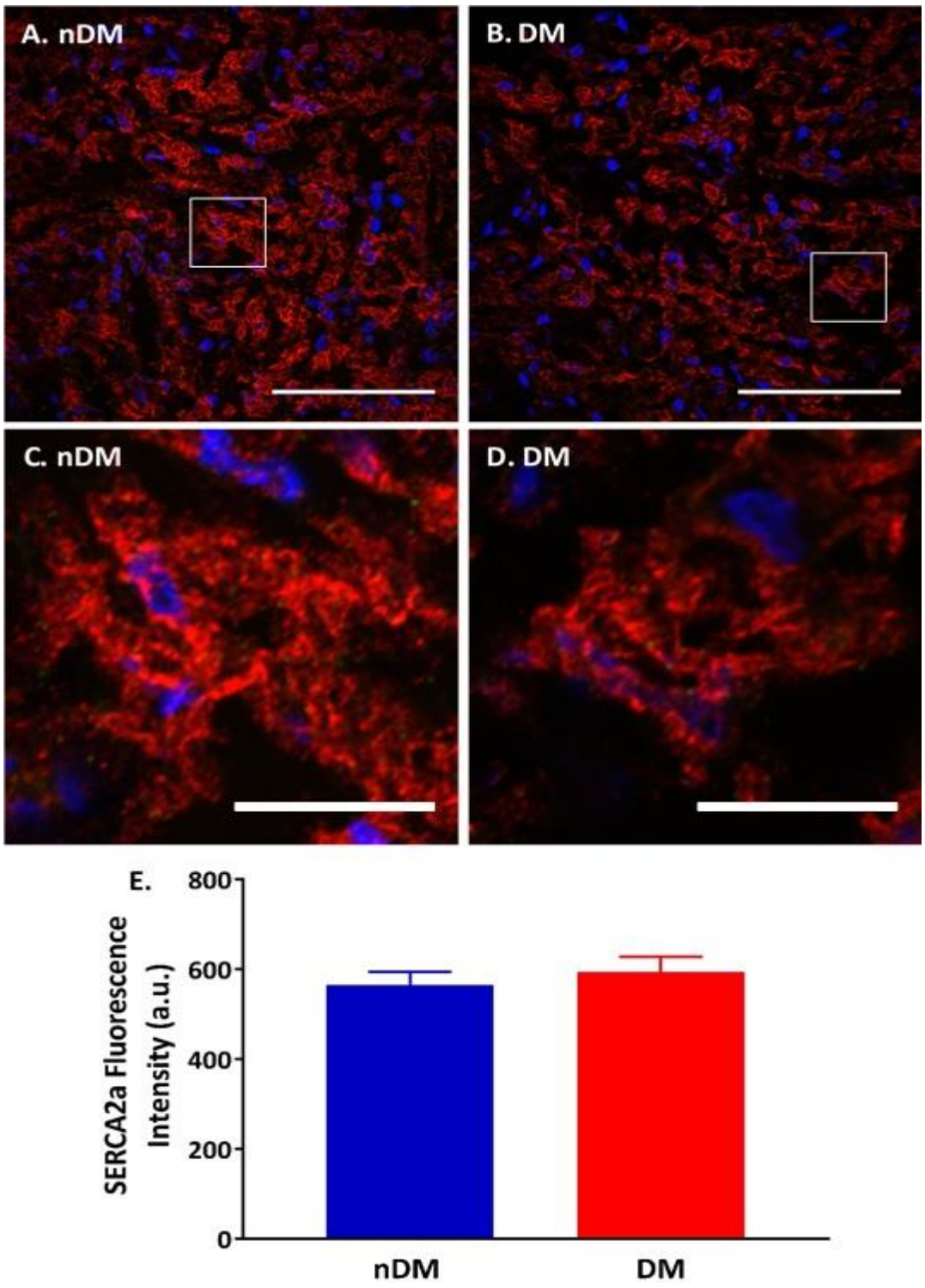

Figure 5.5. Sarco(endo)plasmic reticulum Ca^{2+}-ATPase 2a immuno-labelling in the sinoatrial node. Representative (A. and C.) non-diabetic (nDM) and (B. and D.) diabetic (DM) sinoatrial node (SAN) sarco(endo)plasmic reticulum Ca^{2+}-ATPase 2a (**SERCA2a**, **red**) and **nuclei** (**blue**) immunofluorescence labelling. (C. and D.) The magnified image shows the intracellular sarcoplasmic reticulum labelling pattern. (E.) No significant difference was seen in SERCA2a intensity between the nDM and DM SAN. nDM n=5 and DM n=5, 60x NA 1.4, (A. and B.) 50µm scale bar, (C. and D.) 10µm scale bar, (E.) mean ± SEM, *p<0.05*, unpaired t test.

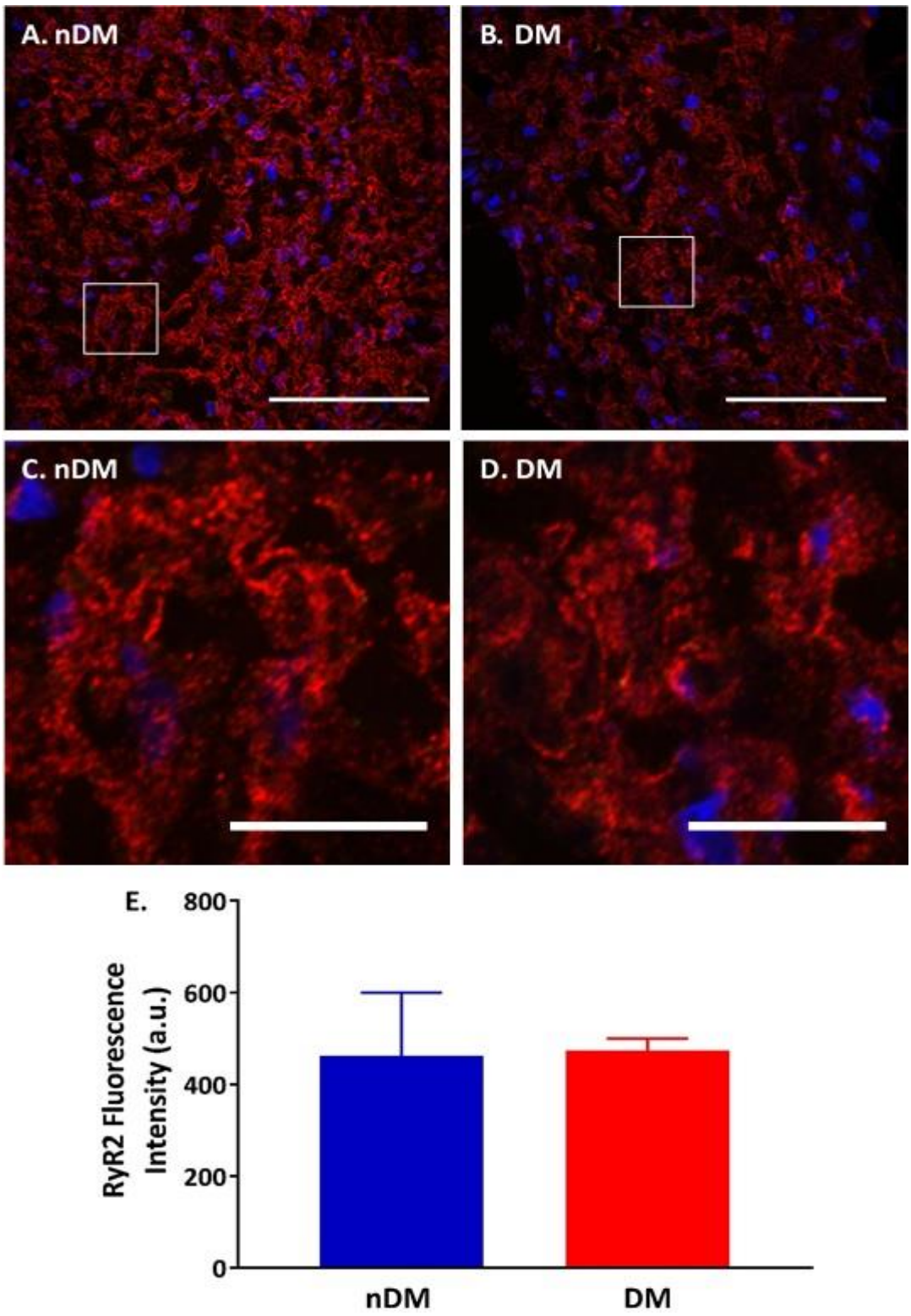

Figure 5.6. Ryanodine receptor 2 immuno-labelling in the sinoatrial node. Representative (A. and C.) non-diabetic (nDM) and (B. and D.) diabetic (DM) sinoatrial node (SAN) ryanodine receptor 2 (**RyR2**, **red**) and **nuclei** (**blue**) immunofluorescence labelling. (C. and D.) The magnified image displays intracellular labelling pattern. (E.) No significant difference was seen in RyR2 intensity between nDM and DM SAN. nDM n=3 and DM n=4, 60x NA 1.4, (A. and B.) 50µm scale bar, (C. and D.) 10µm scale bar, (E.) mean ± SEM, *p>0.05*, Mann-Whitney test.

5.4.2.5 No difference in M_2 receptor immuno-labelling location, pattern and intensity in the type 2 diabetic sinoatrial node

Having found no change in the location, pattern and intensities of key proteins for both SAN clocks and cx45, immuno-labelling for cholinergic protein (M_2 receptor) were also compared between the nDM and DM SAN. M_2 receptor immuno-labelling and intensity quantification for the nDM and DM SAN is presented in **Figure 5.7**. In nDM and DM SAN cardiomyocytes, the M_2 receptor presented a partial sarcolemmal labelling pattern. No obvious M_2 receptor labelling was observed intracellularly. There was no significant difference in the M_2 receptor signal intensity between the nDM and DM SAN (nDM 371 ± 86 versus DM 587 ± 93, *p=0.13*). This suggests M_2 receptor cellular location and expression is not altered in DM.

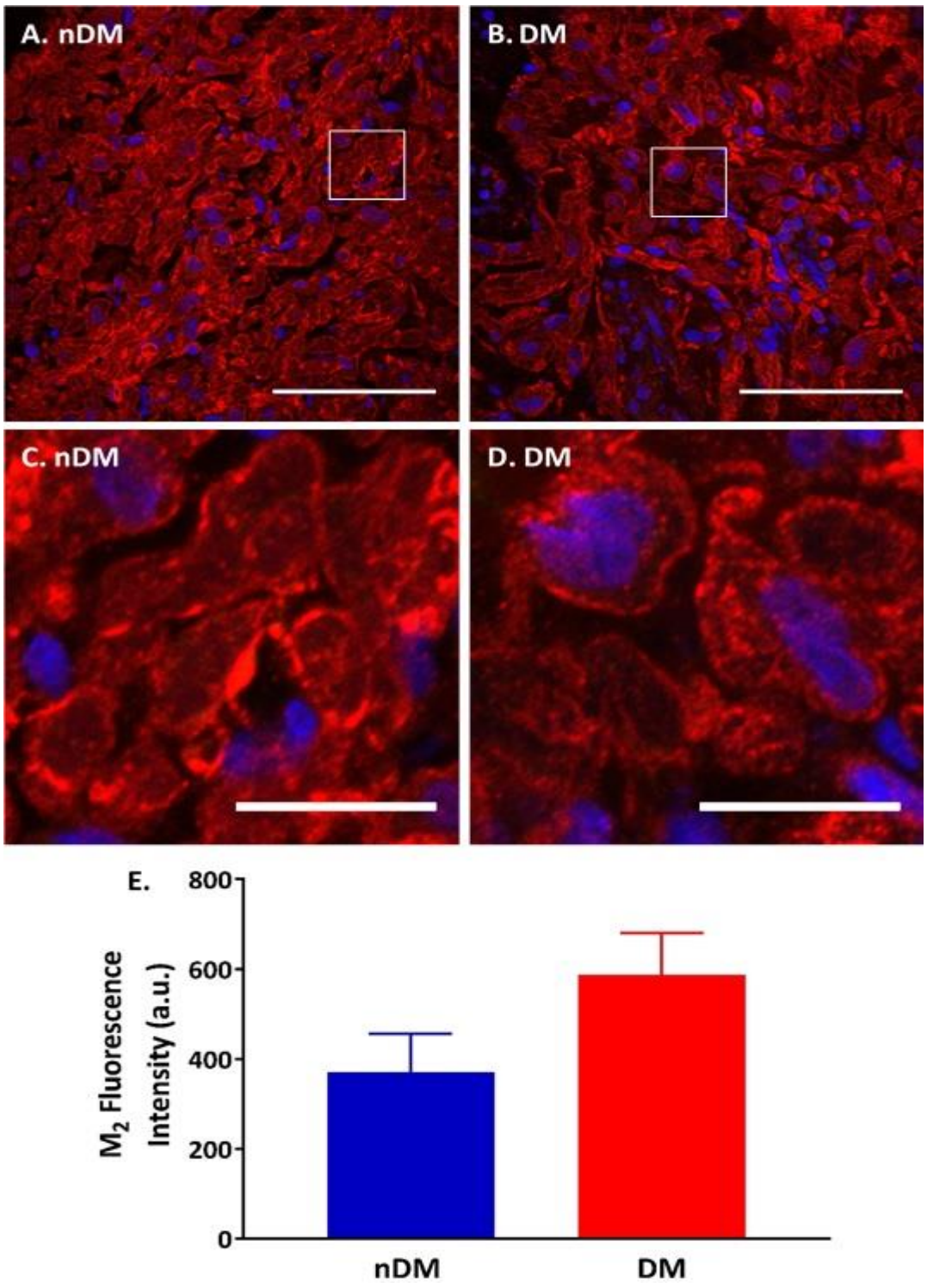

Figure 5.7. Muscarinic type 2 receptor immuno-labelling in the sinoatrial node. Representative (A. and C.) non-diabetic (nDM) and (B. and D.) diabetic (DM) sinoatrial node (SAN) muscarinic type 2 receptor (M_2, red) and nuclei (blue) immunofluorescence labelling. (C. and D.) The magnified image shows a partial membrane labelling pattern. (E.) No significant difference was seen in M_2 intensity between nDM and DM SAN. nDM n=5 and DM n=6, 60x NA 1.4, (A. and B.) 50µm scale bar, (C. and D.) 10µm scale bar, (E.) mean ± SEM, *p>0.05*, unpaired t test.

5.4.3 Histology of the type 2 diabetic sinoatrial node

Following immuno-labelling evaluation of key Vm and Ca^{2+} clock, cx45 and cholinergic proteins, the nDM and DM SAN were investigated for fibrosis around, and fat accumulation around or within, the cardiomyocytes in the SAN.

5.4.3.1 No difference in fibrosis levels in the diabetic sinoatrial node

Masson's trichrome stain was used to evaluate the extent of connective tissue that stained blue among the nDM and DM SAN cardiomyocytes as a measure of fibrosis, as well as other possible cell types (fibroblasts, connective tissue cells, immune cells within the SAN region (379)) that stained purple **(Figure 5.8)**. As can be observed by the blue staining surrounding the SAN, the SAN is relatively separated from the surrounding right atrial myocardium. The SAN cardiomyocytes are small, interweaving and less organised compared to right atrial cardiomyocytes. The intra-SAN fibrosis levels were quantified (i.e. excluding the physiological connective border surrounding the SAN and right atria). No obvious fibrotic lesions and no difference in the level of fibrosis were observed around the cardiomyocytes of the SAN between nDM and DM. This was further confirmed by quantification of the percentage of the tissue attributed to fibrosis staining, which was not significantly different between groups (nDM 12.0 ± 0.9% versus DM 9.5 ± 1.2%, *p=0.16*).

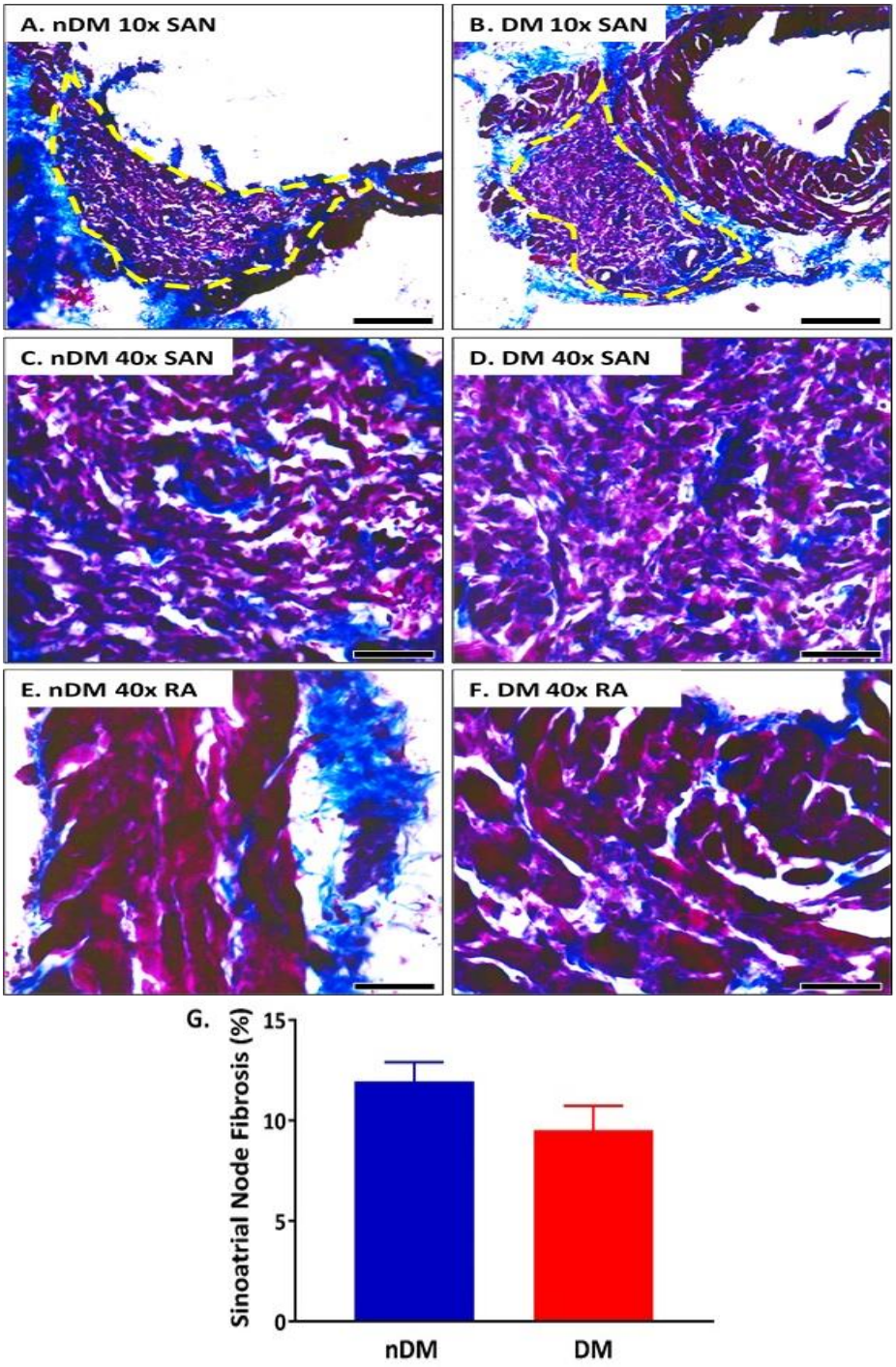

Figure 5.8. Fibrosis in the sinoatrial node. Representative (A., C. and E.) non-diabetic (nDM) and (B., D. and F.) diabetic (DM) Masson's trichrome stained sinoatrial node (SAN) and right atria (RA) labelling **connective tissue** (fibrosis measure) in **blue** and **cardiomyocytes** and other cells in **purple**. (A. and B.) 10x images with the SAN region outlined in yellow and neighbouring right atria. (C. and D.) 40x images of the nDM and DM SAN. (E. and F.) 40x images of the nDM and DM right atria. (G.) No significant difference was found in fibrosis levels between nDM and DM SAN. nDM n=5 and DM n=6, (A. and B.) 10x, 200µm scale bar, (C. – F.) 40x, 50µm scale bar, (G.) mean ± SEM, *p>0.05*, unpaired t test.

5.4.3.2 No difference in fat accumulation in the diabetic sinoatrial node

Oil Red O stain was used to label fat droplets that stained red within or surrounding the SAN cardiomyocytes (and other cell types within the SAN region (379)) that stained pink / purple **(Figure 5.9)**. Only a very limited number of fat droplets were present within or surrounding the SAN cardiomyocytes, and no difference in fat quantity was found between nDM and DM (nDM 0.24 ± 0.14% versus DM 0.14 ± 0.13%, *p=0.65*). Outside of the SAN, more fat accumulation was observed, which most likely is extra-pericardial fat that surrounds the heart. This was not quantified because during cardiac excision, excess tissue, including extra-pericardial fat, was trimmed away, so the labelled fat cannot provide a representative accurate quantitative measure of the total fat that might have accumulated around the atrium. Nonetheless, no obvious fat infiltration into the SAN / atrial myocardium was observed. Collectively, these findings suggest that fibrosis and fat levels do not contribute to the decreased intrinsic HR in DM.

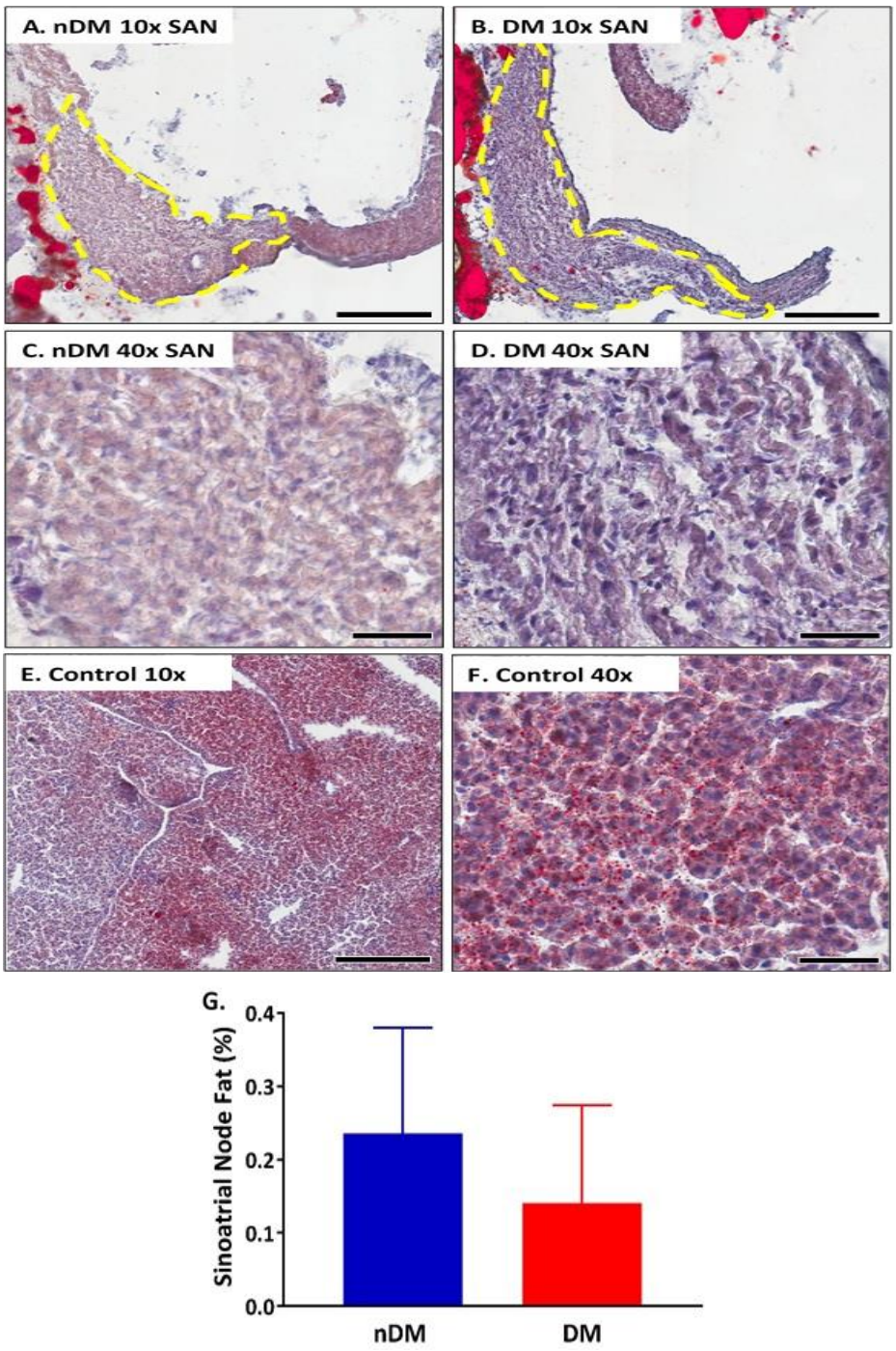

Figure 5.9. Fat in the sinoatrial node. Representative Oil Red O stained (A. and C.) non-diabetic (nDM) and (B. and D.) diabetic (DM) sinoatrial node (SAN), and (E. and F.) positive control (liver tissue section) labelling **fat droplets** in **red**, **cardiomyocytes** and other cells in **pink / purple** and **nuclei** in **purple**. (A. and B.) 8x images with the SAN region outlined in yellow and neighbouring right atria and (E.) liver tissue control. (D. and E.) 40x images of the nDM and DM SAN and (F.) liver tissue control. (G.) No significant difference was seen in fat infiltration in the SAN between nDM and DM. nDM n=6 and DM n=5, (A., B. and E.) 8x, 300µm scale bar, (C., D. and F.) 40x, 50µm scale bar, (G.) mean ± SEM, *p>0.05*, unpaired t test.

5.5. Discussion

In this study, the gross morphology, as well as the cellular location, pattern, and expression of the Vm and Ca^{2+} clock, cx45 and cholinergic proteins were compared between the nDM and DM SAN using immunofluorescence. The nDM and DM SAN were also investigated for fibrosis and the accumulation and infiltration of fat droplets using histology stains. The primary findings of this chapter are: (a) no differences were observed in the location and pattern of the Vm and Ca^{2+} clock, cx45 and M_2 receptor proteins between the nDM and DM SAN, (b) no differences were found in immuno-labelling intensities (as a measure of protein levels) of cx45, HCN4, NCX1, SERCA2a, RyR2 and M_2 receptor between the nDM and DM SAN, (c) no obvious fibrotic lesions were found between the nDM and DM SAN, and (d) no difference in fibrosis and fat droplets or infiltration between the nDM and DM SAN.

5.5.1 Immuno-labelling location and pattern of cx45, sinoatrial node clocks and cholinergic proteins

Robust pacemaking is dependent on the location and intra-cellular spatial arrangement of the various proteins (86, 87, 378). The lack of obvious differences observed in the cellular location and pattern of the Vm and Ca^{2+} clock, cx45 and cholinergic proteins, opposed to my hypothesis, suggests that for the proteins investigated in this study at this stage of the DM disease altered cellular protein distribution is not accountable for the lower intrinsic HR in DM. However, these macro-scale observations were determined using confocal microscopy, which has a limited resolution (~250 nm) thereby unable to differentiate between two neighbouring proteins (or protein clusters). A more detailed nanoscale analysis of subcellular microdomain arrangement or possible DM microdomain remodelling would be required using super-resolution microscopy to further confirm these findings (378, 380).

5.5.1.1 Cx45

As shown in this study and by others, cx45 immuno-labelling presents a punctate labelling pattern in the nDM and DM SAN cardiomyocytes (381-383). However, in both nDM and DM SAN, this immuno-labelling was not exclusive to the sarcolemma, where cardiomyocytes are expected to couple, and additional non-specific immuno-labelling was present intracellularly and localised to the nuclei. The reports on cx45 expression within the cardiac conduction system (CCS) / heart have been varying and conflicting, which is in part attributed to non-specific cx45 antibodies (100, 103, 105). For example, studies have shown cx45 antibodies cross-react with cx43 protein within the heart (103, 105). This is not expected to be the case in the nDM and DM SAN as cx43 is not expressed in the SAN centre but suggests the lack of cx45-specific antibodies. The presence of a strong cx45 protein expression / band in the nDM left ventricle (LV) tissue compared to nDM and DM SAN tissue can be observed by western blot (see Figure 3.ii in the Appendix). This suggests that the cx45 antibody used in my study for western blotting and immunofluorescence is likely to be non-specific as cx45 expression in the rat working myocardium is found to be lower in comparison to the rat SAN / CCS (103, 105). Cx45 expression within the DM SAN is likely to require further investigation, possibly with sarcolemmal staining (such as wheat germ agglutinin (384)), such that cx45 localised to the sarcolemma can be determined. As sarcolemmal immuno-labelling observed might also be non-specific, the use of an additional cx45 antibody would be important to validate these results.

Cx alterations have been investigated in relation to DM arrhythmias in type 1 and type 2 DM SAN (197, 385). In the type 1 DM rat SAN, with significantly prolonged cycle length and conduction time, mRNA expression revealed significantly increased cx45 compared to control

(236, 260). No other significant differences in mRNA expression were found for cx40 and cx43 in the SAN, right atria or right ventricle (236, 260). Cx43 protein expression is not found in the SAN centre, however, cx43 mRNA expression is detected but is still significantly lower than mRNA expression in the SAN periphery and right atrial tissues (32). In contrast, cx45, cx43 and cx40 mRNA levels in the SAN of Goto-Kakizaki lean type 2 DM rats were all significantly decreased compared to control (197). However, this effect might be attributed to a lean versus obese type 2 DM model and / or an age-induced effect as the rats were 12 – 13 months of age (197) (versus 19 – 22 weeks old in this study). Nonetheless, these mRNA findings were not followed up by investigation of protein expression, which would provide a further understanding of conduction alterations in these DM SAN models. Due to the lack of specificity of the cx45 antibody used in my study, I cannot conclude on whether cx45 alterations (protein expression and immunofluorescence (location and pattern)) are responsible for the lower intrinsic HR in the DM ZDF heart and requires investigation in future.

5.5.1.2 Sinoatrial node clocks

My data are in agreement with previous studies showing that HCN4 is located on the sarcolemma of the nDM and DM SAN cardiomyocytes (47, 381, 386). No obvious intracellular HCN4 labelling was found in the nDM or DM SAN, which is suggestive of unaltered HCN4 protein translation or trafficking (381). NCX1, SERCA2a and RyR2 immuno-labelling were all predominantly seen on or close to the sarcolemma and intracellularly (86, 317, 387, 388). However, whether the intracellular labelling of these proteins is truly attributed to either the T-tubule or SR network within the SAN cardiomyocytes, or is due to non-specific antibody binding is difficult to confirm from these nDM and DM SAN images as SAN cardiomyocytes are small, poorly aligned, interweaving and unorganised, and thereby difficult to acquire in a

longitudinal orientation in comparison to atrial or ventricular cardiomyocytes (14, 39). Moreover, SAN cardiomyocytes are shown to lack a well-developed T-tubule (described to be short, narrow and irregular) and SR network (16, 45, 86). Pacemaking is thought to occur beneath the sarcolemma of SAN cardiomyocytes (16). The NCX1, SERCA2a and RyR2 immuno-labelling might suggest a greater T-tubule and SR network presence in the rat SAN cardiomyocytes in comparison to the rabbit SAN cardiomyocytes (16, 86, 387, 388). This would require further confirmation such as wheat germ agglutinin T-tubule labelling of the rat SAN cardiomyocyte membrane (384). These differences might potentially be attributed to species-specific differences in pacemaking and HR.

5.5.1.3 Cholinergic protein

In my study, M_2 receptor immuno-labelling presented a partial sarcolemma labelling pattern in the nDM and DM SAN. This is in contrast to a previous study where M_2 receptor immuno-labelling was observed on the entire sarcolemma in the ferret SAN (did not investigate the rat SAN) (145). This difference in the M_2 receptor labelling pattern is likely to be the result of species-specific differences.

5.5.2 Immuno-labelling intensities of the clocks, cx45 and cholinergic proteins

The semi-quantitative intensity analysis, carried out in parallel with western blotting (Chapter 3), was also used to determine protein expression changes within the nDM and DM SAN cryosections. However, in contrast to the western blot data presented in Chapter 3, no changes in the intensity were found by immunofluorescence. The western blot data presented unchanged cx45 (requires confirmation due to non-specificity of antibody), significantly

increased HCN4, significantly increased NCX1, unchanged SERCA2a and significantly increased M_2 receptor protein expression. RyR2 could not be evaluated by western blotting due to low amounts of total protein obtained from the SAN samples, with RyR2 immuno-labelling suggesting expression is not altered between the nDM and DM SAN. However, due to the protein expression differences presented via western blotting versus immunofluorescence for other proteins, RyR2 protein expression should also be investigated via western blotting in future.

Whilst the majority of proteins analysed did not show similar results for the two methods of expression quantification, potential reasons for the differences observed between immunofluorescence and western blotting data could include: (a) immunofluorescence utilised one 20 µm cryosection per SAN sample to determine possible protein changes, which might not be a sufficient representative of the SAN, (b) due to different antibodies being used for immunofluorescence and western blotting (NCX1, RyR2 and the M_2 receptor, see below) and / or all the antibodies used for immunofluorescence were polyclonal, so the specificity of the labelling could be questioned (i.e. non-specific labelling was quantified as compared to only analysing the correct molecular weight band via western blot), (c) immunofluorescence technique was not sensitive enough to detect small protein changes, and (d) technical variability such as confocal imaging on the different days. As a result of the above factors, it is possible that subtle protein expression alterations were masked in the DM SAN using immunofluorescence.

The lack of difference detected using immunofluorescence for the proteins that were altered using western blot (significantly increased HCN4, NCX1 and M_2 receptor) is likely to be

attributed to non-specific polyclonal antibody binding used for immunofluorescence and its quantification. The more sensitive western blots presented several non-specific bands for HCN4. For NCX1 and M_2 receptor protein expression, different monoclonal antibodies were used for western blotting compared to the polyclonal antibodies used for immunofluorescence. The different antibodies for NCX1, RyR2 and the M_2 receptor (details provided in Chapter 2, Table 2.4 and Table 2.15) were used due to non-specific and / or the inability of the immuno-labelling antibodies to detect bands at the correct molecular band for western blotting or vice versa.

5.5.3 The structure of the type 2 diabetic sinoatrial node

The presence of lesions and the level of fibrosis, as well as, fat droplets and infiltration in the SAN between the nDM and DM was not different. This finding did not support the hypothesis of increased fibrosis and fat deposition in the DM SAN altering SAN structure, HR generation and AP propagation.

5.5.3.1 The absence of lesions in the diabetic sinoatrial node

No obvious (fibrotic) lesions were observed with an absence of HCN4 protein expression between the nDM and DM SAN tissue, which suggests no significant loss of pacemaking cardiomyocytes or formation of replacement fibrosis. This is in contrast to the disease identified as sinus node dysfunction where oxidised Ca^{2+} / calmodulin-dependent protein kinase II (CaMKII) has been found to promote SAN cardiomyocyte apoptosis and / or fibrosis through an angiotensin II-mediated pathway (232, 233, 372). Angiotensin II is also known to be increased in DM, however, the levels of angiotensin II in my DM ZDF model, and whether these levels are sufficient to promote oxidation of CaMKII at this stage of the DM disease,

remains unknown (389). Apoptosis can also result due to chronic activation of CaMKII due to continuous β-adrenergic input that has also been found to be increased in my DM model (165, 371). Although the level of active or oxidised CaMKII between the nDM and DM SAN is unknown, this might suggest no difference in active or oxidised CaMKII at this stage of the DM disease.

5.5.3.2 Sinoatrial node, fibrosis and diabetes

SAN cardiomyocytes are normally nested in connective tissue / fibrosis, therefore, the presence of some fibrosis in both nDM and DM SAN was not surprising (14, 30, 32, 33). However, the lack of increased fibrosis in the DM SAN was surprising as type 1 and type 2 DM has been extensively associated with increased cardiac fibrosis (180, 365, 366, 390-393), however not necessarily in the SAN.

The accumulation of extracellular matrix and its cross-linking is responsible for cardiac stiffening, which contributes to dysfunction in the DM myocardium (365, 390). The mechanisms involved include DM / hyperglycaemia-induced increase in advanced glycation end products (a post-translational modification that adds sugar moieties to proteins), neurohumoral activation, reactive oxygen species, proinflammatory cytokines, growth factors and adipokines that collectively promote fibroblast activation, proliferation and extracellular matrix production (233, 365, 394-398). The expression of profibrotic factors such as transforming growth factor and connective tissue growth factor are also involved (392, 399, 400). The glycosylated proteins cross-link to form advanced glycosylation end products, which become resistant to proteolysis and degradation thereby resulting in fibrosis accumulation (394, 398, 401, 402). As mentioned in the previous section above, the increased oxidative

stress is associated with increases in chronically activated CaMKII (366, 397). Chronically active CaMKII has also been known to activate pro-inflammatory signalling resulting in the recruitment of immune cells and eventual fibrosis (94). Commonly, there is the accumulation of type I and III collagen in both type 1 and type 2 DM (365, 390).

Increased extracellular matrix production by activated fibroblasts has not yet been shown in the SAN of DM experimental animal models, but has been associated with ageing (162, 361). The absence of any one of the above factors in my relatively young 19 – 22 week-old DM ZDF rats might limit fibrosis accumulation in the SAN at this stage of the DM disease. The presence of fibrosis and ischemic lesions have been reportedly observed in the SAN of post-mortem samples of humans with type 2 DM compared to control, however, this was not quantified and no nDM control images were presented for comparison (162). This presence of fibrosis could again be attributed to an age effect (DM group 56 – 73 years versus control group 44 – 56 years) (162, 361). As mentioned, in type 1 DM SAN, oxidised-CaMKII has been identified as a perpetrator for increased SAN apoptosis and fibrosis (230, 233). It might be the lack of sufficient oxidative stress and / or oxidised-CaMKII in the SAN of the ZDF model of DM during this stage of the DM disease that prevented apoptosis and an increase in fibrosis levels.

5.5.3.3 Sinoatrial node, fat and diabetes

Other than the liver, the heart is the second organ to deal with the most lipid fluxes. Nevertheless, excess lipid accumulation is prevented by balancing lipid uptake and oxidation / utilisation (403, 404). The primary source of energy fuel for ATP generation in the heart is via fatty acids (~70%) and the remaining sources being glucose, lactate, ketone bodies and amino acids (404). Alterations in fatty acid oxidation can occur in diseases, such as obesity,

diabetes and heart failure, resulting in structural damage, such as fat droplet and adipose tissue accumulation, contractile dysfunction, fibrosis and cardiomyocyte apoptosis, which in turn is suggested to occur due to mitochondrial dysfunction and oxidative stress (404-410). An increase in plasma free fatty acids, as present in DM, has been linked to an increase in cardiac fatty acid uptake (405, 406, 408-411).

Furthermore, type 1 and type 2 DM has been associated with increased lipotoxicity, which includes tissue fat accumulation, altered fat distribution and adiposopathy in non-adipose tissues such as the heart (ventricle), liver, muscle and pancreatic-islets (410, 412-416). In obese and DM rodent models, an increase in fat droplets within ventricular cardiomyocytes has been shown, which most likely occurred due to increased cardiac expression of proteins involved in fatty acid uptake and storage (410, 415, 417). The presence of lipid droplets can be observed without infiltration of adipocytes in ventricular myocardium (410). Additionally, significantly increased fat tissue in the SAN of a metabolic syndrome rat model was observed compared to the control (55, 404). Therefore, the lack of fat droplets within or around the cardiomyocytes of the SAN in our DM model was unexpected. The absence of fat droplets in the SAN of the DM ZDF rats might also be attributed to their relatively young age and / or the mild high fat diet of the rats.

It has been suggested that cardiomyocytes adapt to the increase in free fatty acid availability by increasing oxidation / utilisation (415, 418). This coping ability is partly regulated by the peroxisome proliferator-activated receptor α (PPAR(-α)) transcription factor (419-421). PPARs function to control the expression of proteins involved in lipid and glucose metabolism (422, 423), with all three PPAR isoforms (α, β / δ, γ) expressed in the heart (422, 423). However,

whether there are SAN tissue-specific differences in PPAR expression remains unknown. Fatty acid and PPAR-α binding trigger the expression of proteins implicated in fatty acid metabolism (424, 425). It is proposed that lipotoxicity might result due to DM disease progression and continued exposure to fatty acids, causing impairment in this transcriptional regulation or via a PPAR-α independent mechanism (415, 418). PPAR-α knockout mice present significantly increased cardiac lipid accumulation, hypoglycaemia (426), no difference to *in vivo* HR on knockout at 16 or 32 weeks of age, abnormal mitochondria, cardiac fibrosis and inflammation (423, 427, 428). Furthermore, other than metabolism, PPAR-α and associated ligands have an anti-fibrotic, anti-inflammatory, anti-oxidative and anti-apoptotic effects (422, 429). It is possible the lack of fat droplets and fibrosis in DM SAN is due to adaptation to this 'for now' coping mechanism for which further investigation is required to confirm.

5.6. Summary

This study has successfully compared the cellular location and pattern of the key SAN clocks and cholinergic proteins between the nDM and DM SAN. No obvious differences were found in cellular location or pattern of SAN clock and cholinergic proteins. This suggests that the location of the key proteins responsible for HR generation and their cholinergic regulators are not altered in the DM SAN. Gross SAN structure, lesion presence, fibrosis and fat accumulation were also not different in the DM SAN. Collectively, my data suggest that the cellular location of the investigated proteins and gross structural changes are not responsible for the decreased intrinsic HR observed in DM.

CHAPTER 6

The Effects of Anaesthetics on Blood Glucose and Heart Rate in Type 2 Diabetes

6.1. Introduction

General anaesthetics result in the loss of consciousness and sensation (430, 431). Due to this net effect, anaesthetics have proven to be particularly useful during surgeries for either treatment or experimental applications, as well as experimental euthanasia (i.e. organ excision) for animal welfare and ethical reasons (432-434). No uniting theory exists of how anaesthetic effects are brought about as they are known to act on multiple proteins and differential degrees of behavioural responses (loss of consciousness, sensation, immobility, analgesia) are facilitated by different anaesthetics (430, 431, 434). The effects of an anaesthetic are exerted on many physiological systems (435, 436). Their actions are time and concentration-dependent, and can also be influenced by metabolic and physiological status, and even vary between strains of experimental animal models (435, 437). Their direct targets include the central and peripheral nervous systems (depress transmission, decrease metabolic rate and oxygen usage), vital organs (heart, lung, liver) and vasculature (435, 436, 438-440). Pertinently, these are all targets of anaesthetics isoflurane and sodium pentobarbital (435, 436, 438-440), which were used in my PhD studies.

Anaesthetics, including isoflurane and sodium pentobarbital, predominantly interact with voltage-gated (Na^+, Ca^{2+}, K^+) and ligand-gated (gamma-aminobutyric acid type A ($GABA_A$, chloride channel), nicotinic, N-methyl-D-aspartate (NMDA, glutamate receptor)) ion channels and G-protein coupled receptors (β-adrenergic) present on the cell membranes of neurones and target organs (430, 431, 435, 436, 438, 439, 441-451). Typically, excitatory channels / mechanisms are inhibited (nicotinic, glutamate and serotonin receptor) and inhibitory channels / mechanisms are promoted ($GABA_A$ and glycine receptor) (431, 434, 439, 442, 452). Generalised outcomes involve depressed ganglionic transmission, reduced sympathetic tone,

vasodilation but with increased coronary and cerebral blood flow, and decreased metabolic activity (435, 453-455). Anaesthetics can directly affect cardiovascular function or indirectly through effects on other systems (436). Understanding the effects of different anaesthetics is limited by the lack of knowledge on how neuronal networks or specific anaesthetic actions on proteins impact behavioural outcomes (434). The duration and concentration of the anaesthetic influences the rate of recovery from anaesthesia after their withdrawal (456).

Isoflurane is an inhalation / volatile anaesthetic with quick induction and elimination effects (435, 456-459). Isoflurane effects occur quickly due to the rapid exchange at the lung to blood transition (440). In relation to the cardiovascular system, in humans and rabbits, isoflurane increases *in vivo* heart rate (HR), but slightly decreases cardiac output and systemic vascular resistance, and consequently mean arterial pressure drops (440, 460, 461). However, significantly decreased *in vivo* HR (compared to the conscious state (435)), respiratory rate and mean blood pressure is found in rodents in a concentration-dependent manner (1.5 – 5% isoflurane) (437). In the isolated guinea-pig heart, direct application of isoflurane in the perfusion buffer decreased intrinsic (*ex vivo*) HR, lengthened atrioventricular conduction time and reduced left ventricular (LV) pressure in a concentration-dependent manner (~0.14 – 0.51 mM) (453, 454, 462). Sodium pentobarbital (belonging to a class of drugs known as barbiturates) is administered as an injectable anaesthetic. In comparison to isoflurane, the onset of effects is slow and long-lasting (436, 457, 463). Sodium pentobarbital (40 mg/kg (464), 50 mg/kg (465)) maintains a relatively stable *in vivo* HR, but decreases cardiac output, myocardial contractility, mean arterial blood pressure and increases peripheral vascular resistance in rodents (464-466). However, decreasing *in vivo* HR with increasing duration of exposure to sodium pentobarbital is observed, as well (467). Direct comparison of isoflurane

and sodium pentobarbital found sodium pentobarbital to be less cardio-depressive compared to isoflurane in the rat cardiovascular system (sodium pentobarbital presented higher HR, LV ejection fraction and fractional shortening) (468, 469). Echocardiography data obtained in conscious rats was not different from echocardiography data obtained in sodium pentobarbital anaesthetised rats (468).

Additionally, anaesthetics can also influence blood glucose. Isoflurane anaesthesia results in significant hyperglycaemia (433, 470-475). Comparatively, sodium pentobarbital has no effects on blood glucose compared to non-anaesthetised controls (475-479). Fasting serum blood glucose was found to be significantly increased in low (1.5%) and high (2.3%) concentrations of isoflurane compared to sodium pentobarbital (50 mg/kg) anaesthesia in rats (475, 480). The mechanisms suggested to be involved in the isoflurane-induced increase in blood glucose will be explored in the discussion section 6.5.1 below.

In my studies, an isoflurane specific effect on blood glucose was noticed in the non-diabetic (nDM) animals during the immunohistochemistry study. The nDM blood glucose measurements were higher during isoflurane use, in agreement with the literature (433, 470-475), however in contrast to findings using urethane anaesthesia (165). As described by the studies above, effects of anaesthetics on the cardiovascular system, especially *in vivo* HR, and on blood glucose are well studied (440, 442, 470, 474, 476, 477). However, the possible effects of anaesthetics on intrinsic HR due to residual anaesthetic or a direct effect on the sinoatrial node (SAN) cardiomyocytes is unknown. As isoflurane is more rapidly eliminated compared to sodium pentobarbital, the return to baseline of intrinsic HR of isolated hearts could be expected to occur sooner with isoflurane compared to sodium pentobarbital. In this study, I

aimed to compare the effects of anaesthetics isoflurane and sodium pentobarbital on blood glucose, *in vivo* HR and intrinsic HR in the nDM and type 2 diabetic (DM) animals.

6.2. Aims and hypothesis

The **aim** of this study was to compare the effects of anaesthetics isoflurane and sodium pentobarbital on standard cardiovascular measurements, such as blood glucose, *in vivo* HR and intrinsic HR between nDM and DM animals.

In the nDM and DM animals, I **hypothesised** an increase in blood glucose, a decrease to *in vivo* HR and an increase to intrinsic HR on use of isoflurane compared to sodium pentobarbital.

6.3. Methodology

Detailed methodology used in this study can be found in Chapter 2. Experimental techniques applied here include echocardiography, heart tissue retrieval, Langendorff, LabChart and statistical analysis.

6.4. Results

6.4.1 Animal characterisation

Table 6.1 presents the standard measurements for the Zucker Diabetic Fatty (ZDF) rats. The data shown here has previously been presented in Chapters 3 – 5, with the inclusion of data from additional animals ($ZDF^{fa/+,\ +/+}$ n=+1, $ZDF^{fa/fa}$ n=+2). These data were collected using

sodium pentobarbital and isoflurane anaesthesia. The ZDF$^{fa/fa}$ rats presented markedly increased blood glucose compared to their ZDF$^{fa/+,\ +/+}$ littermates, demonstrating their diabetic (DM) phenotype. The ZDF$^{fa/fa}$ rats with a 'high' blood glucose reading above the maximum reading of 33.3 mmol/L on the glucometer (11 out of 30 rats (5 from the isoflurane group and 6 from the sodium pentobarbital group)) were only excluded from the blood glucose analysis in Table 6.1, Figure 6.1 and Figure 6.2. The ZDF$^{fa/fa}$ rats also presented significantly decreased *in vivo* and intrinsic HR compared to ZDF$^{fa/+,\ +/+}$. There was no weight difference between the ZDF$^{fa/+,\ +/+}$ and ZDF$^{fa/fa}$ animals.

Table 6.1. Animal characteristics from non-diabetic (nDM) and diabetic (DM) rats. Mean ± SEM, nDM n=30, DM n=30, unpaired t test or Mann-Whitney test (blood glucose only).

Parameter	nDM (ZDF$^{fa/+,\ +/+}$)	DM (ZDF$^{fa/fa}$)	*P value*
Weight (g)	381 ± 4	393 ± 5	*>0.05*
Blood glucose (mmol/L)	13.2 ± 0.8	31.5 ± 0.5	* *<0.0001*
***In vivo* heart rate (bpm)**	329 ± 7	289 ± 7	* *<0.001*
***Ex vivo* intrinsic heart rate (bpm)**	185 ± 7	144 ± 5	* *<0.0001*

6.4.2 Anaesthetics and blood glucose

6.4.2.1 The effect of time on blood glucose with isoflurane or sodium pentobarbital

To investigate the time-dependent effect of anaesthetic exposure on nDM and DM blood glucose, blood glucose measurements from two-time points were compared (**Figure 6.1A** and **Figure 6.1B**). Blood glucose measurements were taken at 5-minutes and 20-minutes following

isoflurane or sodium pentobarbital anaesthesia in the nDM and DM animals. A significant interaction between the duration of isoflurane exposure and DM on blood glucose was observed (interaction *p<0.01*). A significant DM effect with blood glucose was found between nDM and DM animals at both time points using isoflurane (*p<0.001*, Figure 6.1A). The nDM animals presented significantly increased blood glucose with prolonged exposure to isoflurane (nDM 5-minutes 8.8 ± 0.7 mmol/L versus nDM 20-minutes 19.4 ± 1.3 mmol/L, *p<0.01*, Figure 6.1A). In contrast, the DM animals exhibited no alterations in blood glucose with prolonged exposure to isoflurane (DM 5-minutes 31.2 ± 1.4 mmol/L versus DM 20-minutes 32.6 ± 0.5 mmol/L, *p>0.05*, Figure 6.1A). This suggests a time-dependent increase in blood glucose with isoflurane in nDM animals, but not in DM animals.

There was no significant interaction between the duration of sodium pentobarbital exposure and DM on blood glucose (interaction *p>0.05*). A significant DM effect with blood glucose was found between nDM and DM animals at both time points using sodium pentobarbital (*p<0.001*, Figure 6.1B). The nDM (nDM 5-minutes 9.3 ± 0.4 mmol/L versus nDM 20-minutes 11.1 ± 0.5 mmol/L, *p<0.05*, Figure 6.1B) and DM (DM 5-minutes 29.1 ± 0.7 mmol/L versus DM 20-minutes 32.0 ± 0.5 mmol/L, *p<0.05*, Figure 6.1B) animals presented a small but significant increase in blood glucose with prolonged exposure to sodium pentobarbital. In nDM and DM animals, this suggests a time-dependent increase in blood glucose with sodium pentobarbital.

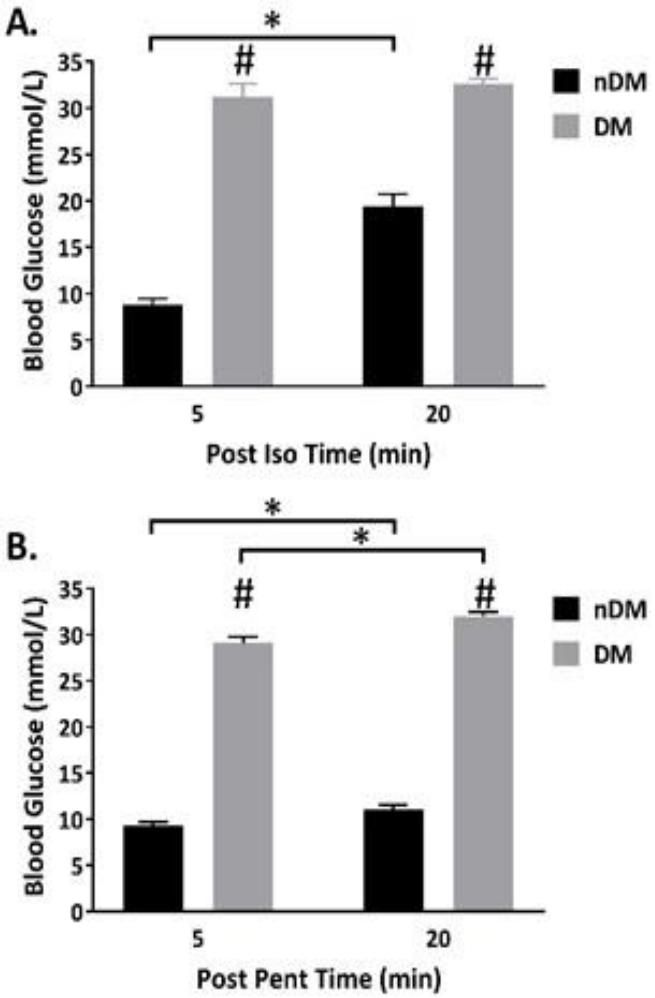

Figure 6.1. Time effect of anaesthetic isoflurane (Iso) and sodium pentobarbital (Pent) on blood glucose in non-diabetic (nDM) and diabetic (DM) animals. (A. and B.) Iso and Pent blood glucose measurements in nDM and DM animals taken 5-minutes or 20-minutes post anaesthetic exposure. (A.) n=3 per group, (B.) nDM n=10 and DM n=9, mean ± SEM, # nDM vs. DM $p<0.001$, * blood glucose vs. time of anaesthetic exposure in nDM or DM $p<0.05$, (A. and B.) two-way ANOVA with repeated measures, Holm-Sidak post hoc test.

6.4.2.2 Comparison of isoflurane and sodium pentobarbital effects on blood glucose at two-time points

To compare whether there were differences in blood glucose depending on the anaesthetic used, blood glucose measurements during isoflurane and sodium pentobarbital anaesthesia of the nDM and DM animals were compared at the two-time points. Additional data were

added to the DM sodium pentobarbital group at 5-minutes, and the nDM and DM groups of both anaesthetics at 20-minutes compared to Figure 6.1. The blood glucose measurements at 5-minutes post-anaesthetic exposure of isoflurane or sodium pentobarbital in nDM (isoflurane 8.8 ± 0.7 mmol/L versus sodium pentobarbital 9.3 ± 0.4 mmol/L, *p>0.05*) and DM (isoflurane 31.2 ± 1.4 mmol/L versus sodium pentobarbital 29.5 ± 0.6 mmol/L, *p>0.05*) animals were not different (**Figure 6.2A** and **6.2B**). However, blood glucose readings at 20-minutes post-anaesthesia in nDM animals were significantly increased using isoflurane compared to sodium pentobarbital (isoflurane 19.6 ± 1.1 mmol/L versus sodium pentobarbital 10.9 ± 0.3 mmol/L, *p<0.001*, **Figure 6.2C**). No effect of anaesthesia was found between isoflurane and sodium pentobarbital in the DM animals at 20-minutes (isoflurane 32.4 ± 0.3 mmol/L versus sodium pentobarbital 31.3 ± 0.6 mmol/L, *p>0.05*, **Figure 6.2D**). This suggests that in nDM animals, the increased exposure to the anaesthetic isoflurane influences blood glucose significantly more than sodium pentobarbital.

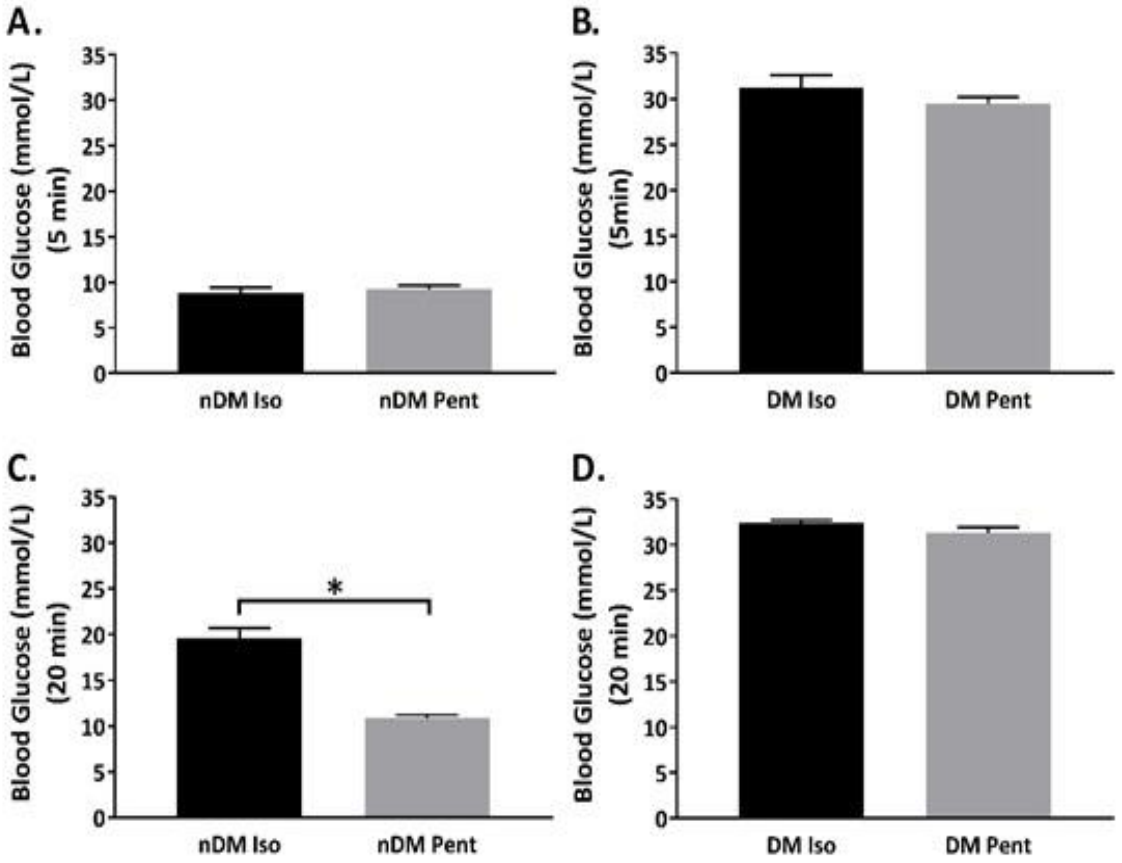

Figure 6.2. Comparison of anaesthetics isoflurane (Iso) and sodium pentobarbital (Pent) on blood glucose at two-time points in non-diabetic (nDM) and diabetic (DM) animals. (A. and B.) Comparison of Iso and Pent blood glucose measurements in nDM and DM animals taken 5-minutes after anaesthesia. (C. and D.) Comparison of Iso and Pent blood glucose measurements in nDM and DM animals taken 20-minutes after anaesthesia. (A.) n=3 (Iso) and n=10 (Pent), (B.) n=3 (Iso) and n=11 (Pent), (C.) n=8 (Iso) and n=22 (Pent) and (D.) n=5 (Iso) and n=15 (Pent). Mean ± SEM, * *p<0.0001*, (A., B. and D.) unpaired t test and (C.) Mann-Whitney test.

6.4.3 Anaesthetics and heart rate

To evaluate whether there was a differential effect of anaesthesia on *in vivo* and intrinsic HR in DM, the *in vivo* and intrinsic HR data obtained during isoflurane or sodium pentobarbital anaesthesia were compared between nDM and DM animals. In the nDM group, a significantly higher *in vivo* HR was found during exposure to sodium pentobarbital compared to isoflurane (isoflurane 312 ± 7 bpm versus sodium pentobarbital 343 ± 8 bpm, *p<0.05*, **Figure 6.3A**),

however, no difference was observed to *in vivo* HR in the DM group (isoflurane 290 ± 11 bpm versus sodium pentobarbital 289 ± 10 bpm, *p>0.05*, **Figure 6.3B**). The intrinsic HR was not different between the type of anaesthetic used in the nDM (isoflurane 203 ± 13 bpm versus sodium pentobarbital 177 ± 8 bpm, *p>0.05*, **Figure 6.3C**) or the DM (isoflurane 150 ± 9 bpm versus sodium pentobarbital 141 ± 6 bpm, *p>0.05*, **Figure 6.3D**) group. In nDM, this suggests sodium pentobarbital is less cardio-depressive, at least in terms of *in vivo* HR, compared to isoflurane.

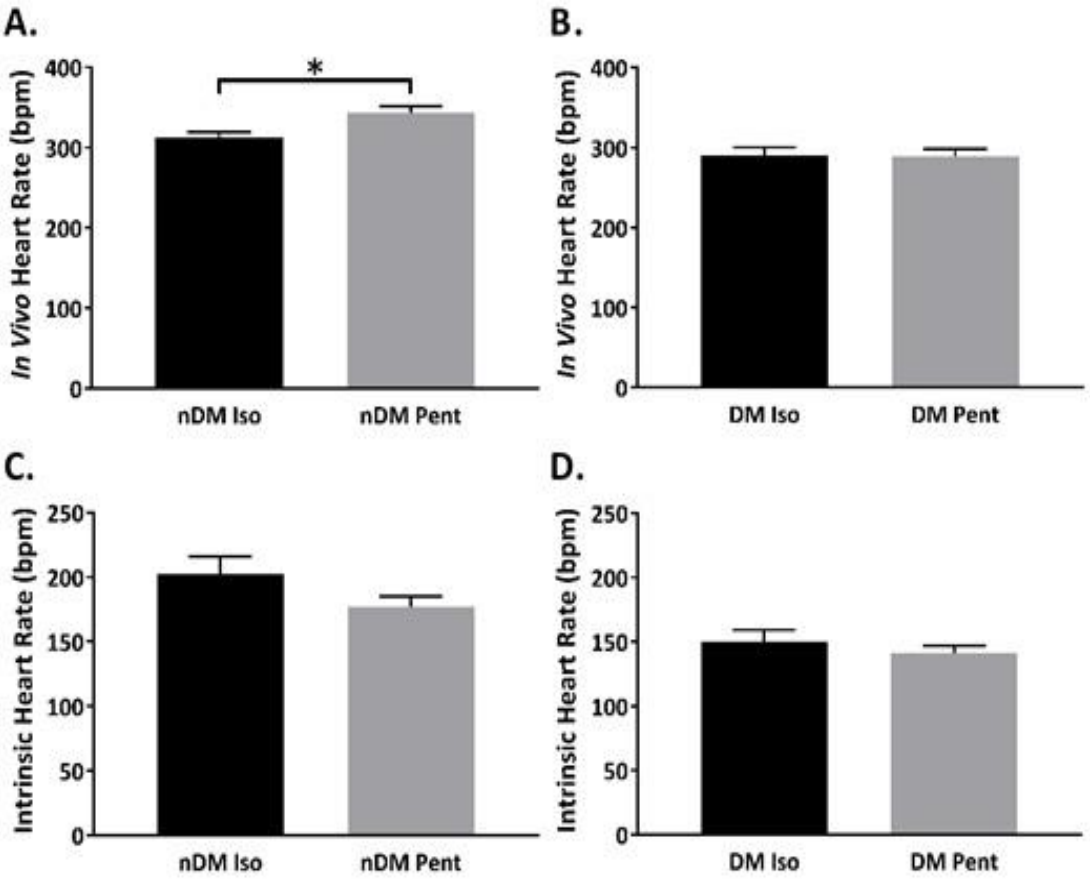

Figure 6.3. Comparisons of anaesthetics isoflurane (Iso) and sodium pentobarbital (Pent) effects on *in vivo* and *ex vivo* intrinsic heart rate (HR) in non-diabetic (nDM) and diabetic (DM) animals. (A. and B.) Iso and Pent *in vivo* HR measurements in nDM and DM animals. (C. and D.) Iso and Pent intrinsic HR measurements in nDM and DM isolated rat hearts. (A.) n=8 (Iso) and n=10 (Pent), (B.) n=9 (Iso) and n=12 (Pent), (C.) n=8 (Iso) and n=19 (Pent) and (D.) n=9 (Iso) and n=19 (Pent). Mean ± SEM, * *p<0.05*, (A. – D.) unpaired t test.

6.5. Discussion

In this chapter, the effects of anaesthetics isoflurane and sodium pentobarbital on blood glucose, *in vivo* HR and intrinsic HR were compared between the nDM and DM animals. The findings of this study are: (a) time-dependent exposure of nDM animals to isoflurane or sodium pentobarbital significantly increased blood glucose, (b) time-dependent exposure of DM animals to sodium pentobarbital but not isoflurane significantly increased blood glucose, (c) in nDM animals 20-minute exposure to isoflurane significantly increased blood glucose compared to sodium pentobarbital, (d) markedly lower *in vivo* HR in nDM during isoflurane compared to sodium pentobarbital, and (e) no difference in intrinsic HR between animals anaesthetised with either isoflurane or sodium pentobarbital.

6.5.1 Anaesthetic effects on blood glucose

The time-dependent increase in blood glucose during isoflurane (nDM animals only) and sodium pentobarbital (nDM and DM animals) suggests increased anaesthetic exposure impacts blood glucose, which was more potent during isoflurane exposure.

In the DM animals, the lack of a time-dependent increase in blood glucose on isoflurane use might be limited by the small 'n' value (n=3, no exclusions were made in this group due to 'high' blood glucose readings). Likewise, the lack of a difference in blood glucose between isoflurane and sodium pentobarbital at 20-minutes exposure might also be due to the small 'n' value for the DM isoflurane group (n=5, 4 exclusions were made in this group due to 'high' blood glucose readings). More 'n' values in future are required to confirm the current results. A lack of an anaesthetic difference in the DM animals could potentially be due to DM-induced

impairments in glucose metabolism and insulin secretion that hamper isoflurane-induced time-dependent increase in blood glucose (203, 481, 482). However, this seems unlikely as blood glucose is also markedly increased in DM patients anaesthetised with isoflurane measured at 30-minutes (483) and 60-minutes (433) into surgery (433, 483, 484). This suggests blood glucose is also expected to rise in the DM animals. The nDM and DM blood glucose values at 20-minutes during isoflurane and sodium pentobarbital exposure presented in my study are higher compared to *in vivo* blood glucose values from 8-hour fasted nDM and DM ZDF rats (166, 182), suggesting anaesthesia in general increases blood glucose levels.

As described in section 6.1, isoflurane is known to acutely increase blood glucose levels, while, sodium pentobarbital has no significant effect (470-480). The time-frame for the onset of an isoflurane-induced increase in blood glucose is likely to depend on the concentration of isoflurane administered. In mice, significant increases in blood glucose have been reported after 10-minutes of 1.5 – 2% (but not 1%) isoflurane exposure (472) and 30-minutes of 2% isoflurane exposure (470). In rats, significant increases in blood glucose have been found after 5-minutes (in contrast to my study) and 30-minutes of 3 – 4% isoflurane exposure (473, 475). This increase in blood glucose was attributed to the significantly decreased plasma insulin in the isoflurane groups compared to sodium pentobarbital (440, 475, 480). However, my findings of a significant time-dependent increase in blood glucose in the nDM and DM animals using sodium pentobarbital are in contrast to the literature. The literature investigating sodium pentobarbital effects on blood glucose over time present small fluctuations to blood glucose, as in the controls (non-anaesthetised), but remains insignificant (476, 477, 479). Reasons for this significant difference in my data remain unknown, however, the difference in blood glucose on sodium pentobarbital exposure between 5-minutes and 20-minutes (nDM

~1.9 mmol/L and DM ~2.9 mmol/L) is comparable to the changes presented in the literature (476, 477, 479).

This blood glucose modulation, is in part, suggested to arise from isoflurane and sodium pentobarbital effects on the opening and closing of the ATP-sensitive K^+ channel (K_{ATP}) channels that inhibit and promote insulin release from pancreatic β-cells respectively (435, 475, 485, 486). K_{ATP} channel-dependent insulin secretion is found to be inhibited by isoflurane but not by sodium pentobarbital. Glucose mediated insulin secretion requires mitochondria to increase cytosolic ATP that in turn closes the K_{ATP} channels depolarising the plasma membrane. The depolarisation allows Ca^{2+} entry via Ca^{2+} channels that results in increased intracellular Ca^{2+} ($[Ca^{2+}]_i$) (485, 487). This increased $[Ca^{2+}]_i$ triggers exocytosis of the insulin secretory granules to merge with the plasma membrane (487, 488). It is likely that limited K_{ATP} channel-dependent insulin secretion brings about the increase in blood glucose present in nDM on isoflurane use. In DM, the K_{ATP} channels are suggested to be over-active remaining in an open state and thereby limiting insulin secretion (489, 490). This mechanism cannot explain the absence of a significant isoflurane increase in blood glucose compared to sodium pentobarbital (i.e. if isoflurane is able to further suppress insulin secretion) but on the other hand, might explain the blood glucose comparability of sodium pentobarbital and isoflurane in DM at 20-minute exposure (i.e. insulin secretion is depressed in DM and neither anaesthetic influences this pathway). Again, this could be clarified with larger ‘n’ values and without the limitation of the maximal reading of 33.3 mmol/L on the glucometer.

6.5.2 Anaesthetic effects on heart rate

6.5.2.1 *In vivo* heart rate

The significantly reduced *in vivo* HR in nDM during isoflurane compared to sodium pentobarbital suggests isoflurane might be more cardio-depressive in relation to *in vivo* HR. This result was in support of the hypothesis in the nDM group, but not the DM group. The lack of *in vivo* HR difference in DM might be due to disease-induced alterations on the autonomic and / or cardiovascular system. As described in section 6.1, sodium pentobarbital has been shown to be less cardio-depressive in the rat cardiovascular system in comparison to isoflurane (these studies used lower sodium pentobarbital (25-30 mg/kg) and isoflurane concentration (3% for induction then maintained on 1.5%)) (468, 469). Sodium pentobarbital presented *in vivo* HR readings that were similar to the conscious state in comparison to isoflurane (~421 bpm conscious versus ~442 bpm sodium pentobarbital versus ~363 bpm isoflurane) (468). Additionally, other cardiac parameters (LV systolic function, LV diastolic wall thickness and LV end-diastolic diameter) measured during sodium pentobarbital were closer to values obtained in the conscious nDM animals in comparison to isoflurane (468). Other studies in nDM rats have also shown similar minimal effects of sodium pentobarbital at higher concentrations on *in vivo* HR, cardiac output and blood pressure (~379 bpm (40 mg/kg) (491) and ~422 bpm conscious versus ~335 bpm (35 mg/kg) anaesthetised (492)). These values are close to the values obtained in the nDM rats in this study (~30-35 mg/kg ~343 bpm). However, some studies report that sodium pentobarbital lowers *in vivo* HR more compared to isoflurane (2% isoflurane ~320 bpm versus 65 mg/kg sodium pentobarbital ~272 bpm (493)) or has similar values (2.5-3% isoflurane ~369 bpm versus 75 mg/kg sodium pentobarbital ~387 bpm (455, 494)). In one study that presented lower *in vivo* HR during sodium pentobarbital anaesthesia compared to isoflurane, administration of propranolol (β-adrenergic blocker) and atropine (M_2 receptor antagonist) had lower responses of decreasing and increasing HR

respectively compared to isoflurane suggesting attenuated baroreflexes (493). This effect would not appear to increase *in vivo* HR in the nDM animals, or on the other hand, my findings suggest that isoflurane might dampen the baroreflexes to a greater degree than sodium pentobarbital. The increase to *in vivo* HR might arise due to other cardiac parameters being affected (decreased cardiac output and / or contractility, see section 6.5.2.2 below).

Both isoflurane and sodium pentobarbital cause inhibition of the voltage-gated K^+, Na^+ and Ca^{2+} channels, which in the heart, is likely to account for their negative chronotropic and inotropic effects (434, 439, 468, 495, 496). However, isoflurane might exert more potent effects on the cardiovascular (and autonomic) system compared to sodium pentobarbital. Isoflurane depresses myofilament Ca^{2+} sensitivity and reduces SR Ca^{2+} content (497), which might contribute to a lower *in vivo* HR. In isolated guinea-pig ventricular cardiomyocytes, isoflurane has been found to have a biphasic effect on AP duration that is concentration-dependent (498). At low concentrations (1.26%) AP duration at 50% and 90% was significantly increased, whereas at high concentrations (3.77%) AP duration at 50% and 90% was significantly decreased (498). This biphasic effect was attributed to the dominance of inhibitory actions on the delayed-rectifier K^+ channel at low concentrations, whereas at high concentrations a dominance of inhibitory actions on the L-type Ca^{2+} channel and an acceleration of their inactivation (498). In the nDM animals, this might suggest that the prevalence of isoflurane-induced effects on the delayed-rectifier K^+ channel prolong AP duration and thereby decrease *in vivo* HR, although, this would require further investigation. It would also be interesting to determine the effects on *in vivo* HR with further concentration increases of isoflurane. While sodium pentobarbital-induced increase to *in vivo* HR has been attributed to the arterial baroreceptor reflex (499). In DM, the lack of an *in vivo* HR difference

between the use of isoflurane and sodium pentobarbital might be attributed to DM-induced alterations to voltage-gated K^+, Na^+ and Ca^{2+} channels and / or compromised baroreceptor reflex (500). Also, sodium pentobarbital has been shown to reduce acetylcholine levels in the rat atria and ventricular myocardium (unknown in the SAN) (501). This decrease in acetylcholine has been suggested to contribute to the anti-arrhythmic properties and increase *in vivo* HR induced by sodium pentobarbital (501).

More generically, barbiturate anaesthesia such as sodium pentobarbital presents concentration-dependent cardiac depression, however, their effects are suggested to be not as pronounced as the cardiac depression induced by volatile anaesthesia such as isoflurane (461). Volatile anaesthetics have also been proposed to slow SAN firing and prolong conduction (461). It might also be speculated that isoflurane modulates both intrinsic SAN firing and autonomic activity, while sodium pentobarbital largely acts via the autonomic system (see section 6.5.2.3 below).

6.5.2.2 *Ex vivo* intrinsic heart rate

Recovery from anaesthesia can result in altered *in vivo* HR and cardiac function for several hours (449). Therefore, data obtained from an isolated heart preparation might be influenced by residual anaesthesia used before the experiment or its respective effects (436). However, no difference in intrinsic HR of hearts between nDM or DM rats, excised during isoflurane or sodium pentobarbital anaesthesia, was observed. This did not support my hypothesis of increased intrinsic HR after isoflurane use. In agreement with my finding, no significant difference in intrinsic HR has been reported for hearts excised using anaesthetics isoflurane (concentration not mentioned) or sodium pentobarbital (50 mg/kg), however, cardiac output

and LV contractility was significantly greater in the isoflurane group compared to sodium pentobarbital (502). Additionally, post-induced ischemia, the hearts from the isoflurane group recovered more quickly than the sodium pentobarbital group (502). This suggests the possibility that the performance of an isolated Langendorff heart during basal conditions (other parameters excluding intrinsic HR) or an experimental protocol might be influenced by the anaesthetic during excision of the heart (502, 503). In other studies, no difference in intrinsic HR was found between non-anaesthetised animals compared to sodium pentobarbital anaesthetised (503). Washout of isoflurane containing perfusion buffer in isolated guinea-pig hearts returned intrinsic HR to initial values (453, 462). In line with these studies, no intrinsic HR difference was found between isoflurane or sodium pentobarbital anaesthetic use in nDM or DM hearts, however, it is plausible that the anaesthetics might affect cardiac parameters other than intrinsic HR.

6.5.2.3 Is isoflurane a more potent autonomic system depressor than sodium pentobarbital?

In nDM animals, the *in vivo* HR during isoflurane was significantly lower compared to sodium pentobarbital without a difference in intrinsic HR between anaesthetic regimes. This suggests that the *in vivo* HR differences might arise from changes in anaesthetic actions on the autonomic system. These data suggest that isoflurane is a more potent autonomic / sympathetic depressor compared to sodium pentobarbital, even if it is acting through similar initial target proteins (such as the voltage-gated (Na^+, Ca^{2+}, K^+) and ligand-gated ($GABA_A$, nicotinic, NMDA) ion channels). Although, this anaesthetic interaction might not necessarily be through the same site on the protein or present comparable downstream mechanisms (431, 435, 439, 440, 442-444, 446). Isoflurane might have more pronounced effects on inhibiting excitatory pathways and / or promoting inhibitory pathways. As described in section

6.5.2.1, it might be that isoflurane affects the autonomic system and the cardiovascular system more potently than sodium pentobarbital, which might largely affect the autonomic system. A study comparing basal and reactive plasma catecholamine levels found sodium pentobarbital to have greater suppressive effects on the autonomic nervous system compared to isoflurane in rabbit (504). This is in contrast to what my data might suggest even though the findings of the former study are not a direct measure of cardiac sympathetic activity, as anaesthetics can exert differential depressive effects to different sympathetic outflows to different organs (505).

Furthermore, this effect appears to be species-dependent. Isoflurane significantly increases *in vivo* HR in humans (506, 507), but significantly decreases HR in rodents (437, 462, 508), with both effects being concentration-dependent. This differential effect is likely to arise due to the differences in the autonomic drive to the heart in both species. DM-induced cardiac autonomic changes might also account for the lack of an *in vivo* HR difference between the use of isoflurane and sodium pentobarbital in DM rats. Rats present a sympathetically driven higher basal *in vivo* HR compared to the parasympathetically driven lower *in vivo* HR in humans (154, 156, 157, 165, 166). In humans, isoflurane displays concentration-dependent decreases in parasympathetic and sympathetic nerve activity thereby reducing heart rate variability (HRV) and increasing *in vivo* HR (i.e. less autonomic / parasympathetic influence and increased SAN intrinsic pacemaking influence) (507). Although no literature on the effects of isoflurane on HRV in the rat was found, isoflurane is found to depress baroreceptor control of *in vivo* HR in rats (509). This is also in contrast to sodium pentobarbital effects that induce *in vivo* HR increases due to the baroreceptor reflex (499). Sodium pentobarbital anaesthesia has been shown to increase HRV, which was also significantly correlated to plasma concentrations of

neuropeptides in rats (510). To the best of my knowledge, I have not found research comparing the effects of isoflurane and sodium pentobarbital on HRV in rodents. Together, these studies might support the viewpoint that isoflurane might be more depressive to autonomic pathways than sodium pentobarbital.

On the other hand, the lower *in vivo* HR due to isoflurane is not through greater autonomic depression, but seems to occur at the cardiac level. This would explain why the effects of both anaesthetics are rapidly reversible after wash out in the isolated hearts, hence the lack of an intrinsic HR difference. Whether these *in vivo* HR decreasing effects of isoflurane are attributed to increased depression at the autonomic and / or cardiac level, and the cause for different HR responses in DM, requires further clarity. The specific effects enabling these *in vivo* HR differences are likely to be due to specific mechanisms of anaesthetic action for which further research in this field is required.

6.6. Summary

This chapter has compared the effects of isoflurane and sodium pentobarbital on blood glucose, *in vivo* HR and intrinsic HR in nDM and DM. The effects of the anaesthetics on blood glucose and HR emphasise the importance of using an anaesthetic suited to the experimental questions or model. Furthermore, the lack of effects in the DM animals suggests that the effects of anaesthetics are altered in diseased states, as previously suggested in the DM ZDF model (182, 206).

CHAPTER 7

General Discussion

7.1. Summary of key findings

The overall **aim** of this thesis was to investigate the underlying mechanisms of the decreased intrinsic heart rate (HR) in type 2 diabetes (DM). My study is the first to evaluate protein expression and function in the type 2 DM SAN. My findings present changes to both the Vm and Ca^{2+} clocks and the cholinergic system in regards to protein expression and / or function, which provides a novel understanding of type 2 DM SAN remodelling and HR regulation.

In regards to protein expression (Chapter 3), in the DM SAN, I found significantly increased hyperpolarisation-activated cyclic nucleotide-gated channel 4 (HCN4 / I_f), Na^+-Ca^{2+} exchanger 1 (NCX1 / I_{NCX1}), phospholamban, muscarinic type 2 (M_2) receptor and total Ca^{2+} / calmodulin-dependent protein kinase II (CaMKII) protein expression. Although there was significantly increased phospholamban expression, this did not present an altered SERCA2a to phospholamban ratio. The absence of a decrease in the key SAN clock proteins or SERCA2a to phospholamban ratio presented no simple explanation that could account for the lower intrinsic HR in DM. Given the unexpected protein expression findings, I went on to examine the functional contribution of a Vm clock protein (HCN4) and a Ca^{2+} clock protein (SERCA2a) to intrinsic HR in nDM and DM hearts. The significantly increased M_2 receptors suggested that the non-neuronal intrinsic cholinergic system activity might be implicated in intrinsic HR modulation and decrease present in DM, therefore, the intrinsic HR responsiveness using an M_2 stimulus was also investigated.

In relation to protein function (Chapter 4), I found significantly decreased intrinsic HR in nDM but no change to intrinsic HR in DM hearts with HCN4 inhibition, significantly decreased intrinsic HR in DM but no effect to intrinsic HR in nDM hearts with external Ca^{2+} ($[Ca^{2+}]_o$) and

no difference in decreasing intrinsic HR response between nDM and DM hearts with M_2 stimulus. This suggested non-functional HCN4 channels, compromised Ca^{2+} handling and cycling that I suggest is due to compromised SERCA2a activity and unaltered contribution from the cholinergic systems in the DM SAN.

I also examined SAN tissue morphology. This was explored to determine whether lesions, fibrosis and / or fat accumulation disrupted pacemaking and propagation of the action potential (AP) in the DM SAN. For the immunohistochemistry study (Chapter 5), I found no observed lesions or difference in fibrosis or fat levels between the nDM and DM SAN. This suggested a significant loss of SAN cardiomyocytes, fibrosis and fat presence was not responsible for the lower intrinsic HR in DM.

Due to the observed increase in blood glucose on isoflurane use in nDM, I also went on to explore the effects of anaesthetics isoflurane and sodium pentobarbital on blood glucose, *in vivo* HR and intrinsic HR in nDM and DM rats. The anaesthetic findings are not summarised or discussed any further in this chapter and can be referred to in Chapter 6. The discussion sections below will focus on the potential molecular mechanisms underlying the key findings.

7.2. Altered HCN4 (Vm clock) in type 2 diabetes

Given the mismatch in the significantly increased HCN4 protein expression but the absence of a declining intrinsic HR response on HCN4 inhibition in DM, suggests non-functional HCN4 channels in the DM SAN. To explore why this might be, the regulation of HCN4 channels,

intrinsic pacemaking regulation by cAMP and phosphorylation, and possible DM alterations are considered in the sections below.

7.2.1 The regulation of HCN channels

The open probability of the HCN channel is governed by two processes. (1) Hyperpolarisation of the sarcolemma (activated ~<-40 mV), which is detected by the voltage sensor in the transmembrane region. (2) Binding of cyclic nucleotides (predominantly cyclic adenosine monophosphate (cAMP)) to the intracellular C-terminal region (**Figure 7.1**) (132, 511-516), which includes the cyclic nucleotide-binding domain (513, 517). The HCN channel pore is autoinhibited by the C-terminal cyclic nucleotide-binding domain region in the absence of cAMP (513, 517). cAMP binding relaxes this autoinhibition by causing conformational shifts that form a gating ring promoting tetramerisation and channel opening (512, 518). The addition of cAMP increases the radius of the C-terminal cyclic nucleotide-binding domain region by 4-fold (519). These alterations to channel kinetics result in HCN channels becoming active at less negative potentials (341, 514, 520, 521). β-adrenergic (shift to less negative potentials) and cholinergic (shift to more negative potentials) modulation of HCN4 is predominantly thought to occur by cAMP binding effects (515). The affinity and shift in voltage of HCN4 and HCN2 to cAMP are quite large (~+25 mV) compared to isoforms HCN1 and HCN3 (least modulated) (512, 514, 517, 522, 523). This suggests controlling the intrinsic SAN cAMP concentration is key for optimal HCN4 and HCN2 channel opening.

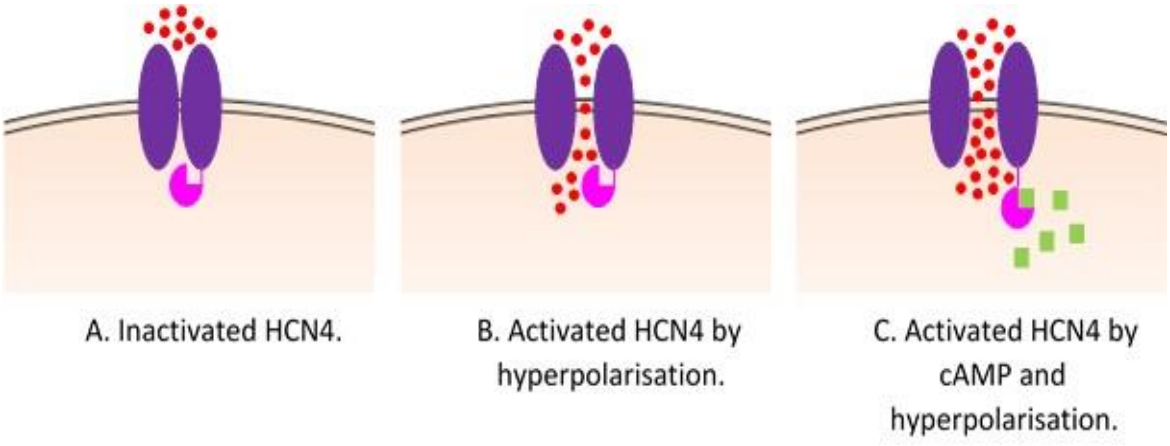

Figure 7.1. The regulation of hyperpolarisation-activated cyclic nucleotide-gated channel 4. (A.) The hyperpolarisation-activated cyclic nucleotide-gated channel 4 (**HCN4**, **purple** transmembrane structure) with its **cyclic-nucleotide binding domain** (**pink**) in an inactivated closed state (i.e. no hyperpolarisation or cyclic adenosine monophosphate (cAMP) binding). (B.) HCN4 in an activated state permitting entry of **Na^+** and **K^+** (**red dots**) induced by hyperpolarisation only. (C.) HCN4 in an activated state permitting entry of **Na^+** and **K^+** induced by **cAMP** (**green squares**) binding to the cyclic-nucleotide binding domain and hyperpolarisation. Original figure.

7.2.2 The intrinsic regulation of pacemaking by cAMP and phosphorylation

As described in Chapter 1 section 1.3.6.1, β-adrenergic input activates Gα stimulatory protein ($G_{\alpha s}$) that activates Ca^{2+}-inhibited adenylyl cyclases (isoforms 5 and 6) that use ATP to generate cAMP, while M_2-cholinergic input inhibits these mechanisms (91, 147). However, SAN cardiomyocytes have been shown to have a ~3-fold greater intrinsic (basal) level of cAMP compared to ventricular cardiomyocytes (16, 81, 87). This greater level of cAMP is attributed to continuously active Ca^{2+}-activated adenylyl cyclases (isoforms 1 and 8) that are independent of β-adrenergic input induced activation in the SAN cardiomyocytes (16, 50, 93). Although SAN cardiomyocytes also express Ca^{2+}-inhibited adenylyl cyclases (isoforms 5 and 6), the Ca^{2+}-activated adenylyl cyclases allow intrinsic cAMP generation and thereby have the

ability to regulate intrinsic HR (50). In pacemaking cardiomyocytes, β-adrenergic or intrinsically generated cAMP can directly bind to HCN4 and increase the rate of diastolic depolarisation (132). cAMP levels are in turn regulated by phosphodiesterases (524, 525). High continuous intrinsic phosphodiesterase activity has also been found in the SAN (526, 527). Inhibition of phosphodiesterase activity (more cAMP for HCN4 and protein kinase A (PKA) enabled phosphorylation), significantly increased spontaneous local Ca^{2+} releases (LCRs) / firing rate (~55%), with a major contribution arising from the inhibition of phosphodiesterase isoform 3 and 4 (~47%) (98, 526-528). A summary of these mechanisms is presented in **Figure 7.2**.

In pacemaking and ventricular cardiomyocytes, cAMP activates PKA and the Ca^{2+}-calmodulin complex activates CaMKII (16, 81, 94, 97, 525). Both kinases are capable of phosphorylating RyR2, phospholamban and L-type Ca^{2+} channels (16, 21, 50, 94). The phosphorylation of RyR2 increases its open probability, phosphorylation of phospholamban relieves SERCA2a inhibition, and phosphorylation of L-type Ca^{2+} channels increases Ca^{2+} influx and recovery from inactivation (16, 21, 94, 97). In accord with high intrinsic cAMP levels, there are also greater intrinsic levels of PKA and CaMKII phosphorylation in SAN cardiomyocytes compared to ventricular cardiomyocytes (16). It is likely that basal intrinsic pacemaking depends on phosphorylation of both PKA and CaMKII sites on pacemaking proteins as inhibition of either PKA or CaMKII reduced rabbit SAN cardiomyocyte spontaneous LCRs and firing rate (16, 81, 97, 270). However, it must be noted that studies performing CaMKII inhibition in mouse found no difference in basal intrinsic HR (96, 529). This might suggest species-specific differences in intrinsic HR control. Together, these findings show intrinsic HR generation is partly controlled

by levels of cAMP and a balance of phosphorylation of pacemaking proteins by kinases and phosphodiesterases.

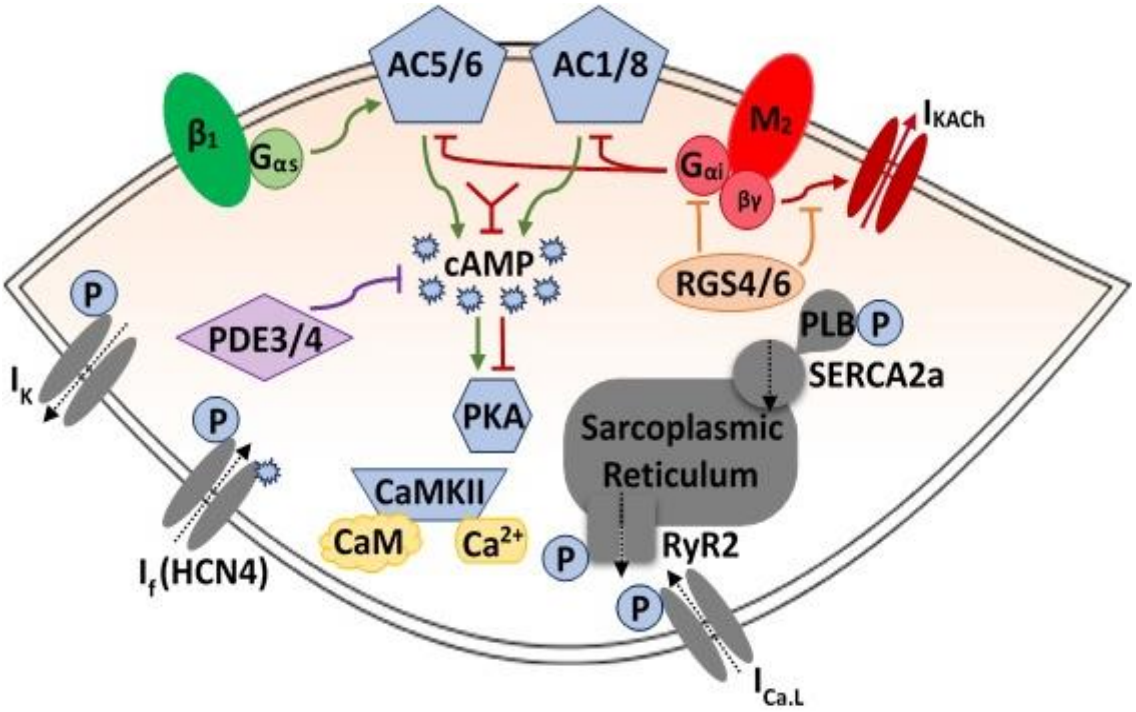

Figure 7.2. Pacemaking regulation by cyclic adenosine monophosphate and phosphorylation within the sinoatrial node. The basic **intrinsic** (facilitated by adenylyl cyclases (AC) isoforms 1 and 8) and **β-adrenergic** (facilitated by G-protein α stimulatory ($G_{\alpha s}$) induced activation of AC isoforms 5 and 6) pathways generate cyclic adenosine monophosphate (cAMP) within the sinoatrial node (SAN). cAMP, in turn, activates protein kinase A (PKA). Ca^{2+} / calmodulin-dependent protein kinase II (CaMKII) is activated by increases in intracellular Ca^{2+} and calmodulin (CaM) binding. PKA and / or CaMKII phosphorylate, denoted by 'P', several pacemaking proteins such as hyperpolarisation-activated cyclic nucleotide-gated channel 4 (I_f / HCN4), L-type Ca^{2+} channel ($I_{Ca,L}$), K^+ channels (I_K), ryanodine receptor 2 (RyR2) and the sarco(endo)plasmic regulator Ca^{2+}-ATPase 2a (SERCA2a) inhibitor phospholamban (PLB). This pathway is highlighted in **green**. cAMP breakdown in the SAN is regulated by phosphodiesterase activity of isoforms 3 and 4 (**PDE3 / 4**) highlighted in **purple**. The **cholinergic** pathway begins with the activation of the muscarinic type 2 (M_2) receptor by acetylcholine. This triggers the activation of the G-protein α inhibitory ($G_{\alpha i}$) that inhibits AC activity and thereby cAMP levels. The G-protein βγ inhibitory ($G_{\beta\gamma i}$) activates the acetylcholine K^+ channel (I_{KACh}) that hyperpolarises the SAN cardiomyocyte. This pathway is highlighted in **red**. Cholinergic activity in the SAN is controlled by regulators of G-protein signalling isoforms 4 and 6 (**RGS4 / 6**) highlighted in **orange**. Original figure.

7.2.3 Can a possible lack of intrinsic cAMP and phosphorylation explain low intrinsic heart rate in type 2 diabetes?

A diminished expression and / or activity of Ca^{2+}-activated adenylyl cyclases might prevent intrinsic cAMP production in the DM SAN. This would not simply limit cAMP-induced HCN4 activity, but also PKA activity and thereby phosphorylation of other proteins involved in intrinsic HR generation (RyR2, phospholamban, L-type Ca^{2+} channels) or might increase dependency for CaMKII mediated phosphorylation. A significant increase in total and active CaMKII has been found in the right atrial appendage from DM patients and right ventricular tissue from DM ZDF rats (207). However, whether this will translate into increased active CaMKII in the DM SAN requires investigation as physiologically tissue-specific differences exist (16). It also remains to be clarified whether phosphorylation of both PKA and CaMKII sites on pacemaking proteins is required for intrinsic pacemaking in the rat SAN. Additionally, despite the significantly increased M_2 receptors, the lack of an augmented declining intrinsic HR response to M_2 stimulation in DM might also be due to decreased expression and / or activity of the Ca^{2+}-activated adenylyl cyclases, as one effect of the cholinergic response is to inhibit adenylyl cyclases which limits cAMP production (131).

A possible lack of intrinsic cAMP would also account for the declining intrinsic HR in DM with increasing $[Ca^{2+}]_o$. If phosphorylation of both PKA and CaMKII sites on phospholamban is needed (see section 7.3.3 below), then in the DM SAN, the reduced phosphorylation of phospholamban at the PKA site serine-16 might limit faster Ca^{2+} uptake by SERCA2a in the intrinsic 'physiological' and increasing $[Ca^{2+}]_o$ setting. This might occur despite the likelihood of increased $[Ca^{2+}]_o$ induced activation of CaMKII and increased phosphorylation of phospholamban at the CaMKII site threonine-17 (16). Graded inhibition of PKA activity

resulted in a graded reduction of phosphorylated phospholamban and spontaneous beating rate in rabbit SAN cardiomyocytes, which also indicates that phosphorylation of both PKA and CaMKII sites on pacemaking proteins is required for the maintenance of normal intrinsic pacemaking (81).

The levels of cAMP, adenylyl cyclase isoforms 1 and 8, and phosphodiesterase isoforms 3 and 4 have not previously investigated in the DM SAN. Measuring cAMP levels is difficult and has not been performed directly in DM, however, there are assessments of downstream proteins and regulators. PKA activity has been found to be decreased in the type 1 DM heart and high glucose cultured cardiomyocytes (530, 531). This might suggest decreased levels of cAMP and / or PKA in DM. Additionally, Ca^{2+}-inhibited phosphodiesterase isoform 5 activity has been found to be increased in the DM ventricle with their inhibition proving to be beneficial (532, 533). This might suggest an increased breakdown of cAMP in DM.

7.2.4 Can a possible lack of hyperpolarisation explain non-functional HCN4 channels and the lower intrinsic heart rate in type 2 diabetes?

In the DM SAN, increased diastolic intracellular Ca^{2+} ($[Ca^{2+}]_i$) and / or intracellular Na^+ ($[Na^+]_i$) might limit hyperpolarisation of the membrane potential and therefore activation of the HCN4 channels (334, 534). This increased $[Ca^{2+}]_i$ and $[Na^+]_i$ might arise from decreased SERCA2a and, increased forward and reverse mode NCX1 function (see section 7.3 below) (79, 334, 535).

A limitation / consideration to the experimental data presented in this study is that the apparently non-functional HCN4 in the DM SAN might be the effect of incomplete and / or slow recovery from the previous condition of increasing $[Ca^{2+}]_o$ applied to the DM hearts, which is likely to result in increased $[Ca^{2+}]_i$ and / or $[Na^+]_i$. The already compromised DM hearts might require a longer recovery time than the 30-minute washout period carried out prior to the use of ivabradine. This is supported by the lack of a complete return to initial baseline intrinsic HR following the $[Ca^{2+}]_o$ condition and washout in nDM and DM hearts. However, the most dramatic decline in intrinsic HR for DM hearts was due to the $[Ca^{2+}]_o$ condition (**Chapter 4**, **Figure 4.5**). This might result in a decreased maximum diastolic potential, a more depolarised state rather than hyperpolarised, resulting in a loss of HCN4 activation (334). Such effects have been reported at extremely high levels of $[Ca^{2+}]_o$ (10 mM) rather than at physiological levels, but, it is possible that these effects arise sooner and at the lower $[Ca^{2+}]_o$ tested (maximum of 3 mM in this study) in the compromised DM heart (334). To what degree this potentially increased $[Ca^{2+}]_i$ affects the membrane potential and HCN4 channel activation in the DM SAN *in vivo* remains unknown. Hence, HCN4 activity might be inhibited due to the DM SAN cardiomyocyte membrane potential not reaching hyperpolarising levels to facilitate HCN4 channel opening *in vivo*, *ex vivo* and in this experimental setting. In the DM SAN, the presence of non-functional HCN4 channels would increase dependency on other Vm clock (T-type Ca^{2+} channels and NCX1) and Ca^{2+} clock (RyR2 for LCRs) proteins for diastolic depolarisation.

7.3. SERCA2a (Ca^{2+} clock) and NCX1 (Vm clock) in type 2 diabetes

7.3.1 Can a possible SERCA2a activity decrease and / or NCX1 activity increase explain the lower intrinsic heart rate in type 2 diabetes?

The effects of limiting SERCA2a activity in SERCA2a knockout and NCX1 overexpression models, and what this might suggest are the potential molecular mechanisms altered in the DM SAN cardiomyocytes is explored in the sections below. This provides reasoning for the proposed decreased SERCA2a activity in DM being responsible for the lower intrinsic and the role of the significantly upregulated NCX1 in the DM SAN.

Complete global knockout of SERCA2a is embryonically lethal (536, 537). Inducible cardiomyocyte-specific SERCA2a knockout in mice at four and seven weeks resulted in significantly reduced *in vivo* HR and increased plasma norepinephrine indicating amplified sympathetic input to the heart (354). As can be expected the primary effect of SERCA2a reduction was lengthened $[Ca^{2+}]_i$ decay (repolarisation) in ventricular cardiomyocytes (also seen in heterozygous models) (354, 355, 536). In ventricular cardiomyocytes, the SR Ca^{2+} content was significantly reduced and contributed minimally to the $[Ca^{2+}]_i$ transient, which is expected when SR Ca^{2+} falls below ~50% (329, 354-356). Ca^{2+} transients were primarily generated by increased Ca^{2+} influx through the significantly increased L-type Ca^{2+} channel and to a lesser extent from the significantly increased NCX1 expression and current (354). This enhanced Ca^{2+} influx by the L-type Ca^{2+} channel was also partly due to slow L-type Ca^{2+} channel inactivation (354). The slow inactivation itself was attributed to reduced SR Ca^{2+} content as SR Ca^{2+} release is one mechanism for L-type Ca^{2+} channel inactivation (283, 354, 538, 539). This

provides a compensatory mechanism for the maintenance of Ca^{2+} transients in a compromised SERCA2a function cardiomyocyte. Enhanced $[Ca^{2+}]_i$ decay was attributed to Ca^{2+} extrusion via NCX1 and / or the significantly upregulated plasma membrane Ca^{2+}-ATPase in ventricular cardiomyocytes (354, 355).

Additionally, a mathematical model of SERCA2a reduction in the SAN that integrated the above findings (increased $I_{Ca,L}$, I_{NCX1} and additional RyR2 downregulation proportional to SERCA2a downregulation) presented a lower intrinsic HR with the combined remodelling than SERCA2a reduction alone (317). A significantly greater HR reduction effect was anticipated on ~70% or above SERCA2a downregulation (317). However, a limitation of the mathematical model is that it is unable to take account of all the physiological processes (possible $[Na^+]_i$ accumulation due to increased forward mode NCX1 activity) occurring within the SAN cardiomyocytes which might also affect HR sooner than the ~70% SERCA2a downregulation (317). Another simulation, of ventricular cardiomyocytes, confirmed the maintenance of $[Ca^{2+}]_i$ transients with compromised SERCA2a activity but eventually resulted in increased diastolic $[Ca^{2+}]_i$ and the compensatory mechanisms of increased I_{NCX1} aimed to decrease diastolic $[Ca^{2+}]_i$ (540). The simulation confirmed the above findings from the cardiomyocyte-specific SERCA2a knockout mouse model where upregulation of $I_{Ca,L}$ and I_{NCX1} maintained systolic and diastolic $[Ca^{2+}]_i$ respectively following compromised SERCA2a function (540). This gives rise to the possibility of increased $[Na^+]_i$ via the upregulated NCX1 expression and activity (541). Additionally, chronic SERCA2a inhibition via ablation of phospholamban phosphorylation also resulted in increased $I_{Ca,L}$ but no change in I_{NCX1} in left ventricular cardiomyocytes (542). The change in I_{NCX1} might be brought about during conditions of increased diastolic $[Ca^{2+}]_i$. Unchanged SERCA2a and phospholamban expression but

diminished SERCA2a activity is found in dilated cardiomyopathy failing hearts (253, 298). However, these studies do not report HR or investigate the $I_{Ca,L}$ or I_{NCX}.

As shown by the above studies where SERCA2a activity is either compromised or completely reduced (knockout studies), the increased diastolic $[Ca^{2+}]_i$ promotes NCX1 upregulation and therefore competition with the residual SERCA2a activity. An NCX1 overexpression study with thapsigargin-induced partial inhibition of SERCA2a (to mimic diseased conditions) in ventricular cardiomyocytes reported similar findings to SERCA2a compromised or knockdown studies (317, 351, 354, 355). As with the SERCA2a compromised and knockout studies, this suggests NCX1 upregulation compensates for reduced SERCA2a activity. This same study also predicted in a mouse ventricular cardiomyocyte a ~2.4-fold increase in NCX1 activity compensates for a ~28% decrease in SERCA2a activity (351). This greater NCX1 increase for a smaller reduction in SERCA2a highlights the lower efficiency of NCX1 compared to SERCA2a for $[Ca^{2+}]_i$ decay during repolarisation. This fold increase is greater than the increase I identified in NCX1 (1.5-fold) in the DM SAN.

In an NCX1 overexpression model of heart failure, failing cardiomyocytes presented decreased $[Ca^{2+}]_i$ transients and SR Ca^{2+} content with no change in $I_{Ca,L}$ (358). The effects of NCX1 overexpression in the failing cardiomyocytes was corrected using an NCX1 inhibitor peptide (partial NCX1 inhibition by XIP) that resulted in normalised SR Ca^{2+} release and refilling, SR Ca^{2+} content and $[Ca^{2+}]_i$ transients (358). Surprisingly, there was no effect on diastolic $[Ca^{2+}]_i$ on NCX1 inhibition. The acceleration of $[Ca^{2+}]_i$ decay upon NCX1 inhibition in normal and failing ventricular cardiomyocytes was suggested to be due to increased $[Ca^{2+}]_i$ activating SERCA2a; similar increased $[Ca^{2+}]_i$ effects on stimulating SERCA2a have also been reported by others

(318, 319, 358). This suggests that inhibition of NCX1 even in a compromised myocyte might have beneficial effects, however, the effect of XIP on NCX1 inhibition on *in vivo* HR remains to be determined.

7.3.2 What does this suggest for pacemaking mechanisms in the type 2 diabetic sinoatrial node and intrinsic heart rate?

The proposed mechanisms discussed here are in relation to the above literature on limiting SERCA2a activity, my research findings and my suggestion of a decreased SERCA2a activity in the DM SAN. I will also highlight / speculate on a number of mechanisms that might be altered as either a cause for the lower DM intrinsic HR or a consequence / compensation to disrupted SERCA2a activity.

As shown by the above models, an effect of reduced SERCA2a expression and / or activity results in increased expression and activity of NCX1 (317, 354, 355, 536, 540). In the DM SAN, NCX1 protein expression has been found to be significantly increased, however, an increase in NCX1 activity requires confirmation. Although the SERCA2a to phospholamban ratio remained unchanged between the nDM and DM SAN, the declining DM intrinsic HR on $[Ca^{2+}]_o$ could suggest compromised SERCA2a activity. The primary responsibility for the maintenance of the DM intrinsic HR was thought to predominantly be attributable to the activity of SERCA2a and to a lesser extent on NCX1 with increasing SAN cardiomyocyte Ca^{2+} load via L-type Ca^{2+} channels and NCX1 (16, 78, 83, 253, 318, 319, 328, 329). Compromised SERCA2a activity in the DM SAN would prolong $[Ca^{2+}]_i$ decay and there would be an increased dependency on NCX1 for Ca^{2+} extrusion. This would lengthen repolarisation in the DM SAN thereby might be partially responsible for the lower intrinsic HR in DM.

Moreover, with compromised SERCA2a and continued Ca^{2+} extrusion by the significantly increased NCX1, it might be expected that SR Ca^{2+} content would be reduced. Yet, the lack of difference in the caffeine-induced intrinsic HR response in the nDM and DM hearts suggests unchanged SR Ca^{2+} content in DM (direct investigation is required). As described in Chapter 4 section 4.5.3.1, SR SERCA2a uptake and RyR2 release characteristics can be altered without changes to the SR Ca^{2+} content (354, 357). Whether there are alterations to RyR2 release characteristics requires direct investigation in future. As SR Ca^{2+} content is not reduced in DM, this might suggest SR Ca^{2+} contribution to the $[Ca^{2+}]_i$ transient is not comparable to the nDM SR Ca^{2+} contribution, particularly if Ca^{2+} influx in the DM SAN cardiomyocytes has not changed, otherwise more Ca^{2+} is depleted from the SAN cardiomyocyte than replaced. Though whether or not SR Ca^{2+} contribution is altered, this also suggests increased Ca^{2+} influx via L-type Ca^{2+} channels and to a lesser extent NCX1 in the DM SAN. If SR RyR2 Ca^{2+} contribution is reduced then increased Ca^{2+} influx is needed to maintain the $[Ca^{2+}]_i$ transient or if SR RyR2 Ca^{2+} contribution is unaltered then more Ca^{2+} influx is needed to replace the released SR Ca^{2+} as there is increased NCX1-SERCA2a competition. Although L-type Ca^{2+} channel expression was not altered in the DM SAN, it is possible that channel activity is altered possible via reduced SR RyR2 Ca^{2+} contribution and / or increased modulation via CaMKII (313, 329, 347, 348, 356). The activity of L-type Ca^{2+} channels could also be investigated in future.

7.3.3 Can a possible decrease in phospholamban phosphorylation explain the suggested compromised SERCA2a activity with unchanged SERCA2a protein expression in the type 2 diabetic sinoatrial node?

As mentioned in section 7.2.2 above, a decrease in PKA and active CaMKII results in a decrease in phosphorylation of phospholamban and this decrease at either phospholamban phosphorylation site will limit SERCA2a activity. Similar decreases might be occurring in the DM SAN and be accountable for the compromised SERCA2a activity and low intrinsic HR. It has been suggested phospholamban phosphorylation increases SERCA2a Ca^{2+} transport by >3-fold (316, 543).

In type 1 DM rats, decreased SERCA2a activity was attributed to significantly decreased SERCA2a and phospholamban protein expression, a significantly increased phospholamban to SERCA2a ratio, and significantly decreased phospholamban phosphorylation as serine-16 (PKA site) and threonine-17 (CaMKII site) in the left ventricle (LV) (257). In obese rats with hyperglycaemia, obesity also resulted in a significant decrease in phospholamban phosphorylation at serine-16 and phospholamban phosphorylation at serine-16 to phospholamban ratio with unchanged SERCA2a, phospholamban protein expression and ratio in the LV (544). Similar significant decreases in phospholamban phosphorylation at serine-16 with unchanged protein expression of SERCA2a and phospholamban have been reported in ventricular tissue of other animal models and human heart failure accounting for reduced SERCA2a function (545-548). These studies, suggest phosphorylation at both serine-16 and threonine-17 sites might be required for maximal SERCA2a activity. Decreased intrinsic

phosphorylation at either site would reduce SERCA2a activity accounting for the lower intrinsic HR within the DM SAN.

7.4. The cardiac cholinergic systems in type 2 diabetes

The markedly increased M_2 receptors with a lack of an increased response to carbachol (M_2 stimulus) in DM compared to nDM suggests a dissociation in the cholinergic responses at the SAN cardiomyocyte level. Although, this suggests no difference in the contribution from the cholinergic systems to intrinsic HR in nDM and DM hearts, the lack of a difference in responsiveness might have implications for *in vivo* HR and cardiac function in DM. Increased cholinergic responsiveness might be important for countering the effects of sympathetic hyperactivity in DM (165). In addition to the possible reasons (unchanged protein expression of K_{ACh}, I_{KACh} desensitisation and deactivation, and a mismatch in the expression of M_2 receptors and Gαβγ inhibitory protein ($G_{\alpha\beta\gamma i}$)) described in Chapter 4 section 4.5.4, another potential reason for the dissociation and potential implications for the lack of augmented cholinergic responsiveness in DM is discussed below.

As mentioned in Chapter 1 section 1.6, neuronal and non-neuronal cholinergic input mediated acetylcholine release stimulates the M_2 receptor that triggers $G_{\alpha\beta\gamma i}$ activation (128, 147, 149). $G_{\alpha\beta\gamma i}$ activation occurs by exchanging guanosine diphosphate (GDP) on the $G_{\alpha i}$ (inactivated state) for guanosine-5'-triphosphate (GTP, activated state) that enables dissociation of $G_{\alpha i}$ and $G_{\beta\gamma i}$ subunits (549, 550). $G_{\alpha i}$ inhibits adenylyl cyclase activity thereby limits cAMP production and $G_{\beta\gamma i}$ directly activates K_{ACh} causing hyperpolarisation (128, 147, 149, 550). The duration of this $G_{\alpha i}$ and $G_{\beta\gamma i}$ activity is dependent on the activated GTP-bound $G_{\alpha i}$ subunit (549, 550).

Termination of this activity occurs via $G_{\alpha i}$ mediated hydrolysis of GTP, which requires the molecular regulator of G-protein signalling (RGS) proteins to increase the rate of $G_{\alpha i}$ mediated hydrolysis (~2000-fold) that would otherwise be slow, returning the G_i subunits to their inactivated GDP bound state (550, 551). Specific isoforms of the RGS proteins in the SAN / heart inhibit cholinergic signalling at the cardiomyocyte level (**Figure 7.2**) (550-554).

RGS4 mRNA levels have been shown to be greater in the SAN compared to atria and have been associated with cholinergic control of HR (550, 552, 555). RGS4 knockout mice exhibited significantly enhanced *in vivo* bradycardia and / or intrinsic HR responses to carbachol compared to control suggesting a role for RGS4 in regulating cholinergic signalling and effects in the SAN (552, 555). Other studies implicate RGS6 (rather than RGS4) in this regulatory process (556-558). The upregulation of RGS4 protein has also been reported in cardiomyopathy and heart failure (559). Collectively, these studies suggest that RGS4 and RGS6 are involved in limiting and inhibiting $G_{\alpha i}$ and $G_{\beta\gamma i}$ cholinergic signalling and effects within cardiomyocytes. In the type 1 DM heart decreased *in vivo* HR response to carbachol was attributed to enhanced desensitisation and decay of I_{KACh} as a result of increased RGS4 (217). A similar increase in RGS4 and / or RSG6 expression might exist that limits increased M_2 receptor activation-induced cholinergic signalling and effects to *in vivo* HR within the DM SAN cardiomyocytes.

In DM ZDF rats during urethane anaesthesia, cardiac sympathetic nerve activity was increased and *in vivo* β-adrenergic HR responsiveness was unchanged using dobutamine (α- / β-adrenergic agonist) (165). On the other hand, in conscious DM ZDF rats, an increased *in vivo* β-adrenergic HR responsiveness with isoprenaline (β-adrenergic agonist) has been found

(166), whereas β-adrenergic HR responsiveness was reduced with dobutamine (182). The reasons for these differences have been suggested to be due to the different β-adrenergic agonists used and / or their different potencies (166), but might also be due to the conscious versus anaesthetised state. In the DM ZDF rats, significantly increased parasympathetic nerve activity has also been found (Bussey *et al*., unpublished data), however, whether there is increased *in vivo* cardiac chronotropic cholinergic responsiveness has not been investigated. My data in the isolated DM ZDF heart shows no difference in the chronotropic cholinergic responsiveness between the nDM and DM hearts. Furthermore, a prolonged *in vivo* HR recovery to baseline following the use of the β-adrenergic agonist isoprenaline in conscious DM ZDF rats has also been shown (166). This was suggested to be comparable to post-exercise prolonged *in vivo* HR recovery in DM patients (166, 560). HR recovery after exercise and stress is suggested to be an indicator of parasympathetic function in humans and rats (561, 562). In line with this, the prolonged *in vivo* HR recovery might be suggested as a result of parasympathetic withdrawal in DM. However, as described above, the parasympathetic nerve activity to the heart in the DM rats was increased (Bussey *et al*., unpublished data), so the prolonged *in vivo* HR recovery in DM (166), might instead suggest alterations in cholinergic signalling and effects within DM SAN cardiomyocytes (rather than parasympathetic withdrawal). This is supported by my data showing no difference in intrinsic HR response to M_2 stimulus between nDM and DM hearts, despite the significantly upregulated M_2 receptor in DM. However, DM ZDF parasympathetic responses at baseline versus recovery following a stressor might differ and therefore requires investigation in nDM and DM to clarify this viewpoint. The lack of an augmented neuronal or non-neuronal intrinsic cholinergic response at the cardiomyocyte level might limit direct (offset sympathetic hyperactivity) and indirect (cholinergic anti-inflammatory pathway, reduces ATP consumption) beneficial cardio-

protective cholinergic signalling and effects within the DM SAN cardiomyocytes *in vivo* (159, 301, 563).

7.5. Limitations

7.5.1 Protein expression study

For my protein expression study, two SAN samples with the closest intrinsic HRs were pooled together to form one 'n' and obtain sufficient protein for western blotting. Due to this small quantity of SAN protein, nitrocellulose membranes were typically stripped 3 – 4 times. The order that the proteins were stripped was altered to prevent technical bias. This might account for some variability present in the protein expression levels. The small quantity of protein also prevented comparison of RyR2 protein expression in the nDM and DM SAN which requires study in future. The phospholamban monomer was not detected in my western blots possibly due to the low 37°C heating used rather than the higher 95°C heating for western blot SAN sample preparation. The low heat was used to prevent SERCA2a protein aggregation, but might not have been sufficient to monomerise the phospholamban protein. This might be important as phospholamban monomers rather than phospholamban pentamers have been suggested to interact directly with SERCA2a, however, other studies indicate the opposite, and the exact mechanism of monomer and pentamer phospholamban-SERCA2a interaction still remains disputed (564, 565).

7.5.2 Langendorff study

The limitations of the Langendorff experiments include the length of the entire protocol, the lack of time controls and that different conditions ($[Ca^{2+}]_o$, ivabradine, carbachol, and caffeine) were tested on the same nDM and DM hearts, which could have had additive effects on

intrinsic HR. These functional assessments were not carried out in separate animal groups due to the cost of the ZDF rats and financial constraints on the research study. However, the duration and order for each condition tested and washout was kept the same between groups. Moreover, the decline in baseline HRs (i.e. an indirect time control, **Figure 4.5**, **Chapter 4**) followed a similar pattern for nDM and DM hearts, and no significant difference was found following normalisation of the nDM and DM baselines. This indirectly suggests that the decline in cardiac viability and HR occurs to the same degree in the nDM and DM hearts. The lack of return to initial baseline intrinsic HR following washout of the different conditions might have resulted due to insufficient washout periods causing additive effects of the different conditions. The initial intrinsic HRs were lower in my study compared to those reported in the literature (not attributed to DM) (566) possibly due to the coronary flow-dependent perfusion I used rather than coronary pressure-dependent perfusion. The Langendorff buffers used for nDM and DM hearts had similar glucose concentrations without fatty acids, the normal energy substrate for the heart (404). Thus, the buffer did not represent the most physiological (nDM) or pathophysiological (DM) substrates of energy metabolism, which might have affected intrinsic HR generation. Nonetheless, cardiomyocytes contain an endogenous source of fatty acids that would be readily used in the absence of fatty acids in the buffer (567). However, the levels of endogenous fatty acids and their usage might also differ between the nDM and DM hearts. Furthermore, the usage of the endogenous fatty acids reserves might be accountable for the declining cardiac viability during the course of the Langendorff experiment.

7.5.3 The Zucker Diabetic Fatty rat as a model for type 2 diabetes

In the ZDF$^{fa/fa}$ rats, a dysfunctional leptin receptor due to a missense mutation prevents the rats from a sense of satiety (199, 202, 568). Therefore, about 12-weeks of age the rats develop

the obese type 2 DM phenotype presenting hyperglycaemia, hyperlipidemia, insulin resistance and obesity due to hyperphagia and slightly high fat diet (Purina 5008, LabDiet®) (202-204). The DM ZDF model is considered a spontaneous model of DM and closely parallels the clinical phenotype of DM in humans, in particular, obesity, insulin resistance, hyperglycaemia and hyperlipidemia (569). Furthermore, the pattern of insulin resistance is similar in ZDF rats and humans, insulin resistance is initially overthrown via hyperinsulinemia that is enabled by pancreatic β-cell compensatory responses to give normoglycaemia (3, 203, 482, 570). The hyperinsulinemia compensatory response is eventually inadequate and fails due to increased β-cell apoptosis that re-introduces hyperglycaemia and the onset of the DM phenotype (203, 570, 571). Additionally, a comparable overlap of cardiovascular disease biomarkers in human and DM ZDF rats was found via urinary peptidomic analysis (572). However, the precise characteristics of DM in humans cannot be replicated in all currently available experimental animal models including the DM ZDF rats due to DM disease complexity and heterogeneity (569). An obvious difference between DM in humans and the DM ZDF rats is the dysfunctional leptin receptor, which is not commonly a contributor to the development of DM in humans. Nonetheless, the DM ZDF model is still considered a commendable experimental animal model of human DM (569).

7.5.4 The rat sinoatrial node as a model for the human sinoatrial node

In this research, the rat SAN was used as a model to investigate intrinsic causes accountable for the lower intrinsic HR in DM. Although the intrinsic HR in rats compared to humans is considerably higher, the proteins and isoforms investigated in this thesis for intrinsic SAN pacemaking, propagation and modulation are fundamentally the same and are also expressed

in humans (32, 124, 165). The intrinsic HR differences between the rat and human might arise due to differences in other proteins not studied here, protein densities, phosphorylation levels, intrinsic regulators, localisation and ultrastructure (14, 16, 21, 32). For these very reasons, there might be different DM-induced effects on human intrinsic SAN remodelling. The findings presented here might also be different with reduced or increased DM duration. Unfortunately, the use of experimental animal models is the abundantly available means to investigate SAN disease as human SAN samples cannot be sampled operatively and would only be obtained post-mortem, and even so are likely to be accompanied by other multifactorial limitations, such as different DM disease durations, other (cardiovascular) co-morbidities and age.

7.5.5 Anaesthetic study

One limitation of the anaesthetic study includes the lack of *in vivo* conscious HR data in the nDM and DM rats. This was not carried out due to the lab being unequipped for *in vivo* conscious telemetry measurements in rats. Another limitation / consideration of the experimental data presented in this thesis is that two anaesthetics were used for different studies. Sodium pentobarbital was used for data presented in Chapters 3 and 4, and isoflurane was used for data presented in Chapter 5. Other than the anaesthetic effects on blood glucose, *in vivo* HR and intrinsic HR, it is possible that sodium pentobarbital and isoflurane have influenced the Langendorff experiments and experimental outcomes differently due to different mechanistic actions. It is also possible that the anaesthetics might have influenced the nDM and DM animals differently (see Chapter 6).

7.6. Future directions

7.6.1 Investigating non-functional HCN4 channels in the type 2 diabetic sinoatrial node

To evaluate the cause for non-functional HCN4 channels in the DM SAN, the levels of cAMP using ELISA should be investigated first. If cAMP levels are found to be altered in DM, then the expression of adenylyl cyclase isoforms 1 and 8, and phosphodiesterase isoforms 3 and 4 could be investigated between the nDM and DM SAN using western blotting to determine the cause for the intrinsic cAMP change. An imbalance in this cAMP regulation could account for the decreased intrinsic activity of pacemaking proteins and therefore lower intrinsic HR in DM. The membrane potential of an isolated SAN cardiomyocyte and / or the AP of an isolated SAN preparation in nDM and DM could also be compared to determine if membrane potential reaches hyperpolarisation levels in order to facilitate HCN4 channel opening and / or the extent of alteration to the slope of diastolic depolarisation using electrophysiological patch-clamp techniques. Due to the absence of an intrinsic HR decrease upon HCN4 inhibition using ivabradine (up to 10 µM) in DM, it would also be interesting to determine whether a HCN4 inhibitory effect could eventually be achieved in the DM hearts upon longer ivabradine exposure and / or use of a higher concentration, however, higher concentrations are known to induce off-target effects on the L-type Ca^{2+} channels (325). This would clarify whether the lack of an intrinsic HR reduction in DM is due to the pre-dispositioned lower intrinsic HR or due to the HR dependency of HCN4 inhibition with ivabradine.

7.6.2 Direct targeting of SERCA2a and NCX1, and phosphorylation status of phospholamban in the type 2 diabetic sinoatrial node

To validate the proposed decreased SERCA2a and increased NCX1 activity in the DM SAN, a more direct approach targeting SERCA2a and NCX1 activity should be explored. The effect of inhibiting SERCA2a and NCX1 using thapsigargin and XIP peptide respectively on intrinsic HR could be investigated between the nDM and DM isolated hearts using Langendorff (358). Also, the phosphorylation status of phospholamban at both the PKA and CaMKII sites, an indicator of phospholamban activity, could be determined by western blotting.

7.6.3 Investigating the lack of an increased cardiac cholinergic response in the type 2 diabetic sinoatrial node

To determine the cause for the lack of an increased cardiac cholinergic response to carbachol despite the significantly increased M_2 receptors in the DM SAN, the expression and activity of the neuronal and non-neuronal cardiac cholinergic system components could be investigated. For the neuronal pathway, the activity, desensitisation and decay of I_{KACh} using patch-clamp of the SAN cardiomyocytes, as well as the expression of G_i, RGS4 and RGS6 using western blotting warrant further exploration. For the non-neuronal intrinsic cholinergic pathway, the expression of the choline acetyltransferase (enzyme for acetylcholine synthesis), vesicular acetylcholine transporter, acetylcholinesterase (enzyme for acetylcholine breakdown) and choline transporter (responsible for re-uptake) should be compared in the nDM and DM SAN using western blotting.

Collectively, this research will provide further insight into the dysfunction responsible for the lower intrinsic HR in the DM SAN for which there are likely to be multiple causes as presented in this thesis.

7.7. Research significance

Previously research has primarily focused on characterising DM-induced innervation changes to the SAN. Little was known about the possible intrinsic protein remodelling occurring within the type 2 DM SAN cardiomyocytes. As shown by my findings in this thesis the intrinsic SAN changes occur alongside the autonomic changes (Bussey *et al*., unpublished data) (165). In the short term, my research is the first to highlight pathological SAN clock protein remodelling in type 2 DM, which affects intrinsic HR generation rather than propagation or modulation. In the long term, the ZDF rat model could further be used to research the additional causes for the alterations in the Vm and Ca^{2+} clock proteins as mentioned in the future direction section 7.6, as well as, the age of onset of these intrinsic SAN changes. Despite the limitations of available human SAN (as mentioned in section 7.5.4), available post-mortem SAN investigation is also needed for comparison of the DM rat SAN and DM human SAN, and / or research could be followed up in larger more comparable animals. This is important due to the differences in intrinsic and autonomic control of *in vivo* HR, as physiologically humans have a lower *in vivo* HR compared to rats and pathophysiologically DM patients present increased basal *in vivo* HR compared to decreased basal *in vivo* HR in rats (31, 166, 182, 193, 206). A greater understanding of the intrinsic SAN molecular changes alongside autonomic alterations adds value by allowing better insight into how to start preventing or treating impaired HR control in DM patients in the clinical setting at the earliest stages of HR dysfunction onset. The

ultimate aim being better DM HR prognosis and therapeutics, however, much more research is required to understand DM-induced impaired HR control.

7.8. Conclusion

The globally increasing prevalence of DM will parallel DM HR dysfunction and healthcare burdens. In this research, I have identified novel type 2 DM-induced alterations to both the intrinsic Vm and Ca^{2+} clocks, in relation to protein expression and function, that helps to understand the lower intrinsic HR in the type 2 DM SAN.

Appendix

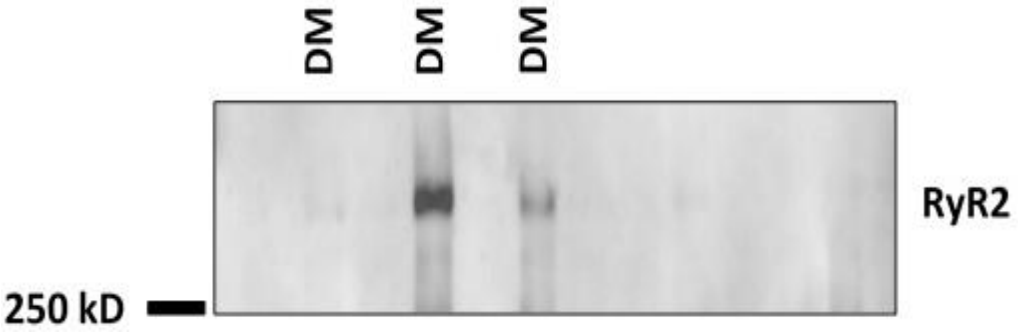

Figure 3.i. Ryanodine receptor 2 expression within the sinoatrial node. (A.) Western blot of ryanodine receptor 2 (RyR2) in the diabetic (DM, n=3) sinoatrial node (SAN) tissue. RyR2 expression was only detected in 3 out of a total 13 SAN homogenate samples. Interestingly, RyR2 expression was more readily detectable in the DM SAN. This might imply greater RyR2 expression within the DM SAN, however justification requires additional studies, potentially pooling more than two SANs to yield sufficient amounts of total protein.

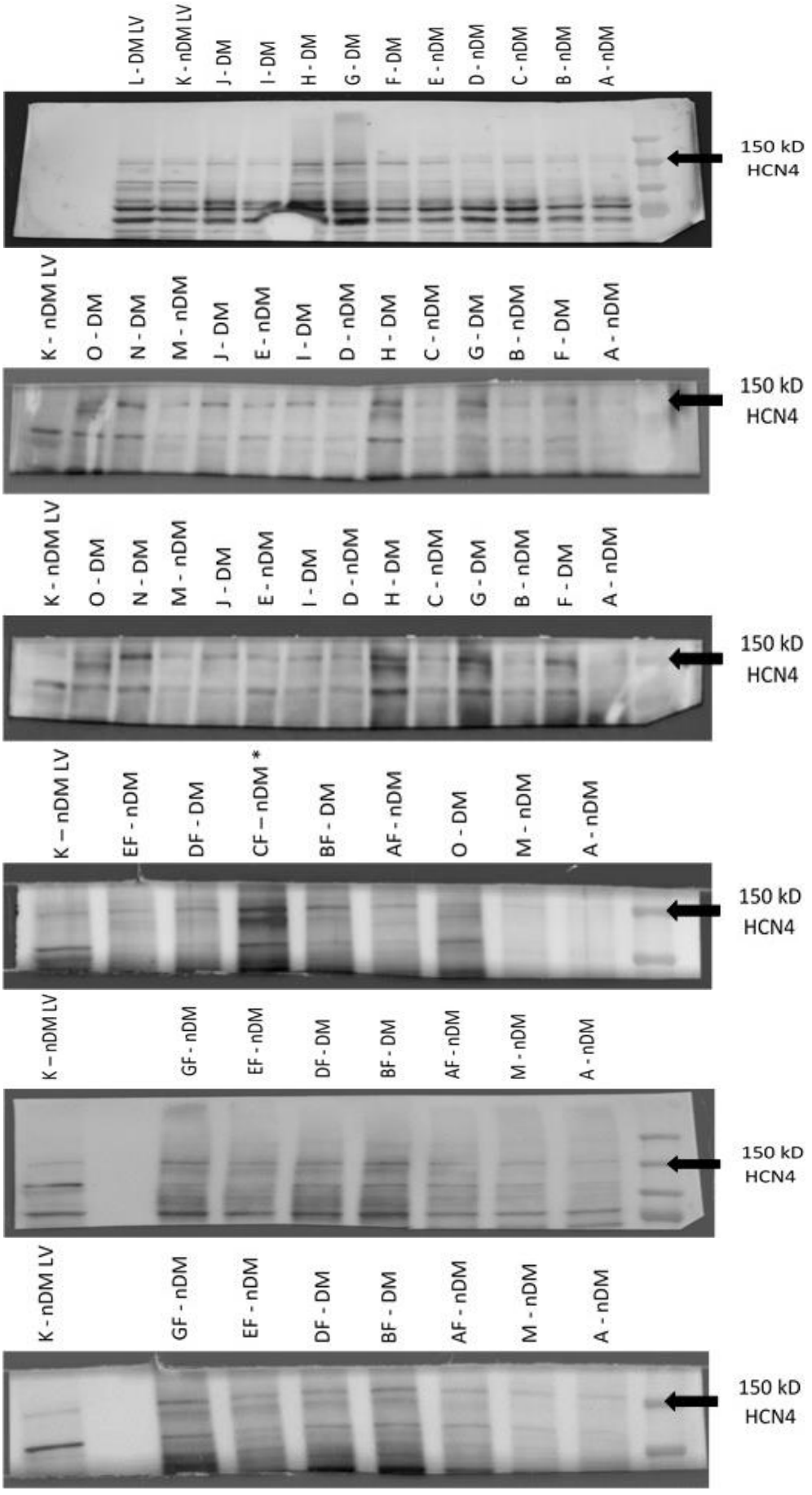
L - DM LV
K - nDM LV
J - DM
I - DM
H - DM
G - DM
F - DM
E - nDM
D - nDM
C - nDM
B - nDM
A - nDM
150 kD
HCN4
K - nDM LV
O - DM
N - DM
M - nDM
J - DM
E - nDM
I - DM
D - nDM
H - DM
C - nDM
G - DM
B - nDM
F - DM
A - nDM
150 kD
HCN4
K - nDM LV
O - DM
N - DM
M - nDM
J - DM
E - nDM
I - DM
D - nDM
H - DM
C - nDM
G - DM
B - nDM
F - DM
A - nDM
150 kD
HCN4
K – nDM LV
EF - nDM
DF - DM
CF – nDM *
BF - DM
AF - nDM
O - DM
M - nDM
A - nDM
150 kD
HCN4
K – nDM LV
GF - nDM
EF - nDM
DF - DM
BF - DM
AF - nDM
M - nDM
A - nDM
150 kD
HCN4
K - nDM LV
GF - nDM
EF - nDM
DF - DM
BF - DM
AF - nDM
M - nDM
A - nDM
150 kD
HCN4

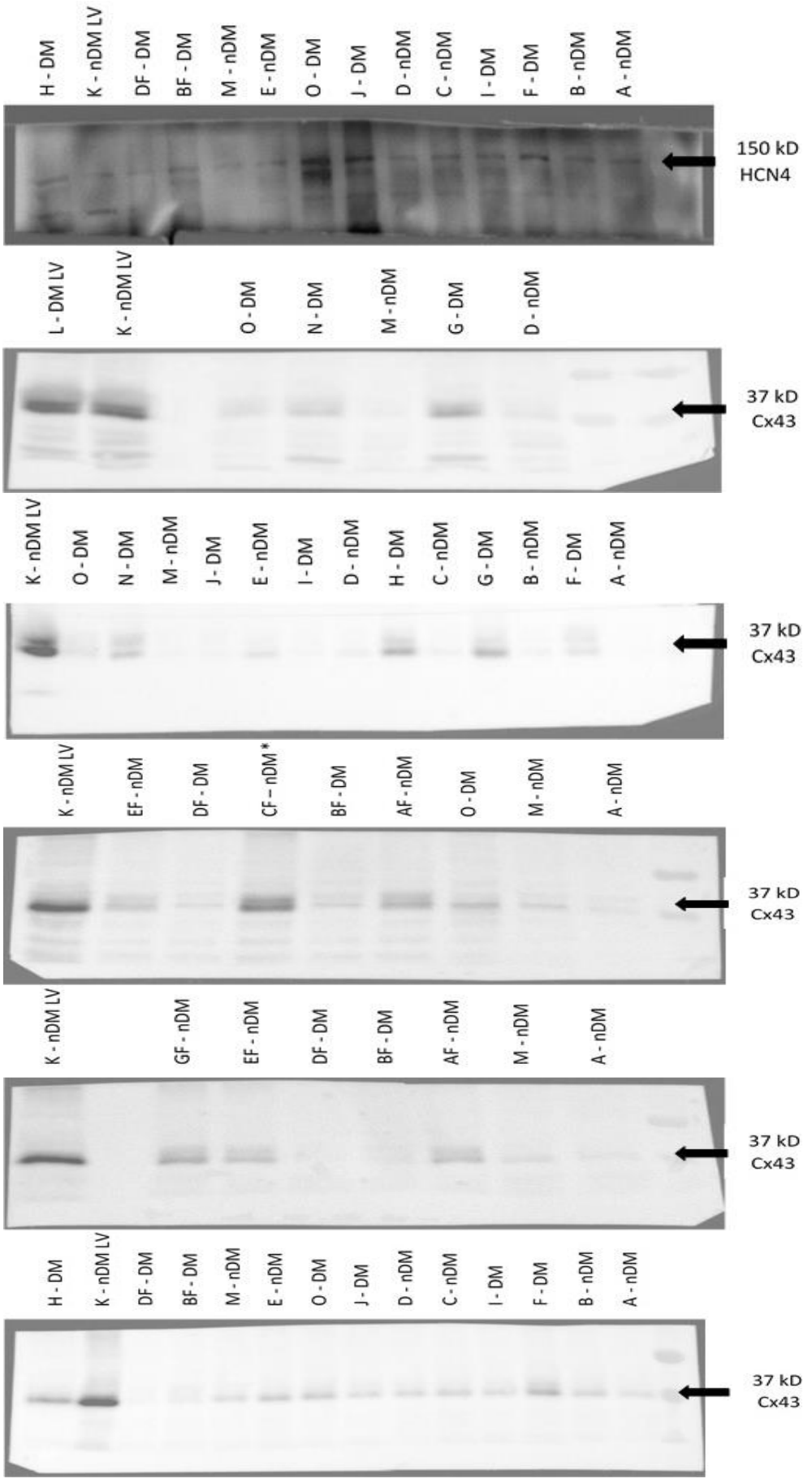
H - DM
K - nDM LV
DF - DM
BF - DM
M - nDM
E - nDM
O - DM
J - DM
D - nDM
C - nDM
I - DM
F - DM
B - nDM
A - nDM
150 kD
HCN4
L - DM LV
K - nDM LV
O - DM
N - DM
M - nDM
G - DM
D - nDM
37 kD
Cx43
K - nDM LV
O - DM
N - DM
M - nDM
J - DM
E - nDM
I - DM
D - nDM
H - DM
C - nDM
G - DM
B - nDM
F - DM
A - nDM
37 kD
Cx43
K - nDM LV
EF - nDM
DF - DM
CF – nDM*
BF - DM
AF - nDM
O - DM
M - nDM
A - nDM
37 kD
Cx43
K - nDM LV
GF - nDM
EF - nDM
DF - DM
BF - DM
AF - nDM
M - nDM
A - nDM
37 kD
Cx43
H - DM
K - nDM LV
DF - DM
BF - DM
M - nDM
E - nDM
O - DM
J - DM
D - nDM
C - nDM
I - DM
F - DM
B - nDM
A - nDM
37 kD
Cx43

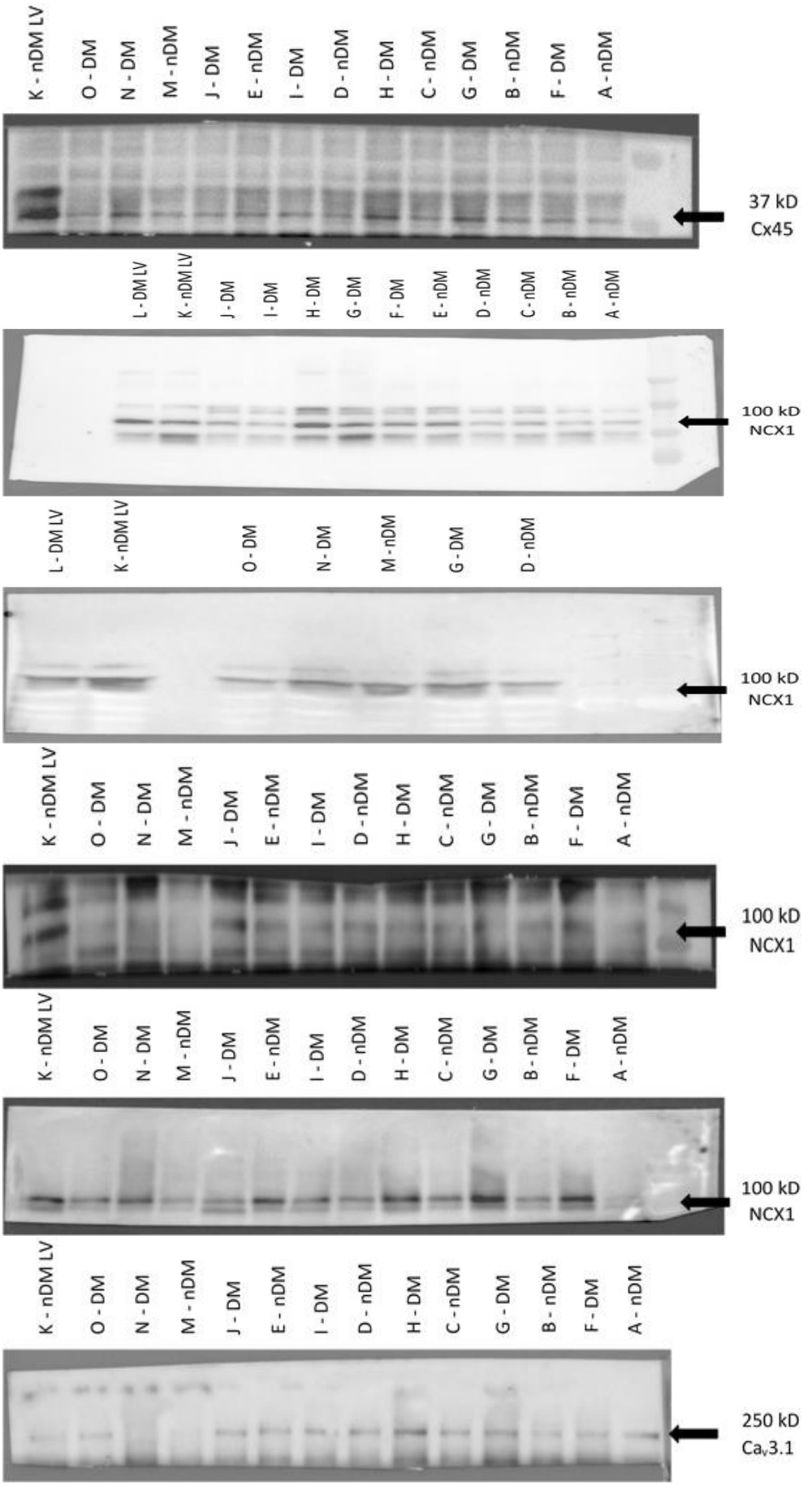
K - nDM LV
O - DM
N - DM
M - nDM
J - DM
E - nDM
I - DM
D - nDM
H - DM
C - nDM
G - DM
B - nDM
F - DM
A - nDM
37 kD
Cx45
L - DM LV
K - nDM LV
J - DM
I - DM
H - DM
G - DM
F - DM
E - nDM
D - nDM
C - nDM
B - nDM
A - nDM
100 kD
NCX1
L - DM LV
K - nDM LV
O - DM
N - DM
M - nDM
G - DM
D - nDM
100 kD
NCX1
K - nDM LV
O - DM
N - DM
M - nDM
J - DM
E - nDM
I - DM
D - nDM
H - DM
C - nDM
G - DM
B - nDM
F - DM
A - nDM
100 kD
NCX1
K - nDM LV
O - DM
N - DM
M - nDM
J - DM
E - nDM
I - DM
D - nDM
H - DM
C - nDM
G - DM
B - nDM
F - DM
A - nDM
100 kD
NCX1
K - nDM LV
O - DM
N - DM
M - nDM
J - DM
E - nDM
I - DM
D - nDM
H - DM
C - nDM
G - DM
B - nDM
F - DM
A - nDM
250 kD
Cav3.1

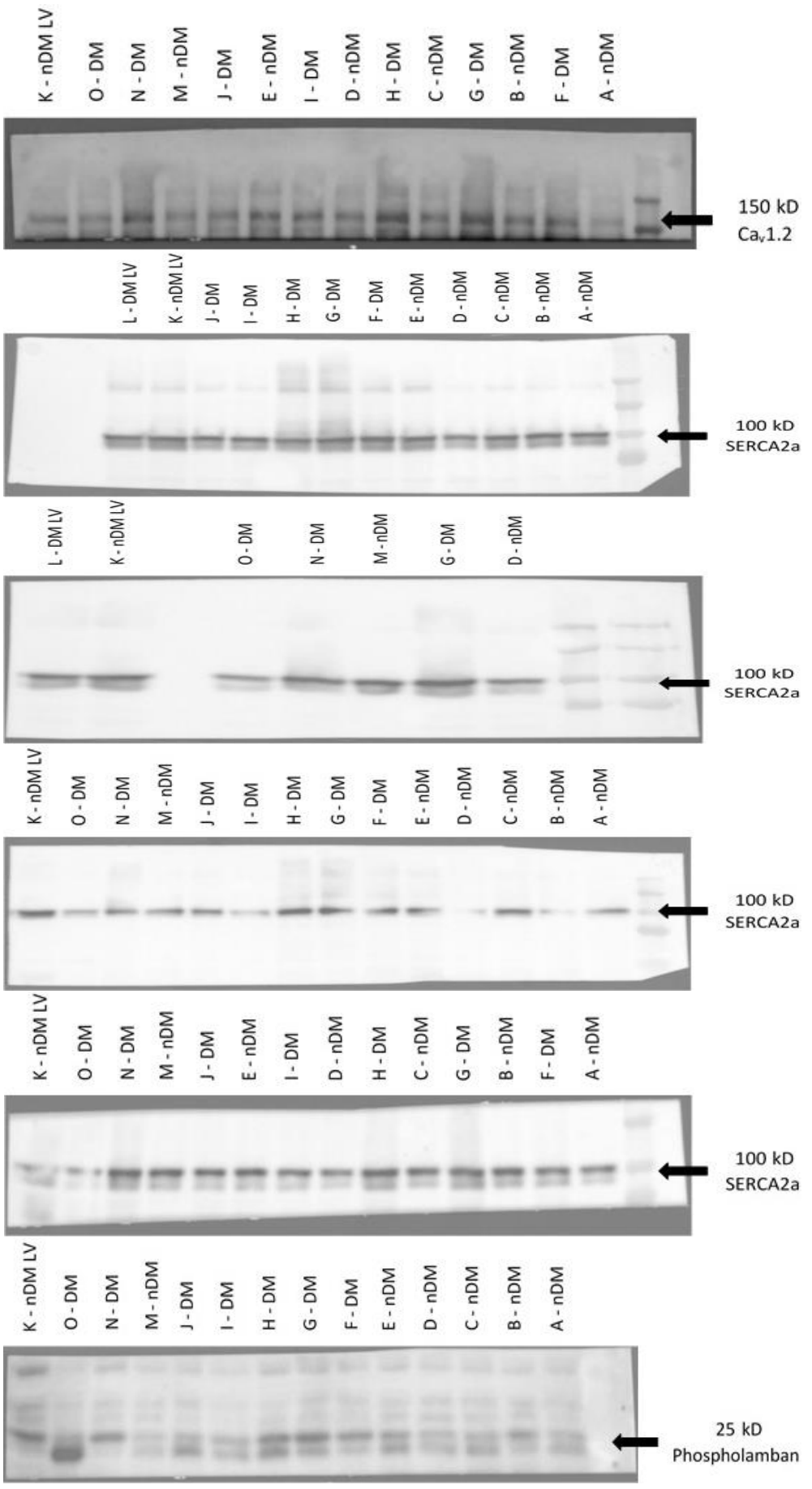
K - nDM LV
O - DM
N - DM
M - nDM
J - DM
E - nDM
I - DM
D - nDM
H - DM
C - nDM
G - DM
B - nDM
F - DM
A - nDM
150 kD
Cav1.2
L - DM LV
K - nDM LV
J - DM
I - DM
H - DM
G - DM
F - DM
E - nDM
D - nDM
C - nDM
B - nDM
A - nDM
100 kD
SERCA2a
L - DM LV
K - nDM LV
O - DM
N - DM
M - nDM
G - DM
D - nDM
100 kD
SERCA2a
K - nDM LV
O - DM
N - DM
M - nDM
J - DM
I - DM
H - DM
G - DM
F - DM
E - nDM
D - nDM
C - nDM
B - nDM
A - nDM
100 kD
SERCA2a
K - nDM LV
O - DM
N - DM
M - nDM
J - DM
E - nDM
I - DM
D - nDM
H - DM
C - nDM
G - DM
B - nDM
F - DM
A - nDM
100 kD
SERCA2a
K - nDM LV
O - DM
N - DM
M - nDM
J - DM
I - DM
H - DM
G - DM
F - DM
E - nDM
D - nDM
C - nDM
B - nDM
A - nDM
25 kD
Phospholamban

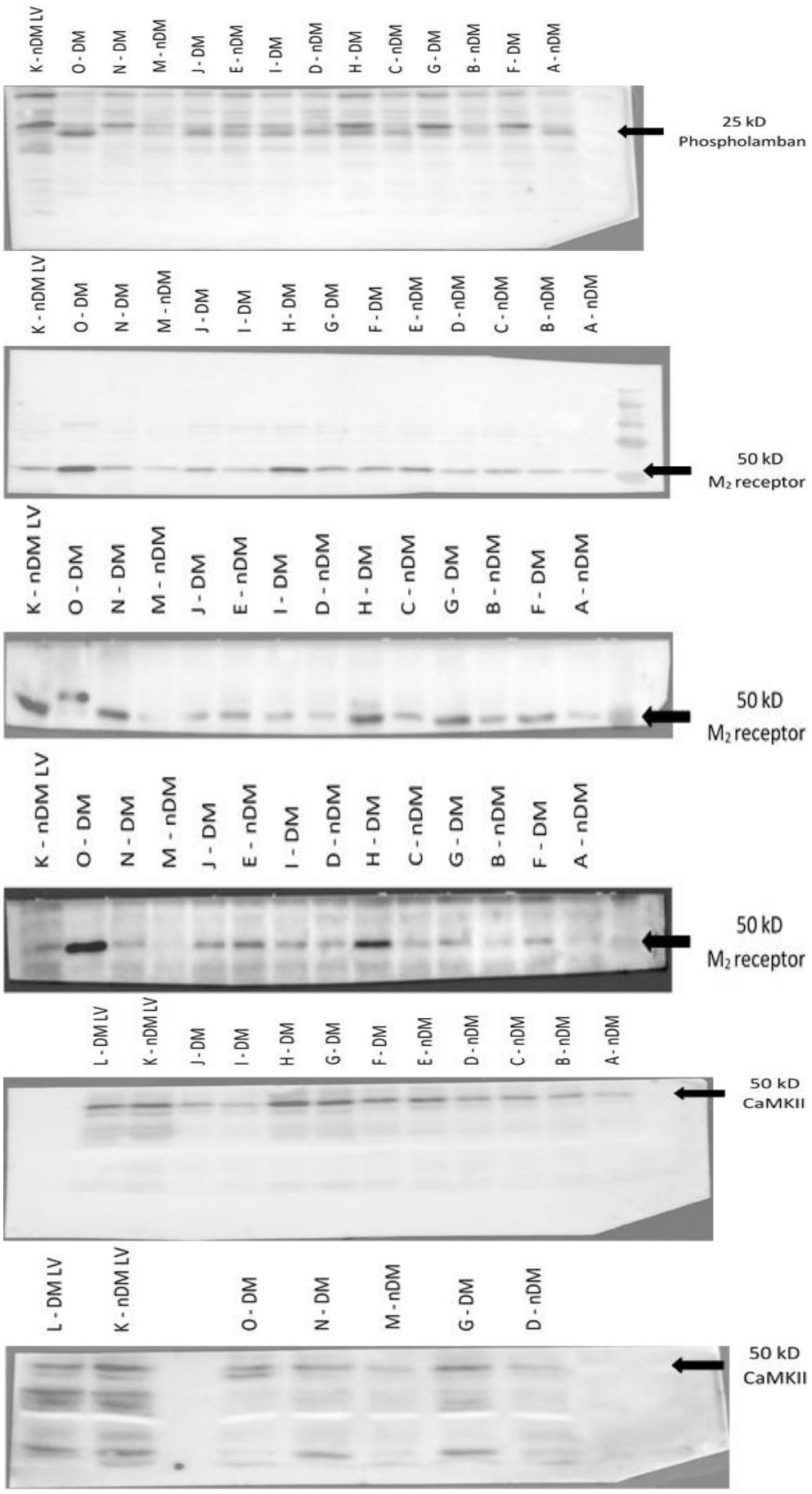
K - nDM LV
O - DM
N - DM
M - nDM
J - DM
E - nDM
I - DM
D - nDM
H - DM
C - nDM
G - DM
B - nDM
F - DM
A - nDM
25 kD
Phospholamban
K - nDM LV
O - DM
N - DM
M - nDM
J - DM
I - DM
H - DM
G - DM
F - DM
E - nDM
D - nDM
C - nDM
B - nDM
A - nDM
50 kD
M2 receptor
K - nDM LV
O - DM
N - DM
M - nDM
J - DM
E - nDM
I - DM
D - nDM
H - DM
C - nDM
G - DM
B - nDM
F - DM
A - nDM
50 kD
M2 receptor
K - nDM LV
O - DM
N - DM
M - nDM
J - DM
E - nDM
I - DM
D - nDM
H - DM
C - nDM
G - DM
B - nDM
F - DM
A - nDM
50 kD
M2 receptor
L - DM LV
K - nDM LV
J - DM
I - DM
H - DM
G - DM
F - DM
E - nDM
D - nDM
C - nDM
B - nDM
A - nDM
50 kD
CaMKII
L - DM LV
K - nDM LV
O - DM
N - DM
M - nDM
G - DM
D - nDM
50 kD
CaMKII

K - nDM LV
O - DM
N - DM
M - nDM
J - DM
I - DM
H - DM
G - DM
F - DM
E - nDM
D - nDM
C - nDM
B - nDM
A - nDM
50 kD
CaMKII
K - nDM LV
O - DM
N - DM
M - nDM
J - DM
E - nDM
I - DM
D - nDM
H - DM
C - nDM
G - DM
B - nDM
F - DM
A - nDM
50 kD
CaMKII
L - DM LV
K - nDM LV
J - DM
I - DM
H - DM
G - DM
F - DM
E - nDM
D - nDM
C - nDM
B - nDM
A - nDM
37 kD
GAPDH
L - DM LV
K - nDM LV
O - DM
N - DM
M - nDM
G - DM
D - nDM
37 kD
GAPDH
K - nDM LV
O - DM
N - DM
M - nDM
J - DM
I - DM
H - DM
G - DM
F - DM
E - nDM
D - nDM
C - nDM
B - nDM
A - nDM
37 kD
GAPDH
K - nDM LV
O - DM
N - DM
M - nDM
J - DM
E - nDM
I - DM
D - nDM
H - DM
C - nDM
G - DM
B - nDM
F - DM
A - nDM
37 kD
GAPDH

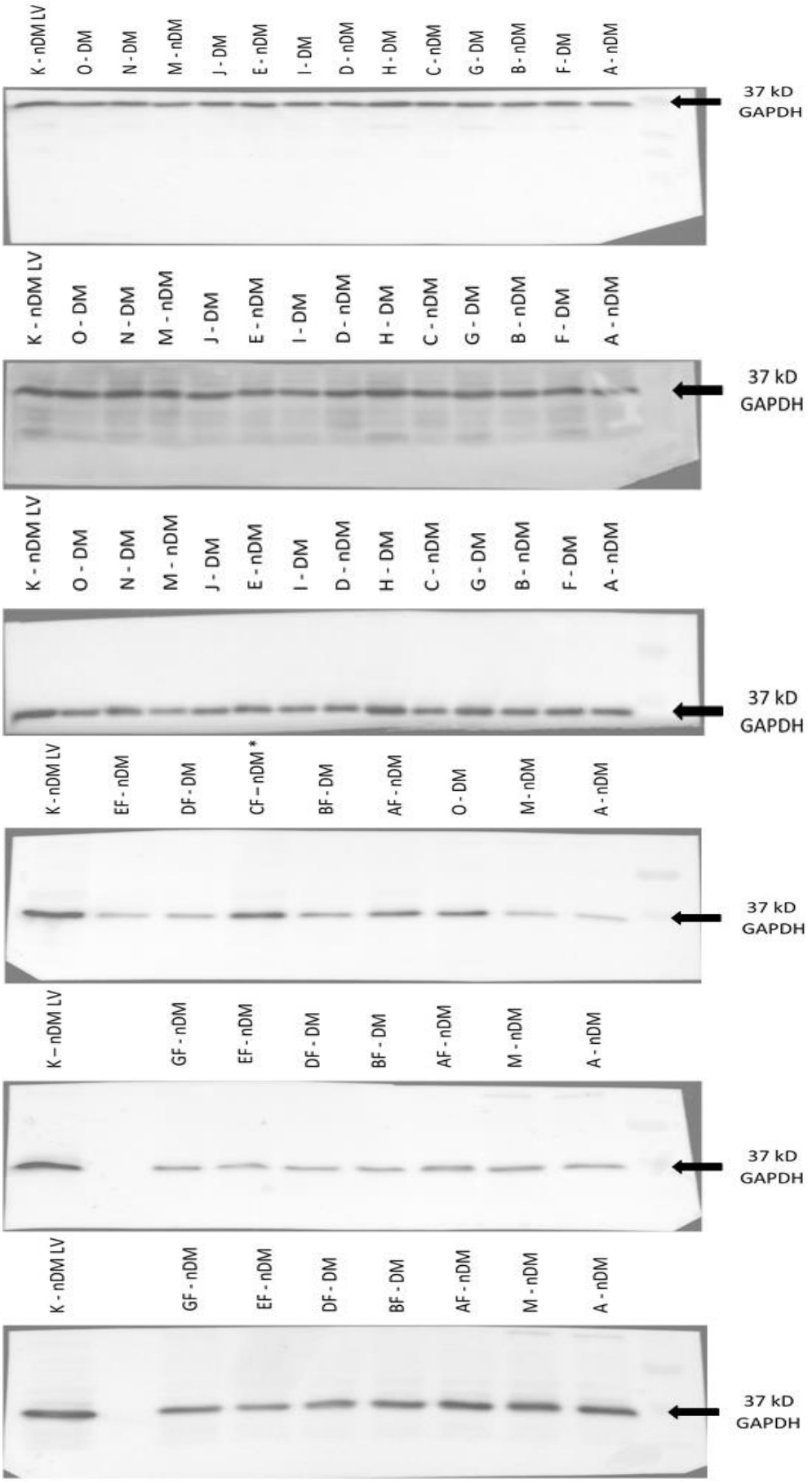
K - nDM LV
O - DM
N - DM
M - nDM
J - DM
E - nDM
I - DM
D - nDM
H - DM
C - nDM
G - DM
B - nDM
F - DM
A - nDM
37 kD
GAPDH
K - nDM LV
O - DM
N - DM
M - nDM
J - DM
E - nDM
I - DM
D - nDM
H - DM
C - nDM
G - DM
B - nDM
F - DM
A - nDM
37 kD
GAPDH
K - nDM LV
O - DM
N - DM
M - nDM
J - DM
E - nDM
I - DM
D - nDM
H - DM
C - nDM
G - DM
B - nDM
F - DM
A - nDM
37 kD
GAPDH
K - nDM LV
EF - nDM
DF - DM
CF – nDM *
BF - DM
AF - nDM
O - DM
M - nDM
A - nDM
37 kD
GAPDH
K – nDM LV
GF - nDM
EF - nDM
DF - DM
BF - DM
AF - nDM
M - nDM
A - nDM
37 kD
GAPDH
K - nDM LV
GF - nDM
EF - nDM
DF - DM
BF - DM
AF - nDM
M - nDM
A - nDM
37 kD
GAPDH

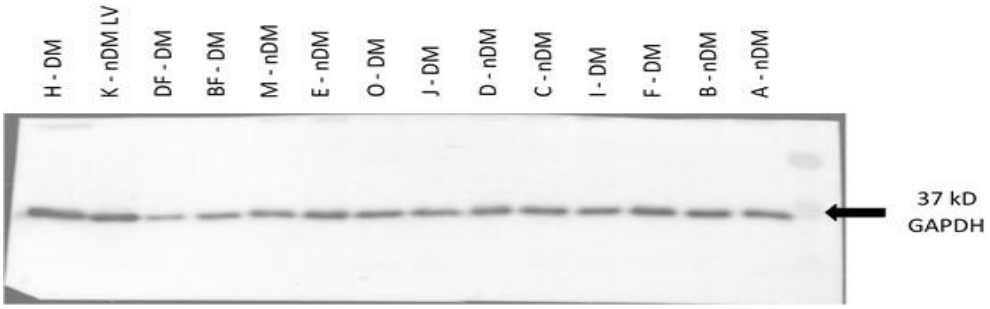

Figure 3.ii. Western blot technical replicates for all non-diabetic (nDM) and diabetic (DM) sinoatrial node (SAN) samples and left ventricular (LV) sample(s) for all proteins investigated. The arrow refers to the protein band of interest and the nearest molecular weight protein marker. Abbreviations: hyperpolarisation-activated cyclic nucleotide-gated channel 4 (HCN4), connexin 43 (cx43), connexin 45 (cx45), Na^{+}-Ca^{2+} exchanger 1 (NCX1), transient type Ca^{2+} channel ($Ca_v3.1$), long-lasting type Ca^{2+} channel ($Ca_v1.2$), sarco(endo)plasmic reticulum Ca^{2+}-ATPase 2a (SERCA2a), muscarinic type 2 (M_2) receptor, Ca^{2+} / calmodulin-dependent protein kinase II (CaMKII) and glyceraldehyde-3-phosphate dehydrogenase (GAPDH). * Sample was excluded due to observed higher levels of cx43 contamination.

References

1. Sun H, Guan Y, Wang L, Zhao Y, Lv H, Bi X, et al. Influence of diabetes on cardiac resynchronization therapy in heart failure patients: a meta-analysis. BMC Cardiovasc Disord. 2015;15:25.
2. Abel ED. Insulin signaling in heart muscle: lessons from genetically engineered mouse models. Curr Hypertens Rep. 2004;6(6):416-23.
3. Kahn BB. Type 2 diabetes: when insulin secretion fails to compensate for insulin resistance. Cell. 1998;92(5):593-6.
4. Halter JB, Musi N, McFarland Horne F, Crandall JP, Goldberg A, Harkless L, et al. Diabetes and cardiovascular disease in older adults: current status and future directions. Diabetes. 2014;63(8):2578-89.
5. Bloomgarden ZT. Cardiovascular disease and diabetes. Diabetes Care. 2003;26(1):230-7.
6. Wild S, Roglic G, Green A, Sicree R, King H. Global prevalence of diabetes: estimates for the year 2000 and projections for 2030. Diabetes Care. 2004;27(5):1047-53.
7. Roglic G. WHO Global report on diabetes: A summary. International Journal of Noncommunicable Diseases. 2016;1(1):3-8.
8. Walker AM, Patel PA, Rajwani A, Groves D, Denby C, Kearney L, et al. Diabetes mellitus is associated with adverse structural and functional cardiac remodelling in chronic heart failure with reduced ejection fraction. Diab Vasc Dis Res. 2016;13(5):331-40.
9. Movahed MR. Diabetes as a risk factor for cardiac conduction defects: a review. Diabetes Obes Metab. 2007;9(3):276-81.
10. Toto RD. Heart disease in diabetic patients. Semin Nephrol. 2005;25(6):372-8.
11. Goraya TY, Leibson CL, Palumbo PJ, Weston SA, Killian JM, Pfeifer EA, et al. Coronary atherosclerosis in diabetes mellitus: a population-based autopsy study. J Am Coll Cardiol. 2002;40(5):946-53.
12. Dawson A, Morris AD, Struthers AD. The epidemiology of left ventricular hypertrophy in type 2 diabetes mellitus. Diabetologia. 2005;48(10):1971-9.
13. Christoffels VM, Moorman AF. Development of the cardiac conduction system: why are some regions of the heart more arrhythmogenic than others? Circ Arrhythm Electrophysiol. 2009;2(2):195-207.
14. Boyett MR, Honjo H, Kodama I. The sinoatrial node, a heterogeneous pacemaker structure. Cardiovasc Res. 2000;47(4):658-87.
15. Moorman AFM, Christoffels VM. Cardiac chamber formation: Development, genes, and evolution. Physiological Reviews. 2003;83(4):1223-67.
16. Vinogradova TM, Tagirova Sirenko S, Lakatta EG. Unique Ca(2+)-Cycling Protein Abundance and Regulation Sustains Local Ca(2+) Releases and Spontaneous Firing of Rabbit Sinoatrial Node Cells. Int J Mol Sci. 2018;19(8).
17. Boyett MR. 'And the beat goes on.' The cardiac conduction system: the wiring system of the heart. Exp Physiol. 2009;94(10):1035-49.
18. Mak KH, Moliterno DJ, Granger CB, Miller DP, White HD, Wilcox RG, et al. Influence of diabetes mellitus on clinical outcome in the thrombolytic era of acute myocardial infarction. GUSTO-I Investigators. Global Utilization of Streptokinase and Tissue Plasminogen Activator for Occluded Coronary Arteries. J Am Coll Cardiol. 1997;30(1):171-9.
19. Soltysinska E, Speerschneider T, Winther SV, Thomsen MB. Sinoatrial node dysfunction induces cardiac arrhythmias in diabetic mice. Cardiovasc Diabetol. 2014;13:122.
20. Howarth FC, Al-Sharhan R, Al-Hammadi A, Qureshi MA. Effects of streptozotocin-induced diabetes on action potentials in the sinoatrial node compared with other regions of the rat heart. Mol Cell Biochem. 2007;300(1-2):39-46.
21. Monfredi O, Maltsev VA, Lakatta EG. Modern concepts concerning the origin of the heartbeat. Physiology (Bethesda). 2013;28(2):74-92.

22. Podlaha R, Falk A. The prevalence of diabetes mellitus and other risk factors of atherosclerosis in bradycardia requiring pacemaker treatment. Horm Metab Res Suppl. 1992;26:84-7.
23. Mandrioli D, Ceci F, Balbi T, Ghimenton C, Pierini G. SEM, TEM, and IHC Analysis of the Sinus Node and Its Implications for the Cardiac Conduction System. Anat Res Int. 2013;2013:961459.
24. Wasada T, Katsumori K, Hasumi S, Kasanuki H, Arii H, Saeki A, et al. Association of sick sinus syndrome with hyperinsulinemia and insulin resistance in patients with non-insulin-dependent diabetes mellitus: report of four cases. Intern Med. 1995;34(12):1174-7.
25. Movahed MR, Hashemzadeh M, Jamal MM. Increased prevalence of third-degree atrioventricular block in patients with type II diabetes mellitus. Chest. 2005;128(4):2611-4.
26. Hasslacher C, Wahl P. Diabetes Prevalence in Patients with Bradycardiac Arrhythmias. Acta Diabetol Lat. 1977;14(5-6):229-34.
27. Zaccardi F, Khan H, Laukkanen JA. Diabetes mellitus and risk of sudden cardiac death: a systematic review and meta-analysis. Int J Cardiol. 2014;177(2):535-7.
28. Shahreyar M, Mupiddi V, Choudhuri I, Sra J, Tajik AJ, Jahangir A. Implantable cardioverter defibrillators in diabetics: efficacy and safety in patients at risk of sudden cardiac death. Expert Rev Cardiovasc Ther. 2015;13(8):897-906.
29. Junttila MJ, Pelli A, Kentta TV, Friede T, Willems R, Bergau L, et al. Appropriate Shocks and Mortality in Patients With Versus Without Diabetes With Prophylactic Implantable Cardioverter Defibrillators. Diabetes Care. 2020;43(1):196-200.
30. Dobrzynski H, Li J, Tellez J, Greener ID, Nikolski VP, Wright SE, et al. Computer three-dimensional reconstruction of the sinoatrial node. Circulation. 2005;111(7):846-54.
31. Vinik AI, Ziegler D. Diabetic cardiovascular autonomic neuropathy. Circulation. 2007;115(3):387-97.
32. Chandler NJ, Greener ID, Tellez JO, Inada S, Musa H, Molenaar P, et al. Molecular architecture of the human sinus node: insights into the function of the cardiac pacemaker. Circulation. 2009;119(12):1562-75.
33. Sanchez-Quintana D, Cabrera JA, Farre J, Climent V, Anderson RH, Ho SY. Sinus node revisited in the era of electroanatomical mapping and catheter ablation. Heart. 2005;91(2):189-94.
34. Sanchez-Quintana D, Anderson RH, Cabrera JA, Climent V, Martin R, Farre J, et al. The terminal crest: morphological features relevant to electrophysiology. Heart. 2002;88(4):406-11.
35. Tellez JO, Dobrzynski H, Greener ID, Graham GM, Laing E, Honjo H, et al. Differential expression of ion channel transcripts in atrial muscle and sinoatrial node in rabbit. Circ Res. 2006;99(12):1384-93.
36. Chandler N, Aslanidi OV, Buckley D, Inada S, Birchall S, Atkinson A, et al. Computer Three-Dimensional Anatomical Reconstruction of the Human Sinus Node and a Novel Paranodal Area. Anat Rec. 2011;294(6):970-9.
37. Yamamoto M, Dobrzynski H, Tellez J, Niwa R, Billeter R, Honjo H, et al. Extended atrial conduction system characterised by the expression of the HCN4 channel and connexin45. Cardiovascular Research. 2006;72(2):271-81.
38. Opthof T, de Jonge B, Mackaay AJ, Bleeker WK, Masson-Pevet M, Jongsma HJ, et al. Functional and morphological organization of the guinea-pig sinoatrial node compared with the rabbit sinoatrial node. J Mol Cell Cardiol. 1985;17(6):549-64.
39. James TN, Sherf L, Fine G, Morales AR. Comparative ultrastructure of the sinus node in man and dog. Circulation. 1966;34(1):139-63.
40. Verheijck EE, Wessels A, van Ginneken AC, Bourier J, Markman MW, Vermeulen JL, et al. Distribution of atrial and nodal cells within the rabbit sinoatrial node: models of sinoatrial transition. Circulation. 1998;97(16):1623-31.
41. Schram G, Pourrier M, Melnyk P, Nattel S. Differential distribution of cardiac ion channel expression as a basis for regional specialization in electrical function. Circ Res. 2002;90(9):939-50.
42. Linscheid N, Logantha S, Poulsen PC, Zhang S, Schrolkamp M, Egerod KL, et al. Quantitative proteomics and single-nucleus transcriptomics of the sinus node elucidates the foundation of cardiac pacemaking. Nat Commun. 2019;10(1):2889.
43. Shinagawa Y, Satoh H, Noma A. The sustained inward current and inward rectifier K+ current in pacemaker cells dissociated from rat sinoatrial node. J Physiol. 2000;523 Pt 3:593-605.

44. Marvin WJ, Jr., Chittick VL, Rosenthal JK, Sandra A, Atkins DL, Hermsmeyer K. The isolated sinoatrial node cell in primary culture from the newborn rat. Circ Res. 1984;55(2):253-60.
45. Ayettey AS, Navaratnam V. The T-tubule system in the specialized and general myocardium of the rat. J Anat. 1978;127(Pt 1):125-40.
46. Keith A, Flack M. The Form and Nature of the Muscular Connections between the Primary Divisions of the Vertebrate Heart. J Anat Physiol. 1907;41(Pt 3):172-89.
47. Dobrzynski H, Anderson RH, Atkinson A, Borbas Z, D'Souza A, Fraser JF, et al. Structure, function and clinical relevance of the cardiac conduction system, including the atrioventricular ring and outflow tract tissues. Pharmacol Ther. 2013;139(2):260-88.
48. Sano T, Yamagishi S. Spread of Excitation from the Sinus Node. Circ Res. 1965;16:423-30.
49. Verkerk AO, van Borren MM, Peters RJ, Broekhuis E, Lam KY, Coronel R, et al. Single cells isolated from human sinoatrial node: action potentials and numerical reconstruction of pacemaker current. Conf Proc IEEE Eng Med Biol Soc. 2007;2007:904-7.
50. Lakatta EG, Maltsev VA, Vinogradova TM. A coupled SYSTEM of intracellular Ca2+ clocks and surface membrane voltage clocks controls the timekeeping mechanism of the heart's pacemaker. Circ Res. 2010;106(4):659-73.
51. Zhang H, Vassalle M. Role of dual pacemaker mechanisms in sinoatrial node discharge. J Biomed Sci. 2000;7(2):100-13.
52. Sohn HG, Vassalle M. Cesium effects on dual pacemaker mechanisms in guinea pig sinoatrial node. J Mol Cell Cardiol. 1995;27(1):563-77.
53. Kreitner D. Electrophysiological Study of the 2 Main Pacemaker Mechanisms in the Rabbit Sinus Node. Cardiovascular Research. 1985;19(5):304-18.
54. Nikmaram MR, Boyett MR, Kodama I, Suzuki R, Honjo H. Variation in effects of Cs+, UL-FS-49, and ZD-7288 within sinoatrial node. Am J Physiol. 1997;272(6 Pt 2):H2782-92.
55. Albarado-Ibanez A, Avelino-Cruz JE, Velasco M, Torres-Jacome J, Hiriart M. Metabolic syndrome remodels electrical activity of the sinoatrial node and produces arrhythmias in rats. PLoS One. 2013;8(11):e76534.
56. Parveen S. The cardiac conduction system in the SERCA2 knockout mouse model of heart failure (Unpublished MRes literature review). University of Manchester, Manchester, UK. 2012.
57. Ford LE, Podolsky RJ. Intracellular calcium movements in skinned muscle fibres. J Physiol. 1972;223(1):21-33.
58. Frank GB. The current view of the source of trigger calcium in excitation-contraction coupling in vertebrate skeletal muscle. Biochem Pharmacol. 1980;29(18):2399-406.
59. Zhang L, Kelley J, Schmeisser G, Kobayashi YM, Jones LR. Complex formation between junctin, triadin, calsequestrin, and the ryanodine receptor. Proteins of the cardiac junctional sarcoplasmic reticulum membrane. J Biol Chem. 1997;272(37):23389-97.
60. Bers DM. Calcium fluxes involved in control of cardiac myocyte contraction. Circ Res. 2000;87(4):275-81.
61. Vinogradova TM, Zhou YY, Maltsev V, Lyashkov A, Stern M, Lakatta EG. Rhythmic ryanodine receptor Ca2+ releases during diastolic depolarization of sinoatrial pacemaker cells do not require membrane depolarization. Circ Res. 2004;94(6):802-9.
62. Difrancesco D, Noble D, Denyer JC, Difrancesco D. The Contribution of the Pacemaker Current (If) to Generation of Spontaneous Activity in Rabbit Sinoatrial Node Myocytes. J Physiol-London. 1991;434:23-40.
63. Wettwer E, Amos GJ, Posival H, Ravens U. Transient outward current in human ventricular myocytes of subepicardial and subendocardial origin. Circ Res. 1994;75(3):473-82.
64. Dobrzynski H, Boyett MR, Anderson RH. New insights into pacemaker activity: promoting understanding of sick sinus syndrome. Circulation. 2007;115(14):1921-32.
65. Xu Y, Dong PH, Zhang Z, Ahmmed GU, Chiamvimonvat N. Presence of a calcium-activated chloride current in mouse ventricular myocytes. American journal of physiology Heart and circulatory physiology. 2002;283(1):H302-14.
66. Lipp P, Laine M, Tovey SC, Burrell KM, Berridge MJ, Li W, et al. Functional InsP3 receptors that may modulate excitation-contraction coupling in the heart. Curr Biol. 2000;10(15):939-42.

67. Ju YK, Liu J, Lee BH, Lai D, Woodcock EA, Lei M, et al. Distribution and functional role of inositol 1,4,5-trisphosphate receptors in mouse sinoatrial node. Circ Res. 2011;109(8):848-57.
68. Chen B, Wu Y, Mohler PJ, Anderson ME, Song LS. Local control of Ca2+-induced Ca2+ release in mouse sinoatrial node cells. J Mol Cell Cardiol. 2009;47(5):706-15.
69. Bogdanov KY, Vinogradova TM, Lakatta EG. Sinoatrial nodal cell ryanodine receptor and Na(+)-Ca(2+) exchanger: molecular partners in pacemaker regulation. Circ Res. 2001;88(12):1254-8.
70. Guo J, Ono K, Noma A. A sustained inward current activated at the diastolic potential range in rabbit sino-atrial node cells. J Physiol. 1995;483 (Pt 1):1-13.
71. Mitsuiye T, Shinagawa Y, Noma A. Sustained inward current during pacemaker depolarization in mammalian sinoatrial node cells. Circ Res. 2000;87(2):88-91.
72. Zhang H, Holden AV, Boyett MR. Sustained inward current and pacemaker activity of mammalian sinoatrial node. J Cardiovasc Electrophysiol. 2002;13(8):809-12.
73. Maltsev VA, Lakatta EG. Dynamic interactions of an intracellular Ca(2+) clock and membrane ton channel clock underlie robust initiation and regulation of cardiac pacemaker function. Cardiovascular Research. 2008;77(2):274-84.
74. Mangoni ME, Traboulsie A, Leoni AL, Couette B, Marger L, Le Quang K, et al. Bradycardia and slowing of the atrioventricular conduction in mice lacking CaV3.1/alpha1G T-type calcium channels. Circ Res. 2006;98(11):1422-30.
75. Zhou Z, Lipsius SL. T-type calcium current in latent pacemaker cells isolated from cat right atrium. J Mol Cell Cardiol. 1994;26(9):1211-9.
76. Lyashkov AE, Behar J, Lakatta EG, Yaniv Y, Maltsev VA. Positive Feedback Mechanisms among Local Ca Releases, NCX, and ICaL Ignite Pacemaker Action Potentials. Biophys J. 2018;114(8):2024.
77. Hagiwara N, Irisawa H, Kameyama M. Contribution of two types of calcium currents to the pacemaker potentials of rabbit sino-atrial node cells. J Physiol. 1988;395:233-53.
78. Bassani JW, Bassani RA, Bers DM. Relaxation in rabbit and rat cardiac cells: species-dependent differences in cellular mechanisms. J Physiol. 1994;476(2):279-93.
79. Bers DM. Cardiac excitation-contraction coupling. Nature. 2002;415(6868):198-205.
80. Vinogradova TM, Brochet DX, Sirenko S, Li Y, Spurgeon H, Lakatta EG. Sarcoplasmic reticulum Ca2+ pumping kinetics regulates timing of local Ca2+ releases and spontaneous beating rate of rabbit sinoatrial node pacemaker cells. Circ Res. 2010;107(6):767-75.
81. Vinogradova TM, Lyashkov AE, Zhu W, Ruknudin AM, Sirenko S, Yang D, et al. High basal protein kinase A-dependent phosphorylation drives rhythmic internal Ca2+ store oscillations and spontaneous beating of cardiac pacemaker cells. Circ Res. 2006;98(4):505-14.
82. Bodi I, Mikala G, Koch SE, Akhter SA, Schwartz A. The L-type calcium channel in the heart: the beat goes on. J Clin Invest. 2005;115(12):3306-17.
83. Bers DM, Perez-Reyes E. Ca channels in cardiac myocytes: structure and function in Ca influx and intracellular Ca release. Cardiovasc Res. 1999;42(2):339-60.
84. Mesirca P, Torrente AG, Mangoni ME. Functional role of voltage gated Ca(2+) channels in heart automaticity. Front Physiol. 2015;6:19.
85. Huser J, Lipsius SL, Blatter LA. Calcium gradients during excitation-contraction coupling in cat atrial myocytes. J Physiol. 1996;494 (Pt 3):641-51.
86. Lyashkov AE, Juhaszova M, Dobrzynski H, Vinogradova TM, Maltsev VA, Juhasz O, et al. Calcium cycling protein density and functional importance to automaticity of isolated sinoatrial nodal cells are independent of cell size. Circ Res. 2007;100(12):1723-31.
87. Liu J, Sirenko S, Juhaszova M, Ziman B, Shetty V, Rain S, et al. A full range of mouse sinoatrial node AP firing rates requires protein kinase A-dependent calcium signaling. J Mol Cell Cardiol. 2011;51(5):730-9.
88. Mackenzie L, Roderick HL, Berridge MJ, Conway SJ, Bootman MD. The spatial pattern of atrial cardiomyocyte calcium signalling modulates contraction. J Cell Sci. 2004;117(Pt 26):6327-37.
89. Bers DM, Grandi E. Calcium/Calmodulin-dependent Kinase II Regulation of Cardiac Ion Channels. J Cardiovasc Pharm. 2009;54(3):180-7.
90. Ginsburg KS, Bers DM. Modulation of excitation-contraction coupling by isoproterenol in cardiomyocytes with controlled SR Ca2+ load and Ca2+ current trigger. J Physiol. 2004;556(Pt 2):463-80.

91. Najafi A, Sequeira V, Kuster DW, van der Velden J. beta-adrenergic receptor signalling and its functional consequences in the diseased heart. Eur J Clin Invest. 2016;46(4):362-74.
92. Schuessler RB, Boineau JP, Bromberg BI. Origin of the sinus impulse. J Cardiovasc Electrophysiol. 1996;7(3):263-74.
93. Mattick P, Parrington J, Odia E, Simpson A, Collins T, Terrar D. Ca2+-stimulated adenylyl cyclase isoform AC1 is preferentially expressed in guinea-pig sino-atrial node cells and modulates the I(f) pacemaker current. J Physiol. 2007;582(Pt 3):1195-203.
94. Hegyi B, Bers DM, Bossuyt J. CaMKII signaling in heart diseases: Emerging role in diabetic cardiomyopathy. J Mol Cell Cardiol. 2019;127:246-59.
95. Wu Y, Anderson ME. CaMKII in sinoatrial node physiology and dysfunction. Front Pharmacol. 2014;5:48.
96. Wu Y, Gao Z, Chen B, Koval OM, Singh MV, Guan X, et al. Calmodulin kinase II is required for fight or flight sinoatrial node physiology. Proc Natl Acad Sci U S A. 2009;106(14):5972-7.
97. Vinogradova TM, Zhou YY, Bogdanov KY, Yang D, Kuschel M, Cheng H, et al. Sinoatrial node pacemaker activity requires Ca(2+)/calmodulin-dependent protein kinase II activation. Circ Res. 2000;87(9):760-7.
98. Vinogradova TM, Sirenko S, Lukyanenko YO, Yang D, Tarasov KV, Lyashkov AE, et al. Basal Spontaneous Firing of Rabbit Sinoatrial Node Cells Is Regulated by Dual Activation of PDEs (Phosphodiesterases) 3 and 4. Circ Arrhythm Electrophysiol. 2018;11(6):e005896.
99. Gaertner TR, Kolodziej SJ, Wang D, Kobayashi R, Koomen JM, Stoops JK, et al. Comparative analyses of the three-dimensional structures and enzymatic properties of alpha, beta, gamma and delta isoforms of Ca2+-calmodulin-dependent protein kinase II. J Biol Chem. 2004;279(13):12484-94.
100. van der Velden HM, Jongsma HJ. Cardiac gap junctions and connexins: their role in atrial fibrillation and potential as therapeutic targets. Cardiovasc Res. 2002;54(2):270-9.
101. Hulsmans M, Clauss S, Xiao L, Aguirre AD, King KR, Hanley A, et al. Macrophages Facilitate Electrical Conduction in the Heart. Cell. 2017;169(3):510-22 e20.
102. Vozzi C, Dupont E, Coppen SR, Yeh HI, Severs NJ. Chamber-related differences in connexin expression in the human heart. J Mol Cell Cardiol. 1999;31(5):991-1003.
103. van Veen AA, van Rijen HV, Opthof T. Cardiac gap junction channels: modulation of expression and channel properties. Cardiovasc Res. 2001;51(2):217-29.
104. Verheijck EE, van Kempen MJ, Veereschild M, Lurvink J, Jongsma HJ, Bouman LN. Electrophysiological features of the mouse sinoatrial node in relation to connexin distribution. Cardiovasc Res. 2001;52(1):40-50.
105. Coppen SR, Dupont E, Rothery S, Severs NJ. Connexin45 expression is preferentially associated with the ventricular conduction system in mouse and rat heart. Circ Res. 1998;82(2):232-43.
106. Coppen SR, Kodama I, Boyett MR, Dobrzynski H, Takagishi Y, Honjo H, et al. Connexin45, a major connexin of the rabbit sinoatrial node, is co-expressed with connexin43 in a restricted zone at the nodal-crista terminalis border. J Histochem Cytochem. 1999;47(7):907-18.
107. Atkinson AJ, Logantha SJ, Hao G, Yanni J, Fedorenko O, Sinha A, et al. Functional, anatomical, and molecular investigation of the cardiac conduction system and arrhythmogenic atrioventricular ring tissue in the rat heart. J Am Heart Assoc. 2013;2(6):e000246.
108. Jansen JA, van Veen TA, de Bakker JM, van Rijen HV. Cardiac connexins and impulse propagation. J Mol Cell Cardiol. 2010;48(1):76-82.
109. Verheule S, Kaese S. Connexin diversity in the heart: insights from transgenic mouse models. Front Pharmacol. 2013;4:81.
110. Kreuzberg MM, Sohl G, Kim JS, Verselis VK, Willecke K, Bukauskas FF. Functional properties of mouse connexin30.2 expressed in the conduction system of the heart. Circ Res. 2005;96(11):1169-77.
111. Kawashima T. The autonomic nervous system of the human heart with special reference to its origin, course, and peripheral distribution. Anat Embryol (Berl). 2005;209(6):425-38.
112. Shen MJ, Zipes DP. Role of the Autonomic Nervous System in Modulating Cardiac Arrhythmias. Circulation Research. 2014;114(6):1004-21.
113. Jamali HK, Waqar F, Gerson MC. Cardiac autonomic innervation. J Nucl Cardiol. 2016.
114. Batulevicius D, Pauziene N, Pauza DH. Key anatomic data for the use of rat heart in electrophysiological studies of the intracardiac nervous system. Medicina (Kaunas). 2004;40(3):253-9.

115. Coote JH, Chauhan RA. The sympathetic innervation of the heart: Important new insights. Auton Neurosci. 2016;199:17-23.
116. Ulphani JS, Cain JH, Inderyas F, Gordon D, Gikas PV, Shade G, et al. Quantitative analysis of parasympathetic innervation of the porcine heart. Heart Rhythm. 2010;7(8):1113-9.
117. Rodefeld MD, Beau SL, Schuessler RB, Boineau JP, Saffitz JE. Beta-adrenergic and muscarinic cholinergic receptor densities in the human sinoatrial node: identification of a high beta 2-adrenergic receptor density. J Cardiovasc Electrophysiol. 1996;7(11):1039-49.
118. Crick SJ, Wharton J, Sheppard MN, Royston D, Yacoub MH, Anderson RH, et al. Innervation of the human cardiac conduction system. A quantitative immunohistochemical and histochemical study. Circulation. 1994;89(4):1697-708.
119. Zaglia T, Mongillo M. Cardiac sympathetic innervation, from a different point of (re)view. J Physiol. 2017;595(12):3919-30.
120. James TN. Cardiac innervation: anatomic and pharmacologic relations. Bull N Y Acad Med. 1967;43(12):1041-86.
121. Armour JA. Functional anatomy of intrathoracic neurons innervating the atria and ventricles. Heart Rhythm. 2010;7(7):994-6.
122. Coote JH. Myths and realities of the cardiac vagus. J Physiol. 2013;591(17):4073-85.
123. Gordan R, Gwathmey JK, Xie LH. Autonomic and endocrine control of cardiovascular function. World J Cardiol. 2015;7(4):204-14.
124. Opthof T. The normal range and determinants of the intrinsic heart rate in man. Cardiovasc Res. 2000;45(1):177-84.
125. Zhao M, Hagler HK, Muntz KH. Regulation of alpha 1-, beta 1-, and beta 2-adrenergic receptors in rat heart by norepinephrine. Am J Physiol. 1996;271(5 Pt 2):H1762-8.
126. McPherson GA, Molenaar P, Malta E. The affinity and efficacy of naturally occurring catecholamines at beta-adrenoceptor subtypes. J Pharm Pharmacol. 1985;37(7):499-501.
127. Bristow MR, Ginsburg R, Umans V, Fowler M, Minobe W, Rasmussen R, et al. Beta 1- and beta 2-adrenergic-receptor subpopulations in nonfailing and failing human ventricular myocardium: coupling of both receptor subtypes to muscle contraction and selective beta 1-receptor down-regulation in heart failure. Circ Res. 1986;59(3):297-309.
128. Dhein S, van Koppen CJ, Brodde OE. Muscarinic receptors in the mammalian heart. Pharmacol Res. 2001;44(3):161-82.
129. Dukes ID, Vaughan Williams EM. Effects of selective alpha 1-, alpha 2-, beta 1-and beta 2-adrenoceptor stimulation on potentials and contractions in the rabbit heart. J Physiol. 1984;355:523-46.
130. de Lucia C, Eguchi A, Koch WJ. New Insights in Cardiac beta-Adrenergic Signaling During Heart Failure and Aging. Front Pharmacol. 2018;9:904.
131. Campbell AP, Smrcka AV. Targeting G protein-coupled receptor signalling by blocking G proteins. Nat Rev Drug Discov. 2018.
132. DiFrancesco D, Tortora P. Direct activation of cardiac pacemaker channels by intracellular cyclic AMP. Nature. 1991;351(6322):145-7.
133. Bois P, Renaudon B, Baruscotti M, Lenfant J, DiFrancesco D. Activation of f-channels by cAMP analogues in macropatches from rabbit sino-atrial node myocytes. J Physiol. 1997;501 (Pt 3):565-71.
134. Liao Z, Lockhead D, Larson ED, Proenza C. Phosphorylation and modulation of hyperpolarization-activated HCN4 channels by protein kinase A in the mouse sinoatrial node. J Gen Physiol. 2010;136(3):247-58.
135. Takasago T, Imagawa T, Shigekawa M. Phosphorylation of the cardiac ryanodine receptor by cAMP-dependent protein kinase. J Biochem. 1989;106(5):872-7.
136. Camors E, Valdivia HH. CaMKII regulation of cardiac ryanodine receptors and inositol triphosphate receptors. Front Pharmacol. 2014;5:101.
137. Tsien RW, Bean BP, Hess P, Lansman JB, Nilius B, Nowycky MC. Mechanisms of Calcium-Channel Modulation by Beta-Adrenergic Agents and Dihydropyridine Calcium Agonists. Journal of Molecular and Cellular Cardiology. 1986;18(7):691-710.
138. Reuter H. Calcium channel modulation by neurotransmitters, enzymes and drugs. Nature. 1983;301(5901):569-74.

139. Hicks MJ, Shigekawa M, Katz AM. Mechanism by which cyclic adenosine 3':5'-monophosphate-dependent protein kinase stimulates calcium transport in cardiac sarcoplasmic reticulum. Circ Res. 1979;44(3):384-91.
140. Koss KL, Kranias EG. Phospholamban: a prominent regulator of myocardial contractility. Circ Res. 1996;79(6):1059-63.
141. Noma A, Kotake H, Irisawa H. Slow inward current and its role mediating the chronotropic effect of epinephrine in the rabbit sinoatrial node. Pflugers Arch. 1980;388(1):1-9.
142. Bennett PB, Begenisich TB. Catecholamines modulate the delayed rectifying potassium current (IK) in guinea pig ventricular myocytes. Pflugers Arch. 1987;410(1-2):217-9.
143. Li GR, Feng J, Wang Z, Fermini B, Nattel S. Adrenergic modulation of ultrarapid delayed rectifier K+ current in human atrial myocytes. Circ Res. 1996;78(5):903-15.
144. Li DL, Liu BH, Sun L, Zhao M, He X, Yu XJ, et al. Alterations of muscarinic acetylcholine receptors-2, 4 and alpha7-nicotinic acetylcholine receptor expression after ischaemia / reperfusion in the rat isolated heart. Clin Exp Pharmacol Physiol. 2010;37(12):1114-9.
145. Dobrzynski H, Marples DD, Musa H, Yamanushi TT, Henderson Z, Takagishi Y, et al. Distribution of the muscarinic K+ channel proteins Kir3.1 and Kir3.4 in the ventricle, atrium, and sinoatrial node of heart. J Histochem Cytochem. 2001;49(10):1221-34.
146. McMorn SO, Harrison SM, Zang WJ, Yu XJ, Boyett MR. A direct negative inotropic effect of acetylcholine on rat ventricular myocytes. Am J Physiol. 1993;265(4 Pt 2):H1393-400.
147. Saternos HC, Almarghalani DA, Gibson HM, Meqdad MA, Antypas RB, Lingireddy A, et al. Distribution and function of the muscarinic receptor subtypes in the cardiovascular system. Physiol Genomics. 2018;50(1):1-9.
148. DiFrancesco D, Tromba C. Inhibition of the hyperpolarization-activated current (if) induced by acetylcholine in rabbit sino-atrial node myocytes. J Physiol. 1988;405:477-91.
149. Ito H, Tung RT, Sugimoto T, Kobayashi I, Takahashi K, Katada T, et al. On the mechanism of G protein beta gamma subunit activation of the muscarinic K+ channel in guinea pig atrial cell membrane. Comparison with the ATP-sensitive K+ channel. J Gen Physiol. 1992;99(6):961-83.
150. Logothetis DE, Kurachi Y, Galper J, Neer EJ, Clapham DE. The beta gamma subunits of GTP-binding proteins activate the muscarinic K+ channel in heart. Nature. 1987;325(6102):321-6.
151. Krapivinsky G, Krapivinsky L, Wickman K, Clapham DE. G beta gamma binds directly to the G protein-gated K+ channel, IKACh. J Biol Chem. 1995;270(49):29059-62.
152. Jeevaratnam K, Chadda KR, Huang CL, Camm AJ. Cardiac Potassium Channels: Physiological Insights for Targeted Therapy. J Cardiovasc Pharmacol Ther. 2018;23(2):119-29.
153. DiFrancesco D, Tromba C. Muscarinic control of the hyperpolarization-activated current (if) in rabbit sino-atrial node myocytes. J Physiol. 1988;405:493-510.
154. Furlan R, Guzzetti S, Crivellaro W, Dassi S, Tinelli M, Baselli G, et al. Continuous 24-hour assessment of the neural regulation of systemic arterial pressure and RR variabilities in ambulant subjects. Circulation. 1990;81(2):537-47.
155. Fink AM, Bronas UG, Calik MW. Autonomic regulation during sleep and wakefulness: a review with implications for defining the pathophysiology of neurological disorders. Clin Auton Res. 2018;28(6):509-18.
156. Sayin H, Chapuis B, Chevalier P, Barres C, Julien C. Assessment of cardiac autonomic tone in conscious rats. Auton Neurosci. 2016;194:26-31.
157. Oosting J, Struijker-Boudier HA, Janssen BJ. Autonomic control of ultradian and circadian rhythms of blood pressure, heart rate, and baroreflex sensitivity in spontaneously hypertensive rats. J Hypertens. 1997;15(4):401-10.
158. Grodner AS, Lahrtz HS, Pool PE, Braunwald E. Neurotransmitter control of sinoatrial pacemaker frequency in isolated rat atria and in intact rabbits. Circ Res. 1970;27(6):867-73.
159. Saw EL, Kakinuma Y, Fronius M, Katare R. The non-neuronal cholinergic system in the heart: A comprehensive review. J Mol Cell Cardiol. 2018;125:129-39.
160. Kakinuma Y, Akiyama T, Sato T. Cholinoceptive and cholinergic properties of cardiomyocytes involving an amplification mechanism for vagal efferent effects in sparsely innervated ventricular myocardium. FEBS J. 2009;276(18):5111-25.

161. Rana OR, Schauerte P, Kluttig R, Schroder JW, Koenen RR, Weber C, et al. Acetylcholine as an age-dependent non-neuronal source in the heart. Auton Neurosci. 2010;156(1-2):82-9.
162. Hostiuc S, Popescu A, Gutu ED, Rusu MC, Pop F. Electrical conduction system apoptosis in type II diabetes mellitus. Rom J Morphol Embryol. 2013;54(4):953-9.
163. Giacco F, Brownlee M. Oxidative stress and diabetic complications. Circ Res. 2010;107(9):1058-70.
164. Webb K, Absi M, Logantha S, Zaborska K, Gurney A, Heagarty A, et al. Obesity increases the propensity for atrial arrhythmias. Eur Heart J. 2017;38:637-.
165. Thaung HP, Baldi JC, Wang HY, Hughes G, Cook RF, Bussey CT, et al. Increased Efferent Cardiac Sympathetic Nerve Activity and Defective Intrinsic Heart Rate Regulation in Type 2 Diabetes. Diabetes. 2015;64(8):2944-56.
166. Cook RF, Bussey CT, Mellor KM, Cragg PA, Lamberts RR. beta1 -Adrenoceptor, but not beta2 -adrenoceptor, subtype regulates heart rate in type 2 diabetic rats in vivo. Exp Physiol. 2017;102(8):911-23.
167. Billman GE. Heart rate variability - a historical perspective. Front Physiol. 2011;2:86.
168. Monfredi O, Lyashkov AE, Johnsen AB, Inada S, Schneider H, Wang R, et al. Biophysical characterization of the underappreciated and important relationship between heart rate variability and heart rate. Hypertension. 2014;64(6):1334-43.
169. Black N, D'Souza A, Wang Y, Piggins H, Dobrzynski H, Morris G, et al. Circadian rhythm of cardiac electrophysiology, arrhythmogenesis, and the underlying mechanisms. Heart Rhythm. 2019;16(2):298-307.
170. Wang Y, D'Souza A, Johnsen A, Olieslagers S, Cox C, Bucchi A, et al. Circadian rhythm in heart rate is due to an intrinsic circadian clock in the sinus node. Eur Heart J. 2016;37:618-.
171. Schroeder EB, Chambless LE, Liao D, Prineas RJ, Evans GW, Rosamond WD, et al. Diabetes, glucose, insulin, and heart rate variability: the Atherosclerosis Risk in Communities (ARIC) study. Diabetes Care. 2005;28(3):668-74.
172. Stevens MJ, Raffel DM, Allman KC, Dayanikli F, Ficaro E, Sandford T, et al. Cardiac sympathetic dysinnervation in diabetes: implications for enhanced cardiovascular risk. Circulation. 1998;98(10):961-8.
173. Gusso S, Hofman P, Lalande S, Cutfield W, Robinson E, Baldi JC. Impaired stroke volume and aerobic capacity in female adolescents with type 1 and type 2 diabetes mellitus. Diabetologia. 2008;51(7):1317-20.
174. Pedersen TM, Boardman NT, Hafstad AD, Aasum E. Isolated perfused working hearts provide valuable additional information during phenotypic assessment of the diabetic mouse heart. PLoS One. 2018;13(10):e0204843.
175. Goncalves AC, Tank J, Diedrich A, Hilzendeger A, Plehm R, Bader M, et al. Diabetic hypertensive leptin receptor-deficient db/db mice develop cardioregulatory autonomic dysfunction. Hypertension. 2009;53(2):387-92.
176. Stuckey DJ, Carr CA, Tyler DJ, Aasum E, Clarke K. Novel MRI method to detect altered left ventricular ejection and filling patterns in rodent models of disease. Magn Reson Med. 2008;60(3):582-7.
177. Senador D, Kanakamedala K, Irigoyen MC, Morris M, Elased KM. Cardiovascular and autonomic phenotype of db/db diabetic mice. Exp Physiol. 2009;94(6):648-58.
178. Daniels A, van Bilsen M, Janssen BJ, Brouns AE, Cleutjens JP, Roemen TH, et al. Impaired cardiac functional reserve in type 2 diabetic db/db mice is associated with metabolic, but not structural, remodelling. Acta Physiol (Oxf). 2010;200(1):11-22.
179. Daniels A, Linz D, van Bilsen M, Rutten H, Sadowski T, Ruf S, et al. Long-term severe diabetes only leads to mild cardiac diastolic dysfunction in Zucker diabetic fatty rats. Eur J Heart Fail. 2012;14(2):193-201.
180. Fredersdorf S, Thumann C, Ulucan C, Griese DP, Luchner A, Riegger GA, et al. Myocardial hypertrophy and enhanced left ventricular contractility in Zucker diabetic fatty rats. Cardiovasc Pathol. 2004;13(1):11-9.
181. Baynes J, Murray DB. Cardiac and renal function are progressively impaired with aging in Zucker diabetic fatty type II diabetic rats. Oxid Med Cell Longev. 2009;2(5):328-34.

182. Bussey CT, de Leeuw AE, Lamberts RR. Increased haemodynamic adrenergic load with isoflurane anaesthesia in type 2 diabetic and obese rats in vivo. Cardiovasc Diabetol. 2014;13:161.
183. Hillis GS, Woodward M, Rodgers A, Chow CK, Li Q, Zoungas S, et al. Resting heart rate and the risk of death and cardiovascular complications in patients with type 2 diabetes mellitus. Diabetologia. 2012;55(5):1283-90.
184. Stettler C, Bearth A, Allemann S, Zwahlen M, Zanchin L, Deplazes M, et al. QTc interval and resting heart rate as long-term predictors of mortality in type 1 and type 2 diabetes mellitus: a 23-year follow-up. Diabetologia. 2007;50(1):186-94.
185. Valensi P, Attali JR, Sachs RN, Palsky D, Lanfranchi J, Sebaoun J. [Abnormalities of 24 hour (Holter) ECG monitoring in diabetics: involvement of cardiac autonomic neuropathy and/or insulin therapy]. Diabete Metab. 1985;11(6):337-42.
186. Ruwald MH, Zareba W, Jons C, Zhang C, Ruwald AC, Olshansky B, et al. Influence of diabetes mellitus on inappropriate and appropriate implantable cardioverter-defibrillator therapy and mortality in the Multicenter Automatic Defibrillator Implantation Trial-Reduce Inappropriate Therapy (MADIT-RIT) Trial. Circulation. 2013;128(7):694-701.
187. Carnethon MR, Yan L, Greenland P, Garside DB, Dyer AR, Metzger B, et al. Resting heart rate in middle age and diabetes development in older age. Diabetes Care. 2008;31(2):335-9.
188. Galderisi M, Anderson KM, Wilson PW, Levy D. Echocardiographic evidence for the existence of a distinct diabetic cardiomyopathy (the Framingham Heart Study). Am J Cardiol. 1991;68(1):85-9.
189. Borer JS, Tardif JC. Efficacy of ivabradine, a selective I(f) inhibitor, in patients with chronic stable angina pectoris and diabetes mellitus. Am J Cardiol. 2010;105(1):29-35.
190. Goit RK, Khadka R, Sharma SK, Limbu N, Paudel BH. Cardiovascular autonomic function and vibration perception threshold in type 2 diabetes mellitus. J Diabetes Complications. 2012;26(4):339-42.
191. Wang L, Cui L, Wang Y, Vaidya A, Chen S, Zhang C, et al. Resting heart rate and the risk of developing impaired fasting glucose and diabetes: the Kailuan prospective study. Int J Epidemiol. 2015;44(2):689-99.
192. Podlaha R, Falk A. The Prevalence of Diabetes-Mellitus and Other Risk-Factors of Atherosclerosis in Bradycardia Requiring Pacemaker Treatment. Horm Metab Res. 1992;26:84-7.
193. Ziegler D, Zentai CP, Perz S, Rathmann W, Haastert B, Doring A, et al. Prediction of mortality using measures of cardiac autonomic dysfunction in the diabetic and nondiabetic population: the MONICA/KORA Augsburg Cohort Study. Diabetes Care. 2008;31(3):556-61.
194. Bernardi L, Ricordi L, Lazzari P, Solda P, Calciati A, Ferrari MR, et al. Impaired Circadian Modulation of Sympathovagal Activity in Diabetes - a Possible Explanation for Altered Temporal Onset of Cardiovascular-Disease. Circulation. 1992;86(5):1443-52.
195. Spallone V, Bernardi L, Ricordi L, Solda P, Maiello MR, Calciati A, et al. Relationship between the Circadian-Rhythms of Blood-Pressure and Sympathovagal Balance in Diabetic Autonomic Neuropathy. Diabetes. 1993;42(12):1745-52.
196. Wang P, Chatham JC. Onset of diabetes in Zucker diabetic fatty (ZDF) rats leads to improved recovery of function after ischemia in the isolated perfused heart. Am J Physiol Endocrinol Metab. 2004;286(5):E725-36.
197. Howarth FC, Qureshi MA, Jayaprakash P, Parekh K, Oz M, Dobrzynski H, et al. The Pattern of mRNA Expression Is Changed in Sinoatrial Node from Goto-Kakizaki Type 2 Diabetic Rat Heart. J Diabetes Res. 2018;2018:8454078.
198. Panagia M, Schneider JE, Brown B, Cole MA, Clarke K. Abnormal function and glucose metabolism in the type-2 diabetic db/db mouse heart. Can J Physiol Pharmacol. 2007;85(3-4):289-94.
199. Phillips MS, Liu Q, Hammond HA, Dugan V, Hey PJ, Caskey CJ, et al. Leptin receptor missense mutation in the fatty Zucker rat. Nat Genet. 1996;13(1):18-9.
200. Griffen SC, Wang J, German MS. A genetic defect in beta-cell gene expression segregates independently from the fa locus in the ZDF rat. Diabetes. 2001;50(1):63-8.
201. Topp BG, Atkinson LL, Finegood DT. Dynamics of insulin sensitivity, -cell function, and -cell mass during the development of diabetes in fa/fa rats. Am J Physiol Endocrinol Metab. 2007;293(6):E1730-5.
202. Zucker LM, Zucker TF. Fatty - New Mutation in Rat. J Hered. 1961;52(6):275-&.

203. Pick A, Clark J, Kubstrup C, Levisetti M, Pugh W, Bonner-Weir S, et al. Role of apoptosis in failure of beta-cell mass compensation for insulin resistance and beta-cell defects in the male Zucker diabetic fatty rat. Diabetes. 1998;47(3):358-64.
204. Paulsen SJ, Vrang N, Larsen LK, Larsen PJ, Jelsing J. Stereological assessment of pancreatic beta-cell mass development in male Zucker Diabetic Fatty (ZDF) rats: correlation with pancreatic beta-cell function. J Anat. 2010;217(5):624-30.
205. Corsetti JP, Sparks JD, Peterson RG, Smith RL, Sparks CE. Effect of dietary fat on the development of non-insulin dependent diabetes mellitus in obese Zucker diabetic fatty male and female rats. Atherosclerosis. 2000;148(2):231-41.
206. Bussey CT, Lamberts RR. Effect of type 2 diabetes, surgical incision, and volatile anesthesia on hemodynamics in the rat. Physiol Rep. 2017;5(14).
207. Daniels LJ, Wallace RS, Nicholson OM, Wilson GA, McDonald FJ, Jones PP, et al. Inhibition of calcium/calmodulin-dependent kinase II restores contraction and relaxation in isolated cardiac muscle from type 2 diabetic rats. Cardiovasc Diabetol. 2018;17(1):89.
208. Hevener A, Reichart D, Janez A, Olefsky J. Female rats do not exhibit free fatty acid-induced insulin resistance. Diabetes. 2002;51(6):1907-12.
209. Janssen SW, Martens GJ, Sweep CG, Ross HA, Hermus AR. In Zucker diabetic fatty rats plasma leptin levels are correlated with plasma insulin levels rather than with body weight. Horm Metab Res. 1999;31(11):610-5.
210. Krebs HA, Henseleit K. Analysis concerning urea formation in animal bodies. H-S Z Physiol Chem. 1932;210:33-66.
211. Sutherland FJ, Hearse DJ. The isolated blood and perfusion fluid perfused heart. Pharmacol Res. 2000;41(6):613-27.
212. Ng FS, Shadi IT, Peters NS, Lyon AR. Selective heart rate reduction with ivabradine slows ischaemia-induced electrophysiological changes and reduces ischaemia-reperfusion-induced ventricular arrhythmias. J Mol Cell Cardiol. 2013;59:67-75.
213. Lauzier B, Vaillant F, Gelinas R, Bouchard B, Brownsey R, Thorin E, et al. Ivabradine reduces heart rate while preserving metabolic fluxes and energy status of healthy normoxic working hearts. American journal of physiology Heart and circulatory physiology. 2011;300(3):H845-52.
214. Yaniv Y, Maltsev VA, Ziman BD, Spurgeon HA, Lakatta EG. The "funny" current (I(f)) inhibition by ivabradine at membrane potentials encompassing spontaneous depolarization in pacemaker cells. Molecules. 2012;17(7):8241-54.
215. Su N, Narayanan N. Enhanced chronotropic and inotropic responses of rat myocardium to cholinergic stimulus with aging. Can J Physiol Pharmacol. 1992;70(12):1618-24.
216. Martinussen HJ, Waldenstrom A, Ronquist G. Carbachol-induced increase in inositol trisphosphate (IP3) content is attenuated by adrenergic stimulation in the isolated working rat heart. Acta Physiol Scand. 1995;153(2):151-8.
217. Krishnaswamy PS, Egom EE, Moghtadaei M, Jansen HJ, Azer J, Bogachev O, et al. Altered parasympathetic nervous system regulation of the sinoatrial node in Akita diabetic mice. J Mol Cell Cardiol. 2015;82:125-35.
218. Konrad D, Vicenzi-Moser R, Vicenzi M, Aldenhoff U, Schwarzl E, Toller W. Combined effects of ivabradine with dobutamine or levosimendan in isolated perfused hearts. Critical Care. 2013;17(2):P228.
219. Ceconi C, Cargnoni A, Francolini G, Parinello G, Ferrari R. Heart rate reduction with ivabradine improves energy metabolism and mechanical function of isolated ischaemic rabbit heart. Cardiovasc Res. 2009;84(1):72-82.
220. Hendrikx M, Toshima Y, Mubagwa K, Flameng W. Muscarinic receptor stimulation by carbachol improves functional recovery in isolated, blood perfused rabbit heart. Cardiovasc Res. 1993;27(6):980-9.
221. Jonkman J, Brown CM. Any Way You Slice It-A Comparison of Confocal Microscopy Techniques. J Biomol Tech. 2015;26(2):54-65.
222. Foldes-Papp Z, Demel U, Tilz GP. Laser scanning confocal fluorescence microscopy: an overview. Int Immunopharmacol. 2003;3(13-14):1715-29.

223. Ridler T, Calvard S. Picture thresholding using an iterative selection method. IEEE trans syst Man Cybern. 1978;8(8):630-2.
224. Laemmli UK. Cleavage of structural proteins during the assembly of the head of bacteriophage T4. Nature. 1970;227(5259):680-5.
225. Motulsky HJ, Brown RE. Detecting outliers when fitting data with nonlinear regression - a new method based on robust nonlinear regression and the false discovery rate. BMC Bioinformatics. 2006;7:123.
226. Erickson JR, Pereira L, Wang L, Han G, Ferguson A, Dao K, et al. Diabetic hyperglycaemia activates CaMKII and arrhythmias by O-linked glycosylation. Nature. 2013;502(7471):372-6.
227. Clark RJ, McDonough PM, Swanson E, Trost SU, Suzuki M, Fukuda M, et al. Diabetes and the accompanying hyperglycemia impairs cardiomyocyte calcium cycling through increased nuclear O-GlcNAcylation. J Biol Chem. 2003;278(45):44230-7.
228. Nishii K, Kumai M, Egashira K, Miwa T, Hashizume K, Miyano Y, et al. Mice lacking connexin45 conditionally in cardiac myocytes display embryonic lethality similar to that of germline knockout mice without endocardial cushion defect. Cell Commun Adhes. 2003;10(4-6):365-9.
229. Lo CW. Role of gap junctions in cardiac conduction and development: insights from the connexin knockout mice. Circ Res. 2000;87(5):346-8.
230. Erickson JR, He BJ, Grumbach IM, Anderson ME. CaMKII in the cardiovascular system: sensing redox states. Physiol Rev. 2011;91(3):889-915.
231. Daniels L, Bell JR, Delbridge LM, McDonald FJ, Lamberts RR, Erickson JR. The role of CaMKII in diabetic heart dysfunction. Heart Fail Rev. 2015;20(5):589-600.
232. Swaminathan PD, Purohit A, Soni S, Voigt N, Singh MV, Glukhov AV, et al. Oxidized CaMKII causes cardiac sinus node dysfunction in mice. J Clin Invest. 2011;121(8):3277-88.
233. Luo M, Guan X, Luczak ED, Lang D, Kutschke W, Gao Z, et al. Diabetes increases mortality after myocardial infarction by oxidizing CaMKII. J Clin Invest. 2013;123(3):1262-74.
234. Zhang Y, Wang Y, Yanni J, Cai X, Qureshi M, Gardiner N, et al. 118Dysfunction of the pacemaker of the heart in the rat model of streptozotocin-induced type I diabetes mellitus. EP Europace. 2017;19(suppl_3):iii12-iii.
235. Huang X, Zhong N, Zhang H, Ma A, Yuan Z, Guo N. Reduced expression of HCN channels in the sinoatrial node of streptozotocin-induced diabetic rats. Can J Physiol Pharmacol. 2017;95(5):586-94.
236. Ferdous Z, Qureshi MA, Jayaprakash P, Parekh K, John A, Oz M, et al. Different Profile of mRNA Expression in Sinoatrial Node from Streptozotocin-Induced Diabetic Rat. PLoS One. 2016;11(4):e0153934.
237. D'Souza A, Bucchi A, Johnsen AB, Logantha SJ, Monfredi O, Yanni J, et al. Exercise training reduces resting heart rate via downregulation of the funny channel HCN4. Nat Commun. 2014;5:3775.
238. Yeh YH, Burstein B, Qi XY, Sakabe M, Chartier D, Comtois P, et al. Funny current downregulation and sinus node dysfunction associated with atrial tachyarrhythmia: a molecular basis for tachycardia-bradycardia syndrome. Circulation. 2009;119(12):1576-85.
239. Zicha S, Fernandez-Velasco M, Lonardo G, L'Heureux N, Nattel S. Sinus node dysfunction and hyperpolarization-activated (HCN) channel subunit remodeling in a canine heart failure model. Cardiovasc Res. 2005;66(3):472-81.
240. He W, Zhang J, Gan T, Xu G, Tang B. Expression of hyperpolarization-activated cyclic nucleotide-gated channel isoforms in a canine model of atrial fibrillation. Exp Ther Med. 2016;12(1):433-6.
241. Zhang Y, Wang Y, Yanni J, Qureshi MA, Logantha S, Kassab S, et al. Electrical Conduction System Remodeling in Streptozotocin-Induced Diabetes Mellitus Rat Heart. Front Physiol. 2019;10:826.
242. Flesch M, Schwinger RH, Schiffer F, Frank K, Sudkamp M, Kuhn-Regnier F, et al. Evidence for functional relevance of an enhanced expression of the Na(+)-Ca2+ exchanger in failing human myocardium. Circulation. 1996;94(5):992-1002.
243. Studer R, Reinecke H, Bilger J, Eschenhagen T, Bohm M, Hasenfuss G, et al. Gene expression of the cardiac Na(+)-Ca2+ exchanger in end-stage human heart failure. Circ Res. 1994;75(3):443-53.
244. Schwinger RH, Wang J, Frank K, Muller-Ehmsen J, Brixius K, McDonough AA, et al. Reduced sodium pump alpha1, alpha3, and beta1-isoform protein levels and Na+,K+-ATPase activity but unchanged Na+-Ca2+ exchanger protein levels in human heart failure. Circulation. 1999;99(16):2105-12.

245. Piper C, Bilger J, Henrichs EM, Schultheiss HP, Horstkotte D, Doerner A. Is myocardial Na+/Ca2+ exchanger transcription a marker for different stages of myocardial dysfunction? Quantitative polymerase chain reaction of the messenger RNA in endomyocardial biopsies of patients with heart failure. Journal of the American College of Cardiology. 2000;36(1):233-41.
246. Choi KM, Zhong Y, Hoit BD, Grupp IL, Hahn H, Dilly KW, et al. Defective intracellular Ca(2+) signaling contributes to cardiomyopathy in Type 1 diabetic rats. American journal of physiology Heart and circulatory physiology. 2002;283(4):H1398-408.
247. Hattori Y, Matsuda N, Kimura J, Ishitani T, Tamada A, Gando S, et al. Diminished function and expression of the cardiac Na+-Ca2+ exchanger in diabetic rats: implication in Ca2+ overload. J Physiol. 2000;527 Pt 1:85-94.
248. Hong TT, Smyth JW, Chu KY, Vogan JM, Fong TS, Jensen BC, et al. BIN1 is reduced and Cav1.2 trafficking is impaired in human failing cardiomyocytes. Heart Rhythm. 2012;9(5):812-20.
249. Schroder F, Handrock R, Beuckelmann DJ, Hirt S, Hullin R, Priebe L, et al. Increased availability and open probability of single L-type calcium channels from failing compared with nonfailing human ventricle. Circulation. 1998;98(10):969-76.
250. Koyama T, Ono K, Watanabe H, Ohba T, Murakami M, Iino K, et al. Molecular and electrical remodeling of L- and T-type Ca(2+) channels in rat right atrium with monocrotaline-induced pulmonary hypertension. Circ J. 2009;73(2):256-63.
251. Takebayashi S, Li Y, Kaku T, Inagaki S, Hashimoto Y, Kimura K, et al. Remodeling excitation-contraction coupling of hypertrophied ventricular myocytes is dependent on T-type calcium channels expression. Biochem Biophys Res Commun. 2006;345(2):766-73.
252. Hasenfuss G, Reinecke H, Studer R, Meyer M, Pieske B, Holtz J, et al. Relation between myocardial function and expression of sarcoplasmic reticulum Ca(2+)-ATPase in failing and nonfailing human myocardium. Circ Res. 1994;75(3):434-42.
253. Schwinger RH, Bohm M, Schmidt U, Karczewski P, Bavendiek U, Flesch M, et al. Unchanged protein levels of SERCA II and phospholamban but reduced Ca2+ uptake and Ca(2+)-ATPase activity of cardiac sarcoplasmic reticulum from dilated cardiomyopathy patients compared with patients with nonfailing hearts. Circulation. 1995;92(11):3220-8.
254. Lyon AR, Nikolaev VO, Miragoli M, Sikkel MB, Paur H, Benard L, et al. Plasticity of surface structures and beta(2)-adrenergic receptor localization in failing ventricular cardiomyocytes during recovery from heart failure. Circ Heart Fail. 2012;5(3):357-65.
255. Meyer M, Schillinger W, Pieske B, Holubarsch C, Heilmann C, Posival H, et al. Alterations of sarcoplasmic reticulum proteins in failing human dilated cardiomyopathy. Circulation. 1995;92(4):778-84.
256. Zhong Y, Ahmed S, Grupp IL, Matlib MA. Altered SR protein expression associated with contractile dysfunction in diabetic rat hearts. Am J Physiol-Heart C. 2001;281(3):H1137-H47.
257. Vasanji Z, Dhalla NS, Netticadan T. Increased inhibition of SERCA2 by phospholamban in the type I diabetic heart. Mol Cell Biochem. 2004;261(1-2):245-9.
258. Yamada KA, Rogers JG, Sundset R, Steinberg TH, Saffitz J. Up-regulation of connexin45 in heart failure. J Cardiovasc Electrophysiol. 2003;14(11):1205-12.
259. Dupont E, Matsushita T, Kaba RA, Vozzi C, Coppen SR, Khan N, et al. Altered connexin expression in human congestive heart failure. J Mol Cell Cardiol. 2001;33(2):359-71.
260. Howarth FC, Nowotny N, Zilahi E, El Haj MA, Lei M. Altered expression of gap junction connexin proteins may partly underlie heart rhythm disturbances in the streptozotocin-induced diabetic rat heart. Mol Cell Biochem. 2007;305(1-2):145-51.
261. Richardson MD, Kilts JD, Kwatra MM. Increased expression of Gi-coupled muscarinic acetylcholine receptor and Gi in atrium of elderly diabetic subjects. Diabetes. 2004;53(9):2392-6.
262. Lee LM, Chang CK, Cheng KC, Kou DH, Liu IM, Cheng JT. Increase of cardiac M2-muscarinic receptor gene expression in type-1 but not in type-2 diabetic rats. Neurosci Lett. 2008;441(2):201-4.
263. Mar GY, Ku PM, Chen LJ, Cheng KC, Li YX, Cheng JT. Increase in cardiac M2-muscarinic receptor expression is regulated by GATA binding protein 4 (GATA-4) in streptozotocin-induced diabetic rats. Int J Cardiol. 2013;167(2):436-41.
264. Livolsi A, Niederhoffer N, Dali-Youcef N, Rambaud C, Olexa C, Mokni W, et al. Cardiac muscarinic receptor overexpression in sudden infant death syndrome. PLoS One. 2010;5(3):e9464.

265. Bohm M, Gierschik P, Jakobs KH, Pieske B, Schnabel P, Ungerer M, et al. Increase of Gi alpha in human hearts with dilated but not ischemic cardiomyopathy. Circulation. 1990;82(4):1249-65.
266. Li N, Csepe TA, Hansen BJ, Dobrzynski H, Higgins RS, Kilic A, et al. Molecular Mapping of Sinoatrial Node HCN Channel Expression in the Human Heart. Circ Arrhythm Electrophysiol. 2015;8(5):1219-27.
267. Boyett MR, Inada S, Yoo S, Li J, Liu J, Tellez J, et al. Connexins in the sinoatrial and atrioventricular nodes. Adv Cardiol. 2006;42:175-97.
268. Koss KL, Grupp IL, Kranias EG. The relative phospholamban and SERCA2 ratio: a critical determinant of myocardial contractility. Basic Res Cardiol. 1997;92 Suppl 1:17-24.
269. Meyer M, Bluhm WF, He H, Post SR, Giordano FJ, Lew WY, et al. Phospholamban-to-SERCA2 ratio controls the force-frequency relationship. Am J Physiol. 1999;276(3):H779-85.
270. Li Y, Sirenko S, Riordon DR, Yang D, Spurgeon H, Lakatta EG, et al. CaMKII-dependent phosphorylation regulates basal cardiac pacemaker function via modulation of local Ca2+ releases. Am J Physiol Heart Circ Physiol. 2016;311(3):H532-44.
271. DiFrancesco D. The role of the funny current in pacemaker activity. Circ Res. 2010;106(3):434-46.
272. Stieber J, Herrmann S, Feil S, Loster J, Feil R, Biel M, et al. The hyperpolarization-activated channel HCN4 is required for the generation of pacemaker action potentials in the embryonic heart. Proc Natl Acad Sci U S A. 2003;100(25):15235-40.
273. Bucchi A, Barbuti A, Difrancesco D, Baruscotti M. Funny Current and Cardiac Rhythm: Insights from HCN Knockout and Transgenic Mouse Models. Front Physiol. 2012;3:240.
274. Kozasa Y, Nakashima N, Ito M, Ishikawa T, Kimoto H, Ushijima K, et al. HCN4 pacemaker channels attenuate the parasympathetic response and stabilize the spontaneous firing of the sinoatrial node. J Physiol. 2018;596(5):809-25.
275. Hoesl E, Stieber J, Herrmann S, Feil S, Tybl E, Hofmann F, et al. Tamoxifen-inducible gene deletion in the cardiac conduction system. J Mol Cell Cardiol. 2008;45(1):62-9.
276. Herrmann S, Stieber J, Stockl G, Hofmann F, Ludwig A. HCN4 provides a 'depolarization reserve' and is not required for heart rate acceleration in mice. EMBO J. 2007;26(21):4423-32.
277. Baruscotti M, Bucchi A, Viscomi C, Mandelli G, Consalez G, Gnecchi-Rusconi T, et al. Deep bradycardia and heart block caused by inducible cardiac-specific knockout of the pacemaker channel gene Hcn4. Proc Natl Acad Sci U S A. 2011;108(4):1705-10.
278. Mesirca P, Alig J, Torrente AG, Muller JC, Marger L, Rollin A, et al. Cardiac arrhythmia induced by genetic silencing of 'funny' (f) channels is rescued by GIRK4 inactivation. Nat Commun. 2014;5:4664.
279. Sanders L, Rakovic S, Lowe M, Mattick PA, Terrar DA. Fundamental importance of Na+-Ca2+ exchange for the pacemaking mechanism in guinea-pig sino-atrial node. J Physiol. 2006;571(Pt 3):639-49.
280. Lytton J. Na+/Ca2+ exchangers: three mammalian gene families control Ca2+ transport. Biochem J. 2007;406(3):365-82.
281. Reuter H, Pott C, Goldhaber JI, Henderson SA, Philipson KD, Schwinger RH. Na(+)--Ca2+ exchange in the regulation of cardiac excitation-contraction coupling. Cardiovasc Res. 2005;67(2):198-207.
282. Armoundas AA, Hobai IA, Tomaselli GF, Winslow RL, O'Rourke B. Role of sodium-calcium exchanger in modulating the action potential of ventricular myocytes from normal and failing hearts. Circ Res. 2003;93(1):46-53.
283. Sham JS, Cleemann L, Morad M. Functional coupling of Ca2+ channels and ryanodine receptors in cardiac myocytes. Proc Natl Acad Sci U S A. 1995;92(1):121-5.
284. Koushik SV, Wang J, Rogers R, Moskophidis D, Lambert NA, Creazzo TL, et al. Targeted inactivation of the sodium-calcium exchanger (Ncx1) results in the lack of a heartbeat and abnormal myofibrillar organization. FASEB J. 2001;15(7):1209-11.
285. Cho CH, Kim SS, Jeong MJ, Lee CO, Shin HS. The Na+ -Ca2+ exchanger is essential for embryonic heart development in mice. Mol Cells. 2000;10(6):712-22.
286. Wakimoto K, Kobayashi K, Kuro OM, Yao A, Iwamoto T, Yanaka N, et al. Targeted disruption of Na+/Ca2+ exchanger gene leads to cardiomyocyte apoptosis and defects in heartbeat. J Biol Chem. 2000;275(47):36991-8.

287. Kaese S, Bogeholz N, Pauls P, Dechering D, Olligs J, Kolker K, et al. Increased sodium/calcium exchanger activity enhances beta-adrenergic-mediated increase in heart rate: Whole-heart study in a homozygous sodium/calcium exchanger overexpressor mouse model. Heart Rhythm. 2017;14(8):1247-53.
288. Pott C, Muszynski A, Ruhe M, Bogeholz N, Schulte JS, Milberg P, et al. Proarrhythmia in a non-failing murine model of cardiac-specific Na+/Ca 2+ exchanger overexpression: whole heart and cellular mechanisms. Basic Res Cardiol. 2012;107(2):247.
289. Groenke S, Larson ED, Alber S, Zhang R, Lamp ST, Ren X, et al. Complete atrial-specific knockout of sodium-calcium exchange eliminates sinoatrial node pacemaker activity. PLoS One. 2013;8(11):e81633.
290. Herrmann S, Lipp P, Wiesen K, Stieber J, Nguyen H, Kaiser E, et al. The cardiac sodiumcalcium exchanger NCX1 is a key player in the initiation and maintenance of a stable heart rhythm. Cardiovascular Research. 2013;99(4):780-8.
291. Torrente AG, Zhang R, Zaini A, Giani JF, Kang J, Lamp ST, et al. Burst pacemaker activity of the sinoatrial node in sodium-calcium exchanger knockout mice. Proc Natl Acad Sci U S A. 2015;112(31):9769-74.
292. Reuter H, Han T, Motter C, Philipson KD, Goldhaber JI. Mice overexpressing the cardiac sodium-calcium exchanger: defects in excitation-contraction coupling. J Physiol. 2004;554(Pt 3):779-89.
293. Ahmmed GU, Dong PH, Song G, Ball NA, Xu Y, Walsh RA, et al. Changes in Ca(2+) cycling proteins underlie cardiac action potential prolongation in a pressure-overloaded guinea pig model with cardiac hypertrophy and failure. Circ Res. 2000;86(5):558-70.
294. Diaz ME, Graham HK, O'Neill S C, Trafford AW, Eisner DA. The control of sarcoplasmic reticulum Ca content in cardiac muscle. Cell Calcium. 2005;38(3-4):391-6.
295. Curran J, Hinton MJ, Rios E, Bers DM, Shannon TR. Beta-adrenergic enhancement of sarcoplasmic reticulum calcium leak in cardiac myocytes is mediated by calcium/calmodulin-dependent protein kinase. Circ Res. 2007;100(3):391-8.
296. Bers DM. Cardiac Na/Ca exchange function in rabbit, mouse and man: what's the difference? J Mol Cell Cardiol. 2002;34(4):369-73.
297. Zhao XY, Hu SJ, Li J, Mou Y, Chen BP, Xia Q. Decreased cardiac sarcoplasmic reticulum Ca2+ -ATPase activity contributes to cardiac dysfunction in streptozotocin-induced diabetic rats. J Physiol Biochem. 2006;62(1):1-8.
298. Munch G, Bolck B, Hoischen S, Brixius K, Bloch W, Reuter H, et al. Unchanged protein expression of sarcoplasmic reticulum Ca2+-ATPase, phospholamban, and calsequestrin in terminally failing human myocardium. J Mol Med (Berl). 1998;76(6):434-41.
299. Wang HS, Arvanitis DA, Dong M, Niklewski PJ, Zhao W, Lam CK, et al. SERCA2a superinhibition by human phospholamban triggers electrical and structural remodeling in mouse hearts. Physiol Genomics. 2011;43(7):357-64.
300. Wang W, Zhu W, Wang S, Yang D, Crow MT, Xiao RP, et al. Sustained beta1-adrenergic stimulation modulates cardiac contractility by Ca2+/calmodulin kinase signaling pathway. Circ Res. 2004;95(8):798-806.
301. Gavioli M, Lara A, Almeida PW, Lima AM, Damasceno DD, Rocha-Resende C, et al. Cholinergic signaling exerts protective effects in models of sympathetic hyperactivity-induced cardiac dysfunction. PLoS One. 2014;9(7):e100179.
302. Livolsi A, Niederhoffer N, Dali-Youcef N, Mokni W, Olexa-Zorn C, Gies JP, et al. Constitutive overexpression of muscarinic receptors leads to vagal hyperreactivity. PLoS One. 2010;5(12):e15618.
303. Ganguly PK, Dhalla KS, Innes IR, Beamish RE, Dhalla NS. Altered norepinephrine turnover and metabolism in diabetic cardiomyopathy. Circ Res. 1986;59(6):684-93.
304. Hoffman RP, Sinkey CA, Anderson EA. Muscle sympathetic nerve activity is higher in intensively versus conventionally treated IDDM subjects. Diabetes Care. 1995;18(3):287-91.
305. Huggett RJ, Scott EM, Gilbey SG, Stoker JB, Mackintosh AF, Mary DA. Impact of type 2 diabetes mellitus on sympathetic neural mechanisms in hypertension. Circulation. 2003;108(25):3097-101.
306. Manzella D, Paolisso G. Cardiac autonomic activity and Type II diabetes mellitus. Clin Sci (Lond). 2005;108(2):93-9.

307. Santulli G, Iaccarino G. Adrenergic signaling in heart failure and cardiovascular aging. Maturitas. 2016;93:65-72.
308. Pfeifer MA, Cook D, Brodsky J, Tice D, Reenan A, Swedine S, et al. Quantitative evaluation of cardiac parasympathetic activity in normal and diabetic man. Diabetes. 1982;31(4 Pt 1):339-45.
309. Akiyama N, Okumura K, Watanabe Y, Hashimoto H, Ito T, Ogawa K, et al. Altered acetylcholine and norepinephrine concentrations in diabetic rat hearts. Role of parasympathetic nervous system in diabetic cardiomyopathy. Diabetes. 1989;38(2):231-6.
310. Dall'ago P, D'Agord Schaan B, da Silva VO, Werner J, da Silva Soares PP, de Angelis K, et al. Parasympathetic dysfunction is associated with baroreflex and chemoreflex impairment in streptozotocin-induced diabetes in rats. Auton Neurosci. 2007;131(1-2):28-35.
311. Maier LS, Bers DM. Calcium, calmodulin, and calcium-calmodulin kinase II: heartbeat to heartbeat and beyond. J Mol Cell Cardiol. 2002;34(8):919-39.
312. Couchonnal LF, Anderson ME. The role of calmodulin kinase II in myocardial physiology and disease. Physiology (Bethesda). 2008;23:151-9.
313. Maier LS, Zhang T, Chen L, DeSantiago J, Brown JH, Bers DM. Transgenic CaMKIIdeltaC overexpression uniquely alters cardiac myocyte Ca2+ handling: reduced SR Ca2+ load and activated SR Ca2+ release. Circ Res. 2003;92(8):904-11.
314. Lai Y, Nairn AC, Gorelick F, Greengard P. Ca2+/calmodulin-dependent protein kinase II: identification of autophosphorylation sites responsible for generation of Ca2+/calmodulin-independence. Proc Natl Acad Sci U S A. 1987;84(16):5710-4.
315. Matalon O, Horovitz A, Levy ED. Different subunits belonging to the same protein complex often exhibit discordant expression levels and evolutionary properties. Curr Opin Struct Biol. 2014;26:113-20.
316. Periasamy M, Bhupathy P, Babu GJ. Regulation of sarcoplasmic reticulum Ca2+ ATPase pump expression and its relevance to cardiac muscle physiology and pathology. Cardiovasc Res. 2008;77(2):265-73.
317. Logantha SJ, Stokke MK, Atkinson AJ, Kharche SR, Parveen S, Saeed Y, et al. Ca(2+)-Clock-Dependent Pacemaking in the Sinus Node Is Impaired in Mice with a Cardiac Specific Reduction in SERCA2 Abundance. Front Physiol. 2016;7:197.
318. Bassani RA, Mattiazzi A, Bers DM. CaMKII is responsible for activity-dependent acceleration of relaxation in rat ventricular myocytes. Am J Physiol. 1995;268(2 Pt 2):H703-12.
319. Schouten VJ. Interval dependence of force and twitch duration in rat heart explained by Ca2+ pump inactivation in sarcoplasmic reticulum. J Physiol. 1990;431:427-44.
320. Kong H, Jones PP, Koop A, Zhang L, Duff HJ, Chen SR. Caffeine induces Ca2+ release by reducing the threshold for luminal Ca2+ activation of the ryanodine receptor. Biochem J. 2008;414(3):441-52.
321. Roy A, Fields WC, Rocha-Resende C, Resende RR, Guatimosim S, Prado VF, et al. Cardiomyocyte-secreted acetylcholine is required for maintenance of homeostasis in the heart. FASEB J. 2013;27(12):5072-82.
322. Roy A, Dakroub M, Tezini GC, Liu Y, Guatimosim S, Feng Q, et al. Cardiac acetylcholine inhibits ventricular remodeling and dysfunction under pathologic conditions. FASEB J. 2016;30(2):688-701.
323. Speranza L, Franceschelli S, Riccioni G. The biological effects of ivabradine in cardiovascular disease. Molecules. 2012;17(5):4924-35.
324. Thollon C, Bedut S, Villeneuve N, Coge F, Piffard L, Guillaumin JP, et al. Use-dependent inhibition of hHCN4 by ivabradine and relationship with reduction in pacemaker activity. Br J Pharmacol. 2007;150(1):37-46.
325. Bois P, Bescond J, Renaudon B, Lenfant J. Mode of action of bradycardic agent, S 16257, on ionic currents of rabbit sinoatrial node cells. Br J Pharmacol. 1996;118(4):1051-7.
326. Bucchi A, Baruscotti M, DiFrancesco D. Current-dependent block of rabbit sino-atrial node I(f) channels by ivabradine. J Gen Physiol. 2002;120(1):1-13.
327. DiFrancesco D, Camm JA. Heart rate lowering by specific and selective I(f) current inhibition with ivabradine: a new therapeutic perspective in cardiovascular disease. Drugs. 2004;64(16):1757-65.
328. Bers DM, Lederer WJ, Berlin JR. Intracellular Ca transients in rat cardiac myocytes: role of Na-Ca exchange in excitation-contraction coupling. Am J Physiol. 1990;258(5 Pt 1):C944-54.

329. Bassani JW, Yuan W, Bers DM. Fractional SR Ca release is regulated by trigger Ca and SR Ca content in cardiac myocytes. Am J Physiol. 1995;268(5 Pt 1):C1313-9.
330. Stieber J, Wieland K, Stockl G, Ludwig A, Hofmann F. Bradycardic and proarrhythmic properties of sinus node inhibitors. Mol Pharmacol. 2006;69(4):1328-37.
331. Huang X, Yang P, Yang Z, Zhang H, Ma A. Age-associated expression of HCN channel isoforms in rat sinoatrial node. Exp Biol Med (Maywood). 2016;241(3):331-9.
332. Bucchi A, Baruscotti M, Nardini M, Barbuti A, Micheloni S, Bolognesi M, et al. Identification of the molecular site of ivabradine binding to HCN4 channels. PLoS One. 2013;8(1):e53132.
333. Tanguay J, Callahan KM, D'Avanzo N. Characterization of drug binding within the HCN1 channel pore. Sci Rep. 2019;9(1):465.
334. Seifen E, Schaer H, Marshall JM. Effect of Calcium on the Membrane Potentials of Single Pacemaker Fibres and Atrial Fibres in Isolated Rabbits Atria. Nature. 1964;202:1223-4.
335. Gonzalez MD, Vassalle M. Role of Oscillatory Potential and Pacemaker Shifts in Digitalis Intoxication of the Sinoatrial Node. Circulation. 1993;87(5):1705-14.
336. Refsum H. Calcium-antagonistic and anti-arrhythmic effects of nifedipine on the isolated rat atrium. Acta Pharmacol Toxicol (Copenh). 1975;37(5):377-86.
337. Hartley EJ, McNeill JH. The effect of calcium oncardiac phosphorylase activation, contractile force and cyclic AMP in euthyroid and hyperthyroid rat hearts. Can J Physiol Pharmacol. 1976;54(4):590-5.
338. Noma A, Irisawa H. Effects of calcium ion on the rising phase of the action potential in rabbit sinoatrial node cells. Jpn J Physiol. 1976;26(1):93-9.
339. Toda N. Electrophysiological effects of potassium and calcium ions in the sino-atrial node in response to sympathetic nerve stimulation. Pflugers Arch. 1969;310(1):45-63.
340. Toda N, West TC. Interaction between Na, Ca, Mg, and vagal stimulation in the S-A node of the rabbit. Am J Physiol. 1967;212(2):424-30.
341. Hagiwara N, Irisawa H. Modulation by intracellular Ca2+ of the hyperpolarization-activated inward current in rabbit single sino-atrial node cells. J Physiol. 1989;409:121-41.
342. Pinnell J, Turner S, Howell S. Cardiac muscle physiology. BJA Education. 2007;7(3):85-8.
343. Tohse N. Calcium-sensitive delayed rectifier potassium current in guinea pig ventricular cells. Am J Physiol. 1990;258(4 Pt 2):H1200-7.
344. Kass RS, Tsien RW. Control of action potential duration by calcium ions in cardiac Purkinje fibers. J Gen Physiol. 1976;67(5):599-617.
345. Lee CO, Vassalle M. Modulation of intracellular Na+ activity and cardiac force by norepinephrine and Ca2+. Am J Physiol. 1983;244(1):C110-4.
346. Ellis D. The effects of external cations and ouabain on the intracellular sodium activity of sheep heart Purkinje fibres. J Physiol. 1977;273(1):211-40.
347. Dzhura I, Wu Y, Colbran RJ, Balser JR, Anderson ME. Calmodulin kinase determines calcium-dependent facilitation of L-type calcium channels. Nat Cell Biol. 2000;2(3):173-7.
348. Kohlhaas M, Zhang T, Seidler T, Zibrova D, Dybkova N, Steen A, et al. Increased sarcoplasmic reticulum calcium leak but unaltered contractility by acute CaMKII overexpression in isolated rabbit cardiac myocytes. Circ Res. 2006;98(2):235-44.
349. Eisner DA, Caldwell JL, Kistamas K, Trafford AW. Calcium and Excitation-Contraction Coupling in the Heart. Circ Res. 2017;121(2):181-95.
350. Winslow RL, Walker MA, Greenstein JL. Modeling calcium regulation of contraction, energetics, signaling, and transcription in the cardiac myocyte. Wiley Interdiscip Rev Syst Biol Med. 2016;8(1):37-67.
351. Terracciano CM, Philipson KD, MacLeod KT. Overexpression of the Na(+)/Ca(2+) exchanger and inhibition of the sarcoplasmic reticulum Ca(2+)-ATPase in ventricular myocytes from transgenic mice. Cardiovasc Res. 2001;49(1):38-47.
352. Trafford AW, Diaz ME, Eisner DA. Coordinated control of cell Ca(2+) loading and triggered release from the sarcoplasmic reticulum underlies the rapid inotropic response to increased L-type Ca(2+) current. Circ Res. 2001;88(2):195-201.

353. Sirenko S, Yang D, Li Y, Lyashkov AE, Lukyanenko YO, Lakatta EG, et al. Ca(2)(+)-dependent phosphorylation of Ca(2)(+) cycling proteins generates robust rhythmic local Ca(2)(+) releases in cardiac pacemaker cells. Sci Signal. 2013;6(260):ra6.
354. Andersson KB, Birkeland JA, Finsen AV, Louch WE, Sjaastad I, Wang Y, et al. Moderate heart dysfunction in mice with inducible cardiomyocyte-specific excision of the Serca2 gene. J Mol Cell Cardiol. 2009;47(2):180-7.
355. Ji Y, Lalli MJ, Babu GJ, Xu Y, Kirkpatrick DL, Liu LH, et al. Disruption of a single copy of the SERCA2 gene results in altered Ca2+ homeostasis and cardiomyocyte function. J Biol Chem. 2000;275(48):38073-80.
356. Bassani JW, Bassani RA, Bers DM. Twitch-dependent SR Ca accumulation and release in rabbit ventricular myocytes. Am J Physiol. 1993;265(2 Pt 1):C533-40.
357. Bode EF, Briston SJ, Overend CL, O'Neill SC, Trafford AW, Eisner DA. Changes of SERCA activity have only modest effects on sarcoplasmic reticulum Ca2+ content in rat ventricular myocytes. J Physiol. 2011;589(Pt 19):4723-9.
358. Hobai IA, Maack C, O'Rourke B. Partial inhibition of sodium/calcium exchange restores cellular calcium handling in canine heart failure. Circ Res. 2004;95(3):292-9.
359. Lomax AE, Rose RA, Giles WR. Electrophysiological evidence for a gradient of G protein-gated K+ current in adult mouse atria. Br J Pharmacol. 2003;140(3):576-84.
360. Kuhar MJ, Murrin LC. Sodium-dependent, high affinity choline uptake. J Neurochem. 1978;30(1):15-21.
361. Csepe TA, Kalyanasundaram A, Hansen BJ, Zhao J, Fedorov VV. Fibrosis: a structural modulator of sinoatrial node physiology and dysfunction. Front Physiol. 2015;6:37.
362. De Maziere AM, van Ginneken AC, Wilders R, Jongsma HJ, Bouman LN. Spatial and functional relationship between myocytes and fibroblasts in the rabbit sinoatrial node. J Mol Cell Cardiol. 1992;24(6):567-78.
363. Fedorov VV, Glukhov AV, Chang R. Conduction barriers and pathways of the sinoatrial pacemaker complex: their role in normal rhythm and atrial arrhythmias. American journal of physiology Heart and circulatory physiology. 2012;302(9):H1773-83.
364. Joyner RW, van Capelle FJ. Propagation through electrically coupled cells. How a small SA node drives a large atrium. Biophys J. 1986;50(6):1157-64.
365. Russo I, Frangogiannis NG. Diabetes-associated cardiac fibrosis: Cellular effectors, molecular mechanisms and therapeutic opportunities. J Mol Cell Cardiol. 2016;90:84-93.
366. Asbun J, Villarreal FJ. The pathogenesis of myocardial fibrosis in the setting of diabetic cardiomyopathy. J Am Coll Cardiol. 2006;47(4):693-700.
367. Miragoli M, Gaudesius G, Rohr S. Electrotonic modulation of cardiac impulse conduction by myofibroblasts. Circ Res. 2006;98(6):801-10.
368. Tse G, Lai ET, Tse V, Yeo JM. Molecular and Electrophysiological Mechanisms Underlying Cardiac Arrhythmogenesis in Diabetes Mellitus. J Diabetes Res. 2016;2016:2848759.
369. de Jong S, van Veen TA, van Rijen HV, de Bakker JM. Fibrosis and cardiac arrhythmias. J Cardiovasc Pharmacol. 2011;57(6):630-8.
370. Glukhov AV, Hage LT, Hansen BJ, Pedraza-Toscano A, Vargas-Pinto P, Hamlin RL, et al. Sinoatrial node reentry in a canine chronic left ventricular infarct model: role of intranodal fibrosis and heterogeneity of refractoriness. Circ Arrhythm Electrophysiol. 2013;6(5):984-94.
371. Feng N, Anderson ME. CaMKII is a nodal signal for multiple programmed cell death pathways in heart. J Mol Cell Cardiol. 2017;103:102-9.
372. Huke S, Knollmann BC. Oxidized CaMKII: a "heart stopper" for the sinus node? J Clin Invest. 2011;121(8):2975-7.
373. Hudson RE. The human pacemaker and its pathology. Br Heart J. 1960;22:153-67.
374. Moss AJ, Davis RJ. Brady-Tachy syndrome. Prog Cardiovasc Dis. 1974;16(5):439-54.
375. Xiao S, Shaw RM. Cardiomyocyte protein trafficking: Relevance to heart disease and opportunities for therapeutic intervention. Trends Cardiovasc Med. 2015;25(5):379-89.
376. Saffitz JE. Protein trafficking in cardiovascular disease: How the science has evolved and where it must go. Trends Cardiovasc Med. 2015;25(5):390-1.

377. Delisle BP, Anson BD, Rajamani S, January CT. Biology of cardiac arrhythmias: ion channel protein trafficking. Circ Res. 2004;94(11):1418-28.
378. Lang D, Glukhov AV. Functional Microdomains in Heart's Pacemaker: A Step Beyond Classical Electrophysiology and Remodeling. Front Physiol. 2018;9:1686.
379. Tirziu D, Giordano FJ, Simons M. Cell communications in the heart. Circulation. 2010;122(9):928-37.
380. Vangindertael J, Camacho R, Sempels W, Mizuno H, Dedecker P, Janssen KPF. An introduction to optical super-resolution microscopy for the adventurous biologist. Methods Appl Fluoresc. 2018;6(2):022003.
381. Yamamoto M, Dobrzynski H, Tellez J, Niwa R, Billeter R, Honjo H, et al. Extended atrial conduction system characterised by the expression of the HCN4 channel and connexin45. Cardiovasc Res. 2006;72(2):271-81.
382. Coppen SR, Gourdie RG, Severs NJ. Connexin45 is the first connexin to be expressed in the central conduction system of the mouse heart. Exp Clin Cardiol. 2001;6(1):17-23.
383. Dobrzynski H, Rothery SM, Marples DD, Coppen SR, Takagishi Y, Honjo H, et al. Presence of the Kv1.5 K(+) channel in the sinoatrial node. J Histochem Cytochem. 2000;48(6):769-80.
384. Crossman DJ, Jayasinghe ID, Soeller C. Transverse tubule remodelling: a cellular pathology driven by both sides of the plasmalemma? Biophys Rev. 2017;9(6):919-29.
385. Wright JA, Richards T, Becker DL. Connexins and diabetes. Cardiol Res Pract. 2012;2012:496904.
386. Liu J, Dobrzynski H, Yanni J, Boyett MR, Lei M. Organisation of the mouse sinoatrial node: structure and expression of HCN channels. Cardiovasc Res. 2007;73(4):729-38.
387. Musa H, Lei M, Honjo H, Jones SA, Dobrzynski H, Lancaster MK, et al. Heterogeneous expression of Ca(2+) handling proteins in rabbit sinoatrial node. J Histochem Cytochem. 2002;50(3):311-24.
388. Allah EA, Tellez JO, Yanni J, Nelson T, Monfredi O, Boyett MR, et al. Changes in the expression of ion channels, connexins and Ca2+-handling proteins in the sino-atrial node during postnatal development. Exp Physiol. 2011;96(4):426-38.
389. Ribeiro-Oliveira A, Jr., Nogueira AI, Pereira RM, Boas WW, Dos Santos RA, Simoes e Silva AC. The renin-angiotensin system and diabetes: an update. Vasc Health Risk Manag. 2008;4(4):787-803.
390. Shimizu M, Umeda K, Sugihara N, Yoshio H, Ino H, Takeda R, et al. Collagen remodelling in myocardia of patients with diabetes. J Clin Pathol. 1993;46(1):32-6.
391. Li CJ, Lv L, Li H, Yu DM. Cardiac fibrosis and dysfunction in experimental diabetic cardiomyopathy are ameliorated by alpha-lipoic acid. Cardiovasc Diabetol. 2012;11:73.
392. Ares-Carrasco S, Picatoste B, Benito-Martin A, Zubiri I, Sanz AB, Sanchez-Nino MD, et al. Myocardial fibrosis and apoptosis, but not inflammation, are present in long-term experimental diabetes. American journal of physiology Heart and circulatory physiology. 2009;297(6):H2109-19.
393. Packer M. Critical role of the epicardium in mediating cardiac inflammation and fibrosis in patients with type 2 diabetes. Diabetes Obes Metab. 2019;21(8):1765-8.
394. Aguilar H, Fricovsky E, Ihm S, Schimke M, Maya-Ramos L, Aroonsakool N, et al. Role for high-glucose-induced protein O-GlcNAcylation in stimulating cardiac fibroblast collagen synthesis. Am J Physiol Cell Physiol. 2014;306(9):C794-804.
395. Fiaschi T, Magherini F, Gamberi T, Lucchese G, Faggian G, Modesti A, et al. Hyperglycemia and angiotensin II cooperate to enhance collagen I deposition by cardiac fibroblasts through a ROS-STAT3-dependent mechanism. Biochim Biophys Acta. 2014;1843(11):2603-10.
396. Souders CA, Bowers SL, Baudino TA. Cardiac fibroblast: the renaissance cell. Circ Res. 2009;105(12):1164-76.
397. Aragno M, Mastrocola R, Alloatti G, Vercellinatto I, Bardini P, Geuna S, et al. Oxidative stress triggers cardiac fibrosis in the heart of diabetic rats. Endocrinology. 2008;149(1):380-8.
398. Singh VP, Bali A, Singh N, Jaggi AS. Advanced glycation end products and diabetic complications. Korean J Physiol Pharmacol. 2014;18(1):1-14.
399. Biernacka A, Cavalera M, Wang J, Russo I, Shinde A, Kong P, et al. Smad3 Signaling Promotes Fibrosis While Preserving Cardiac and Aortic Geometry in Obese Diabetic Mice. Circ Heart Fail. 2015;8(4):788-98.

400. Huynh K, McMullen JR, Julius TL, Tan JW, Love JE, Cemerlang N, et al. Cardiac-specific IGF-1 receptor transgenic expression protects against cardiac fibrosis and diastolic dysfunction in a mouse model of diabetic cardiomyopathy. Diabetes. 2010;59(6):1512-20.
401. Ulrich P, Cerami A. Protein glycation, diabetes, and aging. Recent Prog Horm Res. 2001;56:1-21.
402. Aronson D. Cross-linking of glycated collagen in the pathogenesis of arterial and myocardial stiffening of aging and diabetes. J Hypertens. 2003;21(1):3-12.
403. Park TS, Yamashita H, Blaner WS, Goldberg IJ. Lipids in the heart: a source of fuel and a source of toxins. Curr Opin Lipidol. 2007;18(3):277-82.
404. Schulze PC, Drosatos K, Goldberg IJ. Lipid Use and Misuse by the Heart. Circ Res. 2016;118(11):1736-51.
405. Sharma S, Adrogue JV, Golfman L, Uray I, Lemm J, Youker K, et al. Intramyocardial lipid accumulation in the failing human heart resembles the lipotoxic rat heart. FASEB J. 2004;18(14):1692-700.
406. McGavock JM, Lingvay I, Zib I, Tillery T, Salas N, Unger R, et al. Cardiac steatosis in diabetes mellitus: a 1H-magnetic resonance spectroscopy study. Circulation. 2007;116(10):1170-5.
407. Nyman K, Graner M, Pentikainen MO, Lundbom J, Hakkarainen A, Siren R, et al. Cardiac steatosis and left ventricular function in men with metabolic syndrome. J Cardiovasc Magn Reson. 2013;15:103.
408. van de Weijer T, Schrauwen-Hinderling VB, Schrauwen P. Lipotoxicity in type 2 diabetic cardiomyopathy. Cardiovasc Res. 2011;92(1):10-8.
409. Shimabukuro M, Zhou YT, Levi M, Unger RH. Fatty acid-induced beta cell apoptosis: a link between obesity and diabetes. Proc Natl Acad Sci U S A. 1998;95(5):2498-502.
410. Christoffersen C, Bollano E, Lindegaard ML, Bartels ED, Goetze JP, Andersen CB, et al. Cardiac lipid accumulation associated with diastolic dysfunction in obese mice. Endocrinology. 2003;144(8):3483-90.
411. Boden G. Free fatty acids, insulin resistance, and type 2 diabetes mellitus. Proc Assoc Am Physicians. 1999;111(3):241-8.
412. DeFronzo RA. Insulin resistance, lipotoxicity, type 2 diabetes and atherosclerosis: the missing links. The Claude Bernard Lecture 2009. Diabetologia. 2010;53(7):1270-87.
413. Kusminski CM, Shetty S, Orci L, Unger RH, Scherer PE. Diabetes and apoptosis: lipotoxicity. Apoptosis. 2009;14(12):1484-95.
414. Levin K, Daa Schroeder H, Alford FP, Beck-Nielsen H. Morphometric documentation of abnormal intramyocellular fat storage and reduced glycogen in obese patients with Type II diabetes. Diabetologia. 2001;44(7):824-33.
415. Young ME, Guthrie PH, Razeghi P, Leighton B, Abbasi S, Patil S, et al. Impaired long-chain fatty acid oxidation and contractile dysfunction in the obese Zucker rat heart. Diabetes. 2002;51(8):2587-95.
416. Basu R, Oudit GY, Wang X, Zhang L, Ussher JR, Lopaschuk GD, et al. Type 1 diabetic cardiomyopathy in the Akita (Ins2WT/C96Y) mouse model is characterized by lipotoxicity and diastolic dysfunction with preserved systolic function. Am J Physiol Heart Circ Physiol. 2009;297(6):H2096-108.
417. Zhou YT, Grayburn P, Karim A, Shimabukuro M, Higa M, Baetens D, et al. Lipotoxic heart disease in obese rats: implications for human obesity. Proc Natl Acad Sci U S A. 2000;97(4):1784-9.
418. Young ME, McNulty P, Taegtmeyer H. Adaptation and maladaptation of the heart in diabetes: Part II: potential mechanisms. Circulation. 2002;105(15):1861-70.
419. Leone TC, Weinheimer CJ, Kelly DP. A critical role for the peroxisome proliferator-activated receptor alpha (PPARalpha) in the cellular fasting response: the PPARalpha-null mouse as a model of fatty acid oxidation disorders. Proc Natl Acad Sci U S A. 1999;96(13):7473-8.
420. Kersten S, Seydoux J, Peters JM, Gonzalez FJ, Desvergne B, Wahli W. Peroxisome proliferator-activated receptor alpha mediates the adaptive response to fasting. J Clin Invest. 1999;103(11):1489-98.
421. Barger PM, Kelly DP. PPAR signaling in the control of cardiac energy metabolism. Trends Cardiovasc Med. 2000;10(6):238-45.

422. Lee WS, Kim J. Peroxisome Proliferator-Activated Receptors and the Heart: Lessons from the Past and Future Directions. PPAR Res. 2015;2015:271983.
423. Madrazo JA, Kelly DP. The PPAR trio: regulators of myocardial energy metabolism in health and disease. J Mol Cell Cardiol. 2008;44(6):968-75.
424. Gulick T, Cresci S, Caira T, Moore DD, Kelly DP. The peroxisome proliferator-activated receptor regulates mitochondrial fatty acid oxidative enzyme gene expression. Proc Natl Acad Sci U S A. 1994;91(23):11012-6.
425. Brandt JM, Djouadi F, Kelly DP. Fatty acids activate transcription of the muscle carnitine palmitoyltransferase I gene in cardiac myocytes via the peroxisome proliferator-activated receptor alpha. J Biol Chem. 1998;273(37):23786-92.
426. Djouadi F, Weinheimer CJ, Saffitz JE, Pitchford C, Bastin J, Gonzalez FJ, et al. A gender-related defect in lipid metabolism and glucose homeostasis in peroxisome proliferator- activated receptor alpha- deficient mice. J Clin Invest. 1998;102(6):1083-91.
427. Watanabe K, Fujii H, Takahashi T, Kodama M, Aizawa Y, Ohta Y, et al. Constitutive regulation of cardiac fatty acid metabolism through peroxisome proliferator-activated receptor alpha associated with age-dependent cardiac toxicity. J Biol Chem. 2000;275(29):22293-9.
428. Campbell FM, Kozak R, Wagner A, Altarejos JY, Dyck JR, Belke DD, et al. A role for peroxisome proliferator-activated receptor alpha (PPARalpha) in the control of cardiac malonyl-CoA levels: reduced fatty acid oxidation rates and increased glucose oxidation rates in the hearts of mice lacking PPARalpha are associated with higher concentrations of malonyl-CoA and reduced expression of malonyl-CoA decarboxylase. J Biol Chem. 2002;277(6):4098-103.
429. Lockyer P, Schisler JC, Patterson C, Willis MS. Minireview: Won't get fooled again: the nonmetabolic roles of peroxisome proliferator-activated receptors (PPARs) in the heart. Mol Endocrinol. 2010;24(6):1111-9.
430. Muller CP, Pum ME, Amato D, Schuttler J, Huston JP, Silva MA. The in vivo neurochemistry of the brain during general anesthesia. J Neurochem. 2011;119(3):419-46.
431. Pleuvry BJ. Mechanism of action of general anaesthetic drugs. Anaesthesia & Intensive Care Medicine. 2008;9(4):152-3.
432. Urban BW, Bleckwenn M. Concepts and correlations relevant to general anaesthesia. Br J Anaesth. 2002;89(1):3-16.
433. Behdad S, Mortazavizadeh A, Ayatollahi V, Khadiv Z, Khalilzadeh S. The Effects of Propofol and Isoflurane on Blood Glucose during Abdominal Hysterectomy in Diabetic Patients. Diabetes Metab J. 2014;38(4):311-6.
434. Campagna JA, Miller KW, Forman SA. Mechanisms of actions of inhaled anesthetics. N Engl J Med. 2003;348(21):2110-24.
435. Constantinides C, Murphy K. Molecular and Integrative Physiological Effects of Isoflurane Anesthesia: The Paradigm of Cardiovascular Studies in Rodents using Magnetic Resonance Imaging. Front Cardiovasc Med. 2016;3:23.
436. Doursout MF, Chelly JE. Effects of basal anaesthesia on cardiac function. Br J Anaesth. 1988;60(8 Suppl 1):119S-22S.
437. Kato K, Wakai J, Ozawa K, Sekiguchi M, Katahira K. Different sensitivity to the suppressive effects of isoflurane anesthesia on cardiorespiratory function in SHR/Izm, WKY/Izm, and Crl:CD (SD) rats. Exp Anim. 2016;65(4):393-402.
438. Thompson SA, Wafford K. Mechanism of action of general anaesthetics--new information from molecular pharmacology. Curr Opin Pharmacol. 2001;1(1):78-83.
439. Loscher W, Rogawski MA. How theories evolved concerning the mechanism of action of barbiturates. Epilepsia. 2012;53:12-25.
440. Khan KS, Hayes I, Buggy DJ. Pharmacology of anaesthetic agents II: inhalation anaesthetic agents. BJA Education. 2013;14(3):106-11.
441. Bertaccini EJ. The Molecular Mechanisms of Anesthetic Action: Updates and Cutting Edge Developments from the Field of Molecular Modeling. Pharmaceuticals (Basel). 2010;3(7):2178-96.
442. Khan KS, Hayes I, Buggy DJ. Pharmacology of anaesthetic agents I: intravenous anaesthetic agents. BJA Education. 2013;14(3):100-5.

443. Grasshoff C, Antkowiak B. Effects of isoflurane and enflurane on GABAA and glycine receptors contribute equally to depressant actions on spinal ventral horn neurones in rats. Br J Anaesth. 2006;97(5):687-94.
444. Brannigan G, LeBard DN, Henin J, Eckenhoff RG, Klein ML. Multiple binding sites for the general anesthetic isoflurane identified in the nicotinic acetylcholine receptor transmembrane domain. Proc Natl Acad Sci U S A. 2010;107(32):14122-7.
445. Gilat E, Rubinstein I, Binah O. Effect of sodium pentobarbital on the transmembrane action potential and the slow inward current of guinea pig ventricular myocytes. J Cardiovasc Pharmacol. 1987;10(4):485-8.
446. Bachmann A, Mueller S, Kopp K, Brueggemann A, Suessbrich H, Gerlach U, et al. Inhibition of cardiac potassium currents by pentobarbital. Naunyn Schmiedebergs Arch Pharmacol. 2002;365(1):29-37.
447. Khatter JC, Hoeschen RJ, Dhalla NS. Effects of sodium pentobarbital on rat heart sarcolemma. Res Commun Chem Pathol Pharmacol. 1979;24(1):57-66.
448. Pistis M, Belelli D, McGurk K, Peters JA, Lambert JJ. Complementary regulation of anaesthetic activation of human (alpha6beta3gamma2L) and Drosophila (RDL) GABA receptors by a single amino acid residue. J Physiol. 1999;515 (Pt 1):3-18.
449. Sawyer DC, Lumb WV, Stone HL. Cardiovascular effects of halothane, methoxyflurane, pentobarbital, and thiamylal. J Appl Physiol. 1971;30(1):36-43.
450. Segel LD, Rendig SV. Sodium pentobarbital effects on cardiac function and response to dobutamine. J Cardiovasc Pharmacol. 1986;8(2):392-7.
451. Lotz C, Kehl F. Volatile anesthetic-induced cardiac protection: molecular mechanisms, clinical aspects, and interactions with nonvolatile agents. J Cardiothorac Vasc Anesth. 2015;29(3):749-60.
452. Pocock G, Richards CD. Cellular mechanisms in general anaesthesia. Br J Anaesth. 1991;66(1):116-28.
453. Graf BM, Vicenzi MN, Bosnjak ZJ, Stowe DF. The comparative effects of equimolar sevoflurane and isoflurane in isolated hearts. Anesth Analg. 1995;81(5):1026-32.
454. Stowe DF, Marijic J, Bosnjak ZJ, Kampine JP. Direct comparative effects of halothane, enflurane, and isoflurane on oxygen supply and demand in isolated hearts. Anesthesiology. 1991;74(6):1087-95.
455. Iltis I, Kober F, Dalmasso C, Lan C, Cozzone PJ, Bernard M. In vivo assessment of myocardial blood flow in rat heart using magnetic resonance imaging: effect of anesthesia. J Magn Reson Imaging. 2005;22(2):242-7.
456. Bailey JM. Context-sensitive half-times and other decrement times of inhaled anesthetics. Anesth Analg. 1997;85(3):681-6.
457. Gargiulo S, Greco A, Gramanzini M, Esposito S, Affuso A, Brunetti A, et al. Mice anesthesia, analgesia, and care, Part I: anesthetic considerations in preclinical research. ILAR J. 2012;53(1):E55-69.
458. Lysko GS, Robinson JL, Casto R, Ferrone RA. The stereospecific effects of isoflurane isomers in vivo. Eur J Pharmacol. 1994;263(1-2):25-9.
459. Ruxanda F, Bel L, Ratiu C, Miclaus V, Pestean C, Oana L. Clinical Evaluation in Isoflurane and Sevoflurane Anesthesia in Rat. Bulletin UASVM Veterinary Medicine. 2016;73(2).
460. Marano G, Grigioni M, Tiburzi F, Vergari A, Zanghi F. Effects of isoflurane on cardiovascular system and sympathovagal balance in New Zealand white rabbits. J Cardiovasc Pharmacol. 1996;28(4):513-8.
461. Loushin MK. The Effects of Anesthetic Agents on Cardiac Function. In: Iaizzo PA, editor. Handbook of Cardiac Anatomy, Physiology, and Devices. Totowa, NJ: Humana Press; 2005. p. 171-80.
462. Boban M, Stowe DF, Buljubasic N, Kampine JP, Bosnjak ZJ. Direct comparative effects of isoflurane and desflurane in isolated guinea pig hearts. Anesthesiology. 1992;76(5):775-80.
463. Field KJ, White WJ, Lang CM. Anaesthetic effects of chloral hydrate, pentobarbitone and urethane in adult male rats. Lab Anim. 1993;27(3):258-69.
464. Wixson SK, White WJ, Hughes HC, Jr., Lang CM, Marshall WK. The effects of pentobarbital, fentanyl-droperidol, ketamine-xylazine and ketamine-diazepam on arterial blood pH, blood gases, mean arterial blood pressure and heart rate in adult male rats. Lab Anim Sci. 1987;37(6):736-42.

465. Skolleborg KC, Gronbech JE, Grong K, Abyholm FE, Lekven J. Distribution of cardiac output during pentobarbital versus midazolam/fentanyl/fluanisone anaesthesia in the rat. Lab Anim. 1990;24(3):221-7.
466. Watkins L, Maixner W. The effect of pentobarbital anesthesia on the autonomic nervous system control of heart rate during baroreceptor activation. J Auton Nerv Syst. 1991;36(2):107-14.
467. Buelke-Sam J, Holson JF, Bazare JJ, Young JF. Comparative stability of physiological parameters during sustained anesthesia in rats. Lab Anim Sci. 1978;28(2):157-62.
468. Stein AB, Tiwari S, Thomas P, Hunt G, Levent C, Stoddard MF, et al. Effects of anesthesia on echocardiographic assessment of left ventricular structure and function in rats. Basic Res Cardiol. 2007;102(1):28-41.
469. Redfors B, Shao Y, Omerovic E. Influence of anesthetic agent, depth of anesthesia and body temperature on cardiovascular functional parameters in the rat. Lab Anim. 2014;48(1):6-14.
470. Durand JL, Hosinking W, Jelicks LA. Time course of effects of inhalation anesthesia on blood glucose level in male and female C57BL/6 mice. Horm Metab Res. 2009;41(4):339-41.
471. Pomplun D, Mohlig M, Spranger J, Pfeiffer AF, Ristow M. Elevation of blood glucose following anaesthetic treatment in C57BL/6 mice. Horm Metab Res. 2004;36(1):67-9.
472. Constantinides C, Mean R, Janssen BJ. Effects of isoflurane anesthesia on the cardiovascular function of the C57BL/6 mouse. ILAR J. 2011;52(3):e21-31.
473. Kofke WA, Hawkins RA, Davis DW, Biebuyck JF. Comparison of the effects of volatile anesthetics on brain glucose metabolism in rats. Anesthesiology. 1987;66(6):810-3.
474. Laber-Laird K, Smith A, Swindle MM, Colwell J. Effects of isoflurane anesthesia on glucose tolerance and insulin secretion in Yucatan minipigs. Lab Anim Sci. 1992;42(6):579-81.
475. Zuurbier CJ, Keijzers PJ, Koeman A, Van Wezel HB, Hollmann MW. Anesthesia's effects on plasma glucose and insulin and cardiac hexokinase at similar hemodynamics and without major surgical stress in fed rats. Anesth Analg. 2008;106(1):135-42, table of contents.
476. Illera JC, Gonzalez Gil A, Silvan G, Illera M. The effects of different anaesthetic treatments on the adreno-cortical functions and glucose levels in NZW rabbits. J Physiol Biochem. 2000;56(4):329-36.
477. Johansen O, Vaaler S, Jorde R, Reikeras O. Increased plasma glucose levels after Hypnorm anaesthesia, but not after Pentobarbital anaesthesia in rats. Lab Anim. 1994;28(3):244-8.
478. Bester JF, Nelson JW. A study of the potentiation of pentobarbital anesthesia by glucose and its metabolites. J Am Pharm Assoc Am Pharm Assoc. 1953;42(7):421-4.
479. Guarino MP, Santos AI, Mota-Carmo M, Costa PF. Effects of anaesthesia on insulin sensitivity and metabolic parameters in Wistar rats. In Vivo. 2013;27(1):127-32.
480. Sano Y, Ito S, Yoneda M, Nagasawa K, Matsuura N, Yamada Y, et al. Effects of various types of anesthesia on hemodynamics, cardiac function, and glucose and lipid metabolism in rats. American journal of physiology Heart and circulatory physiology. 2016;311(6):H1360-H6.
481. Stoffel M, Tokuyama Y, Trabb JB, German MS, Tsaar ML, Jan LY, et al. Cloning of rat KATP-2 channel and decreased expression in pancreatic islets of male Zucker diabetic fatty rats. Biochem Biophys Res Commun. 1995;212(3):894-9.
482. Cavaghan MK, Ehrmann DA, Polonsky KS. Interactions between insulin resistance and insulin secretion in the development of glucose intolerance. J Clin Invest. 2000;106(3):329-33.
483. Farrokhnia F, Lebaschi AH, Andalib N. A randomized clinical trial for the effects of halothane and isoflurane anesthesia on blood glucose levels in the diabetic patients. DARU Journal of Pharmaceutical Sciences. 2009;17(1):29-32.
484. Wade T. The anaesthetic practitioner and type 1 diabetes mellitus. J Perioper Pract. 2015;25(1-2):19-23.
485. Maechler P, Wollheim CB. Mitochondrial signals in glucose-stimulated insulin secretion in the beta cell. J Physiol. 2000;529 Pt 1:49-56.
486. Fujimoto K, Bosnjak ZJ, Kwok WM. Isoflurane-induced facilitation of the cardiac sarcolemmal K(ATP) channel. Anesthesiology. 2002;97(1):57-65.
487. Rorsman P. The pancreatic beta-cell as a fuel sensor: an electrophysiologist's viewpoint. Diabetologia. 1997;40(5):487-95.
488. Lang J. Molecular mechanisms and regulation of insulin exocytosis as a paradigm of endocrine secretion. Eur J Biochem. 1999;259(1-2):3-17.

489. Koster JC, Permutt MA, Nichols CG. Diabetes and insulin secretion: the ATP-sensitive K+ channel (K ATP) connection. Diabetes. 2005;54(11):3065-72.
490. Bonfanti DH, Alcazar LP, Arakaki PA, Martins LT, Agustini BC, de Moraes Rego FG, et al. ATP-dependent potassium channels and type 2 diabetes mellitus. Clin Biochem. 2015;48(7-8):476-82.
491. Benessiano J, Levy BI, Michel JB. Instantaneous aortic blood flow measurement with range-gated Doppler flowmeter in anesthetized rat. J Pharmacol Methods. 1985;14(2):99-110.
492. Tuma RF, Irion GL, Vasthare US, Heinel LA. Age-related changes in regional blood flow in the rat. Am J Physiol. 1985;249(3 Pt 2):H485-91.
493. Murakami M, Niwa H, Kushikata T, Watanabe H, Hirota K, Ono K, et al. Inhalation anesthesia is preferable for recording rat cardiac function using an electrocardiogram. Biol Pharm Bull. 2014;37(5):834-9.
494. Bencze M, Behuliak M, Zicha J. The impact of four different classes of anesthetics on the mechanisms of blood pressure regulation in normotensive and spontaneously hypertensive rats. Physiol Res. 2013;62(5):471-8.
495. Davies LA, Hamilton DL, Hopkins PM, Boyett MR, Harrison SM. Concentration-dependent inotropic effects of halothane, isoflurane and sevoflurane on rat ventricular myocytes. Br J Anaesth. 1999;82(5):723-30.
496. Skeehan TM, Schuler HG, Riley JL. Comparison of the alteration of cardiac function by sevoflurane, isoflurane, and halothane in the isolated working rat heart. J Cardiothorac Vasc Anesth. 1995;9(6):706-12.
497. Davies LA, Gibson CN, Boyett MR, Hopkins PM, Harrison SM. Effects of isoflurane, sevoflurane, and halothane on myofilament Ca2+ sensitivity and sarcoplasmic reticulum Ca2+ release in rat ventricular myocytes. Anesthesiology. 2000;93(4):1034-44.
498. Suzuki A, Aizawa K, Gassmayr S, Bosnjak ZJ, Kwok WM. Biphasic effects of isoflurane on the cardiac action potential: an ionic basis for anesthetic-induced changes in cardiac electrophysiology. Anesthesiology. 2002;97(5):1209-17.
499. Manders WT, Vatner SF. Effects of sodium pentobarbital anesthesia on left ventricular function and distribution of cardiac output in dogs, with particular reference to the mechanism for tachycardia. Circ Res. 1976;39(4):512-7.
500. Rowaiye OO, Jankowska EA, Ponikowska B. Baroreceptor sensitivity and diabetes mellitus. Cardiol J. 2013;20(5):453-63.
501. Madan BR, Khanna NK, Jain BK. Effect of pentobarbital and thiopental on the acetylcholine content of the heart and brain. Indian J Physiol Pharmacol. 1969;13(4):265-7.
502. Oguchi T, Kashimoto S, Yamaguchi T, Nakamura T, Kumazawa T. Is pentobarbital appropriate for basal anesthesia in the working rat heart model? J Pharmacol Toxicol Methods. 1993;29(1):37-43.
503. Segal J, Schwalb H, Shmorak V, Uretzky G. Effect of anesthesia on cardiac function and response in the perfused rat heart. J Mol Cell Cardiol. 1990;22(11):1317-24.
504. Duan YF, Winters RW, McCabe PM, Green EJ, Schneiderman N. Basal and reactive plasma catecholamine levels under stress and anesthesia in rabbits. Physiol Behav. 1994;56(3):577-83.
505. Matsukawa K, Ninomiya I, Nishiura N. Effects of anesthesia on cardiac and renal sympathetic nerve activities and plasma catecholamines. Am J Physiol. 1993;265(4 Pt 2):R792-7.
506. Tanaka S, Tsuchida H, Nakabayashi K, Seki S, Namiki A. The effects of sevoflurane, isoflurane, halothane, and enflurane on hemodynamic responses during an inhaled induction of anesthesia via a mask in humans. Anesth Analg. 1996;82(4):821-6.
507. Kato M, Komatsu T, Kimura T, Sugiyama F, Nakashima K, Shimada Y. Spectral analysis of heart rate variability during isoflurane anesthesia. Anesthesiology. 1992;77(4):669-74.
508. Cesarovic N, Nicholls F, Rettich A, Kronen P, Hassig M, Jirkof P, et al. Isoflurane and sevoflurane provide equally effective anaesthesia in laboratory mice. Lab Anim. 2010;44(4):329-36.
509. Lee JS, Morrow D, Andresen MC, Chang KS. Isoflurane depresses baroreflex control of heart rate in decerebrate rats. Anesthesiology. 2002;96(5):1214-22.
510. Dobrek L, Skowron B, Baranowska A, Malska-Wozniak A, Ciesielczyk K, Thor PJ. Spectral heart rate variability and selected biochemical markers for autonomic activity in rats under pentobarbital anesthesia. Polish Annals of Medicine. 2017;24(2):180-7.

511. Wicks NL, Wong T, Sun J, Madden Z, Young EC. Cytoplasmic cAMP-sensing domain of hyperpolarization-activated cation (HCN) channels uses two structurally distinct mechanisms to regulate voltage gating. Proc Natl Acad Sci U S A. 2011;108(2):609-14.
512. Lolicato M, Nardini M, Gazzarrini S, Moller S, Bertinetti D, Herberg FW, et al. Tetramerization dynamics of C-terminal domain underlies isoform-specific cAMP gating in hyperpolarization-activated cyclic nucleotide-gated channels. J Biol Chem. 2011;286(52):44811-20.
513. Wainger BJ, DeGennaro M, Santoro B, Siegelbaum SA, Tibbs GR. Molecular mechanism of cAMP modulation of HCN pacemaker channels. Nature. 2001;411(6839):805-10.
514. Lewis AS, Estep CM, Chetkovich DM. The fast and slow ups and downs of HCN channel regulation. Channels (Austin). 2010;4(3):215-31.
515. Accili EA, Proenza C, Baruscotti M, DiFrancesco D. From funny current to HCN channels: 20 years of excitation. News Physiol Sci. 2002;17:32-7.
516. DiFrancesco D. Characterization of single pacemaker channels in cardiac sino-atrial node cells. Nature. 1986;324(6096):470-3.
517. Viscomi C, Altomare C, Bucchi A, Camatini E, Baruscotti M, Moroni A, et al. C terminus-mediated control of voltage and cAMP gating of hyperpolarization-activated cyclic nucleotide-gated channels. J Biol Chem. 2001;276(32):29930-4.
518. Akimoto M, Zhang Z, Boulton S, Selvaratnam R, VanSchouwen B, Gloyd M, et al. A mechanism for the auto-inhibition of hyperpolarization-activated cyclic nucleotide-gated (HCN) channel opening and its relief by cAMP. J Biol Chem. 2014;289(32):22205-20.
519. Chow SS, Van Petegem F, Accili EA. Energetics of cyclic AMP binding to HCN channel C terminus reveal negative cooperativity. J Biol Chem. 2012;287(1):600-6.
520. DiFrancesco D, Ferroni A, Mazzanti M, Tromba C. Properties of the hyperpolarizing-activated current (if) in cells isolated from the rabbit sino-atrial node. J Physiol. 1986;377:61-88.
521. Mangoni ME, Nargeot J. Properties of the hyperpolarization-activated current (I(f)) in isolated mouse sino-atrial cells. Cardiovasc Res. 2001;52(1):51-64.
522. Wang J, Chen S, Siegelbaum SA. Regulation of hyperpolarization-activated HCN channel gating and cAMP modulation due to interactions of COOH terminus and core transmembrane regions. J Gen Physiol. 2001;118(3):237-50.
523. Stieber J, Stockl G, Herrmann S, Hassfurth B, Hofmann F. Functional expression of the human HCN3 channel. J Biol Chem. 2005;280(41):34635-43.
524. Beavo JA, Brunton LL. Cyclic nucleotide research -- still expanding after half a century. Nat Rev Mol Cell Biol. 2002;3(9):710-8.
525. Leroy J, Vandecasteele G, Fischmeister R. Cyclic AMP signaling in cardiac myocytes. Curr Opin Physiol. 2018;1:161-71.
526. Vinogradova TM, Sirenko S, Lyashkov AE, Younes A, Li Y, Zhu W, et al. Constitutive phosphodiesterase activity restricts spontaneous beating rate of cardiac pacemaker cells by suppressing local Ca2+ releases. Circ Res. 2008;102(7):761-9.
527. Vinogradova TM, Kobrinsky E, Lakatta EG. Dual Activation of Phosphodiesterases 3 and 4 Regulates Basal Spontaneous Beating Rate of Cardiac Pacemaker Cells: Role of Compartmentalization? Front Physiol. 2018;9:1301.
528. Lukyanenko YO, Younes A, Lyashkov AE, Tarasov KV, Riordon DR, Lee J, et al. Ca(2+)/calmodulin-activated phosphodiesterase 1A is highly expressed in rabbit cardiac sinoatrial nodal cells and regulates pacemaker function. J Mol Cell Cardiol. 2016;98:73-82.
529. Gao Z, Singh MV, Hall DD, Koval OM, Luczak ED, Joiner ML, et al. Catecholamine-independent heart rate increases require Ca2+/calmodulin-dependent protein kinase II. Circ Arrhythm Electrophysiol. 2011;4(3):379-87.
530. Bockus LB, Humphries KM. cAMP-dependent Protein Kinase (PKA) Signaling Is Impaired in the Diabetic Heart. J Biol Chem. 2015;290(49):29250-8.
531. Dutta K, Carmody MW, Cala SE, Davidoff AJ. Depressed PKA activity contributes to impaired SERCA function and is linked to the pathogenesis of glucose-induced cardiomyopathy. J Mol Cell Cardiol. 2002;34(8):985-96.
532. Das A, Durrant D, Salloum FN, Xi L, Kukreja RC. PDE5 inhibitors as therapeutics for heart disease, diabetes and cancer. Pharmacol Ther. 2015;147:12-21.

533. Matyas C, Nemeth BT, Olah A, Torok M, Ruppert M, Kellermayer D, et al. Prevention of the development of heart failure with preserved ejection fraction by the phosphodiesterase-5A inhibitor vardenafil in rats with type 2 diabetes. Eur J Heart Fail. 2017;19(3):326-36.
534. Fan X, Ma J, Wan W, Zhang P, Wang C, Wu L. Increased intracellular calcium concentration causes electrical turbulence in guinea pig ventricular myocytes. Sci China Life Sci. 2011;54(3):240-7.
535. Fan XR, Ma JH, Wan W, Zhang PH, Wang C, Wu L. Increased intracellular calcium concentration causes electrical turbulence in guinea pig ventricular myocytes. Sci China Life Sci. 2011;54(3):240-7.
536. Periasamy M, Reed TD, Liu LH, Ji Y, Loukianov E, Paul RJ, et al. Impaired cardiac performance in heterozygous mice with a null mutation in the sarco(endo)plasmic reticulum Ca2+-ATPase isoform 2 (SERCA2) gene. J Biol Chem. 1999;274(4):2556-62.
537. Shull GE, Okunade G, Liu LH, Kozel P, Periasamy M, Lorenz JN, et al. Physiological functions of plasma membrane and intracellular Ca2+ pumps revealed by analysis of null mutants. Ann N Y Acad Sci. 2003;986:453-60.
538. Sipido KR, Callewaert G, Carmeliet E. Inhibition and rapid recovery of Ca2+ current during Ca2+ release from sarcoplasmic reticulum in guinea pig ventricular myocytes. Circ Res. 1995;76(1):102-9.
539. Sham JS. Ca2+ release-induced inactivation of Ca2+ current in rat ventricular myocytes: evidence for local Ca2+ signalling. J Physiol. 1997;500 (Pt 2):285-95.
540. Li L, Louch WE, Niederer SA, Andersson KB, Christensen G, Sejersted OM, et al. Calcium dynamics in the ventricular myocytes of SERCA2 knockout mice: A modeling study. Biophys J. 2011;100(2):322-31.
541. Li L, Louch WE, Niederer SA, Aronsen JM, Christensen G, Sejersted OM, et al. Sodium accumulation in SERCA knockout-induced heart failure. Biophys J. 2012;102(9):2039-48.
542. Brittsan AG, Ginsburg KS, Chu G, Yatani A, Wolska BM, Schmidt AG, et al. Chronic SR Ca2+-ATPase inhibition causes adaptive changes in cellular Ca2+ transport. Circ Res. 2003;92(7):769-76.
543. Tada M, Kirchberger MA, Repke DI, Katz AM. The stimulation of calcium transport in cardiac sarcoplasmic reticulum by adenosine 3':5'-monophosphate-dependent protein kinase. J Biol Chem. 1974;249(19):6174-80.
544. Lima-Leopoldo AP, Leopoldo AS, da Silva DC, do Nascimento AF, de Campos DH, Luvizotto RA, et al. Long-term obesity promotes alterations in diastolic function induced by reduction of phospholamban phosphorylation at serine-16 without affecting calcium handling. J Appl Physiol (1985). 2014;117(6):669-78.
545. Schwinger RH, Munch G, Bolck B, Karczewski P, Krause EG, Erdmann E. Reduced Ca(2+)-sensitivity of SERCA 2a in failing human myocardium due to reduced serin-16 phospholamban phosphorylation. J Mol Cell Cardiol. 1999;31(3):479-91.
546. Brixius K, Wollmer A, Bolck B, Mehlhorn U, Schwinger RH. Ser16-, but not Thr17-phosphorylation of phospholamban influences frequency-dependent force generation in human myocardium. Pflugers Arch. 2003;447(2):150-7.
547. Schmidt U, Hajjar RJ, Kim CS, Lebeche D, Doye AA, Gwathmey JK. Human heart failure: cAMP stimulation of SR Ca(2+)-ATPase activity and phosphorylation level of phospholamban. Am J Physiol. 1999;277(2):H474-80.
548. Sande JB, Sjaastad I, Hoen IB, Bokenes J, Tonnessen T, Holt E, et al. Reduced level of serine(16) phosphorylated phospholamban in the failing rat myocardium: a major contributor to reduced SERCA2 activity. Cardiovasc Res. 2002;53(2):382-91.
549. Hamm HE. The many faces of G protein signaling. J Biol Chem. 1998;273(2):669-72.
550. Mighiu AS, Heximer SP. Controlling Parasympathetic Regulation of Heart Rate: A Gatekeeper Role for RGS Proteins in the Sinoatrial Node. Front Physiol. 2012;3:204.
551. Watson N, Linder ME, Druey KM, Kehrl JH, Blumer KJ. RGS family members: GTPase-activating proteins for heterotrimeric G-protein alpha-subunits. Nature. 1996;383(6596):172-5.
552. Fu Y, Huang X, Piao L, Lopatin AN, Neubig RR. Endogenous RGS proteins modulate SA and AV nodal functions in isolated heart: implications for sick sinus syndrome and AV block. American journal of physiology Heart and circulatory physiology. 2007;292(5):H2532-9.
553. Wieland T, Mittmann C. Regulators of G-protein signalling: multifunctional proteins with impact on signalling in the cardiovascular system. Pharmacol Ther. 2003;97(2):95-115.

554. Mittmann C, Chung CH, Hoppner G, Michalek C, Nose M, Schuler C, et al. Expression of ten RGS proteins in human myocardium: functional characterization of an upregulation of RGS4 in heart failure. Cardiovasc Res. 2002;55(4):778-86.
555. Cifelli C, Rose RA, Zhang H, Voigtlaender-Bolz J, Bolz SS, Backx PH, et al. RGS4 regulates parasympathetic signaling and heart rate control in the sinoatrial node. Circ Res. 2008;103(5):527-35.
556. Wydeven N, Posokhova E, Xia Z, Martemyanov KA, Wickman K. RGS6, but not RGS4, is the dominant regulator of G protein signaling (RGS) modulator of the parasympathetic regulation of mouse heart rate. J Biol Chem. 2014;289(4):2440-9.
557. Yang J, Huang J, Maity B, Gao Z, Lorca RA, Gudmundsson H, et al. RGS6, a modulator of parasympathetic activation in heart. Circ Res. 2010;107(11):1345-9.
558. Posokhova E, Ng D, Opel A, Masuho I, Tinker A, Biesecker LG, et al. Essential role of the m2R-RGS6-IKACh pathway in controlling intrinsic heart rate variability. PLoS One. 2013;8(10):e76973.
559. Stewart A, Huang J, Fisher RA. RGS Proteins in Heart: Brakes on the Vagus. Front Physiol. 2012;3:95.
560. Seshadri N, Acharya N, Lauer MS. Association of diabetes mellitus with abnormal heart rate recovery in patients without known coronary artery disease. Am J Cardiol. 2003;91(1):108-11.
561. Arai Y, Saul JP, Albrecht P, Hartley LH, Lilly LS, Cohen RJ, et al. Modulation of cardiac autonomic activity during and immediately after exercise. Am J Physiol. 1989;256(1 Pt 2):H132-41.
562. Carnevali L, Sgoifo A. Vagal modulation of resting heart rate in rats: the role of stress, psychosocial factors, and physical exercise. Front Physiol. 2014;5:118.
563. Roy A, Guatimosim S, Prado VF, Gros R, Prado MAM. Cholinergic Activity as a New Target in Diseases of the Heart. Molecular Medicine. 2014;20:527-37.
564. Wittmann T, Lohse MJ, Schmitt JP. Phospholamban pentamers attenuate PKA-dependent phosphorylation of monomers. J Mol Cell Cardiol. 2015;80:90-7.
565. Chu G, Dorn GW, 2nd, Luo W, Harrer JM, Kadambi VJ, Walsh RA, et al. Monomeric phospholamban overexpression in transgenic mouse hearts. Circ Res. 1997;81(4):485-92.
566. Merin RG. The isolated heart preparation. Br J Anaesth. 1988;60(8 Suppl 1):28S-34S.
567. Saddik M, Lopaschuk GD. Myocardial Triglyceride Turnover and Contribution to Energy Substrate Utilization in Isolated Working Rat Hearts. Journal of Biological Chemistry. 1991;266(13):8162-70.
568. Bates SH, Kulkarni RN, Seifert M, Myers MG, Jr. Roles for leptin receptor/STAT3-dependent and -independent signals in the regulation of glucose homeostasis. Cell Metab. 2005;1(3):169-78.
569. Wang YW, Sun GD, Sun J, Liu SJ, Wang J, Xu XH, et al. Spontaneous type 2 diabetic rodent models. J Diabetes Res. 2013;2013:401723.
570. Coleman DL, Hummel KP. The influence of genetic background on the expression of the obese (Ob) gene in the mouse. Diabetologia. 1973;9(4):287-93.
571. Marchetti P, Del Prato S, Lupi R, Del Guerra S. The pancreatic beta-cell in human Type 2 diabetes. Nutr Metab Cardiovasc Dis. 2006;16 Suppl 1:S3-6.
572. Siwy J, Zoja C, Klein J, Benigni A, Mullen W, Mayer B, et al. Evaluation of the Zucker diabetic fatty (ZDF) rat as a model for human disease based on urinary peptidomic profiles. PLoS One. 2012;7(12):e51334.